Structure of prion β-oligomers as determined by structural proteomics

by

Jason John Serpa
BSc., University of Victoria, 2005

A Dissertation Submitted in Partial Fulfillment
of the Requirements for the Degree of

DOCTOR OF PHILOSOPHY

in the Department of Biochemistry and Microbiology

Supervisory Committee

Structure of prion β-oligomers as determined by structural proteomics

by

Jason John Serpa
BSc, University of Victoria, 2005

Supervisory Committee

Dr. Christoph H. Borchers, Department of Biochemistry and Microbiology
Supervisor

Dr. Robert D. Burke, Department of Biochemistry and Microbiology
Departmental Member

Dr. John E. Burke, Department of Biochemistry and Microbiology
Departmental Member

Dr. Stephanie M. Willerth, Department of Mechanical Engineering
Outside Member

Abstract

Dr. Christoph H. Borchers, Department of Biochemistry and Microbiology
Supervisor
Dr. Robert D. Burke, Department of Biochemistry and Microbiology
Departmental Member
Dr. John E. Burke, Department of Biochemistry and Microbiology
Departmental Member
Dr. Stephanie M. Willerth, Department of Mechanical Engineering
Outside Member

The conversion of the native monomeric cellular prion protein (PrP^{C}) into an aggregated pathological β-oligomeric (PrP^{β}) and an infectious form (PrP^{Sc}) is the central element in the development of prion diseases. The structure of the aggregates and the molecular mechanisms of the conformational change involved in this conversion are still unknown.

My research hypothesis was that a specific structural rearrangement of normal PrP^{C} monomers leads to the formation of new inter-subunit interaction interfaces in the prion aggregates, leading to aggregation. My approach was to use constraints obtained by structural proteomic methods to create a 3D model of urea-acid induced recombinant prion oligomers (PrP^{β}). My hypothesis was that this model would explain the mechanism of the conformational change involved in the conversion, the early formation of the β-structure nucleation site, and would describe the mode of assembly of the subunits within the oligomer.

I applied a combination of limited proteolysis, surface modification, chemical crosslinking and hydrogen/deuterium exchange (HDX) with mass spectrometry for the differential characterization of the native and the urea-acid converted prion β-oligomer structures to get an insight into the mechanism of the conversion and aggregation. Using HDX, I detected a region of the protein in which backbone amides become more protected from exchange in PrP^{β} compared to PrP^{C}. In order to obtain the inter-residue distance constraints to guide the assembly of the oligomer model, I then applied zero-length and short-range crosslinking to an equimolar mixture of $^{14}N/^{15}N$-metabolically labeled β-oligomer thereby enabling the classification of the crosslinks as either intra-

protein or inter-protein. Working with the Dokholyan group at the University of North Carolina at Chapel Hill, I was able to assemble a structure of the β-oligomer based on the combination of constraints obtained from all methods. By comparing the structures before and after the conversion, I was able to deduce the conformational change, that occurs during the conversion as the rearrangement and disassembly of the beta sheet 1– helix 1 – beta sheet 2 (β1-H1-β2) region from the helix 2 – helix 3 (H2-H3) core, forming new β-sheet nucleation site and resulting in the exposure of hydrophobic residues patches leading to formation of inter-protein contacts within aggregates.

Table of Contents

List of Tables

List of Figures

List of Equations

Acknowledgments

A heartfelt thanks to Dr. Christoph Borchers for seeing a biochemist where few would have seen one. I admire the strength and vision he had to push to be an advisor for a non-traditional student such as myself. His unwavering confidence in me is not easily forgotten and I only hope it has been a worthwhile journey for him as well.

Dr. Borchers provided the mentorship and leadership which offered me the chance to pursue this goal but its realization would also not have been possible without the day-to-day assistance and mentorship of Dr. Evgeniy Petrotchenko. It has been my great fortune to have had the opportunity to learn so much from him.

Thanks also to my committee members Dr. Robert Burke, Dr. John Burke, and Dr. Stephanie Willerth. Your guidance, support, and patience throughout the years was essential and I am appreciative for it. Thanks as well to Dr. Derek Wilson for being a great external examiner.

A special thank-you to Dr. Carol Parker for her countless contributions to critically editing and revising this and all manuscripts. Furthermore, I would like to thank all of the authors and those acknowledged in the data chapter papers presented within. There would be no dissertation without you.

In working with prions, it was often necessary to change laboratory locations and procedures. I would like to give a special thanks to Dr. Juan Ausio, Dr. Fran Nano, and Dr. Chris Upton for sharing space and/or equipment with me through the years.

Thanks to all of the current and past students, post-docs, and staff at the University of Victoria Genome BC Proteomics Centre -- especially those who have studied with the structural proteomics group, and especially Nick Brodie and Karl Makepeace whose growth as leaders in this field has been enjoyable to be a part of. A most honorable mention to Darryl Hardie for always being willing to help me every time I needed assistance.

Lastly, thanks to my ever-supportive family. Jean, for taking on and succeeding in being my single greatest supporter every day along the way. It is easy to forget the down days on such a long journey, but they have come and they have gone with the love and

encouragement she has always offered. Mom and Dad have supported me in everything I have done, so it is not surprising that they have been with me on this voyage as well. With their elegantly simple teachings of being good to everyone and working hard every day, I can see and perhaps have in-part proven that indeed so much is possible. To my brother Terry and sister-in law Laura, I am also thankful to the two of you as well for providing me with much needed encouragement as well.

Dedication

Jean for everything.

Mom and Dad for everything.

Ainsle James Helmcken, for teaching me the importance of learning something new every day.

Edith Mary Helmcken, for teaching me to be confident (you were right, I would become a doctor), seize every day, and never stop dreaming.

Abbreviations

A	Adenosine
aa	Amino acid
AcOH	Acetic acid
ALS	Amyotrophic lateral sclerosis
ANS	1-anilinonapthalene-8-sulfonate fluorescence
APP	Amyloid precursor protein
Arg-C	Clostripain
Asn	Asparagine
Aβ	Amyloid beta
Aβo	Amyloid β oligomers
BS_3	Bis(Sulfosuccinimidyl) suberate
BSE	Bovine spongiform encephalopathy
C1	GPI-anchored C-terminal fragment of PrP^C resulting from α-cleavage at aa110 or 111
C2	GPI-anchored C-terminal fragment or PrP^C resulting from β-cleavage near aa90
CamKII	Calcium/calmodulin-dependent protein kinase II
CBDPS	CyanurBiotinDiPropionylSuccinimde
CD	Circular dichroism
CDI	Conformation-dependent immunoassay
cDNA	Complementary DNA
CID	Collision-induced dissociation
CJD	Creutzfeld-Jakob disease
CNS	Central nervous system
CSF	Cerebrospinal fluid
^{ctm}Prp	Topologically differently processed PrP^C form with C-terminus in the ER lumen
Cu/ZnSOD	Cu/Zn-superoxide dismutase
^{cy}PrP	Topologically differently processed PrP^C form which is non-mebrane bound and found in cytosol
Cys	Cysteine
D178N	Asparagine for aspartic acid subsitiution at codon 178
DLS	Dynamic light scattering
DMD	Discrete molecular dynamics
DMTMM	4-(4, 6-dimethoxy-1,3,5-triazin-2-yl)-4-methylmorpholinium chloride
DSG	Di(N-succinimidyl) glutarate
DSS	Disuccinimidyl suberate
E. coli	*Escherichia coli*
ECD	Electron capture dissociation

EDC	1-Ethyl-3-[3-dimethylaminopropyl]carbodiimide hydrochloride
EGS	Ethylene glycol bis[succinimylsuccinate]
Endo H	Endoglycosidase H
EPR	Electron paramagnetic resonance
ER	Endoplasmic reticulum
ESI	Electrospray ionization
Fabs	Antigen-binding fragments
FFI	Fatal familial insomnia
FPOP	Fast photochemical oxidation of proteins
FT	Fourier transform
FTIR	Fourier transform infrared
GAGs	Glycosaminoglycans
GdnHCl	Guanidine hydrochloride
GFAP	Glial-fibrillary acidic protein
GlcNAc	*N*-Acetylglucosamine
GPCR	G protein coupled receptor
GPI	Glycosylphosphatidylinositol
GPI-SS	GPI-anchor addition sequence
GSS	Gerstmann-Straussler-Scheinker disease
H/D	Hydrogen/deuterium
HD	Hydrophobic domain
HDX	Hydrogen-deuterium exchange
H-E	Hematoxylin-eosin
His	Histidine
HSPG	Heparin sulfate proteoglycans
HuPrP	Human prion protein
iCJD	Iatrogenic CJD
Ile	Isoleucine
kDa	Kilo Dalton
LRP/LR	37 kDa Laminin Receptor Precursor/ 67 kDa Laminin Receptor
LRP1	Low-density lipoprotein receptor related protein
M/M	Methionine homozygote
M/V	Methionine/valine heterozygote
MALDI	Matrix-assisted laser desorption/ionization
MD	Molecular dynamics
Met	Methionine
MS	Mass spectrometry
N	Nitrogen
N1	Soluble N-terminal fragment relaesed from α-cleavage of PrP^C at aa110 or 111
N2	Soluble N-terminal fragment relaesed from β-cleavage of PrP^C near aa90

NaOAc	Sodium acetate
NCAM	Neural cell adhesion molecule
Neu	Neuraminidase
Neu5Ac	N-acetylneuraminic acid
Neu5Gc	N-glyconeuraminic acid
NEUs	Sialidases
Ni-NTA	Nickel-nitrilotriacetic acid
NMDA	*N*-methyl D-aspartate
NMR	Nuclear magnetic resonance
^{Ntm}PrP	Topologically differently processed PrP^{C} form with N-terminus in the ER lumen
OM	Olfactory mucosa
OR	Octarepeat
ORPD	Octarepeat deletion
ORPI	Octapeptide repeat insertions
PCASS	Pyridine carboxylic acid N-hydroxysulfosuccinimide ester
PE	Phosphatidylethanolamine
Phe	Phenylalanine
PICUP	Photo-Induced Cross-linking of Unmodified Protein
PM	Plasma membrane
PMCA	Protein misfolding cyclic amplification
PNGase F	N-glycosidase F
POPG	Palmitoyl-oleoyl-phosphatidylglycerol
Pro	Proline
PrP 27-30	β-structure rich, insoluble, protease-resistant core obtained from enriched fracions of PrP^{Sc}
PrP5	Prion Protein and Plasmid Production Platform Facility
PrP^{C}	Native (non-infectious) prion protein
PrP^{L}	Lethal oligomeric prion form
PrP^{Sc}	β-structure rich, protease-resistant, insoluble, infectious prion form
PrP^{β}	β-oligomeric form of the prion protein
PTM	Post-translational modification
Pyk2	Protein-tyrosine kinase 2-β
Rab4	Rras-related protein 4
Rab5	Ras-related protein 5
recPrP	Recombinant PrP
recPrP $_{121-231}$	Recombinant PrP $_{121-230}$
$recPrP^{C}$	Recombinant PrP^{C}
RML	Rocky mountain laboratories prion strain
RT-QuIC	Real-time quaking-induced conversion

SAXS	Small x-ray scattering
sCJD	Sporadic CJD
SDS	Sodium dodecyl sulfate
SDS-PAGE	Sodium dodecyl sulfate polyacrylamide gel electrophoresis
Ser	Serine
shed PrP	PrP shed into the medium
ShPrP	Syrian hamster prion protein
ShPrP23-232	Syrian hamster prion protein sequence 23-232
ShPrP90-232	N- and C- terminally truncated syrian hamster prion protein sequence 90-232
$sPrP^{Sc}$	Protease-sensitive PrP^{Sc}
SRP	Signal recognition particle
ST	Sialyltransferase
STEM	Scanning transmission electron microscopy
STI	Stress inducible protein 1
TATA	2,4,6-triazido-1,3,5-triazine
TRAM	Translocating chain associating membrane protein
TRAP	Translocon-associated protein
TREK-1	Two-pore potassium channel protein
Trp	Tryptophan
TSE	Transmissible spongiform encephalopathy
Tyr	Tyrosine
UPS	Ubiquitin-proteasome system
UV	Ultraviolet
V/V	Valine homozygote
Val	Valine
vCJD	Variant Creutzfeld-Jakob disease
Δ-GPI PrP^{Sc}	PrP^{Sc} without GPI-anchor

Chapter 1: Introduction

1.1. Prion

Transmissible spongiform encephalopathies (TSEs) are a collection of infectious and transmissible neurodegenerative disorders of humans and animals (1,2). These include; bovine spongiform encephalopathy (BSE) of cattle, chronic wasting disease (CWD) of cervids, and scrapie of sheep and goat. Human TSEs include: sporadic Creutzfeld-Jakob disease (CJD) (sCJD), acquired prion diseases (e.g. kuru), inherited prion diseases (e.g. fatal familial insomnia (FFI), and Gerstmann-Sträussler-Scheinker syndrome (GSS)). These invariably fatal infections are most often characterized by brain vacuolation, astrogliosis, neural apoptosis, and an accumulation of an abnormal misfolded prion protein in the central nervous system (3-5). Prions, or "proteinacious infectious particles" (6), were so named, since, despite multiple investigations, no evidence has been shown for a nucleic acid being involved in TSE transmission (7-10), suggesting that the prion protein itself is required for infection (6). The prion protein, therefore, must be the pathogenic agent of these diseases and must be responsible for the highly unusual properties of TSEs.

The conversion of the native PrP^{C} into a pathogenic PrP^{Sc} (^{Sc} indicating scrapie-like) is the central element in the transmission and development of prion diseases (11). Pathogenic, fibril-forming, multimeric, and predominately β-sheet prion protein (PrP^{Sc}) binds to native monomeric α-helix-rich cellular prion protein (PrP^{C}), resulting in the conversion of PrP^{C} to nascent PrP^{Sc}, in a template mediated conversion (12). The major hallmark of the conversion process is the creation of insoluble PrP^{Sc} from PrP^{C} (3,6,13-16). In the central nervous system, these insoluble proteins eventually accumulate as amyloid plaques. These amyloid fibrils and plaques are the late products of the aggregation pathway and are often treated as the explicit effectors of prion disorders (17). However, intermediates or by-products of the transition from PrP^{C} to PrP^{Sc} may actually be the pathogenic forms. β-oligomers (PrP^{β}) are one such intermediate species that may be toxic and may be involved in later stages of the process of PrP^{Sc} assembly (17,18). This underscores the importance of studying PrP^{β} oligomers to gain insight into prion disease pathogenesis.

The study of the molecular mechanisms involved in the conformational changes of PrP^{C}, which lead to the assembly and final structures of the pathogenic prion isoforms, is critical to understanding the aggregation process in prion disease. Conversion of PrP^{C} to $PrP^{ß}$ oligomers can be studied *in vitro* using nonglycosylated recombinantly expressed proteins. Prion oligomers have structural features that are believed to resemble those existing *in vivo* during prion disease pathogenesis. These β-rich forms are inherently challenging to study using conventional structural biology methods, such as liquid-state NMR spectroscopy and X-ray crystallography, due to their poor solubility and heterogeneity. The lack of biophysical techniques suitable for determining high-resolution structures of non-crystalline fibrillar assemblies has been one of the major hurdles in understanding the structure of prion aggregates (19).

To make a more complete characterization of prion aggregate structures, proteomic approaches can be used. Structural proteomics can be defined as the combination of protein chemistry methods, which includes limited proteolysis, surface chemical modification (SM), hydrogen/deuterium exchange (HDX), and chemical crosslinking, in combination with mass spectrometry. By using these methods, specific structural details of protein and protein complexes can be obtained (20) and applied to the study of prion aggregate structure (21,22).

We and others have shown, that during PrP^{C} to PrP^{β} conversion, the prion protein undergoes a significant conformational rearrangement, and for this to occur, there must be a disengagement of the H1 α-helix and a separation of contacts between the β1-H1-β2 domain and the H2-H3 core (22-27). This rearrangement is thought to result in previously buried surfaces becoming exposed to solvent, from which new inter-protein contacts can develop. This conversion is also thought to result in the formation of a β-sheet nucleation site, which can initiate the progression to fibrillar forms.

We have performed a comprehensive study using multiple proteomic techniques for the determination of urea-acid induced prion oligomer structure. A panel of enzymes was used for limited proteolysis. ^{12}C and ^{13}C pyridine carboxylic acid N-hydroxysulfosuccinimide ester (PCAS) was used for the differential modification of lysine, tyrosine, serine, and threonine residues, and differential oxidation of tryptophan and methionine residues using isotopically-labeled hydrogen peroxide was used to obtain

surface-exposure differences resulting from the conversion. HDX was used to assess changes in secondary structure between PrP^{C} and PrP^{β}. We utilized a panel of crosslinking reagents, including zero-length, and short- and long- range reagents, to identify intra- and inter- protein crosslinks by applying crosslinking reactions to an equimolar mixture of $^{14}N/^{15}N$-metabolically labeled PrP^{β}. Pairwise inter-atom distance constraints derived from zero-length and short-range crosslinking experimental data can be incorporated into the force field of discrete molecular dynamics (DMD) simulations to develop a flexible and efficient procedure for experimentally-guided de-novo structure determination. The models developed using DMD simulations can then be validated using other structural-proteomics techniques such as limited proteolysis, SM, HDX, and long-range (>14Å) crosslinking.

We have applied a combination of these structural proteomic methods to compare the structure of PrP^{C} (before and after conversion) with urea-acid induced PrP^{β} oligomers. This has allowed us to assemble a structure of the β-oligomer, based on all of the constraints obtained. Our β-oligomer model supports the rearrangement and disassembly of the β1-H1-β2 region from the H2-H3 core, the consequent development of an apparent β-sheet nucleation site, and the formation of new inter-protein hydrophobic contacts resulting from the change in exposure of hydrophobic residues, as pivotal to the conversion of PrP^{C} to PrP^{β}. The structure we obtained explains the mechanism of the conformational change involved in the conversion and the early formation of the β-structure nucleation site, and describes the mode of assembly of the subunits within the oligomer.

1.1.1. History of prion disease

Scrapie, a fatal and contagious disease of sheep, is thought to be the first recorded member of animal TSEs. It was first clearly described as an infectious disease of sheep in the eighteenth century in Germany and England, and is thought to have its origins in Europe during the Middle Ages (28). Infected sheep appeared to lack coordination over voluntary muscle movements, as evidenced by their consistent rubbing against fences in an effort to stay upright, inevitably succumbing to the disease (29).

The transmissibility of scrapie was accidentally demonstrated when a flock of Scottish sheep were inoculated against louping ill with a vaccine inadvertently produced from a

formalin extract of brain tissue from a scrapie infected sheep. This resulted in nearly 10% of the flock developing scrapie within 2 years (2,28). Further studies established that scrapie could be experimentally transmitted to sheep (30) and mice (31) by inoculation of cell free lysates. In humans, the acquired TSE known as kuru, meaning "shivering" or "trembling", was first considered to be caused by a slow viral infection with a long incubation time (32) which was thought to be propagated by the ritualistic cannibalistic practices of some tribes of highlanders of New Guinea (2,32). Infected individuals also exhibited ataxia, a predominant symptom of scrapie, and a shivering-like tremor which ultimately resulted in complete motor incapacity and death within 9 months (29,32). In brain samples of these patients, typical "plaque" lesions, similar to those from scrapie-infected sheep, contained characteristic collections of extracellular proteinaceous material (29). In 1959, William Hadlow highlighted the similarities between the aetiological, epizootiological, clinical, and pathological features of scrapie and kuru brain lesions, suggesting that both were the result of a slow virus (33). Carlton Gajdusek et al. (34) showed that intracerebral inoculation of kuru-victim brain homogenate to chimpanzees resulted in transmission of kuru. In 1959, Igor Klatzo described kuru and CJD as also exhibiting similarities in pathology in the central nervous system tissues as determined by light microscopy (35). It was then confirmed that other human forms of disease, such as CJD (36) and inherited prion disease GSS (37), could also be transmitted to other animals via intracerebral inoculation.

The infectious agent of these diseases was determined to be relatively small, because filtered homogenates remained infectious, which led to the original conclusion that a slow virus with an unusually long incubation time between onset of symptoms and pathogen exposure was responsible (38). In 1967, Tikvah Alper (7) demonstrated that the infectious agent was so small that it *excluded* viruses and that it was also extremely resistant to UV and ionizing radiation which normally inactivates viruses. Infectivity was also shown to be more sensitive to UV at 237nm instead of 254nm (39), suggesting that the agent was not composed of nucleic acids (7,40).

The nature of the infectious agent remained unanswered and was hypothesised to be a nucleoprotein complex or a replicating polysaccharide (6). In 1982, Prusiner et al. (6,41) reported a 1000-fold enrichment of infectivity from brain homogenate by a series of steps

including limited proteinase-K digestion, polyethylene-glycol precipitation, micrococcal-nuclease digestion, and sucrose-gradient centrifugation. These enriched samples were inactivated by treatments which destroy protein function (i.e., exposure to urea, guanidine hydrochloride (GdnHCl), diethylpyrocarbonate, sodium dodecyl sulfate (SDS), or phenol, or increased exposure to proteinase K), and were not inactivated by treatments which abolish nucleic acid activity, such as UV irradiation and nuclease treatments (42). Astonishingly, these experiments indicated that a protein in the enriched infective fraction was responsible for transmission and infection. This protein migrated on SDS-PAGE to 27-30 kDa (PrP 27-30) and, in studies with hamsters, was determined to be present *only* in infected brains and not in brains from healthy specimens. It was found to be inseparable from and required for infectivity (6,43-46).

1.1.2. The prion phenomenon

In 1967, J.S. Griffith was the first to outline the protein-only hypothesis, stating that an infectious protein could be one that an animal is genetically equipped to make, but that the animal either does not make, does not make correctly, or does not make in that form (47). Stanley Prusiner (6) coined the term "prion" for proteinacious infective particle in 1982, underscoring the fact that the prion protein was required for infection and suggested a protein-only hypothesis for TSEs. The infectious prion protein supports this hypothesis as it is devoid of informational nucleic acid, and yet is able to propagate by recruiting normal cellular prion protein and inducing an "autocatalytic" conformational change of the native form to the disease-associated PrP^{Sc}. The protein-only hypothesis was once highly controversial; however, it is now widely accepted as a result of recent progress creating autocatalytic PrP^{Sc} conformers *in vitro*, even though these have variations in specific infectivity (48-56).

The conversion of the native monomeric α-helix rich cellular prion protein (PrP^{C}) into a pathogenic, fibril-forming, multimeric, and predominately β-sheet, prion protein (PrP^{Sc}) is now recognized as the central element in the transmission and development of prion diseases (11,57). The major feature of the conversion process is the creation of insoluble PrP^{Sc} from PrP^{C} (3,13-15). Prion proteins are characterized by this template-induced conformational change, which leads to the conversion of the native structure and

formation of the pathological protein aggregates (24,58-60). The molecular details of this process, however, are currently unknown.

Determining the structure and assembly of aggregated prion protein (PrP^{Sc}) continues to be extensively studied (1.6.2. PrP^{Sc} structure), but it may not necessarily reflect the form(s) of the infectious prion. In fact, prion infectivity should not be equated with protease resistance (e.g. PrP^{Sc}), *a priori* (61). Indeed, it has been demonstrated that in the absence of detectable PrP^{Sc}, prion diseases can still occur (62). The infectious unit within a population of PrP^{Sc} can be as low as 1:100,000 or less (61). It is not clear if infectious protease-sensitive prion ($sPrP^{Sc}$) are a minor but distinct component in a mixture of different molecules, or an infectious aggregate of identical PrP molecules (61). This emphasises the need to develop model systems and strategies to obtain residue-level resolution structural details of variably infective intermediate prion isoforms. These structures would provide insights into the formation of the β-structure nucleation site, the overall conversion mechanism, the assembly of oligomer subunits, and the interplay of structure with infectivity and disease progression.

1.2. Prion diseases

Animals that can be infected with TSEs include; cattle, sheep, goats, mule deer, white-tailed deer, elk, moose, and domestic cats (Table 1) The human form of prion diseases are divided into three categories; infectious (see 1.2.1. Acquired prion diseases: kuru, iatrogenic CJD, variant CJD), inherited (see 1.2.2. Inherited prion diseases: Familial CJD, Fatal familial insomnia, Gerstmann-Sträussler-Scheinker disease), spontaneous (see 1.2.3. Sporadic prion diseases: sporadic CJD (sCJD)), each of which is based on the route of transmission (3) (Table 1). The majority of prion diseases are sporadic with only approximately 1% attributable to an external source (63).

TSE disease	Natural host species affected	Route of transmission
Variant Creutzfeldt–Jakob disease (vCJD)	Humans	Ingestion of BSE-contaminated food. Two cases associated with transfusion of blood from vCJD-infected blood donor
Sporadic Creutzfeldt–Jakob disease	Humans	Unknown. Somatic mutation or spontaneous conversion of PrP^{C} into PrP^{Sc}?
Iatrogenic Creutzfeldt–Jakob disease	Humans	Accidental medical exposure to CJD-contaminated tissues or tissue products
Familial Creutzfeldt–Jakob disease	Humans	Associated with germline mutations in *PRNP* gene
Gerstmann–Sträussler–Scheinker syndrome	Humans	Associated with germline mutations in *PRNP* gene
Fatal familial insomnia	Humans	Associated with germline mutations in *PRNP* gene
Kuru	Humans	Ritualistic cannibalism
Scrapie	Sheep, goats and mouflon	Acquired (for example, ingestion), horizontal transmission, vertical transmission unclear
Bovine spongiform encephalopathy (BSE)	Cattle	Ingestion of BSE-contaminated meat and bonemeal
Chronic wasting disease	Mule deer, white-tailed deer, Rocky mountain elk and moose	Acquired (for example, ingestion), horizontal transmission, vertical transmission unclear
Feline spongiform encephalopathy	Domestic and zoological cats	Ingestion of BSE-contaminated food
Transmissible mink encephalopathy	Farmed mink	Acquired (ingestion) but source unknown
Exotic ungulate encephalopathy	Zoological greater kudu, nyala and oryx	Ingestion of BSE-contaminated food

Table 1: Transmissible spongiform encephalopathies, natural host species, and route of transmission.
Table indicating a number of TSE diseases, the natural host species they infect and their route of transmission. Reprinted from Mabbott et al. (64).

The clinical signs attributable to each prion syndrome can vary between prion disease types (65). In humans, a prolonged, clinically silent incubation can exceed 50 years (66). Definitive diagnosis of prion diseases generally requires post-mortem brain tissue-analysis; however, improvements have been made in diagnosis of sporadic CJD using cerebrospinal fluid (CSF) and olfactory mucosa (OM) (67) (see 1.2.3. Sporadic prion diseases: sporadic CJD (sCJD)). Despite improvements in diagnosis, these progressive diseases are invariably fatal and no treatments are currently available (67).

1.2.1. Acquired prion diseases: kuru, iatrogenic CJD, variant CJD

Infectious prion diseases include kuru, iatrogenic CJD (iCJD), and variant CJD (vCJD). These diseases have been confined to unusual and rare conditions (68). The most well-known occurrences of human prion diseases of dietary origin is kuru caused by cannibalistic consumption of infected humans (see also 1.1.1. History of prion disease) and variant CJD (vCJD), caused by consumption of BSE infected cattle. Although rare, it is the transmissibility of these untreatable disorders that has had a major impact on public policy and public health (69).

1.2.2. Inherited prion diseases: Familial CJD, Fatal familial insomnia, Gerstmann-Sträussler-Scheinker disease

The three inherited prion diseases include: familial CJD, fatal familial insomnia (FFI), and Gerstmann-Sträussler-Scheinker disease (GSS). Approximately 15% of prion disease cases can be attributed to an inheritable autosomal dominant pathogenic mutation of *PRNP* (70,71). *PRNP* mutations predispose individuals to the production of misfolded PrP during their lifetimes (65).

There are more than 40 (72) pathogenic mutations and polymorphic variants of *PRNP* associated with inheritable prion diseases, and these include 1,2, or 4-9 octapeptide repeat insertions (ORPI) between codons 51 and 91, a 2 octarepeat deletion (ORPD), and point mutations resulting in missense and stop amino acid substitutions (68) (Figure 1).

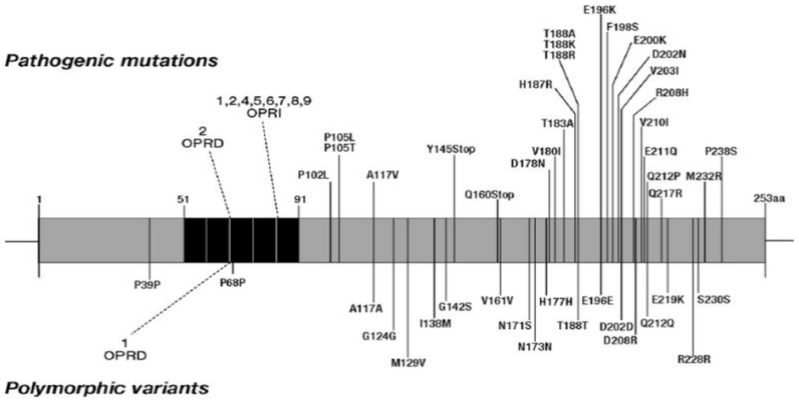

Figure 1: Pathogenic mutations and polymorphic variants of human *PRNP*.

Pathogenic mutations associated with human prion disease (displayed above coding sequence) include 1, 2, or 4-9 octapeptide repeat insertions (ORPI) between codons 51 and 91 and a 2 octarepeat deletion (ORPD). Polymorphic variants are displayed beneath the coding sequence. Reprinted from Wadsworth et al. (68).

How pathogenic *PRNP* mutations are involved in inherited prion diseases is unknown. Most of these mutations are located in the globular C-terminal portion of PrP^{C} and therefore are thought to destabilize PrP^{C}, thereby facilitating the conformational conversion of PrP^{C} to PrP^{Sc} (73-75), although it has been demonstrated that this is not always due to a straightforward decrease in the thermal stability of mutated PrP^{C} (76,77).

Clinical symptoms for all inherited CJDs are variable among all 3 forms and can include variable combinations of: cerebellar ataxia, progressive dementia, myoclonus, chorea, seizures, and amyotrophic features (68). Although histological features of

spongiform encephalopathy may not always be present, PrP immunochemistry is usually positive (78). Because inherited prion diseases can mimic other neurodegenerative conditions (e.g. Alzheimer's disease) and have extensive phenotypic variability between them, analysis of the *PRNP* gene is suggested for the diagnosis of any dementia and presenile ataxia, even for those where a history of neurodegenerative illness in the family is not present (78-80).

1.2.3. Sporadic prion diseases: sporadic CJD (sCJD)

Sporadic CJD (sCJD) accounts for 85% of human prion disease cases (81). Unlike inherited prion diseases, unique *PRNP* mutations have not been identified (3). The mechanism underlying the initiation of these diseases is unknown. A number of hypotheses have been described to illustrate how disease-causing prions arise (3), including somatic mutation of *PRNP*, animal to human horizontal transmission (32), and spontaneous conversion of PrP^{C} to PrP^{Sc} (82-84).

Typical presentations for sCJD include rapidly progressive dementia, which may be accompanied by myoclonus and cerebellar ataxia, followed by a median 4-5 month akinetic-mute state prior to death (65). Within 12 months, approximately 90% of patients succumb to the disease (65). The mean age of onset is 60 years, with no preference to patient sex; however, for unknown reasons, the rate of sCJD incidences begins to fall after 70 years of age (85,86).

A wide variability in pathological lesions and clinical signs are observed in sCJD patients (67). These appear to depend on the glycotype of the protease-resistant PrP and the *PRNP* codon-129 status, whether polymorphic for either methionine or valine (87-90). Detection of non-specific 14-3-3 proteins, cerebrospinal markers for neuronal injury, provides a diagnostic sensitivity of 94% and a specificity of 85% (91). Real-time quaking-induced conversion (RT-QuIC) seeding assays for PrP^{Sc} are nearly 100% sensitive and specific using either cerebrospinal fluid (CSF) or olfactory mucosa (OM) samples (67). Neuropathological studies confirm spongiform, astrocytosis, and neuronal loss in sCJD patients (68). Despite high rates for positive identification of PrP^{Sc} using immunohistochemistry, amyloid plaques may not be present in all sCJD cases (92,93).

1.3. Why Study Prions

Studying prion conversion and structure is important to aid in improved understanding of the conversion phenomenon and the development of therapeutics. These studies are also crucial to mitigate the devastating economic impact of TSEs (particularly BSE), and technologies developed to study these prions are transferable to other neurodegenerative diseases.

Despite the lack of treatment, there are promising avenues being pursued. In 2003, White et al. (96) used animal models to show that monoclonal antibodies recognizing PrP^{C} and PrP^{Sc} can inhibit prion replication and delay disease development. These antibodies act by reducing the half-life of PrP^{C}, which is coupled to and leads to a decrease in PrP^{Sc} (97). Low molecular-weight compounds (e.g. chloropromazine and quinacrine (98)), which have been in clinical use for other diseases and are capable of crossing the blood-brain barrier, have also been studied as therapeutics. Unfortunately, no anti-prion effects of these chemicals have been demonstrated in animal models (99). Without a more detailed understanding of the prion-conversion mechanism and the structure of infectious prion forms, rational structure-based drug-design strategies are limited. Perrier et al. (100) demonstrated this strategy by searching a library of more than 200,000 compounds *in compuo* for molecules that mimic the basic polymorphism and spatial orientation of PrP^{C} residues 168, 172, 215, and 219. This search yielded 2 compounds that exhibited some inhibitive effects on the formation of PrP^{Sc} in a dose-dependent manner.

The economic impact of TSEs in humans is low. CJD, for example, is a rare disease with a world-wide incidence rate of 1-2 cases per million people (1.11 incidences per million in Canada in 2016) (101). However, BSE can have a devastating economic impact (102). For example, in 2003, when the first case of BSE in Canada was reported, beef and cattle prices dropped rapidly and international borders were closed immediately, resulting in total losses to the Canadian economy of $6 billion in the first year after the borders were closed (103).

Advances in prion research may be directly applicable to other neurodegenerative diseases in which aggregates are believed to transmit disease in a ‘prion-like’ mechanism (94,95). Proteins involved in these diseases include: amyloid beta (Aβ), tau, and α-

synuclein (Alzheimer's disease), superoxide dismutase 1 (SOD1) (amyotrophic lateral sclerosis), and possibly huntingtin (Huntington's chorea) (104). Advancements in the treatments of all of these diseases require a clearer understanding of the conversion mechanism that occurs in vivo. The similarity between the etiology of these diseases and prion-related disease means that technologies developed for prions can be used to study these other diseases.

In order to understand prion diseases, it is critical to understand the details of prion biosynthesis and the posttranslational processes that are involved in PrP^{C} to PrP^{Sc} conversion. Furthermore, the interconnectedness between native prion function and the structure of misfolded isoforms and roles in infectivity, conversion, and pathogenesis need to be further elucidated -- and all of these features remain undetermined.

1.4. Prion protein biosynthesis

To understand the role PrP^{β} and PrP^{Sc} plays in prion diseases, it is important to determine the genetic origins of the protein. Studies have found the same gene coding for all protein forms (PrP^{C}, PrP^{β}, and PrP^{Sc}), and the differences between the forms could not be explained by variations in amino acid sequences, suggesting that post-translational events are responsible for the differences between them. Differences in post-translational modifications between these prion isoforms have also not been found. For this reason, the conversion of PrP^{C} to PrP^{β} or PrP^{Sc} appears unlikely to be the result of posttranslational modifications, although this too has not yet been fully established.

1.4.1. Prion molecular genetics

The enrichment of PrP 27-30 was the first step required for determining the genetic origins of the prion protein. This was accomplished in 1984 by Prusiner et al. (44) who determined the sequence of the N-terminal region of the protein, despite the presence of multiple populations of different truncated N-terminal regions resulting from the limited proteinase K digestion used in the enrichment procedure. A cDNA for PrP 27-30 was sequenced and cloned using poly$(A)^{+}$ RNA from scrapie-infected brain tissue (16,105) and was found to encode a protein containing no less than 240 amino acids (106). This PrP mRNA was determined to be the product of the host's single nuclear gene (29). A single chromosomal gene *PRNP*, encodes for this PrP protein (106). Based on its

location on the short arm of human chromosome 20 (84) and the high sequence (89%) similarity between human and rodent mammalian orders, the *PRNP* gene has revealed considerable evolutionary conservation during over 50 million years (107-109).

The entire open reading frame for the PrP^{C} gene contains an unusual structure having a 56 to 82 bp noncoding region followed by a 10 kb intron sequence then the 2 kb coding exon (106,110-112). Within the 5`-flanking region of the PrP gene, there is no TATA box, rather it contains three repeats of the 9 base pair sequence GCCCCGCCC at positions 284, 304, and 334 (106). Such GC-rich repeats are recognized as a common feature among promotor regions of "housekeeping" genes (106,113), which are genes that are ubiquitously expressed and have an activity required by cells, but whose expression is not environmentally controlled (16,106,114).

During development, PrP expression is highly regulated (84,115). *In-situ* hybridization of mouse embryos revealed PrP mRNA within 13.5 days in the developing spinal cord, brain, peripheral nervous system, nerve trunks, and ganglia of the sympathetic nervous system (115). In the brains of adult animals, the mRNA for PrP is constitutively expressed and is found in the highest amounts in neurons of Purkinje cells of the cerebellum and in the large neurons of the neocortex (114). There is no apparent expression bias between healthy and infected individuals (16,105,114).

The gene product of *PRNP* was not scrapie-specific, as it has the same primary structure regardless if it came from the cDNA of a scrapie infected animal or from a normal healthy animal (16,105) and, paradoxically, although it had already been shown that PrP 27-30 from infected individuals was resistant to proteinase-K digestion, the PrP produced in the healthy animal was sensitive to proteinase-K proteolysis (16).

These results suggested that there was only one gene for PrP and the different properties between prion isoforms could not be explained by variations in the amino acid sequence and was therefore, likely to be the result of either conformational differences or differences in post-translational modification between the two isoforms (105,106).

1.4.2. PrP post-translational modifications

PrP is expressed with a 23 amino acid N-terminal signal sequence targeting newly synthesized peptide to the endoplasmic reticulum (ER). In the rough ER, a host of modifications occur including cleavage of the N-terminal signal peptide, creation of

disulfide bond, glycosylation, and attachment of Glycosylphosphatidylinositol (GPI)-anchor (Figure 2).

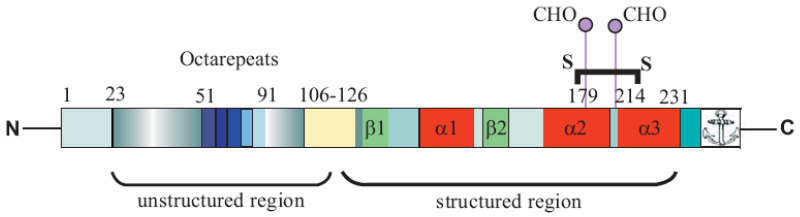

Figure 2: Schema of the mouse PrP^{C} protein.
N-terminal signal sequence residues 1-22 are removed in the endoplasmic reticulum. Residues 23-121 represent the unstructured N-terminal region and contain 5 octarepeat regions. Within the prion globular domain are two small β-sheets (aa128-130 and aa106-126; light green) and three α-helices (aa143-153, aa171-192, aa199-226; red). Glycosylation sites (at Asn 180 and Asn 196), disulfide bond (aa 179 and aa-214) and GPI-anchor at C-terminus as illustrated. Reprinted from Kupfer et al. (11).

In the ER, the 23-amino acid N-terminal sequence is cleaved and a single disulfide bond between Cys-179 and Cys-214 is formed (116), acting as a tether between helices H2 and H3 (see 1.6.1. PrP^{C} structure).

Glycosylation of PrP within the ER was one of the first post-translational modifications studied. From PrP cDNA cloning it was determined that there were two potential asparagine (Asn) glycosylation sites (Asn-181 and Asn-197) (117). It has since been demonstrated that, in the ER, PrP is posttranslationally modified by the attachment of up to two N-linked carbohydrates at these predicted sites (1,118,119). Digesting PrP^{Sc} with the endoglycosidase peptide-N-glycosidase F (PNGase F) results in a 20-22kDa product, representing a loss of approximately 7kDa, consistent with an approximate 3kDa mass loss per potential glycosylation site, as previously observed with other Asn-linked oligosaccharides (117). PNGase F cleaves Asn-linked oligosaccharides with either high- or low-mannose cores between the Asn and the most proximal *N*-Acetylglucosamine (GlcNAc) (117). Treatment with Endoglycosidase H (Endo H), on the other hand, does not show marked digestion of PrP 27-30, by SDS-PAGE (117). Endo H cleaves the β-1,4-link between two GlcNAc moieties in Asn-linked oligosaccharides with low-mannose cores (117). This indicates that the oligosaccharides on both PrP^{C} and PrP^{Sc} are

sufficiently complex (containing a high-mannose core) as they are released by PNGase F but not Endo H (117).

Further post-translational processing can occur in the ER, as a GPI anchor may be attached to the prion protein in the ER after cleavage of the carboxy-terminal signal sequence at Ser-231 (1,120,121). GPI-anchored PrP's association with specific membrane rafts is facilitated by this GPI anchor. These rafts are important as they can serve as membrane microdomains where a dynamic association between specific lipids can form, resulting in platforms from which specific membrane proteins can associate and interact (122-125).

The diversity of prion proteins is increased because multiple topologically different prion isoforms can be created via PrP localization and co-translational targeting in the ER (1,126) (Figure 3). These forms include PrP^{C}, the predominant form, which is fully translocated in the lumen of the ER; ^{ctm}Prp, with its C terminus in the lumen; ^{Ntm}PrP with its N-terminus in the lumen; and ^{cy}PrP a non-membrane-bound isoform located in the cytosol (Figure 3) (1,126-130).

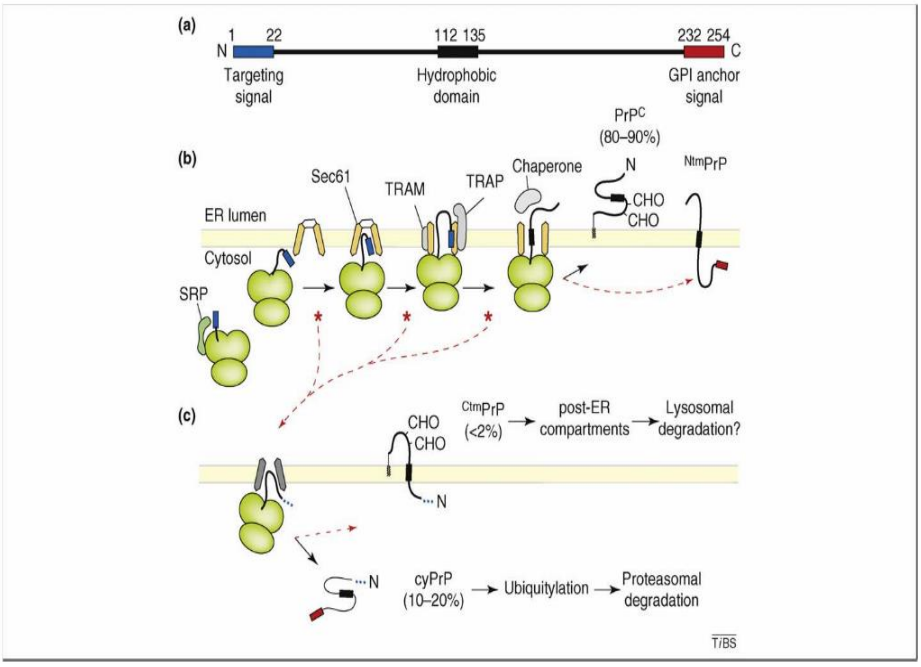

Figure 3: Summary of the generation of multiple prion isoforms via co-translational targeting and PrP localization into the ER.
A) Line diagram of PrP with N-terminal sequence (aa1-22; blue), hydrophobic domain (aa112-135; black) and GPI anchor signal (aa232-254; red). B) Significant stages in PrP translocation. Signal recognition particle (SRP)

recognizes N-terminal signal sequence as it emerges from the ribosome. The Sec61 translocon in the ER lumen interacts with the signal sequence and in coordination with accessory factors translocating chain associating membrane protein (TRAM) and translocon-associated protein (TRAP) complex open the gates for translocation through the lumen. Chaperones may prevent slippage back to the cytosol. Red asterisks indicate known or potential areas of inefficiencies relating to signal sequence and may lead to slippage of the N-terminal in the cytosol in translocation. 80-90% or PrP (PrP^{C}) is GPI-anchored to lumen and glycosylated (CHO) as illustrated. ^{Ntm}PrP is a rare prion form where the hydrophobic domain inserts into the ER lumen. C) N-terminal signal inefficiencies can lead to either ^{ctm}PrP or cytosolic ^{cy}PrP. Signal sequence represented as an ellipsis to indicate that signal-cleaved and signal-containing molecules can be present depending on step from which slippage as illustrated in B) occurred. If the translocon is initiated by HD, ^{ctm}PrP is produced and may ultimately be decreased by lysosomal degradation. If HD does not engage with translocon, ^{cy}PrP is produced which is ultimately degraded by proteasome. Reprinted from Chakrabarti et al. (131).

After processing and folding in the ER, PrP is trafficked through the Golgi apparatus where additional processing -- i.e., the addition of complex sugars onto the N-linked oligosaccharides -- occurs (1) prior to its transport to the cell surface. In the trans-Golgi, sialic acids, a family of 9-carbon containing acidic monosaccharides, are attached to the terminal positions of N- and O-linked glycans of PrP^{C} (132). Sialic acids on the surface of mammalian cells are important in establishing a "self-associated molecular pattern" that assists the immune system in recognizing "self" from "altered-self" and "non-self" (133,134). Sialic acid residues are abundant on the surface of mammalian cells, with an estimated local concentration of 100mM on the cell-surface glycocalyx (135).

Glycan sialylation can have a profound effect on the pI of PrP^{C}. For example, full-length mouse prion protein has a pI of 9.6 with a charge at pH 7.5 of +9.5 (119), while glycan sialylation results in pI that can be highly heterogeneous based on the specific sialylation patterns and can vary between pH 9.6 and acidic pH (119,136). During conversion from PrP^{C} to PrP^{Sc}, the sialylated glycan status is carried forward to the new structure (137,138).

Details of the biosynthesis of PrP has not led to a conclusive mechanism for the conversion between the two isoforms, indicating that it could be the result of an as-yet-

undetermined posttranslational modification, or more likely, the result of a posttranslational process.

1.4.3. Conversion of PrP^{C} to PrP^{Sc} is a posttranslational process

In the absence of a biosynthetic or posttranslational modification that specifically described the basis for the conversion of PrP^{C} to PrP^{Sc}, it was hypothesized that that the differences between the two isoforms were the result of a posttranslational process (84). In 1990, Borchelt *et al*. (139) used pulse-chase experiments with [^{35}S] methionine to show that incorporation to PrP^{C} was almost immediate, while incorporation to PrP^{Sc} was observed only several hours later. These studies also demonstrated that -- despite static mRNA concentrations (16,106) -- synthesis and degradation of PrP^{C} is rapid while PrP^{Sc} synthesis is slow and rather than degrade, it accumulates (139). Furthermore, kinetic studies have established that PrP^{Sc} is converted from PrP^{C}, and that the conversion to PrP^{Sc} occurs at different rates which are presumably dependent on these posttranslational events (139).

The conversion of PrP^{C} to PrP^{Sc} is thought to occur either in an endocytic compartment immediately after internalization, or on the plasma membrane (PM) where primary contact between exogenous PrP^{Sc} and endogenous PrP^{C} can occur (63,140-145). The PM and ER are both central to the conversion but may be differentially involved (63).

The importance of the PM in conversion is illustrated by studies where conversion is prevented by releasing PrP^{C} from the cell surface or by exposing PrP^{C} to anti-PrP antibodies (141,146). PrP^{Sc} formation is also delayed by introduction of Suramin, a chemical that inhibits PrP^{C} trafficking to the PM (147). Cell-free amplification systems have demonstrated that both membrane raft constituents and the GPI anchor are important elements for the conversion to PrP^{Sc} (148,149).

Immunofluorescence and cell-fractionation studies have established that the ER compartment may play a significant role in PrP^{Sc} conversion upon retrograde transfer of PrP^{Sc} toward the ER (150). In infected cells, the release of PrP^{C} and PrP^{Sc} into the medium is associated with exosomes, secreted membranous vesicles from fusion of plasma membrane with multivesicular endosomes (151). This is indicative of exocytic fusion as the fate of PrP^{Sc}-containing lysosomal and endosomal compartments (63). Fevrier et al. (151) demonstrated that PrP^{Sc}-containing exosomes might play a pivotal

role in the spread of prions as they are infectious and may be integrally involved in the intercellular membrane exchange of PrP^{Sc}.

To better understand TSEs, it is necessary to elucidate the normal cellular function of prion protein. Determining the role of PrP^{C} in animals may indicate interactions with protein partners or ligands present *in vivo* that could influence or be involved in initiating the conformational change to misfolded prion forms.

1.5. Prion function

The amino acid sequence of PrP has greater than 90% sequence homology among mammals (152), suggesting its importance in basic physiological processes (63,153). Identifying the role of PrP^{C}, and how its conversion to misfolded isoforms impacts "regular" PrP^{C} activity, can be significant for understanding prion disease-related neurodegeneration (154,155).

In mice, ablation of the PrP gene (*Prn-p* $^{0/0}$) gene does not appear to be deleterious, as these mice behave and develop normally for at least seven months (83). However, these mice have an increased susceptibility to seizures (156), exhibit greater locomotive activity (157), display cellular degradation in old age (158), and have aberrant sleep patterns (159). Prion protein may also act as an antioxidant itself and may be involved in antioxidant functions via other proteins such as Cu/Zn-superoxide dismutase (Cu/ZnSOD) (155,156,160-172). Furthermore, expression of PrP^{C} has been shown to promote the cellular uptake of copper (161,173) as shown by studies demonstrating PrP^{C} endocytosis after copper exposure to cells (154,174).

Recently, studies have revealed numerous PrP^{C} binding partners (Figure 4) (175-177). PrP^{C} interacts with a number of these ligands in neurons, activating various processes, including neuritogenesis, neuroprotection, differentiation, regulation of protein synthesis, and myelin homeostasis (177-192). Based on its ability to bind a variety of different ligands, it is hypothesized that PrP^{C} has a primary function as a cell surface scaffolding protein (176). In order to validate GPI-anchored PrP^{C} in signal transduction, complexes between transmembrane receptors and PrP^{C} needed to be verified (191). Indeed, such interactions have been determined with purinergic receptors (193), α7 nicotinic acetylcholine receptor (178), G protein coupled receptor (GPCR), Adgrg6 (192), ionotroptic glutamate receptors (194,195), and group I metabotropic glutamate receptors

(183,196,197) (Figure 4). These interactions support PrP^C as an extracellular scaffolding protein with an ability to organize multiprotein complexes at the surface of the cell (176,177,191).

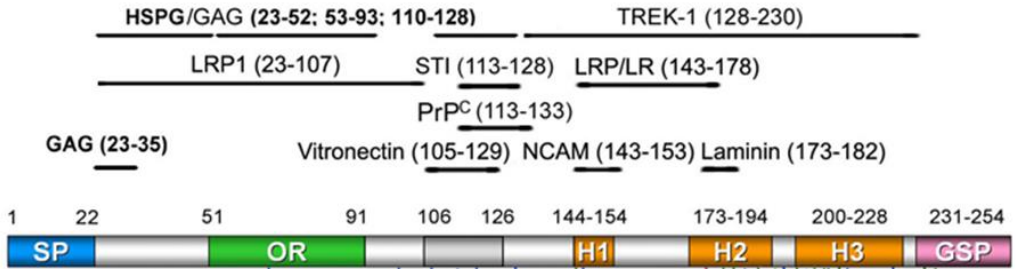

Figure 4: Binding sites of mouse PrP^C ligands exhibiting neurotrophic activity.

Amino acid residue numbers for determined binding sites to PrP^C are indicated in parenthesis. PrP^C schematic drawing includes N-terminal signal peptide sequence (blue), octapeptide repeats (green), hydrophobic domain (grey), regions of α-helical structure (orange), GPI-anchor sequence (purple). Ligands listed include heparin sulfate proteoglycans (HSPG), glycosaminoglycans (GAGs), two-pore potassium channel protein (TREK-1), low-density lipoprotein receptor related protein (LRP1), stress inducible protein 1(STI), 37 kDa laminin receptor precursor/ 67 kDa laminin receptor (LRP/LR), neural cell adhesion molecule (NCAM). Reprinted from Martins et al.(177).

In order to reconcile all of the observed ligand interactions of PrP^C, it has been suggested that soluble PrP^C can act as a signaling molecule which interacts with neighbouring cells in a soluble form or via exosomes (198). PrP^C can be released from exosomes after fusion of multivesicular bodies, or alternatively, GPI-anchored PrP^C can operate as a protein involved in dynamic cell surface scaffolding (198). The ability of PrP^C to act as a scaffold for numerous transmembrane and intracellular molecules results in diverse signaling events that are dependent on the cell types and developmental stage, the expression levels of PrP^C and/or its partner proteins, endocytic trafficking, and the accessibility of specific ligands (176). These properties may explain the various --and at times conflicting -- functions attributed to PrP^C (176).

1.6. Prion structure

The structures of all prion isoforms, with the exception of PrP^C, remain unresolved. The structure of PrP^{Sc} has been extensively studied, and a number of different models

have been proposed (see 1.6.2. PrP^{Sc} structure). The structural characterization of intermediate oligomeric forms has also been extensive, but, to date, no high-resolution structures have been determined.

1.6.1. PrP^{C} structure

In 1996, the conformation of the mouse autonomously-folded C-terminal domain PrP^{c}(121-231) ($MoPrP^{C}_{121-231}$) was determined by NMR (199). This structure contained three alpha-helices (H1, H2, H3) and a two-stranded antiparallel β-sheet (β1, β2) (Figure 5A) (199). Both cysteines (Cys-179 and Cys-214) are disulfide bound, and tether the H2 and H3 helices to each other (199) (Figure 5A). The twisted V-shaped arrangement created by H2 and H3, creates a scaffold to which H1 and the short β2 sheet are anchored (199). Hydrophobic interactions were found to stabilize the polypeptide fold (199) (Figure 5B).

In 1997, the full-length recombinant murine prion protein ($MoPrP^{C}_{23-231}$) was characterized (200). This structure revealed that the C-terminal domain structure as determined for $MoPrP^{C}_{121-231}$ (199) is preserved in the full-length intact $MoPrP^{C}_{23-231}$(200) and the additional large N-terminal polypeptide segment (aa23- aa120) is flexibly disordered (200) (Figure 6). This structure accommodates the addition of GPI-anchor at Ser 230, glycosylation at Asn-181 and Asn-197 as illustrated on NMR determined human PrP^{C} structure (Figure 6).

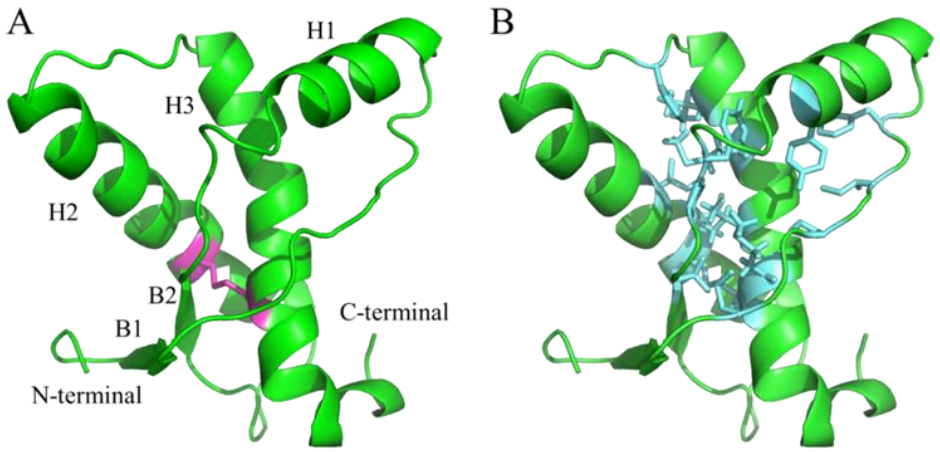

Figure 5: NMR determined structure of mouse $PrP^{C}_{121-231}$ (PDB:1ag2)(105).

A) Secondary structural motifs α-helices (H1, H2, H3), β-sheets (B1, B2), and disulfide bond between Cys179 and Cys214 (pink) and both N- and C-terminal as indicated. B) Amino acid residues making up the hydrophobic core (blue) of PrP^{C}; Met 134, Pro 137, Ile 139, Phe 141 of β1-H1 loop; Tyr 150 of H1, Tyr 157, Pro 158, of H1-β2 loop; Val 161 of β2; Cys 179, Val 180, Ile 184 of H2; His 198 of H2-H3 loop; Val 203, Met 206, Val 210, Met 213, Cys 214 of H3. Figure created using PyMOL (201) (PDB:1ag2) (106).

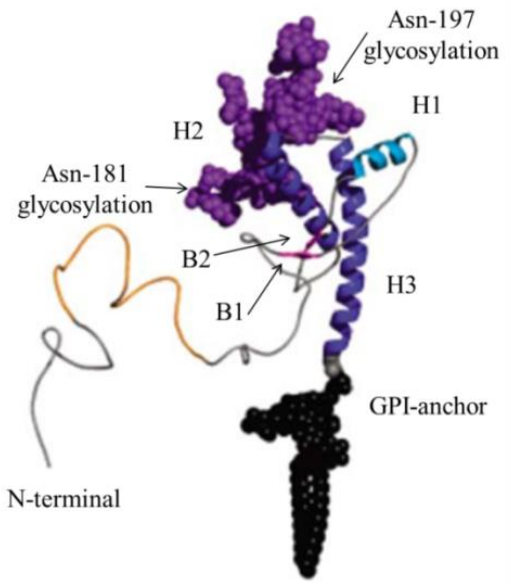

Figure 6: NMR determined structure of human PrP^{C}.
Human PrP^{C} structure illustrating the octarepeat region (residues aa51-91, orange), two β-sheets (β1, β2, magenta), α-helix H1 (light blue), α-helices H2, H3 (dark purple), glycosylation sites at Asn-181 and Asn-197 (purple), and black GPI-anchor at Ser 230 of C-terminal. Residues aa125-228 from NMR structure (PDB 1QLX (202) with flexible N-terminal region, sugars, and GPI-anchor modelled in. Reprinted from DeMarco et al. (203).

1.6.2. PrP^{Sc} structure

PrP^{Sc} and PrP 27-30 are difficult to study as they have a propensity to aggregate and are generally insoluble. Despite these challenges, a large array of experimental techniques including electron microscopy (23,24,58,204-208), limited proteolysis (41,209-213), circular dichroism (CD) (214), Fourier transform infrared (FTIR) spectroscopy (13,215,216), x-ray fibre diffraction (58,217,218), molecular dynamics (219-224), sequence analysis (223,225), modeling by threading analysis (24), crosslinking (226), electron crystallography (58,227), electron spin resonance (EPR)

spectroscopy (228), hydrogen-deuterium exchange (HDX) (229,230), surface modification (25,231), antibody epitope mapping (231), small x-ray scattering (SAXS) (232), solid state NMR (224), and electron tomography (233) have been used to study the structures of PrP^{Sc} and PrP 27-30. Secondary structure assessments (CD and FTIR) and the resistance of these proteins to proteinase K underscore and confirm the conformational change from PrP^{C} to PrP^{Sc}. Unfortunately, the structure and details of the mechanisms of these changes are still unknown.

1.6.2.1. Secondary structure assessments PrP^{Sc} and PrP 27-30

The conversion of PrP^{C} to PrP^{Sc} requires considerable structural rearrangement and is the fundamental event in propagation and infectivity (13). Experimental approaches such as CD, FTIR, and HDX suggest a strong shift in secondary structure (from α-sheet rich to β-sheet rich) upon conversion of PrP^{C} to PrP^{Sc} or PrP 27-30 (Table 2). A high content of β-sheet structure, as observed for PrP^{Sc} or PrP 27-30, results in an increased tendency for the formation of larger-order aggregates, both *in vivo* and *in vitro* (205,234).

	PrP^{C}	$recPrP_{121-230}$	PrP 27-30	PrP 27-30	PrP 27-30	PrP^{Sc}	PrP^{Sc}	Δ-GPI PrP^{Sc}
α-helix	42%	40%	17%	21%	0%	30%	20%	0%
β-sheet	3%	7%	47%	54%	43%	43%	34%	~75%
turn	32%	53%	31%	9%	57%	11%	46%	~25%
coil	23%		5%	16%		16%		
reference	(13)	(199)	(215)	(13)	(214)	(13)	(214)	(230)
method	FTIR	NMR	FTIR	FTIR	CD	FTIR	CD	HDX

Table 2: Comparison of secondary structural element predictions for prion isoforms.
An overview of secondary structure element predictions tabulated using CD, FTIR, HDX, and NMR with prion isoforms PrP^{C}, recombinant $PrP_{121-230}$ ($recPrP_{121-231}$), PrP 27-30, PrP^{Sc}, and PrP^{Sc} without GPI-anchor (Δ-GPI PrP^{Sc}). Reprinted from Requena et al. (235).

1.6.2.2. Protease resistance

PrP^{C} is completely and rapidly degraded by proteinase K. PrP^{Sc} is resistant to complete protease digestion *in vitro* (236). Proteinase K cleaves PrP^{Sc} obtained from brain tissues, removing ~66 N-terminal region amino acids and leaving the protease-resistant 'core' protein (PrP 27-30) (6,16,29,43). Prion protein *in vivo* is found in both a protease-

sensitive conformational state (PrP^{C} or $sPrP^{Sc}$) and in a protease-resistant state (PrP^{Sc} or PrP 27-30).

1.6.2.3. PrP^{Sc} and PrP 27-30 models

One of the first models for PrP 27-30 was developed by Huang et al (237) in 1996 (Figure 7A). This model used data from CD and FTIR-spectroscopy secondary-structure predictions to guide the modeling such that the final structure would have 30% α-helix and 45% β-sheet content (237). Nearly half of the α-helical structure of PrP^{C} becomes β-sheet in this PrP^{Sc} conformation (13,214). Further spectroscopic studies of PrP fragments and a variety of secondary-structure prediction methods (74,238) suggested that two of the four helices of PrP^{C} (PrP^{C} structure at that time was presumed to have four α-helices (74)) were converted to β-sheet structure in PrP 27-30 (237), while disulfide-bonded H2 and H3 remained as α-helices (Figure 7A). This data was used in a combinatorial packing approach where non-polar residues on the surface of the α-helices interact with the hydrophobic surfaces of the β-sheets (237) (Figure 7A).

In 2002, Wille *et al.* revised the model based on electron crystallography data (23) (Figure 7B-C). This model maintained H2 and H3 in their native arrangement, as in their previous model, but the anti-parallel β-sheet, as previously published (237) (Figure 7 A), did not agree with measurements obtained for the 2D crystals. The structure was adjusted by introducing either a trimeric or a hexameric subunit organization with right- or left- handed β-helical structures (Figure 7B-C) (237), where each helix is formed by triangular progressive coils (or rungs) (223). The structure of PrP^{Sc} 106, a construct with residues 141-176 deleted, was also studied (23). The corresponding FTIR data revealed that most of the 36 deleted residues of PrP^{Sc} 106 were converted to β-sheet in PrP 27-30 and difference mapping between the two forms suggested that the deleted residues of PrP^{Sc} 106 were part of two extra rungs on the β-helix fold of PrP 27-30 (Figure 7B-C). In 2004, the model was revised to accommodate N-linked sugars in order to match the improved electron crystallographic data (Figure 7D-E). Threading analysis (239) was used to obtain a left-handed β-helical fold scaffold to assemble the aa 89-175 region, H2 and H3 helices remained, and a trimeric subunit arrangement was determined to be optimal (24) (Figure 7D-E).

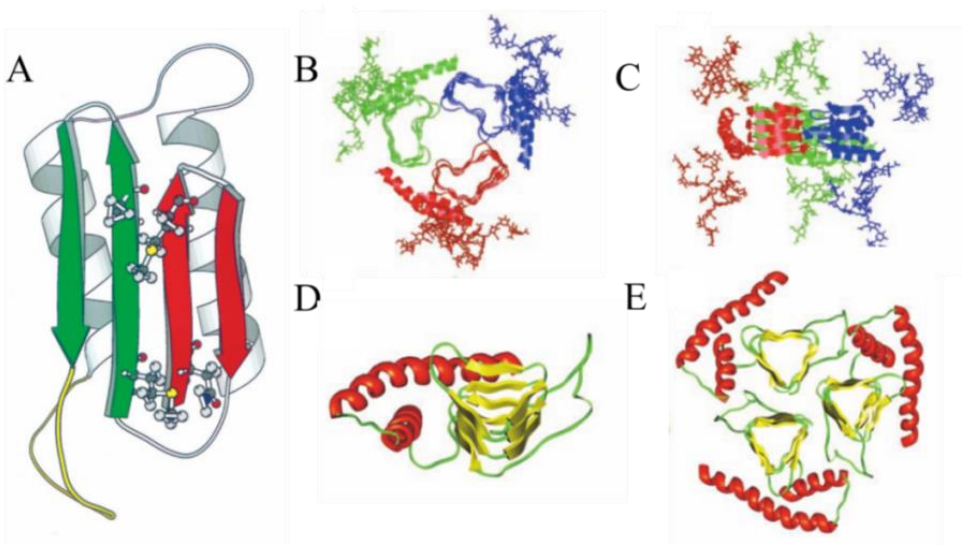

Figure 7: Predicted models for PrP 27-30.
A) Predicted model of PrP 27-30 reprinted from from Huang et al. (237). H2 and H3 helices (grey) are maintained as in native PrP^{C} structure. Residues aa90–aa177 become a four-strand mixed β-sheet (green and red). Asn108, Met112, Met129, and Ala133 are implicated in the species barrier to transmission and are indicated as ball and sticks. In yellow is the putative interface for PrP^{C} to PrP^{Sc} interaction. B-C) Predicted right-handed β-helical model reprinted from Wille et al. (23). Top-view (B) and side view (C). Three subunits shown (green, red, blue). H2 and H3 helices are maintained (outside periphery of helical stack) and glycosylation at Asn-181 and Asn-197 is illustrated protruding from H2-H3 bundles. D-E) Predicted model of PrP 27-30 reprinted from Govaerts et al. (24) modelling residues aa89-aa174 into a left-handed β-helical fold (yellow β-sheet core with green loops). H2 and H3 helices are maintained (red). PrP 27-30 monomer (D) and trimeric model of PrP 27-30 (E) (Govaerts et al. (24)).

In 2004, DeMarco et al. (220) described a model of PrP^{Sc} protofibril based on low-pH molecular dynamics (MD) simulations. The model used D147N mutant Syrian-hamster PrP^{Sc} simulated with low pH and the disulfide bond intact (220). The dimensions of the non-branching fibril model fit the published 2D PrP^{Sc} crystal projection maps previously published by Wille et al (23), including the accommodation of the fibril glycosylation (220). The model had a 3_1 axis of symmetry and two oligomerization sites which could explain monomer addition along the fibril axis (220) (Figure 8). Furthermore, the model showed only minimal exposure of both the N- and C-terminal regions, consistent with

proteinase K resistance, and had the discontinuous epitopes of the PrP^{Sc}-specific antibody 15B3 (240) in close proximity when more than two subunits were present (220).

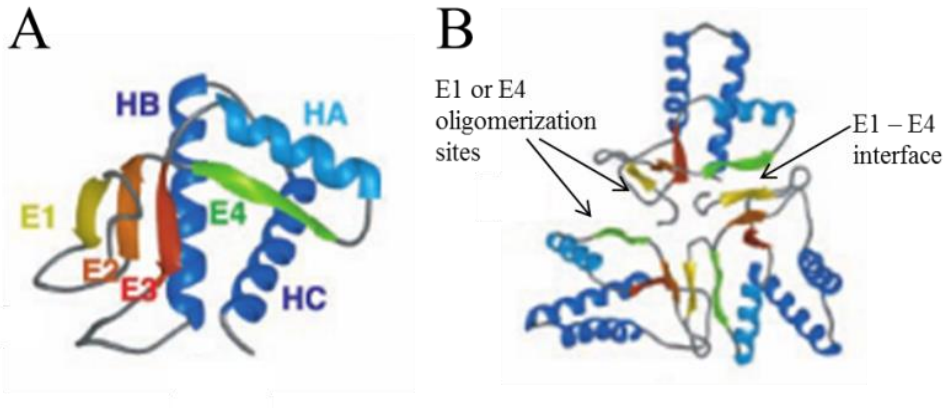

Figure 8: Predicted protofibril model for hamster PrP 27-30 using D147N mutant and low pH MD simulations (220).
A) PrP^{Sc} monomer showing maintenance of all three α-helices H1 (HA), H2 (HB), and H3 (HC) in their native conformation and creation of an extended conformation as β-sheets in the N-terminus of the protein. E1(yellow) represents extended conformation of residues aa116-aa119, E2 (orange) is an extended β1 (residues aa129-aa131) spanning residues aa129-aa132, E3 (red) is an extended form of β2 (residues aa161-aa163) spanning residues aa160-aa164, and E4 (green) represents residues aa135-aa140 (220). B) The non-branching protofibril contains a 3_1 axis of symmetry. The E1-E4 interface is shown as well as the proposed E1 and E4 oligomerization sites allowing for protofibril growth along the fibril axis (220). Reprinted from DeMarco et al. (220).

Langedijk et al. (223) also used MD simulations in combination with multiple sequence alignments and homology modeling to create an alternative left-handed β-helix model of human PrP 27-20 $_{92\text{-}228}$. This model also maintains H2 and H3 in the native conformation, and -- rather than the three rung left-handed β-helices described by Govaerts et al. (described above) (24) -- this model contains a two-runged left-hand β-helix stabilized by stacking and backbone-backbone hydrogen bonding between sidechains in adjacent rungs (223) (Figure 9).

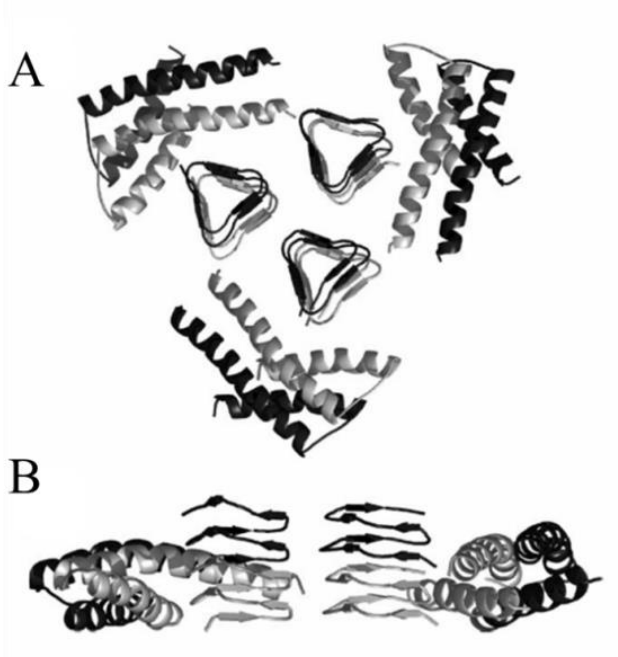

Figure 9: Top and side view of human PrP^{Sc} 27-30 model with two-rung left-hand β-helix core (223).
A) Top-view of human PrP^{Sc}_{92-228} hexamer. H2 and H3 is maintained in native conformation and is shown in periphery (black and grey helices), double runged left-hand β-helix core (at centre). B) Side view of hexamer showing core stacking and H2 H3 subunit stacking (223). Reprinted from Langedijk et al. (216).

In 2007, the Surewicz group described a model for recombinantly expressed D178N human PrP_{90-231} converted to fibril and based on HDX (229), site directed spin labelling, and EPR spectroscopy (228). In this model, the core region, as indicated by HDX and site-directed spin labeling, is located between residues ~aa169-aa221 (containing H2 and most of H3) and this region is predicted to refold into intermolecularly hydrogen-bonded β-strands which maintain the native disulfide bond, resulting in a core region which stacks into a parallel in-register β-sheet structure (228) (Figure 10).

.

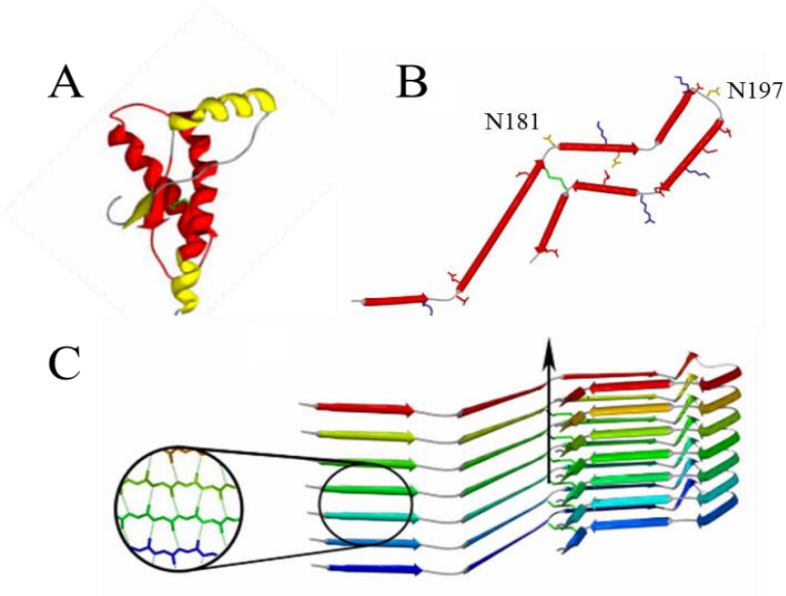

Figure 10: Human recombinant PrP amyloid fibril model proposed by Cobb et al. (228) as a parallel in-register β-sheet structure.
A) Monomeric natively folded human PrP^{C} $_{120-231}$. Region representing the amyloid core in this model shown in red. B) Model of PrP $_{159-219}$ amyloid core. Native disulfide bond (green) is maintained. Potential glycosylation sites at Asn181 and Asn197 are indicated. Charged residues are coloured blue (positive) and red (negative). C) In-register parallel stacking motif for the nearly planar monomers. Long axis of the fibril indicated by arrow. Network of intermolecular hydrogen bonding shown with inset. Reprinted from Cobb et al. (228).

Like the Surewicz group (228), Groveman et al. (224) also described a model for recombinant hamster prion PrP $_{90-231}$ amyloids that were initially seeded with homogenate from scrapie-infected hamster brain tissue. This model also contains parallel in-register intermolecular β-sheet architecture and is based on solid-state NMR and scanning transmission electron microscopy (STEM), and was optimized using energy minimization and MD simulations (224). The dimensions of this fibril model were in agreement with published electron and atomic force microscopy measurements for under-glycosylated prion fibrils from scrapie-infected transgenic mice expressing anchorless prion protein (208). However, this model can accommodate glycosylation and maintains the native disulfide bond while the C-terminal regions (residues aa124-aa227) of each subunit (including regions representing H1, H2, and H3) refold into extended chains forming fibrils via in-register stacking (224) (Figure 11).

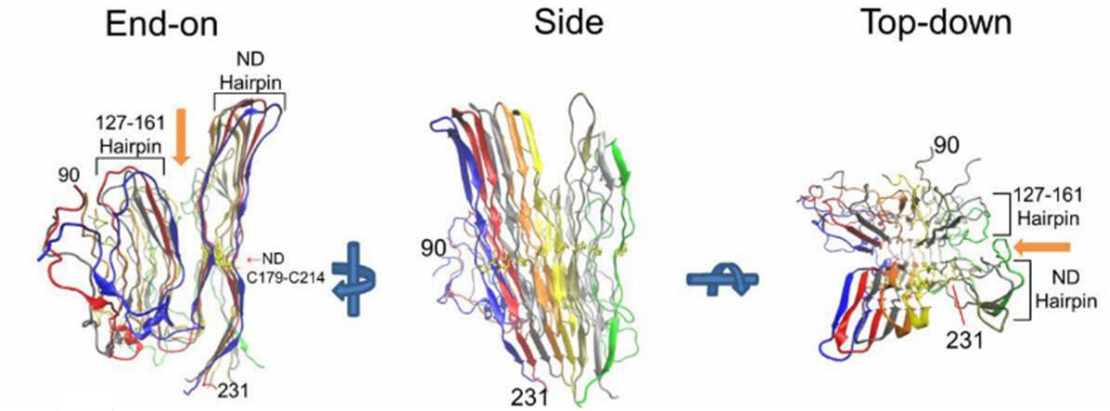

Figure 11: Molecular dynamics simulation of parallel in-register intermolecular β-sheet-based model of PrP fibrils proposed by Groveman et al. (224).

End-on, side, and top-down view of parallel in-register β-sheet based core of fibril created *in vitro* with recombinant hamster prion PrP $_{90\text{-}231}$ initially seeded with homogenate from scrapie-infected hamster brain tissue (224). N-terminal (aa90), C-terminal (aa231), and native disulfide (ND) bond (Cys179-Cys214), ND hairpin, and second hairpin (residues 127-161) are illustrated. Orange arrow indicates region for glycan attachment at Asn181, whose expansion or contraction based on size of glycosylation units added can lead to varying fibril dimensions and shape ("celery stalk" or half-pipe) (224). Reprinted from Groveman et al. (224).

Recently, Vazquez-Fernandez et al. (31) used electron cryomicroscopy to create a non-atomistic cartoon model of GPI-anchorless fibril purified from Rocky Mountain Laboratories (RML) prion strain-infected transgenic mice expressing GPI-anchorless prion (206). Like the model recently proposed by Terry et al. (233) for *ex vivo* prion fibrils, the Vazquez-Fernandez model is also a model of a paired double-helix of prion protein fibrils (206) (Figure 12). Structural constraints obtained by electron cryomicroscopy -- especially the Fourier transform analysis -- show a 4.8 Å cross-β signal indicative of β-strand stacking in the direction of the fibril axis which was used to determine that each PrP^{Sc} molecule is conformationally rearranged in a four-rung β-solenoid arrangement (206) (Figure 12). The model does not indicate which residues are involved in β-strands, connecting loops or turns, and the disulfide bond, which is expected to be present, is not accommodated in the model (206). Despite this, the authors suggest that this four-rung β-solenoid architecture may hold the key to the templating

mechanism responsible for the *in vivo* replication of infectious prions (206). They hypothesize that this templating is based on the interaction of the lower- or upper- rung of the β-solenoid, and that the edges of these rungs would be exposed and, as proposed by Richardson et al. (241), would be inherently aggregation prone and would propagate their hydrogen-bonding pattern to any amyloidogenic peptide it makes contact with (206,241).

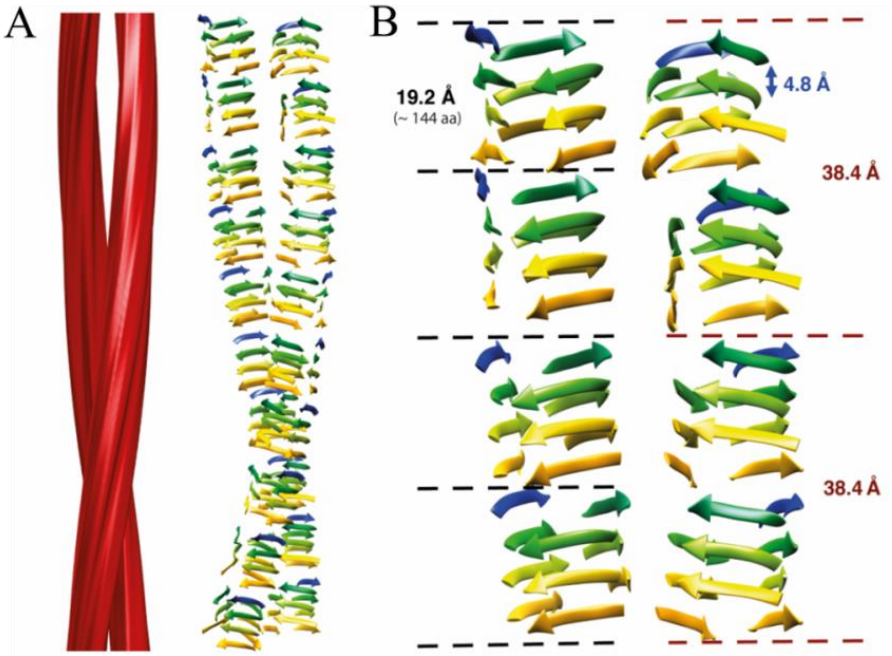

Figure 12: Structural outline of GPI-anchorless PrP 27-30 fibril proposed by Vazquez-Fernandez et al. (206).
A) Three dimensional non-atomistic rendering of a GPI-anchorless PrP 27-30 fibril containing two protofilaments (left) and a cartoon representation of the potential polypeptide configuration within the polypeptide chains (right). B) Zoom in of possible four-rung β-solenoid structure and possible β-stacking of each PrP 27-30 subunit. Critical inter subunit and inter-rung distances are illustrated. Reprinted from Vazquez-Fernandez et al. (206).

Studies of the structure of misfolded prion isoforms have primarily focused on PrP^{Sc} and PrP 27-30. There is still little consensus on the structure and arrangement of the subunits in these assemblies, although recent advances are encouraging.

1.7. Prion protein model systems

Model systems using highly purified recombinant prion protein expressed in bacterial systems have been used extensively for studies of the TSE conformational change. Despite being deficient in both glycosylation and GPI anchor, CD and 1D NMR reveal

that recombinant PrP^{C} ($recPrP^{C}$) folds with a secondary and tertiary structure that is very similar to brain-derived PrP^{C} (199,242,243). Model systems for conformational change allow specific control of most factors that may influence the conversion of PrP^{C} to other prion isoforms. Under numerous solvent conditions, PrP^{C} can spontaneously convert to a soluble, β-sheet rich, oligomeric (PrP^{β}) form that has properties similar to PrP^{Sc} (244), such as protease resistance and an increase in β-sheet content. Study of the conversion mechanism, biophysical characteristics, and structures of such β-oligomers are important, as these oligomers may be infectious neurotoxic forms of PrP (see 1.7.2. β-oligomer) (245).

1.7.1. Mouse and hamster prion protein

Recombinantly-expressed Syrian hamster (*Mesocricetus auratus*) prion protein (ShPrP) has been one of the most commonly used models for structural studies of PrP and its isoforms (246). Importantly, the hamster prion protein sequence has 88.5% sequence identity to that of humans (247), suggesting that the sequence is significantly different from that of human prion protein (HuPrP), which implies a significant barrier to transmission to humans (106,248,249).

1.7.1.1. Expression and purification

In 1996, Mehlhorn *et al*. (246) described a procedure for the expression in *Escherichia coli* (*E. coli*) of Syrian hamster full-length mature prion ($ShPrP_{23-232}$), and its N- and C-terminally truncated form ($ShPrP\ 90-_{223}$). $ShPrP_{90-223}$ was chosen for my experiments because it represents the region corresponding to PrP^{Sc} identified *in vivo* (44,106,246) and carries all of the required features for conversion and aggregation propagation (48,250-252). Swietnicki *et al*. (44,106,244) described the expression of prion protein, which includes a 22-residue N-terminal linker, with a 6x-His tail and a thrombin cleavage site. The protein is expressed as inclusion bodies in the *E. coli* cytoplasm (253). Refolding the expressed protein to its native form is a critical purification step (246,254,255). For detailed expression and purification procedures see 5.2.2. Prion protein expression and urea-acid induced conversion to PrP^{β}.

1.7.2. β-oligomer

PrP^{Sc} cannot always be equated with infectivity (256). In certain disease cases, an animal can harbour high infectivity levels and not display clinical signs of prion disease (257), while in other animals with clinical signs of the disease, PrP^{Sc} is barely or not detectable (258-261). In such cases, PrP^{Sc} may not represent the infective component (256). One explanation for this could be that PrP^{Sc} is a relatively inert component of the disease, with the toxicity resulting from more labile, smaller, possibly oligomeric misfolded species (245,262) which may be formed as side products or intermediates during prion propagation (263,264). Collinge et al. (265) term this lethal intermediate oligomeric conformer, PrP^{L}. A model can be used to illustrate (Figure 13) the potential role of PrP^{L} in TSE pathogenesis while accounting for neurotoxicity of PrP^{Sc} (Figure 13). The model proposes that PrP^{L}, in low amounts, may be tolerated or cleared by the cell but that a neurotoxic threshold may be reached whereby cell death occurs as PrP^{L} accumulates (Figure 13) (265). As the concentration of PrP^{L} increases, PrP^{Sc} accumulates -- this is then followed by phenotypic symptoms and cell death (Figure 13) (265).

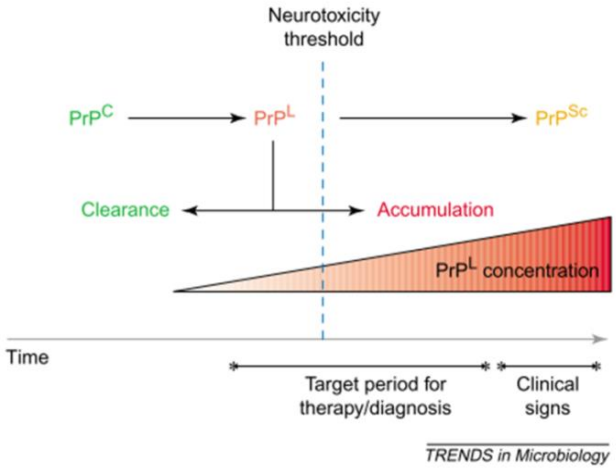

Figure 13: Model of possible molecular pathway of TSE pathogenesis. Illustration of potential pathway of TSE pathogenesis. As PrP^{C} is converted to PrP^{Sc}, the toxic intermediate PrP^{L} is being formed. PrP^{L} in low levels may be tolerated by the cell and may be cleared or degraded. A neurotoxicity threshold limit of PrP^{L} may be reached where the cell can no longer clear or degrade the intermediate and cell death begins. This leads to PrP^{Sc} accumulation and continued cell death with consequent emergence of clinical signs of disease. Reprinted from Hill et al. (265).

Collinge et al. (94) have proposed a mechanism that may explain the lack of toxicity of PrP^{Sc} while still accommodating the autocatalytic nature characteristic of prion propagation (Equation 1) (94). In this mechanism PrP^{L} acts as an intermediate in the template-assisted formation of PrP^{Sc} from PrP^{C} (Equation 1) (94). This process acknowledges that PrP^{L} could be the toxic species and has its levels regulated by the ratio of the initial rate of PrP^{C} conversion to PrP^{L} (k_1) to the rate of PrP^{L} maturation (k_2) (Equation 1) (94).

$$PrP^{Sc} + PrP^{C} \rightarrow PrP^{Sc}{:}PrP^{C} \xrightarrow{k1} PrP^{Sc}{:}PrP^{L} \xrightarrow{k2} PrP^{Sc}{:}PrP^{Sc} \rightarrow PrP^{Sc} + PrP^{Sc}$$

Equation 1: Proposed mechanism of PrP^{Sc} formation of Collinge et al. (94).
A four-step proposed mechanism for PrP^{Sc} formation. This mechanism does not challenge the protein-only hypothesis, as the intermediate state PrP^{L} is a transitional component in the template-assisted progression of PrP^{C} to PrP^{Sc} (94).

Large PrP^{Sc} aggregates are generally more protease resistant than smaller oligomeric PrP^{Sc} (72). In nature, prions from a diseased animal are often mixtures of protease resistant PrP^{Sc} and $sPrP^{Sc}$ (81,218,266-269). Some cases of prion disease contain a high proportion of PrP^{Sc} in a soluble oligomeric $sPrP^{Sc}$ form, which may be responsible for conversion of PrP^{C} to PrP^{Sc} (218,270,271). Therefore, candidate neurotoxic PrP^{L} must include soluble monomeric or oligomeric conformers with varying degrees of protease resistance (265). Unfortunately, many structural studies of oligomers have been done only on components of mature insoluble fibrils (see 1.6.2.3. PrP^{Sc} and PrP 27-30 models) (220). However, more studies need to be done on β-oligomers (PrP^{β}), an intermediate conformer that is soluble, β-sheet rich, has molten globule-like properties, and can have varying degrees of protease sensitivity and infectivity (272-274).

Three models have been proposed describing the mechanism for PrP^{Sc} seeding its host for further production of PrP^{Sc}. 1) The standard catalytic model was introduced by Huang et al. (237) in 1996 and proposed that PrP^{Sc} and PrP^{C} are distinct monomeric stable states, with PrP^{C} to PrP^{Sc} conversion occurring with PrP^{Sc} acting as a catalyst. 2) The nucleated polymerization model hypothesizes that the two prion forms differ primarily in their quaternary structure, with PrP^{C} as a monomer and PrP^{Sc} as intrinsically

multimeric (275,276). Changes in secondary and tertiary structure are suggested to accompany the polymerization-state change (272). 3) The β-nucleation model is a hybrid between the nucleated polymerization and the standard catalytic model (27). This model proposes that PrP^{Sc} is fundamentally in an aggregative state presenting a structure that can induce a highly specific change in PrP^{C} resulting in propagation of PrP^{Sc} (27). Specifically, this conversion occurs by H1 of PrP^{C} unraveling and then contacting and adding to the residues of H1 from aggregated PrP^{Sc} (27).

We and others have described events consistent with the β-nucleation model during PrP^{C} to PrP^{β} conversion. Indeed, such events include a significant conformational rearrangement of PrP^{C} whereby there is a disengagement of the H1 α-helix and a separation of contacts between the β1-H1-β2 domain and the H2-H3 core (see Figure 5) (22-26,277). It is thought that this rearrangement results in changes in which previously buried surfaces become exposed to solvent, from which new inter-protein contacts can develop. This conversion is also thought to result in the formation of a β-sheet nucleation site, which can initiate the development of fibrillar forms.

Different PrP^{β} oligomeric conformers can be created by using different conversion methods, leading to unique conformers that can be differentiated based on a number of biophysical characteristics including proteinase K sensitivity, β-sheet content (determined by CD and FTIR), and varying degrees or absence of infectivity. These oligomers might carry structural features that resemble those of PrP^{L} and which exist *in vivo* during prion disease pathogenesis.

1.7.2.1. Conversion methods, characteristics, and infectivity

The conversion of PrP^{C} to an oligomeric PrP^{β} form can be induced by numerous methods including low pH only (278), low pH with chemical denaturants (279), lipid (280-284), RNA (285), lipid-RNA (50,286), salt (244,279,287-289), lipopolysaccharide (290), shaking (291), dopamine (292), copper (242,293), manganese (294), and SDS (280,295-298) and other detergents (296). The conversion events can be monitored and confirmed using multiple methods such as NMR spectroscopy, CD, dynamic light scattering (DLS), FTIR, proteinase-K assay, and 1-anilinonapthalene-8-sulfonate fluorescence (ANS). PrP^{β} obtained using a particular conversion method may not share

the same biophysical characteristics or infectivity as oligomers created using an alternative conversion method.

The specific infectivity of these isoforms is determined from the amount of agent delivered to a susceptible wild-type host animal in an end-point titration assay (299). This infectivity ranges from high infectivity to minimal or no infectivity. Deleault et al. (284) produced a high titre (2.2×10^6 LD_{50} U/µg PrP) mouse prion *in vitro* using recombinantly expressed PrP and a single endogenous phospholipid cofactor, phosphatidylethanolamine (PE) (300). This provided evidence for cofactors playing an important role in maintaining prion infectivity (51). Cofactors palmitoyl-oleoyl-phosphatidylglycerol (POPG) and RNA in combination with protein misfolding cyclic amplification (PMCA) were required to obtain infective PrP^{Sc} (56,284). This step-wise formation of infectious PrP^{Sc} results in a number of stable non-infectious intermediates on the pathway to PrP^{Sc}. Although it is not clear how closely each intermediate along these cofactor-requiring pathways are to the actual *in vivo* propagation steps, each discrete intermediate may still provide an opportunity to study the generation of infectivity along these intermediate steps (286).

Previously, I have studied strong acid (pH 1) converted Syrian hamster 90-232 β-oligomers (278) using structural proteomics techniques (22,301,302)(see Chapter 2. Use of Proteinase K non-specific digestion for selective and comprehensive identification of inter-peptide crosslinks: Application to prion proteins, Chapter 3. Using multiple structural proteomic approaches for the characterization of prion proteins, Chapter 4: Using isotopically-coded hydrogen peroxide as a surface modification reagent for the structural characterization of prion protein aggregates). Oligomerization and transformation to this β-rich isoform is initiated below pH 2.8 (278). These oligomers may resemble those existing *in vivo* in low-pH environments such as that in the endosome/lysosome (pH 4) and the stomach (pH 1.5-2), which could support the conversion to this oligomeric and fibrillar form (278). A number of biophysical techniques were used to determine properties of these oligomers: CD indicated a dramatic shift to an almost exclusive β-sheet conformation >40% β-sheet, while 12% remain as β-turns or helices (278). Similarly, when incubated with proteinase K, a prominent band at 12kDa remained, indicating at least partial resistance to proteolytic

degradation (278). Unfortunately the infectivity of this conformer has not yet been determined.

Recently, I used structural proteomics to determine the structure of PrP^{β} oligomers created with the urea-mild acid (pH 4) conversion method (303) (see Chapter 5. Structure of prion β-oligomers as determined by structural proteomics with crosslinking constraint-guided molecular dynamic simulations). β-oligomers obtained using this method exhibit an increased resistance to proteinase-K digestion (Figure 37) and an increase in β-sheet structure as determined by CD (11.8% β-sheet content in PrP^{C} and 20.1% in PrP^{β}) (Figure 38). A crosslinking titration assay of PrP^{C} and PrP^{β} shows marked differential formation of the inter-protein crosslinked species on SDS-PAGE gel for PrP^{β} but not for PrP^{C} (Figure 39). Previously, studies on chemical denaturant-induced misfolding of PrP amyloid fibrils have resulted in isoforms with minimal infectivity (48,54). Despite the low infectivity, we and others believe that these isoforms may closely resemble the existing *in vivo* converted species, occurring in an acidic pH environment, comparable to that within endocytic vesicles (18,60,304).

It is important to build a methodological framework from which to study prion oligomeric forms. The well-defined structures of each intermediate or alternately formed oligomer will result in an in-depth understanding of the steps involved in conversion, and can lead to unique opportunities for rational drug design. It is expected that common structural themes among these β-rich forms will become evident, resulting in a much better understanding of the aggregation process in prion diseases. Structural proteomics combined with mass spectrometry is rapidly advancing as the ideal tool for determining the structural details of these oligomeric forms.

1.8. Studying prion conformational change and structure using protein chemistry methods combined with mass spectrometry

Misfolded prion isoforms are inherently challenging to study using conventional structural-biology methods, such as liquid-state NMR spectroscopy and X-ray crystallography, due to their poor solubility and heterogeneity. Despite these difficulties, there have been significant improvements in the structural details of prion aggregate structures (see 1.6.2.3. PrPSc and PrP 27-30 models) by using alternative methods including antibody mapping (300,305-307), computer modeling (74,220,308), electron

microscopy (217,218), infrared spectroscopy (13,17,215,309), protease accessibility (213,305,310), spin labeling (228,311), and X-ray diffraction (13,23,24,227). However, there is still little agreement on the structure of prion oligomers (24,207,220,223,312,313). To expand and improve the characterization of prion isoforms, a combination of structural proteomic approaches must be used.

Structural proteomics can be defined as the combination of contemporary mass spectrometry with protein chemistry methods such as limited proteolysis, SM, HDX, and chemical crosslinking. These methods constitute an integrated set of ready-to-use tools and protocols that can facilitate the fast, efficient, and comprehensive extraction of a set of structural constraints that can lead to the creation of an accurate structural model (20).

Limited proteolysis provides information on the accessibility of residues on the surface of a protein to a large enzymatic probe. The first regions of a protein to be digested will be the most accessible to the enzyme. Limited proteolysis has been used for the characterization of PrP^{β} and PrP^{Sc} using chymotrypsin, pepsin, proteinase K, or trypsin (22,212,310,314). Recently, I have performed limited proteolysis analysis of urea-mild acid induced PrP^{β} using an extensive panel of enzymes: ArgC, AspN, chymotrypsin, GluC, pepsin, and trypsin (see Chapter 5. Structure of prion β-oligomers as determined by structural proteomics with crosslinking constraint-guided molecular dynamic simulations).

Chemical surface modification (SM) provides information on the surface exposure of residues on the protein's surface to small-molecule chemical-modification reagents and can be complimentary to data obtained from limited proteolysis (303). SM studies have been previously reported for the characterization of PrP^{β} and PrP^{Sc} using acetic acid N-hydroxysulfosuccinimide ester (231,315), acetylation and nitration (25,316), methionine oxidation (302,317) (see Chapter 4:), and pyridine carboxylic acid N-hydroxysulfosuccinimide ester (PCASS) (22) (see Chapter 3. Using multiple structural proteomic approaches for the characterization of prion proteins and Chapter 5. Structure of prion β-oligomers as determined by structural proteomics with crosslinking constraint-guided molecular dynamic simulations).

HDX is based on the principle that backbone amide hydrogens can exchange with deuterium and do so at different rates based on their hydrogen bonding status.

Consequently, the deuteration status of backbone amides reflects their involvement in secondary structure (318-320). Numerous prion HDX studies using top-down (22) (see Chapter 3. Using multiple structural proteomic approaches for the characterization of prion proteins) and bottom-up (26,229,230,286,300,321-324) strategies have been reported. Recently, I have used top-down electron capture dissociation (ECD) ECD-FTICR mass spectrometry for determining the deuteration values of specific amino acid residues and the boundaries of secondary structural motifs (325,326) in urea-mild acid induced PrP^{β} oligomers (see Chapter 5. Structure of prion β-oligomers as determined by structural proteomics with crosslinking constraint-guided molecular dynamic simulations).

Crosslinking combined with modern mass spectrometric techniques is an emerging and evolving technology for the structural analysis of proteins and protein complexes (for recent reviews see (20,327-331)). Crosslinking provides distance information between pairwise crosslinked amino acid residues, which are covalently linked. In this approach, crosslinked proteins are enzymatically digested then analysed by LC/MS/MS. Because there is a wide variety of crosslinking reagents (20), with variations in their specificity and spacer arm lengths, these reagents can be used as a "molecular ruler" for structure determination. Crosslinking reagent specificities can include amine to carboxyl specific (e.g. EDC or 4-(4, 6-dimethoxy-1,3,5-triazin-2-yl)-4-methylmorpholinium chloride (DMTMM) with lysine to aspartic or glutamic acid reactivity), amine-reactive (e.g. CyanurBiotinDimercaptoPropionylSuccinimide (CBDPS) with lysines and the N-termini), specific photo-reactive (PICUP with tyrosine to tyrosine), and non-specific photo-reactive (e.g. 2,4,6-triazido-1,3,5-triazine (TATA)). The spacer arm length determines the diameter of the "interaction sphere" around each end of the crosslink, and thus the "tightness" of the distance constraints obtained. These constraints can vary from 14 Å (e.g. CBDPS), to shorter range (e.g. 8 Å DSG and 5 Å TATA) or zero-length crosslinks with <1Å (e.g. EDC and PICUP).

Only a few studies using chemical crosslinking have been performed on PrP^{β} and PrP^{Sc}, and these include crosslinking of SDS-induced PrP^{β} using EDC (332); crosslinking of brain derived PrP27-30 using BS_3 (226), and acid-induced PrP^{β} crosslinked with CBDPS (22,301) (see Chapter 2. Use of Proteinase K non-specific digestion for selective

and comprehensive identification of inter-peptide crosslinks: Application to prion proteins and Chapter 3. Using multiple structural proteomic approaches for the characterization of prion proteins).

When crosslinking prion oligomers, in order to determine if a crosslink occurs within the same protein (intra-protein crosslink) or between two protein molecules (inter-protein crosslinks) I crosslinked an equimolar mixture of ^{14}N- and ^{15}N-PrP$^{\beta}$ (333) (see Chapter 5. Structure of prion β-oligomers as determined by structural proteomics with crosslinking constraint-guided molecular dynamic simulations). This results in distinct signatures for intra- and inter- protein crosslinks in the resulting mass spectra (Figure 36). Distinguishing between inter- and intra-protein crosslinks (334) is critical for guiding the PrP$^{\beta}$ structure and the PrP$^{\beta}$ assembly of subunits. Recently, I applied a panel of crosslinking reagents (DMTMM, PICUP, TATA, ABAS, SDA, DSA, DSG, DSS, and CBDPS) (Figure 45) to the structural characterization of urea-acid induced PrP$^{\beta}$ oligomers (303) (see Chapter 5. Structure of prion β-oligomers as determined by structural proteomics with crosslinking constraint-guided molecular dynamic simulations). 14 intra-protein and 48 inter-protein inter-peptide crosslinks (Appendix A: Table of all urea-acid induced PrPβ intra-protein crosslinked sites identified and Appendix B: Table of all urea-acid induced PrPβ inter-protein crosslinked sites identified) were detected, and these have been used as constraints to guide the structural modeling of these oligomers using crosslinking constraint guided molecular dynamic simulations (CL-DMD) (335) (see Chapter 5. Structure of prion β-oligomers as determined by structural proteomics with crosslinking constraint-guided molecular dynamic simulations).

Pairwise inter-atom distance constraints from crosslinking experimental data can be incorporated into the force field of the discrete molecular dynamics (DMD) simulations to develop a flexible and efficient procedure for experimentally-guided de novo structure determination. Models developed using DMD simulations can then be validated using other structural proteomics techniques such as limited proteolysis, surface modification, HDX, and long-range (>14 Å) crosslinking.

A combination of these structural proteomic methods has been used to compare the structure of PrP^{C} before and after conversion to urea-acid induced PrP$^{\beta}$ oligomers. This

has allowed the assembly of a structure of the β-oligomer, based on all of the constraints obtained. This new β-oligomer model supports the rearrangement and disassembly of the β1-H1-β2 region from the H2-H3 core, the consequent development of an apparent β-sheet nucleation site, and the formation of new inter-protein hydrophobic contacts, resulting from the change in exposure of hydrophobic residues, as pivotal to the conversion of PrP^C to PrP^β. The resulting structure explains the mechanism of the conformational change involved in the conversion, early formation of the β-structure nucleation site and describes the mode of assembly of the subunits within the oligomer.

1.9. Research hypothesis/questions and objectives

My research hypothesis was that a rearrangement of the H1-β2-H2 interface in normal PrP^C monomers leads to the formation of new inter-subunit interaction interfaces in the prion aggregates, thereby leading to aggregation.

My objective was to use constraints obtained by structural proteomic methods to determine the 3D structure of urea-acid induced recombinant prion oligomers (PrP^β). This would explain the mechanism of the conformational change involved in the urea-acid induced conversion, the early formation of the β-structure nucleation site, and would describe the mode of assembly of the subunits within the oligomer.

To determine the 3D structures of the prion PrP oligomers, I used a combination of structural proteomics, which included limited proteolysis, surface modification, HDX exchange, crosslinking, and molecular modelling. To maximize the number of structural constraints, it was necessary to develop methodology that was essential for studying prion aggregates, and would also be universally applicable to other protein systems and aggregates. These included the use of proteinase K digestion for crosslinking experiments (see Chapter 2. Use of Proteinase K non-specific digestion for selective and comprehensive identification of inter-peptide crosslinks: Application to prion proteins) and the introduction of amine reactive reagent PCAS for a differential surface modification approach between PrP^C and acid-induced PrP^β (see Chapter 3. Using multiple structural proteomic approaches for the characterization of prion proteins). I also used PrP^C and acid-induced PrP^β to demonstrate the advantages of combining structural proteomic methods for determining protein structure (see Chapter 3. Using multiple structural proteomic approaches for the characterization of prion proteins).

Furthermore, I expanded the amino acid residues that could be analysed using the differential surface modification approach for the characterization of PrP^{C} and acid-induced PrP^{β} by describing methionine and tryptophan oxidation by use of isotopically-coded hydrogen peroxide combined with mass spectrometry (see Chapter 4: Using isotopically-coded hydrogen peroxide as a surface modification reagent for the structural characterization of prion protein aggregates).

Finally, I applied a combination of limited proteolysis, surface modification, chemical crosslinking and hydrogen/deuterium exchange (HDX) with mass spectrometry to the differential characterization of the native and the urea-acid converted prion β-oligomer structures to get insights into the mechanism of conversion and aggregation (see Chapter 5. Structure of prion β-oligomers as determined by structural proteomics with crosslinking constraint-guided molecular dynamic simulations). By comparing the structures before and after the conversion, conformational changes that occur during the conversion can be deduced. These include the rearrangement and disassembly of the β1-H1-β2 region from the H2-H3 core, the formation of a new β-sheet nucleation site resulting in the exposure of hydrophobic residues patches, which leads to formation of inter-protein contacts within the aggregate.

Chapter 2. Use of Proteinase K non-specific digestion for selective and comprehensive identification of inter-peptide crosslinks: Application to prion proteins

Work in this chapter was a collaborative effort involving two laboratories. Native (PrP^C) and acid-induced oligomeric (PrP^β) prion protein was recombinantly expressed and purified in the laboratory of Dr. David Wishart in the Prion Protein and Plasmid Production Platform Facility (PrP5) (University of Alberta, Edmonton, AB, Canada) and supplied to the Borchers lab at University of Victoria as PrP^C and PrP^β stock solutions. Experimental design was performed by Jason Serpa, Evgeniy Petrotchenko, and Christoph Borchers. Jason Serpa was also responsible for performing all experiments, LC-MALDI-MS/MS acquisition (with assistance from Daryl Hardie), and data analysis. MS modeling based on crosslinking constraints was performed by Mark Berjanski from the Wishart laboratory. Christoph Borchers oversaw the project.

This chapter was adapted in part from the publication (301):

Petrotchenko EV, Serpa JJ, Hardie DB, Berjanski M, Suriyamongkol BP, Wishart DS, Borchers CH. 2012. ***Use of Proteinase K non-specific digestion for selective and comprehensive identification of inter-peptide crosslinks: application to prion proteins*****. Molecular & cellular proteomics, doi: 10.1074/mcp.M111.013524**

2.1. Introduction

Crosslinking analysis provides the distance between two crosslinked amino acid residues, while mass spectrometry provides information on which residues are connected. The basis of this method is a chemical reaction of the crosslinking reagent with functional groups on a protein, leading to the formation of a covalent bond between each end of the reagent and the protein. The distance between two crosslinked sites is determined by the length of the spacer in the crosslinking reagent. Thus, identification of the crosslinked sites on a protein or a protein complex provides spatial information and distance constraints for the two amino acid residues that are connected by the crosslinker.

The use of chemical crosslinking combined with mass spectrometry is a rapidly-developing technique for structural proteomics (20,327,330,331,336-338). In recent years, we and others have been developing an array of crosslinking and modification reagents, software, and methods specifically designed for protein crosslinking experiments combined with MS analysis (334,339-350). For mass spectrometric determination of the crosslinking sites, the crosslinked protein is typically digested with proteolytic enzymes and the peptides are examined by mass spectrometry.

Challenges associated with the crosslinking technique include finding the crosslinked peptides in the complex mixture that often results from this digestion. For this reason, isotopically-coded crosslinkers are often used to produce a distinct signature for the crosslinks in the mass spectra (351).

A crosslinker that can be cleaved with collision-induced dissociation is also highly beneficial because it facilitates identification of the linked peptides and determination of the crosslinking sites by MS/MS sequencing, after a peak corresponding to a crosslink (a crosslinked pair of peptides) has been found (352). In order to simplify the mass spectra and enhance the detectability of the crosslinked peptides, affinity enrichment can also be used (353).

Affinity purification is also important for enriching the sample in crosslinker-containing peptides. Crosslinkers with a biotin moiety incorporated in them, for example, can be enriched on avidin beads. Even these methods, however, will enrich the sample in all types of crosslinks – dead-end and intra-peptide, as well as the more-desirable inter-peptide crosslinks.

Another challenge in crosslinking studies is the lack of suitable cleavage sites. Although trypsin is the most widely used enzyme for proteomics studies, the existence of only a few tryptic cleavage sites in some proteins, including prions, limits the power of this traditional proteolytic enzyme, especially when used with amino-reactive crosslinkers, which target the same amino acids as trypsin and preventing cleavage at the modified sites. This produces high molecular-weight crosslinked peptides, which complicates their mass spectrometric analysis and identification. Furthermore, acid and urea-acid induced PrP^{β} oligomers are only partially digested with trypsin yielding a ~20 and ~13 kDa and ~20 and ~16 kDa fragments respectively (see 3.3.1. Limited Proteolysis and 5.3.4. Limited proteolysis).

To overcome these difficulties, I have examined non-specific protease, proteinase K (PK), as an alternative to trypsin for crosslinking. Using acid-induced PrP^{β} oligomers and crosslinking reagent CBDPS (Figure 14) (342) combined with PK digestion, I reported a series of related inter-peptide crosslink species that have a lower mass than tryptic crosslinks and differ by single amino acid residues, which provides additional confirmation of the crosslink assignments. Proteinase K digestion of crosslinked proteins is necessary to obtain sufficient crosslinking constraints for acid and urea-acid induced PrP^{β} oligomers.

2.2. Materials and methods

All materials were from Sigma-Aldrich, (St. Louis, MO, USA), unless otherwise noted.

2.2.1. Model crosslinked peptide

The model peptide Ac-TRTESTDIKRASSREADYLINKER (Creative Molecules Inc., Victoria, BC, Canada) was crosslinked with an equimolar amount of CBDPS-H8/D8 reagent (CyanurBiotinDiPropionylSuccinimide, Creative Molecules Inc.), as previously described (342). The pH of the mixture was adjusted to 8.0 – 8.5 by the addition of 0.2 M Na_2HPO_4. The reaction mixture was incubated for 30 min at 25^{o}C and quenched with 50 mM ammonium bicarbonate. The crosslinked peptide was then digested with Proteinase K (Invitrogen, Carlsbad, CA, USA) for 1 hour at 37°C at a 1:1 (w:w) enzyme:substrate ratio.

2.2.2. Prion PrP^C protein

All prion constructs were obtained from Dr. David Wishart's laboratory at the University of Alberta via the Prion Protein and Plasmid Production Platform Facility (PrP5) (354), of PrioNet Canada (355). Specifically, a synthetic gene corresponding to the Syrian hamster prion protein sequence 90-232 ($ShPrP_{90-232}$) with a 23-residue N-terminal fusion tag containing 6x-His and a thrombin cleavage site (MGSSHHHHHHSSGLVPRGSHMLE) was synthesized by DNA 2.0. The gene was cloned into a pET15b expression vector between XhoI and EcoRI restriction sites and heat shock transformed into E. coli strain BL21 (DE3). For expression, the transformed cells were grown in 100 mL LB plus 100 µg/mL ampicillin overnight to generate a starter culture. Between 1.5 and 2% of this starter culture was then used to inoculate 1 L of LB media (giving a starting OD_{600} of 0.1). The cells were allowed to reach an OD_{600} between 0.8 and 1.0 before induction with 1 mM IPTG. Twelve to eighteen hours later, the cells were harvested by centrifugation at 5000 rpm for 30 minutes at 4 ºC. The inclusion of the 6x-His tag afforded a standardized nickel affinity purification strategy previously described by Zahn et al. (253). PrP^{β} was generated by exposing the native PrP^C protein to low pH (1.0) for 1 hour and then dialyzing it back to pH 5.5. The details of the purification and PrP^C to PrP^{β} conversion protocol have been described elsewhere (278).

2.2.3. Crosslinking analysis of prion proteins

A 10 µL aliquot of a 1 mg/mL solution of PrP^C and PrP^{β} in PBS was mixed with 1 µL of a 0.5 mM CBDPS-H8/D8 solution in water, prepared from a 50 mM stock solution of the crosslinker in DMSO. The final concentration of the crosslinker reagent was chosen based on the preliminary titration of the reaction mixture where the intensity of the crosslinked dimer band of the β-sheet form of the prion protein (PrP^{β}) on SDS-PAGE was maximized, without the appearance of any non-specific higher-oligomeric crosslinked products of the native non-infectious prion protein (PrP^C). The pH of the mixture was adjusted to 8.0 – 8.5 by the addition of 0.2 M Na_2HPO_4. The reaction mixture was incubated for 30 min at 25°C and quenched with 50 mM ammonium bicarbonate. The crosslinked proteins were then digested with Proteinase K, for 2.5

hours at 37°C at a 1:1 (w:w) enzyme:substrate ratio. A protease inhibitor cocktail (Sigma-Aldrich, P8465) was added to the resulting peptide mixture.

2.2.4. Affinity enrichment of CBDPS crosslinks

Monomeric avidin beads (ThermoFisher, Thermo Scientific, Mississauga, ON, Canada) were used for the affinity enrichment. The mixture was affinity purified with 80 µL of monomeric avidin agarose beads slurry. Beads were washed three times with 120 µL of 1M ammonium acetate and then with water, and the affinity-bound material was eluted with 100 µL of 0.1% TFA and 100 µL of 0.1%TFA/50% acetonitrile. Aliquots from the loading, flow-through, wash, and elution fractions were desalted using Zip-Tips C18 (Millipore), and were analyzed by MALDI-MS.

2.2.5. Nano-ESI-MS analysis

ESI mass spectrometric analyses were performed on the Orbitrap Velos (Thermo Scientific) mass spectrometer, in the positive ion mode. The PK digest was loaded onto a C18 Zip-tip (Millipore, Billerica, MA) and eluted with 60% methanol/0.1%FA. Nano-ESI of the eluate was performed using Proxeon nanoES capillaries (Thermo Scientific) at 1.6kV spray voltage. ESI-MS spectra were acquired manually over an m/z range of 400-2000, using FT detection profile mode with resolution of 60000, isolation width 1 Da. ESI-MS/MS spectra were manually acquired using CID fragmentation in the FT Profile mode, with an isolation width of 2 Da, a collision energy setting of 30%, and a resolution of 60,000. Thermo Scientifics Excalibur software, version 2.1.0 QF03489 build 1140, was used for the data acquisition. Thermo Proteome Discoverer 1.3, Version 1.3.0.339 was used to generate the mgf files.

2.2.6. LC-MALDI analysis

The eluted fractions were combined, concentrated by lyophilization, and were separated by nano-flow reversed-phase HPLC on a 1D Tempo nano-LC system (Eksigent, Dublin, CA) equipped with an LC Packings (Sunnyvale, CA) 0.3 x 5 mm C_{18} PepMap guard column (5 µm particle size, 100 Å pore size), and a 75 µm x 15 cm capillary column packed in-house with Magic C_{18} Aq (Michrom Bioresources Inc., Auburn, CA) particles (5 µm, 100 Å). This capillary LC system was operated at a flow rate of 300 nL/min, using a 55-minute gradient from 5 to 60% acetonitrile (0.1% TFA).

The column effluent was spotted at one-minute intervals (300 nL/spot) onto a stainless steel MALDI target using a Shimadzu (Kyoto, Japan) spotter. The spots were dried, overlaid with 1 mg/mL α-cyano-4-hydroxycinnamic acid matrix solution in 0.1% TFA/50 % acetonitrile, and analyzed by MALDI-MS and MS/MS, using a 4800 MALDI-TOF/TOF (AB Sciex, Concord, ON, Canada). MS/MS spectra were acquired using "CID off", 50 FHWM gate width, and a 1 kV MSMS method. In cases where additional fragmentation was desirable for the unambiguous crosslink assignments, spectra were reacquired using "CID on", and a 2 kV MSMS method.

The mass spectra were analyzed using the ICC-CLASS software (344) and the ICCLMSMS program (341) (version date: August 1, 2011; available free at www.creativemolecules.com/CM_Software.htm). Mass spectra peaklists were generated using Data Explorer Version 4.0 (AB Sciex). The mass spectra from each chromatographic fraction were searched for undeuterated/deuterated CBDPS-crosslinked (D0/D8) doublets using the DX program of the ICC-CLASS software suite, with a peak intensity cutoff of 50 and a mass tolerance setting of 0.01 Da for the 8.05824-Da theoretical mass difference between the masses of the light and heavy isotopes. The D0/D8 mass list obtained was used as "inclusion list" for automatic MS/MS spectra acquisition. The acquired MS/MS spectra were searched for isotopic signatures characteristic of the CID cleavage of crosslinks 401 Da apart, using the ICCLMSMS program. Inter-peptide crosslinks were recognized based on their CID cleavage patterns and were identified by the DXMSMS module of the ICC-CLASS software suite based on the crosslink mass, the masses of the CID-cleavage products, and the masses of the fragments of the crosslink, using the following settings: 100 ppm mass tolerance for the precursor mass; 300 ppm mass tolerance for the MS/MS fragment ions; all possible cleavage sites; and KYST as allowed crosslinking sites.

2.2.7. Molecular modeling

The NMR structure of hamster prion protein (PDB ID 1B10, (243)) was used as the initial template, which covers only residues 125-231. The missing residues from the flexible N-terminus (G68 - G124) were modeled in an extended conformation, and were connected to the initial template via super-positioning, followed by energy minimization of these residues using XPLOR-NIH (356).

MS crosslinking data was converted into distance constraints between the side-chain nitrogen atoms of lysine residues, with an upper limit of 14Å (the length of the crosslink). For G68 -- the N-terminal residue of the N-terminal fusion tag -- the position of the N-terminal nitrogen was used for the distance calculations. An ensemble of 200 models was generated by molecular dynamics in Cartesian space using XPLOR-NIH (356). Specifically, the positions of the N-terminal region (G68 to G124) with respect to the initial template (L125 to G228) was optimized with a simulated annealing protocol that included 6000 steps at 1000ºK, 3000 cooling steps from 1000ºK to 0ºK, followed by 1000 steps of Powell minimization (357). In this initial model, the positions of the backbone atoms of the initial template were kept fixed. Structures were visualized using the molecular modeling program MOLMOL (358).

2.3. Results

2.3.1. Digestion of the crosslinked model peptide

To characterize the types of peptides produced by proteinase K digestion of the inter-peptide crosslinks, I analyzed a digest of the model peptide, Ac-TRTESTDIKRASSREADYLINKER, crosslinked with the CBDPS reagent (Figure 14, Figure 15, Figure 16, Figure 17). CBDPS is a homo-bifunctional NHS-based amine-reactive crosslinker, possessing additional features useful for mass spectrometric analyses, such as isotopic coding, CID-cleavability, and affinity purification (342). Previous studies have shown that both inter- and intra-peptide crosslinks are generated by crosslinking this peptide with CBDPS. Digestion of this crosslinked peptide with proteinase K, a non-specific enzyme, resulted in sets of short, related, inter-peptide CBDPS crosslinks, all of which contained the same crosslinked pair of lysine residues. As can be seen from Figure 14, proteinase K cleaves the peptides at or near the crosslinked residue, leaving two to four residues of each peptide still attached to the crosslinker. This usually results in a set of related isotopically-labeled crosslinks for each crosslinked pair of amino acids. In the example shown in Figure 14, there are multiple crosslinks containing the same pair of crosslinked residues – for example, the crosslinked Lys-Lys pair (K9 to K22) is found six times in the spectrum. Multiple crosslinks often

differed by one amino acid residue, creating a "sequence ladder" around the crosslinking site, which can be used as an additional verification tool for the crosslink assignment.

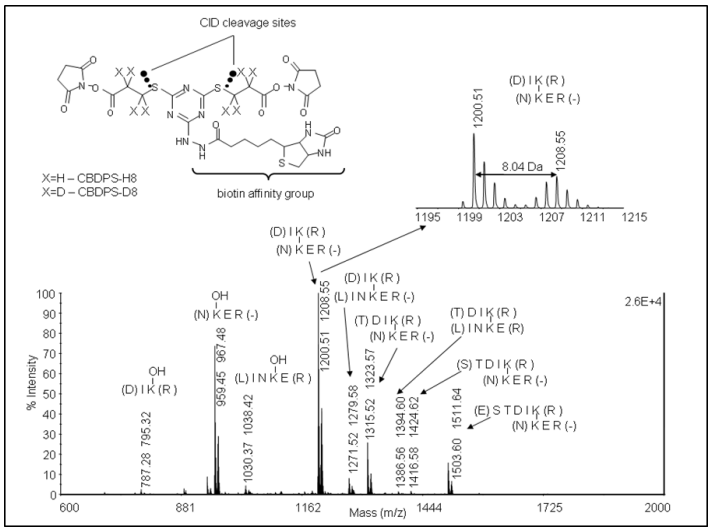

Figure 14: MALDI-MS and MS/MS analysis of the test peptide (Ac-TRTESTDIKRASSREADYLINKER) crosslinked with CBDPS-H8/D8, followed by proteinase K digestion.

MALDI-MS spectrum of the proteinase K digest. As shown in the Inset, crosslinks appear in the spectrum as doublets of signals 8.05 Da apart (theoretical mass difference), due to the isotopic coding of the crosslinking reagent. Reprinted from Petrotchenko et al. (301).

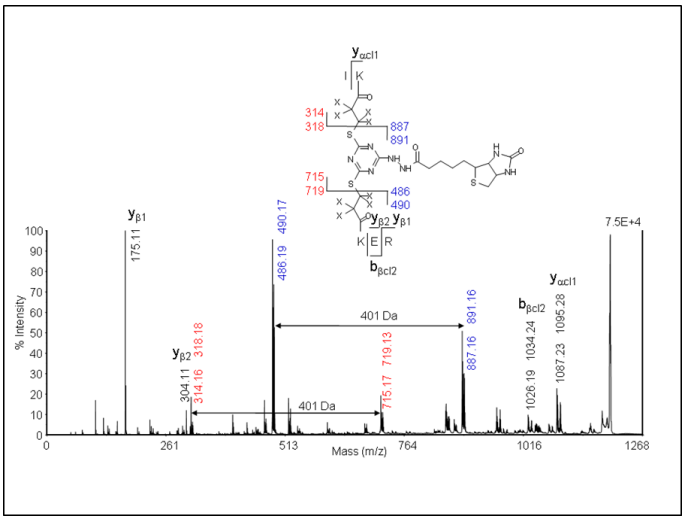

Figure 15: MALDI-MS and MS/MS analysis of the test peptide (Ac-TRTESTDIKRASSREADYLINKER) crosslinked with CBDPS-H8/D8, followed by proteinase K digestion.

MS/MS spectrum of the m/z 1200 inter-peptide IK-KER crosslink. (Note: masses of the isotopically-coded peptide and fragment ion pairs are denoted as vertically aligned pairs of numbers corresponding to light and heavy isotopic

forms; fragment ions are labeled with subscripts α or β, denoting the peptide the originated from; fragments containing portions of the crosslinker and counterpart peptide are labeled with the subscript cl.). Reprinted from Petrotchenko et al. (301).

Due to the molecular weight of the CBDPS crosslinker (ca. 500 Da), the inter-peptide crosslinks fall within the optimum mass range (1100-1500 Da), for MALDI-MS detection and MS/MS sequencing. An example of an MS/MS spectrum is shown in Figure 15. The use of the CID-cleavable crosslinker CBDPS allowed determination of the two component peptides forming the crosslink, by MS/MS. The relatively short sequences from each crosslinked peptide simplify the MS/MS spectra and facilitate the sequence assignment of the crosslinks. It should be noted that the proteinase-K cleavage reaction does not proceed all the way to the K-CBDP-K crosslink, possibly due to steric hindrance from the crosslinker and/or from the connected peptide. Interestingly, in a paper on localization of disulfides, cleavage was variable but sometimes occurred adjacent to the maleimido-butyryl-biocytin (MBB)-modified cysteines, giving peptides as small as CG/GC and SC/SC (359). In this MBB study, smaller peptides would have been buried in the MALDI matrix background. In our case, had the reaction proceeded all the way to the crosslinked residue, the crosslinking sites could not have been localized, so the blockage of the cleavage reaction is essential for the success of these experiments.

Notably, because of the affinity purification of the CBDPS crosslinks, there are also no ion signals from "free" (non-crosslinked) peptides present in the spectrum. Also, because of the digestion with proteinase K, which cleaves to within a few residues of the crosslinks, and the +1 charge on the crosslinks in MALDI MS, the masses of the CBDPS dead-end crosslinks fall in the low-mass region of the spectrum, below the mass range of the inter-peptide crosslinks (as can be seen in Figure 14), while non-crosslinked peptides are cleaved down to very small peptides, diamino acids (359), or possibly even to individual amino acids (360). In effect, this digestion "cleans up" the spectrum and leads to large regions of the spectrum which predominantly contain signals from inter-peptide crosslinks. The MALDI MS/MS spectrum of a CBDPS crosslink is shown in Figure 15. Although the PK digestion is the same, with electrospray ionization (ESI), the spectra are more complex due to the presence of multiply-charged ions (Figure 16), but the presence of the isotopic coding facilitates the recognition of the crosslinks. The presence and

intensities of the structurally-important fragment ions in the ESI-MS/MS spectra are charge- and peptide-dependent, but ESI-MS/MS still gave easily-interpretable results for the +2 charge state (Figure 17). Thus, this analysis can be performed in both ESI and MALDI. Although much of the work in this chapter was performed using MALDI-MS and MS/MS acquisition and analysis, many of the current workflows in the Borchers laboratory have now transitioned to the use of LC/ESI-MS/MS acquisition and analysis.

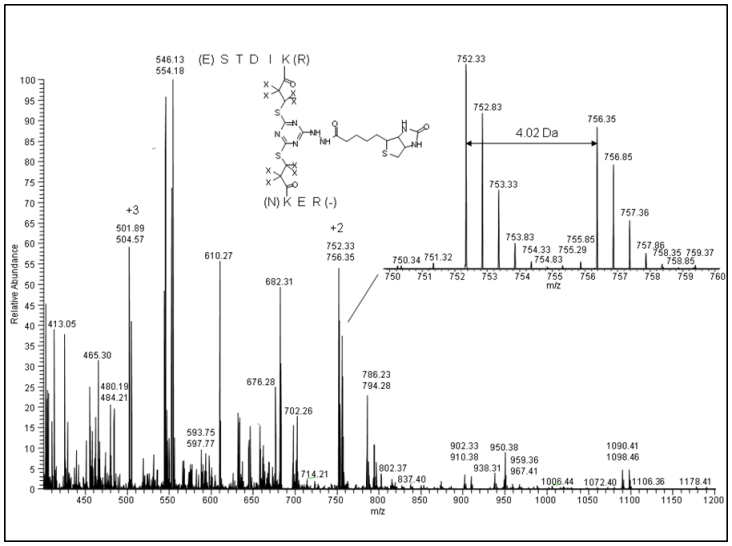

Figure 16: MALDI-MS and MS/MS analysis of the test peptide (Ac-TRTESDKIRASSREADYLINKER) crosslinked with CBDPS-H8/D8, followed by proteinase K digestion.
ESI-MS spectrum of proteinase K digest (inset: expanded region of the doubly-charged molecular ion of the crosslink, showing the isotopic labeling). Reprinted from Petrotchenko et al. (301).

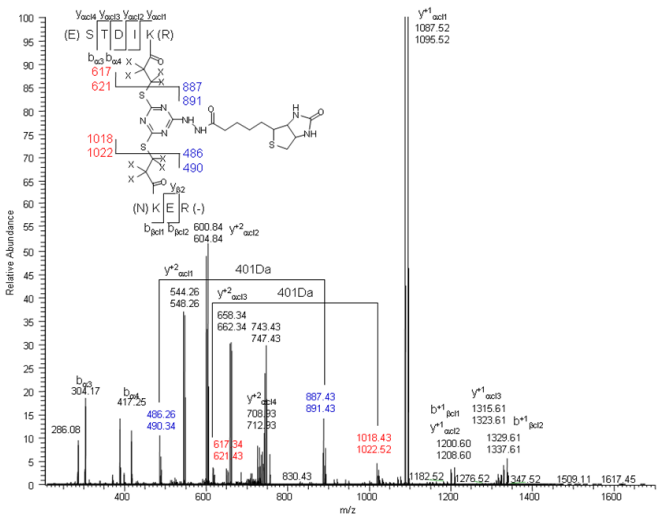

Figure 17: MALDI-MS and MS/MS analysis of the test peptide (Ac-TRTESDKIRASSREADYLINKER) crosslinked with CBDPS-H8/D8, followed by proteinase K digestion.
ESI-MS/MS spectrum of the proteinase K digest. In positive-ion ESI MS/MS, the fragmentation depends on the charge state of the precursor ion. The ESI-MS/MS spectrum of the +2 charge state of the precursor ion is shown. Reprinted from Petrotchenko et al. (301).

Table 3 shows the inter-peptide crosslinks and isotopically-coded CID-cleavage fragments from the CBDPS-crosslinked test peptide in MALDI. A similar pattern of digestion was observed with other crosslinkers, including DSG, DSS, PICUP (361), and EGS (Table 4). For CBDPS, CID-cleavage of the crosslinker bridge of inter-peptide crosslinks produces short linear peptides from each crosslink (the columns labeled "401 1" and "401 2"), which are easy to assign.

Mass (M+H)+	Δ, ppm	Res start	Res end	K	401 1*	401 2	Sequence Peptide 1	Res start	Res end	K	401 1	401 2	Sequence Peptide 2
1200.51	24.4	8	9	9	314.16	715.17	(D)IK(R }	22	24	22	486.19	887.16	(N)KER(-)
1271.52	39.8	8	9	9	314.17	715.18	(D)IK(R }	20	23	22	557.25	958.22	(L)INKE(R)
1315.52	35.5	7	9	9	429.17	830.16	(T)DIK(R }	22	24	22	486.20	887.19	(N)KER(-)
1386.56	26.2	7	9	9	429.17	830.15	(T)DIK(R }	20	23	22	557.25	958.22	(L)INKE(R)
1416.58	24.3	6	9	9	530.27		(S)TDIK(R }	22	24	22	486.20	887.20	(N)KER(-)
1503.60	34.1	5	9	9	617.18		(E)STDIK(R }	22	24	22	486.20	887.21	(N)KER(-)

Table 3: Inter-peptide crosslinks identified by crosslinking test peptide (Ac-TRTESTDIKRASSREADYLINKER) with CBDPS followed by proteinase K digestion.
* The central portion of the crosslinker weighs 401 Da. Due to the symmetrical nature of the crosslinker, cleavage on either side of this central portion leads to two pairs of peaks separated by 401 Da, corresponding to each peptide connected to a portion of the crosslinker. Because all of these

cleaved fragments still contain the isotopically-labeled propionic acid moiety of CBDPS they appear in the spectrum as doublets of peaks (342). Reprinted from Petrotchenko et al. (301).

Mass,	Δ,Peptide 1					Peptide 2			
Da	ppm	start	end	K	Sequence	start	end	K	Sequence
DSG	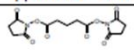								
1317.71	-0.7	5	11	9	(E)STDIKRA(S)	22	24	22	(N)KER(-)
	-9.2	5	10	9	(E)STDIKR(A)	20	23	22	(I)NKE(R)
1544.85	-8.5	5	11	9	(E)STDIKRA(S)	20	24	22	(L)INKER(-)
1598.77	-9.7	5	9	9	(E)STDIK(R)	12	19	Y18	(A)SSREADYL(I)
1694.86	-12.7	5	12	Y18	(A)SSREADYL(I)	19	24	22	(Y)LINKER(-)
1317.71	-0.7	5	11	9	(E)STDIKRA(S)	22	24	22	(N)KER(-)
DSS	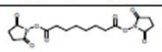								
1132.63	-3.2	5	10	9	(E)STDIKR(A)	22	23	22	(N)KE(R)
	-3.2	5	9	9	(E)STDIK(R)	22	24	22	(N)KER(-)
1261.68	-11.1	4	10	9	(T)ESTDIKR(A)	22	23	22	(N)KE(R)
	-11.1	4	9	9	(T)ESTDIK(R)	22	24	22	(N)KER(-)
1379.76	-11.5	5	9	9	(E)STDIK(R)	20	24	22	(L)INKER(-)
	-11.5	5	10	9	(E)STDIKR(A)	20	23	22	(L)INKE(R)
	-3.2	5	11	9	(E)STDIKRA(S)	22	24	22	(N)KER(-)
1640.83	-14.1	5	9	9	(E)STDIK(R)	12	19	Y18	(A)SSREADYL(I)
1736.90	-12.7	12	20	Y18	(A)SSREADYLI(N)	21	24	22	(I)NKER(-)
EGS	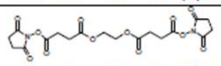								
1220.60	1.7	5	10	9	(E)STDIKR(A)	22	23	22	(N)KE(R)
	1.7	5	9	9	(E)STDIK(R)	22	24	22	(N)KER(-)
1447.74	-16.4	5	11	9	(E)STDIKRA(S)	22	24	22	(N)KER(-)
	-16.4	6	12	9	(S)TDIKRAS(S)	22	24	22	(N)KER(-)
	-16.4	8	15	9	(D)IKRASSRE(A)	22	23	22	(N)KE(R)
1728.80	-13.0	5	9	9	(E)STDIK(R)	12	19	Y18	(A)SSREADYL(I)
1824.85	6.9	12	21	Y18	(A)SSREADYLIN(K)	22	24	22	(N)KER(-)
	6.9	12	20	Y18	(A)SSREADYLI(N)	21	24	22	(I)NKER(-)
	6.9	12	19	Y18	(A)SSREADYL(I)	20	24	22	(L)INKER(-)
	6.9	12	18	Y18	(A)SSREADY(L)	19	24	22	(Y)LINKER(-)
PICUP									
1627.75	23.6	17	21	Y18	(A)DYLIN(K)	14	21	Y18	(S)READYLIN(K)
1774.78	20.5	15	19	Y18	(R)EADYL(I)	10	19	Y18	(K)RASSREADYL(I)
1801.83	18.7	17	21	Y18	(A)DYLIN(K)	10	19	Y18	(K)RASSREADYL(I)
2001.90	16.1	15	21	Y18	(R)EADYLIN(K)	12	21	Y18	(A)SSREADYLIN(K)

Table 4: Inter-peptide crosslinks identified by crosslinking test peptide (Ac-TRTESTDIKRASSREADYLINKER) with DSG, DSS, EGS, and PICUP followed by proteinase K digestion.
Crosslink mass and ppm error listed as well as peptide 1 and 2 start, end, sequence, and the residue involved in the crosslink. Reprinted from Petrotchenko et al. (301).

2.3.2. Proteinase K digestion of crosslinked prions

As a first application of this new method, I then applied the proteinase K digestion method to the crosslinking analysis of native monomeric PrP^{C} and acid-induced PrP^{β}. As described in section 1.4. Prion protein biosynthesis, prion proteins are characterized by template-induced conformational changes which lead to the conversion of the native structure and formation of the pathological protein aggregates (24,58-60).

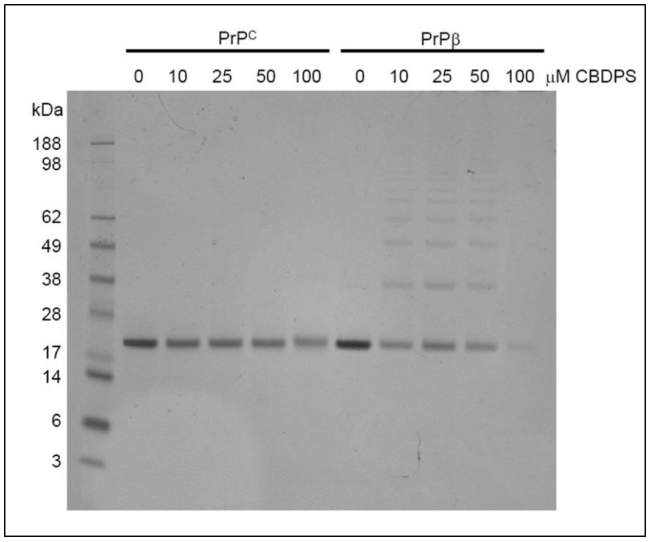

Figure 18: CBDPS crosslinking of PrP^{C} and PrP^{β}.
PrP^{C} and PrP^{β} samples were crosslinked with increasing concentrations of CBDPS and separated by SDS-PAGE. Inter-protein crosslinked species were observed only for the β-oligomer. Reprinted from Petrotchenko et al. (301).

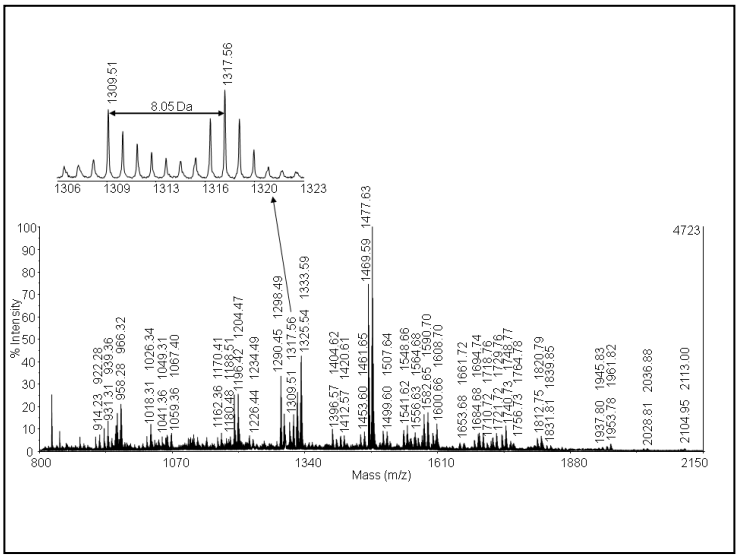

Figure 19: Crosslinking analysis of the prion proteins.
MALDI MS spectrum of an HPLC fraction from a proteinase-K digest of the β-oligomer after crosslinking with CBDPS-H8/D8. Proteins were crosslinked with CBDPS-H8/D8, digested, crosslinks were affinity purified with immobilized avidin, separated by HPLC, and analyzed by MALDI MS and MALDI MS/MS. Inset: differential crosslink, present only in the β-oligomer sample. Reprinted from Petrotchenko et al. (301).

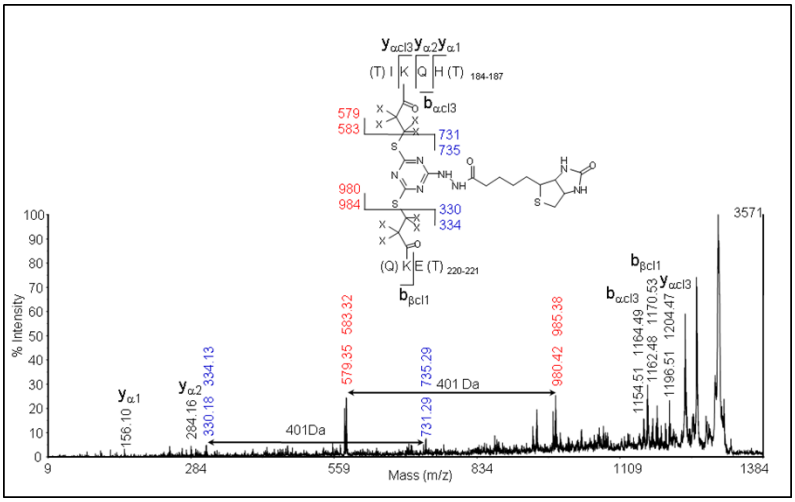

Figure 20: Crosslinking analysis of the prion proteins.
MS/MS spectrum of the 1309 m/z crosslink identified as K185-K220 inter-peptide crosslink. Reprinted from Petrotchenko et al. (301).

I investigated this structural problem using crosslinking combined with mass spectrometry. For the CBDPS crosslinking experiments on PrP^{C} and PrP^{β}, the experimental conditions were optimized so that inter-protein crosslinked species were observed *only* for the β-oligomer Figure 18. I then combined CBDPS crosslinking with proteinase K digestion, and compared the results with CBDPS crosslinking combined with standard tryptic digestion. The use of tryptic digestion did not result in the detection of any inter-peptide crosslinks. Although the CBDPS-crosslinked protein produces a very complex mixture of peptides, amino acids, and crosslinks with proteinase K, I was able to isolate numerous inter-peptide crosslinks (Figure 19 and Figure 20). This strategy produced a broad coverage of the crosslinked sites – as can be seen in Figure 21, every lysine in the protein is represented in multiple crosslinks. In addition, the masses of the inter-peptide crosslinks produced by proteinase-K digestion of the crosslinked protein were suitable for MALDI-MS analysis. Using proteinase K and all of the features designed into the CBDPS crosslinker (CID cleavage, isotopic coding, and affinity purification), a total of over 60 inter-peptide crosslinks were found for the native and the β- forms of the prion protein. Several of these crosslinks were unique to each form of the prion protein (Table 5).

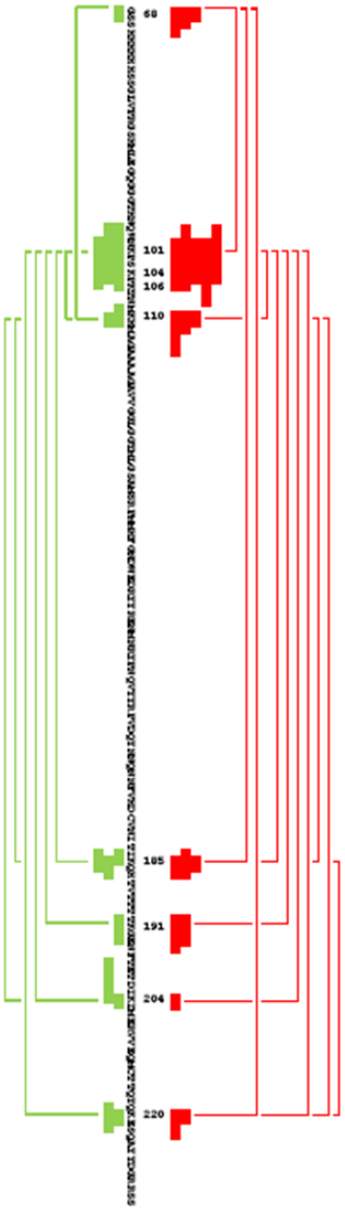

Figure 21: Locations of the inter-peptide crosslinks found for both PrP^{C} (green) and PrP^{β} (red).
Sequences for the peptide components of the Lys-Lys inter-peptide crosslinks are highlighted. Reprinted from Petrotchenko et al. (301).

Mass $(M+H)^+$	Δ, ppm	HPLC fract.	Res start	Res end	K	401 1	401 2	Sequence Peptide 1	Res start	Res end	K	401 1	401 2	Sequence Peptide 2
PrP^C														
955.33	0.9	18	68	68	68	217	618	(-)GS(S)	110	111	110	338	739	(M)KH(M)
1590.74	0.8	18	100	106	101	852	1253	(W)NKPSKPK(T)	110	111	110	338	739	(M)KH(M)
1721.77	11.2	19	100	106	101	852	1253	(W)NKPSKPK(T)	110	112	110		870	(M)KHM(A)
1694.79	25.5	19	100	106	101	852	1253	(W)NKPSKPK(T)	184	186	185		843	(T)IKQ(H)
1740.77	14.9	19	100	106	101	852	1253	(W)NKPSKPK(T)	193	196	194	488		(T)TKGE(N)
1566.73	27.6	20	100	106	101	852	1253	(W)NKPSKPK(T)	204	205	204		715	(I)KI(M)
1752.76	29.4	23	98	105	101	1038	1439	(N)QWNKPSKP(K)	204	205	204	314		(I)KI(M)
1880.81	53.4	23	98	106	101	1166	1567	(N)QWNKPSKPK(T)	204	205	204	314		(I)KI(M)
2012.94	28.3	21	100	106	101	852	1253	(W)NKPSKPK(T)	199	204	204	760		(F)TETDIK(I)
1582.70	16.7	19	100	106	101	852	1253	(W)NKPSKPK(T)	220	221	220		731	(Q)KE(S)
1797.82	12.7	18	100	106	101	852	1253	(W)NKPSKPK(T)	219	222	220			(Y)QKES(Q)
1204.47	21.1	17	110	111	110	338	739	(M)KH(M)	185	187	185	466		(I)KQH(T)
1183.45	44.8	23	110	112	110	314	715	(I)KI(M)	204	205	204	469	870	(M)KHM(A)
1474.59	38.7	24	199	204	204	760	1161	(F)TETDIK(I)	184	185	185	314	715	(T)IK(Q)
$PrP\beta$														
1469.59	37.1	17	68	69	68		618	(-)GS(S)	100	106	101	852	1253	(W)NKPSKPK(T)
1556.63	27.0	16	68	70	68		705	(-)GSS(S)	100	106	101	852	1253	(W)NKPSKPK(T)
1684.68	32.4	17	68	69	68		618	(-)GS(S)	100	108	101	1067	1468	(W)NKPSKPKTN(M)
1693.70	20.4	18	68	71	68		845	(-)GSSH(H)	100	106	101	852	1253	(W)NKPSKPK(T)
1083.36	27.9	17	68	69	68		618	(-)GS(S)	185	187	185	466	867	(I)KQH(T)
1196.42	45.4	17	68	69	68		618	(-)GS(S)	184	187	185	579	980	(T)IKQH(T)
1162.37	33.9	17	68	69	68		618	(-)GS(S)	220	223	220	545	946	(Q)KESQ(S)
2104.97	39.2	16	100	106	101	852	1253	(W)NKPSKPK(T)	100	106	101	852	1253	(W)NKPSKPK(T)
2291.01	38.7	19	100	106	101	852	1253	(W)NKPSKPK(T)	98	105	101	1038	1439	(N)QWNKPSKP(K)
2419.06	55.4	19	100	106	101	852	1253	(W)NKPSKPK(T)	98	106	101	1166	1567	(N)QWNKPSKPK(T)
1721.71	41.7	18	100	106	101	852	1253	(W)NKPSKPK(T)	110	112	110	469	870	(M)KHM(A)
1590.72	27.9	16	100	106	101	852	1253	(W)NKPSKPK(T)	110	111	110		739	(M)KH(M)
1920.81	40.2	18	100	106	101	852	1253	(W)NKPSKPK(T)	110	115	110	668	1069	(M)KHMAGA(A)
1581.65	61.3	17	100	106	101	852	1253	(W)NKPSKPK(T)	185	186	185			(I)KQ(H)
1718.76	33.3	16	100	106	101	852	1253	(W)NKPSKPK(T)	185	187	185			(I)KQH(T)
1831.81	43.2	16	100	106	101	852	1253	(W)NKPSKPK(T)	184	187	185		980	(T)IKQH(T)
1740.73	39.3	17	100	106	101	852	1253	(W)NKPSKPK(T)	193	196	194			(T)TKGE(N)
1854.77	38.8	16	100	106	101	852	1253	(W)NKPSKPK(T)	193	197	194			(T)TKGEN(F)
1566.70	47.3	18	100	106	101	852	1253	(W)NKPSKPK(T)	204	205	204	314	715	(I)KI(M)
1582.66	46.2	17	100	106	101	852	1253	(W)NKPSKPK(T)	220	221	220		731	(Q)KE(S)
1797.76	35.2	15	100	108	101	852	1253	(W)NKPSKPK(T)	220	223	220	545	946	(Q)KESQ(S)
1204.49	7.0	15	110	111	110		739	(M)KH(M)	185	187	185	466	867	(I)KQH(T)
1068.40	41.0	16	110	111	110	338	739	(M)KH(M)	220	221	220	330	731	(Q)KE(S)
1196.44	58.6	16	185	187	185	466	867	(I)KQH(T)	220	221	220		731	(Q)KE(S)
1309.51	35.0	17	184	187	185	579	980	(T)IKQH(T)	220	221	220		731	(Q)KE(S)

Table 5: Inter-lysine CBDPS crosslinks of prion proteins after proteinase K digestion.

Proteins were crosslinked with isotopically-coded CBDPS-H8/D8 reagent, and digested with proteinase K. Crosslinked peptides were affinity enriched using immobilized monomeric avidin beads, and the resulting peptide crosslinks were separated by HPLC and analyzed by MALDI MS and MS/MS. Crosslinks that were unique to the native form of prion are highlighted in gold; those unique to the β-oligomeric form are highlighted in red; those found in both samples are in green. 401 1 and 401 2 are the masses of the CID-cleavage products of the inter-peptide crosslinks, which carry a

specific isotopic signature -- two 4.03-Da doublets of signals, 401 Da apart. Reprinted from Petrotchenko et al. (301)**.**

2.3.3. Molecular modeling

My initial analysis of PrP models indicated that the multiple crosslink-based restraints on K101 could not be satisfied by a single conformation. Therefore, the crosslink-based distance constraints were split into two sets in order to separate K101 crosslinking partners that are located on the opposite sides of the protein: set A included crosslinks K101-K194 and K101-K220; set B included crosslinks K101 – K185 and K101 – K204. This yielded 123 and 200 models, respectively, with no violations of the distance constraints. These models are shown in Figure 22 A-D, and include the aa90-aa124 portion of the N-terminal sequence that could not be determined by NMR spectroscopy. Even a recent NMR-based model of prions was unable to postulate a structure for this flexible portion of the protein (362). Our new model is based on mass spectrometrically-derived crosslinking restraints, and includes the N-terminal flexible region (aa90-123) plus a 23-residue extension to facilitate purification. This model indicates that there is an interaction of the N-terminal part of PrP with the C-terminal portion of helix 2 and helix 2 – helix 3 loop.

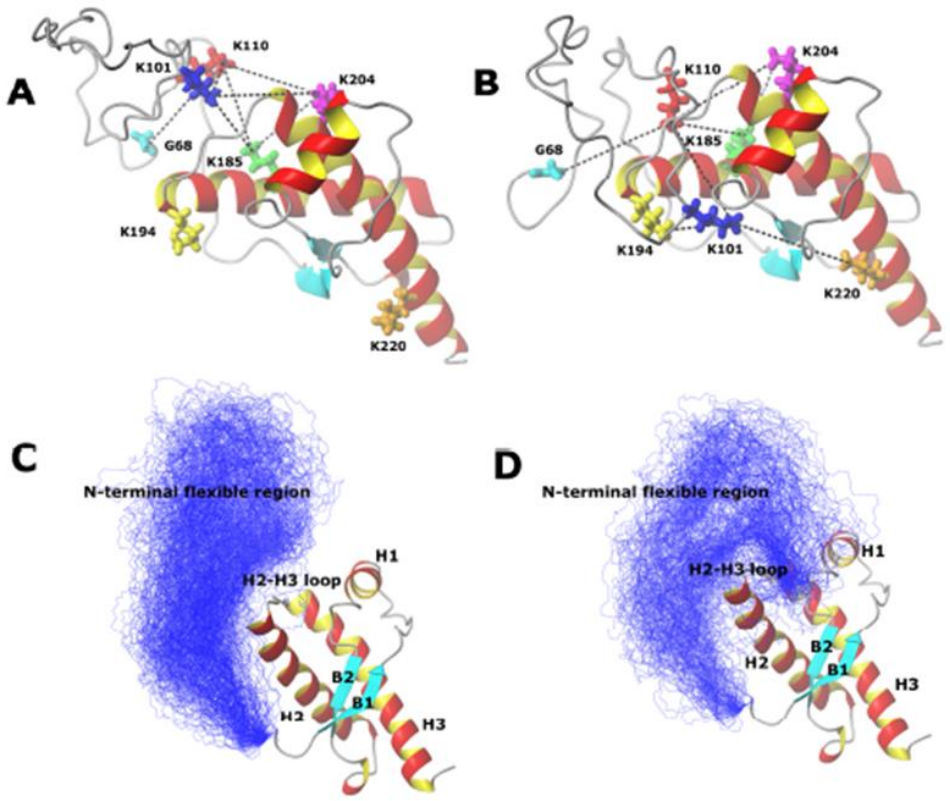

Figure 22: Conformations of the native form of the PrP aa68-aa232 protein, modeled using the inter-lysine crosslink distance restraints. Dashed lines indicate constraints that were applied to the crosslinked residues. Panels A and B show crosslinker distances for constraint sets A and B, respectively. Panels C and D illustrate "open" and "closed" conformational bundles of the flexible N-terminal region (blue lines) that are identified by constraint sets A and B, respectively. B1, B2, H1, H2, and H3 are beta-strands 1 and 2, and helices 1, 2, and 3, respectively. Both conformational bundles are consistent with transient interactions of the N-terminal flexible region with the C-terminal part of helix 2 and the loop between helices 2 and 3. Reprinted from Petrotchenko et al. (301).

2.4. Discussion

The ionization efficiency of MALDI-MS drops as the molecular weight of a peptide increases, so there is always a concern in mass spectrometry-based crosslinking studies as to whether all of the crosslinks present in the digest have been detected. This is even more of a concern for protein sequences that may lack cleavage sites for high-specificity proteolytic enzymes and where these cleavage sites may be blocked by crosslinkers. This can lead both to reduced peptide sensitivity due to the size of the peptide (363-366), thus

leading to increased susceptibility to suppression effects, particularly in complex mixtures, as well as a reduced fragmentation efficiency (366,367). To address this issue, I explored the use of the non-specific proteolytic enzyme proteinase K for the digestion of the crosslinked proteins. Low-specificity enzymes are not often used in proteomics studies because they usually divide the peptide signals among several possible digestion peptide products, and because they complicate the identification of the peptides.

Proteinase K has been used for the study of prions since the early 1980's. In fact, proteinase K was used in initial experiments that proved that the infectious agent in scrapie was, in fact, a protein and not a virus or viroid (see 1.1.1. History of prion disease) (42,368,369). Although in these studies, digestion with proteinase K reduced the infectivity of the samples, it was also noted that resistance to proteinase K correlated with the titer of the infectious agent (43,45). This led to a patented method for the determination of PrP^{C} and PrP^{Sc} in biological samples, such as blood (370).

To overcome the partial resistance of PrP^{β} to proteinase K digestion, fairly high enzyme:substrate ratios were used in our study. In my crosslinking experiments, I found that proteinase K digestion appears to stop within 2-6 residues of crosslinking sites, which may reflect steric hindrance to the approach of the enzyme activity, as well as the reduced enzyme activity which has been reported to occur at high pH (359). Even with very high enzyme:substrate ratios, K-CL-K crosslinks were not observed. An important additional benefit of this method is that proteinase K digestion effectively eliminates the non-informative non-crosslinked (i.e., free) peptides and dead-end crosslinks (i.e., a crosslink where the crosslinker is incorporated into a protein through only one of the two reactive groups of the crosslinker, while the other reactive group remains unreacted with another amino acid residue) from the mass region of the spectra that contains the inter-peptide crosslinks. Dead-end crosslinks, which are the largest group of crosslinks, will be efficiently digested by proteinase K and will fall below the usual mass range of MALDI-MS. In fact, if the minimum sequence length requirement for the proteinase K reaction is 4-6 residues, for CBDPS this would put the non-crosslinked peptide products in a mass range below m/z 600 and the dead-end crosslinks in a mass range below m/z 1000, while most of inter-peptide crosslinks would be observed in the mass range between m/z 1200 and 1800 – the ideal mass range for MALDI-MS/MS fragmentation.

This is a major advantage of this method and is particularly significant for facilitating the detection of inter-peptide crosslinks. In fact, when proteinase K digestion was used for crosslinking studies, we found that any drawbacks due to the enzyme's lack of specificity were more than outweighed by the reduced size of the crosslinked peptides, and the simplicity of the inter-peptide crosslinks produced.

Although the short crosslinked peptides produced could potentially lead to ambiguous crosslinking-site identification in very large or complex systems, the fact that these crosslinks are observed at all provides a starting point for subsequent strategies for their targeted determination, such as the use of alternative enzymes. Removing the digestion restrictions also increases the computational challenges for the crosslinking data analysis software, especially for complex protein systems. As the systems increase in size, further upgrades to search algorithms and automated data processing procedures will; be required. This work has been a focus of the Borchers laboratory (344-346).

Representation of the same crosslinked sites by several inter-peptide crosslinks will certainly reduce the signal from each crosslink. However, as has been noted for other studies using PK on post-translationally modified peptides (359), the presence of these "families" of crosslinks provides additional confirmation of the crosslinking sites. These "families" also provide an additional tool for the recognition and assignment of the inter-peptide crosslinks.

A set of 60 crosslinks was found for PrP^{C} and PrP^{β} (Table 5), including crosslinks that were specific to each form of the protein. Nine PrP^{C} interpeptide crosslinks (Figure 21) were used to model the orientation of the N-terminal region (G68 – G124) with respect to the N-terminal domain of PrP, using 14 Å as the maximum span of the CBDPS crosslinker (Figure 22). To my knowledge, these crosslinks provide the first experimental evidence of an interaction between the flexible N-terminal region of PrP and the C-terminal part of helix 2 and helix 2 – helix 3 loop (Figure 22), the first regions to undergo conformational transition under destabilizing conditions such as low pH (278,371,372). The propensity of these PrP low-stability spots to interact with the extended polypeptide chain of the N-terminal region would be consistent with helix 2 and the H2-H3 loop being involved in interactions between PrP^{C} and PrP^{Sc} during disease propagation.

The detected PrP^{C} inter-peptide crosslinks and the PrP^{C} model are consistent with changes observed in the NMR chemical shifts in helix 2 and the helix 2-helix 3 loop, which were induced by the presence of the flexible N-terminal region in human and hamster prion proteins (202,373). This points to direct interactions between this flexible N-terminal region and these portions of the PrP ^{C}-terminal domain as a cause of the observed chemical-shift changes. Interestingly, a G90 (N-terminus)-to-Glu152 crosslink has been reported using EDC (1-ethyl-3-[3-dimethylaminopropyl]carbodiimide hydrochloride), trypsin, and mass spectrometric detection (332). In our current model, these residues are too far apart to be consistent with the length of an EDC crosslinker. However, the large distance between G90 and E152 could also be associated with the different buffer conditions or/and the different protein constructs that were used in the two studies.

Using proteinase K, a CBDPS crosslink between K185 and K220 was also found, but only in the PrP^{β} protein form. This crosslink could originate either from rearrangements of the PrP structure upon conversion to PrP^{β}, or from intermolecular interactions among the sub-units of the β-oligomer, and it is experimental evidence for the conformational differences between PrP^{C} and PrP^{β}. In the native structure, the distance between K185 and K220 is greater than 26Å, and these two residues are situated on opposite surfaces of the protein, separated by the aa127-aa165 loop. A conformational change involving unfolding of the aa127-aa165 loop would expose residues K185 and K220, which would then be able to be crosslinked. This hypothesis is currently being tested in the Borchers laboratory by other structural proteomics methods, such as limited proteolysis (374), surface modification (375), and hydrogen/deuterium exchange (325,326).

Crosslinking combined with mass spectrometry holds great potential for providing constraint data for molecular modeling studies, especially for flexible portions of proteins that cannot be determined by NMR. EDC, a zero-length crosslinker, combined with tryptic digestion and mass spectrometry, was used to demonstrate crosslinks in a PrP dimer (332), and a G90-G90 crosslink was recently found in PrP^{Sc} using BS3 (11.4 Å spacer length), thus providing the first distance constraint for PrP^{Sc} (226). The structures of PrP^{C}, PrP^{β}, and PrP^{Sc} have also been studied using surface chemical modification with nitration (25,316) or acetylation (25), combined with mass spectrometric detection.

Based on my proof-of-principle experiments, proteinase K combined with cleavable crosslinkers have been shown to be useful for mass spectrometry-based structural proteomics studies of prions and other difficult-to-digest proteins. I am confident that the use of this new technique, combined with molecular modeling, will lead to the determination of the structures of these particularly challenging proteins.

2.5. Conclusion

This study demonstrates the utility of the non-specific enzyme proteinase K for crosslinking combined with mass spectrometry experiments. For the proteins studied thus far, the broad specificity and high activity of this enzyme leads to an extensive digestion of the crosslinked proteins, providing comprehensive coverage of the crosslinked sites. Digestion apparently stops within few residues of the crosslinked sites, producing a very clean mass spectrum containing effectively only inter-peptide crosslinks. Cleavage with proteinase K produces inter-peptide crosslinks with molecular masses suitable for MALDI-MS or ESI-MS detection and MALDI-MS/MS or ESI-MS/MS fragmentation, which greatly facilitates identification of the crosslinked peptides and the crosslinked residues. The digestion produces a series of related inter-peptide crosslink species differing by single amino-acid residues, which provides additional confirmation of the crosslink assignments. These features of proteinase K digestion of crosslinked proteins make it an attractive alternative to high-specificity enzymes for crosslinking applications using mass spectrometric analysis.

Proteinase K digestion was essential for obtaining acid-induced PrP^{β} oligomer crosslinking constraints and was crucial to obtaining of sufficient crosslinking constraints of urea-acid converted PrP^{β} crosslinking constraints using a variety of crosslinking reagents (see Chapter 5. Structure of prion β-oligomers as determined by structural proteomics with crosslinking constraint-guided molecular dynamic simulations). Proteinase K digestion is now a standard procedure in the Borchers for crosslinking studies of other prion oligomers.

Chapter 3. Using multiple structural proteomic approaches for the characterization of prion proteins

Work in this chapter was a collaborative effort involving two laboratories. Native (PrP^C) and acid-induced oligomeric (PrP^β) prion protein was recombinantly expressed and purified in the laboratory of Dr. David S. Wishart in the Prion Protein and Plasmid Production Platform Facility (PrP5) (University of Alberta, Edmonton, AB, Canada) and supplied to the Borchers lab at University of Victoria as PrP^C and PrP^β stock solutions. Experimental design was performed by Jason Serpa, Evgeniy Petrotchenko, Aileen Patterson, and Christoph H. Borchers. HDX experiments and analysis were performed by Jingxi Pan and Evgeniy Petrotchenko. Surface modification and crosslinking, experimentation, LC-MALDI-MSMS and data analysis was performed by Jason Serpa. Christoph Borchers oversaw the project.

This chapter was adapted in part from the publication (22):

Serpa JJ, Patterson AP, Pan J, Han J, Wishart DS, Petrotchenko EV, Borchers CH. 2012. ***Using multiple structural proteomics approaches for the characterization of prion proteins.*** **Journal of Proteomics, 10.1016/j.jprot.2012.10.008.**

3.1. Introduction

Structural proteomics methods, such as limited proteolysis, surface chemical modification, hydrogen/deuterium exchange, and chemical crosslinking, combined with contemporary mass spectrometry, can provide detailed structural information for proteins and protein complexes that are not amenable to traditional biochemical methods (20).

Each structural proteomics method can provide specific orthogonal structural data, such as surface accessibility to large/small probes, hydrogen bonding/the presence of secondary structural motifs, and inter-side chain distances at the single amino acid level. Here, we illustrate the application of a combination of these multiple structural proteomics methods to compare the prion protein structures before (PrP^{C}) and after acid-induced conversion (PrP^{β}), in order to get insights into the conformational changes that occur during this conversion, as well as to characterize the structure of PrP^{β} aggregates.

Several examples of using single structural-proteomics methods to study prion proteins have recently been reported. Limited proteolysis using proteinase K has been used for the characterization of the fibrillar PrP^{Sc} form of prions (212). Differential surface modification studies, using nitration and acetylation, have also recently been reported (25,316). Methionine oxidation of PrP^{C} by hydrogen peroxide has also been successfully assessed (317). Two crosslinking studies have been attempted, using BS3 (226) and using EDC (332). Several bottom-up hydrogen/deuterium exchange studies on prions have also been reported (26,229,230,321).

Combining all of these available approaches to obtain structural information for the protein system studied would allow us to compare the findings from each method, cross-validate the results, and solidify the overall conclusions. In this study, I showed that data on the structural differences between the native and the aggregated forms of the prion protein, obtained from multiple structural proteomics approaches, consistently implicates the same regions of the molecule in the conversion process. This confirms that application of these multiple complementary structural proteomics approaches leads to a reliable structural characterization of protein or protein complexes.

3.2. Materials and methods

All chemicals were from Sigma-Aldrich, unless noted otherwise. Native and acid-induced β-oligomeric Syrian hamster 90-232 prion proteins (278) were obtained from

PrioNet's PrP5 facility (University of Alberta, Canada), where we confirmed the structure of the β-oligomeric prion protein by dynamic light scattering, circular dichroism, 1-anilinonapthalene-8-sulfonate fluorescence, the proteinase-K resistance assay, and NMR.

3.2.1. Limited proteolysis

Limited proteolysis was performed using trypsin or pepsin. The cleaved proteins were separated by SDS-PAGE, and individual bands, corresponding to the proteolytic products of the prion proteins, were excised and identified by trypsin in-gel digestion, followed by MALDI-MS and MALDI-MS/MS analysis of the tryptic peptides. A 35-μg aliquot of each PrP^{C} and PrP^{β} protein was incubated with each enzyme at 1:50 enzyme to substrate ratios at 37 °C in PBS pH 7.4, or in 0.1% acetic acid pH 4.0 for trypsin and pepsin analyses, respectively. Aliquots were taken at 1, 5, 10, 20, and 30 min and were immediately mixed with NuPage lithium dodecyl sulfate (LDS) Sample Buffer 4× (Invitrogen) and stored at -80 °C prior to SDS-PAGE separation. The sites of the limited-proteolysis cleavage were determined from the sequences of the tryptic peptides in the in-gel digests.

3.2.2. Surface modification

PrP^{C} and PrP^{β} proteins were modified with either the light or the heavy forms of the isotopically-coded reagent, pyridine carboxylic acid N-hydroxysulfosuccinimide ester (PCASS-H4,-D4) (Creative Molecules Inc.) for 30 min at 25 °C in PBS pH 7.4. Reaction mixtures were quenched with 50 mM ammonium bicarbonate for 30 min at 25 °C, acidified with 10% acetic acid, combined in 1:1 ratio, and digested with pepsin at a 1:10 enzyme:substrate ratio. The digested peptides were separated by nano-flow reversed-phase HPLC on an Ultimate nano-LC system (LC Packings), equipped with an LC Packings 0.3×5 mm C18 PepMap guard column (5 μm particle size, 100 Å pore size), and a 75 μm×15 cm capillary column packed in-house with Magic C18 Aq (Michrom Bioresources Inc.) particles (5 μm, 100 Å). This capillary LC system was operated at a flow rate of 300 nL/min, using a 55-minute gradient from 5 to 60% acetonitrile (0.1% TFA). The column effluent was spotted at one minute intervals (300 nL/spot) onto a stainless steel MALDI target using a Shimadzu spotter. The spots were dried, overlaid with 0.7 μL of a 4 mg/mL solution of α-cyano-4-hydroxycinnamic acid matrix solution in

0.1% TFA/50% acetonitrile, and analyzed by MALDI-MS using a 4800 MALDI-TOF/TOF (AB SCIEX). MS/MS spectra were acquired using "CID off", 50 FWHM gate width, and a 1 kV MSMS method. In cases where additional fragmentation was needed MALDI-MS/MS was used to give unambiguous assignments -- i.e., additional spectra were acquired using "CID on", and a 2-kV MSMS method.

Mass spectra from each chromatographic fraction were searched for nondeuterated/deuterated (D0/D4) doublets of signals that indicate modification of the peptides with PCASS, using the DX program of the ICC-CLASS software package (Creative Molecules Inc.) (344), with peak intensity cutoff of 50 and a mass tolerance of 0.01 Da for the 4.02508 Da mass difference between the masses of the light and heavy isotopic forms. The modification sites were confirmed by MALDI-MS/MS analysis. MS/MS spectra were assigned using the DXMSMS module of the ICC-CLASS program, with searches limited to dead-ends, no restriction on digestion sites, a user-defined mass increment (Mip mass) of 86.02 Da resulting from the modification, and KYST as allowed modification sites. Specific differences in amino acid residue reactivities were determined based on the ratios of signal intensities for the light and heavy forms of the PCASS-modified peptides from the PrP^{C} and PrP^{β} proteins, respectively.

3.2.3. Hydrogen/Deuterium Exchange

Hydrogen/deuterium exchange experiments were carried out under "exchange-in" conditions, using a two-stage continuous flow mixer, as described previously (325). Briefly, protein solution and D_2O from separate syringes were continuously mixed in 1:4 ratio (80% D_2O final) via a three-way tee which was connected to a 100 μm × 21 cm capillary, providing a labeling time of 10 seconds. The outflow from this capillary was mixed with a quenching solution containing 0.4% formic acid in 80% D_2O from third syringe via a second three-way tee, and injected into a Bruker 12 T Apex-Qe hybrid Fourier Transform mass spectrometer, equipped with an Apollo II electrospray source. In-cell ECD fragmentation experiments were performed with an m/z 900–1200 precursor selection range using a cathode filament current of 1.2 A and a grid potential of 12 V. Approximately 1200 scans were accumulated over the m/z range 250–2600, corresponding to an acquisition time of approximately 30 min for each ECD spectrum. FT-MS calibration was performed using the ECD fragments of PrP^{C}. Deuteration levels

of the amino acid residues' amide groups were determined from centroid masses of the c- and z-ion series (325).

3.2.4. Crosslinking

Crosslinking analysis was performed using the isotopically coded CID-cleavable affinity-purifiable crosslinker, CBDPS-H8/D8 (Creative Molecules Inc.), and proteinase K digestion, as described previously (see Chapter 2. Use of Proteinase K non-specific digestion for selective and comprehensive identification of inter-peptide crosslinks: Application to prion proteins) (301). Briefly, protein samples were crosslinked with 0.05 mM CBDPS-H8/D8 in PBS, the pH was adjusted to 8.0 by the addition of 0.2 M Na_2HPO_4, and the samples were incubated for 30 min at 25 °C. The reaction mixtures were quenched with 50 mM ammonium bicarbonate for 30 min at 25 °C and the crosslinked proteins were digested with proteinase K for 2.5 h at 37 °C at a 1:1 (w:w) enzyme:substrate ratio. Proteinase K was inhibited by the addition of protease inhibitor cocktail (Sigma-Aldrich, P8465) and the crosslinked peptides were enriched on monomeric avidin beads (Thermo). The crosslinks were eluted from the avidin beads with 0.1% TFA 50% acetonitrile, concentrated by lyophilization, and analyzed by LC-MALDI MS and MALDI-MS/MS as described above.

3.3. Results and discussion

The goal of this study was to characterize the structural differences between the two prion protein isoforms, PrP^C and PrP^β, using an array of structural proteomics techniques, including limited proteolysis, surface modification, hydrogen deuterium exchange, and crosslinking. Each method provides unique residue-specific information for the different forms of the protein, and combining the results of the studies on both PrP^C and PrP^β should therefore shed light on the mechanisms of the structural changes which occur during the prion protein conversion.

3.3.1. Limited Proteolysis

Limited proteolysis provides information on the protein's surface accessibility to a large probe, in this case, an enzyme. The method is based on short controlled exposures of the protein to a proteolytic enzyme. The first cleavage of the protein occurs while the overall structure of the protein should still be preserved; thus, these cleavage sites should

be restricted to the outermost regions of the protein surfaces which are accessible to the active site of the proteolytic enzyme. Because most enzymes are medium-sized globular proteins with molecular weights of at least 15–20 kDa, location of the cleavage sites thus reflects the accessibility of these sites to a nearly spherical probe whose diameter corresponds to the size of the enzyme used.

Limited proteolysis of PrP^{C} and PrP^{β} proteins with trypsin showed similar patterns for both samples with less cleavage at the K110 site for PrP^{β} (i.e., a different pattern of bands 1 and 2, Figure 23A). The increased accumulation of the aa84-232 product in the case of PrP^{β}, results from poorer access of the trypsin to the K110 cleavage site and may be an indication of involvement of this region in intra- and/or inter-protein interactions.

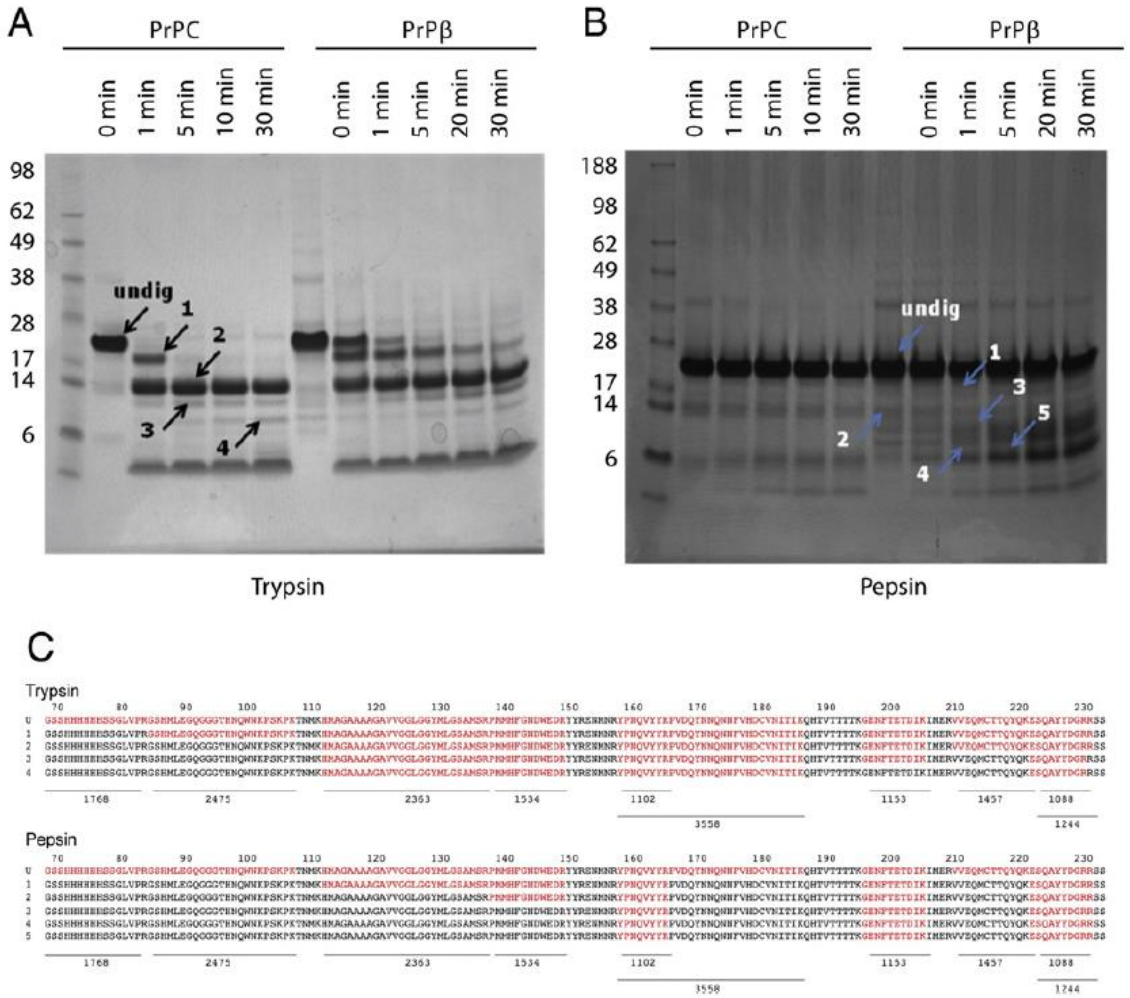

Figure 23: Limited proteolysis analysis of the native and oligomeric Syrian hamster aa90–232 prion proteins.

Native PrP^{C} and PrP^{β} proteins were digested with trypsin (A) or pepsin (B) at 37 °C. Aliquots were taken at the indicated time points, and were separated by SDS-PAGE. The gel was stained with Coomassie blue, and the marked bands were excised for trypsin in-gel digestion and peptide identification by MALDI-MS and MALDI-MS/MS. An aliquot of the reaction mixture was taken before protease addition, and is indicated as "undig". C. Peptides which were identified for each band are shown in red in panels A and B; tryptic peptides are underlined and marked with the corresponding m/z values. Reprinted from Serpa et al. (22).

Both prion isoforms are characterized by a noticeable formation of the residue aa110–232 product (band 2, Figure 23A), which is resistant to tryptic digestion. This indicates protection of the R148, R151, and R156 sites in both forms of the protein. It may indicate the potential of this region to be involved in intra-protein (PrP^{C}) and/or inter-protein (PrP^{β}) interactions. There are no tryptic cleavage sites in the residues aa111–148 portion of the sequence, however, so it is not possible to estimate the accessibility to trypsin of this portion of the protein chain by this method. I had recently shown, based on crosslinking data, that the N-terminal portion (residues aa68–126) of PrP^{C} interacts with the C-terminal portion of H2 (residues aa183–194), the loop between H2 and H3 (residues aa195–202), and the H1 -H3 interface (see Chapter 2. Use of Proteinase K non-specific digestion for selective and comprehensive identification of inter-peptide crosslinks: Application to prion proteins) (301). Residues R148 and R151 are located in the middle of H1, and R156 is located at the C-terminal end of H1. Although the N-terminal region of the PrP^{C} is considered to be a flexible disordered part of the protein (362), it may possibly contribute to the protection of the H1–H3 interface from tryptic cleavage.

Limited-proteolysis experiments with pepsin have shown differential accumulation of products resulting from cleavage in the residues aa149–156 region (bands 3, 4, 5, Figure 23B) of the protein, which corresponds to the C-terminal portion of the amphipathic helix 1. Pepsin is an enzyme which has a substrate preference for hydrophobic residues. Pepsin cleavage at sites within the residue aa149–156 region of PrP^{β} but not PrP^{C} indicates increased exposure of the hydrophobic residues in this region in PrP^{β}. These changes indicate unfolding or rearrangement of this region during the PrP^{C} to PrP^{β} conversion process.

3.3.2. Surface Modification

Surface chemical modification provides information similar to that obtained by limited proteolysis, but in this case the accessibility is to a small hydrophilic probe (a modification reagent) instead of a large probe (an enzyme). By identifying the specific modification sites, chemical modification with water-soluble reagents allows one to determine which functional groups on which specific amino acids are on the protein surface and are exposed to the solvent.

I performed differential surface chemical modification of PrP^{C} and PrP^{β} using the isotopically-coded water-soluble amine-reactive reagent PCASS-H4/-D4. Isotopic coding allowed us to quantitatively determine differences in specific amino acid reactivities between the two forms of the prion protein (Figure 24A). Each form of the protein was modified with either the light or the heavy isotopic forms of the reagent, the reaction mixtures were quenched, combined in a 1:1 equimolar ratio, digested with pepsin, and the digests were analyzed by MALDI LC-MS/MS. Differences in residue reactivities between the two prion isoforms can be determined from the ratios of the signal intensities of the light (H4) and heavy (D4) forms of the modified peptides. These ratios can be translated into the surface accessibilities of functional groups on each residue to a small water-soluble modification reagent.

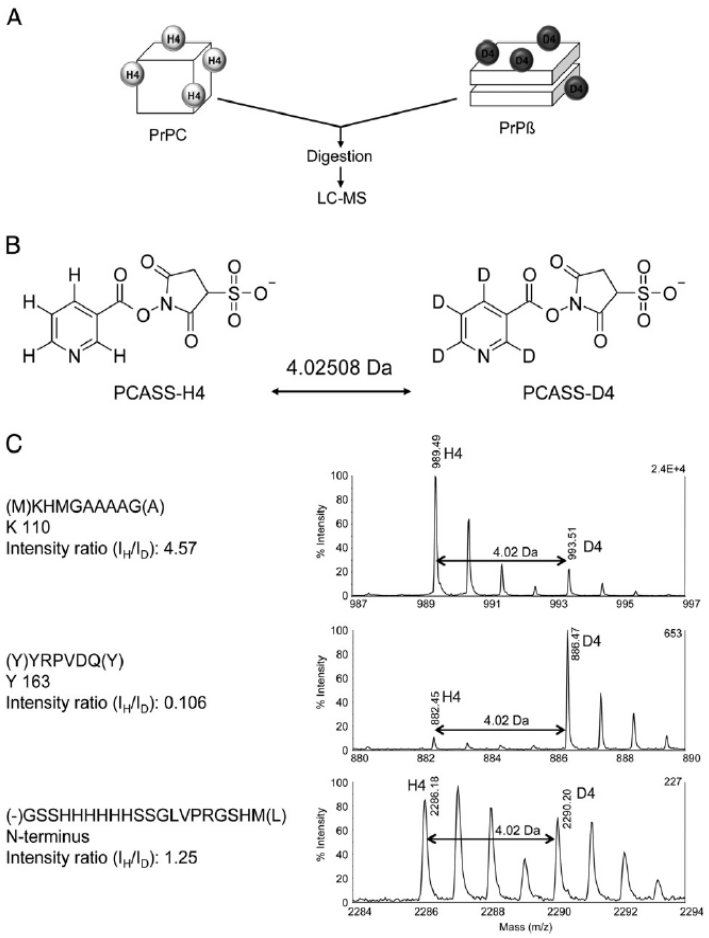

Figure 24: Differential surface modification analysis of the PrP^{C} and PrP^{β}.

A. Scheme of the differential surface modification analysis, using isotopically-coded modification reagents. Each form of protein is modified with light or heavy isotopic forms of the reagent. Reaction mixtures are quenched, combined in a 1:1 ratio, and digested with pepsin, and digests are analyzed by LC-MS/MS. B. Structure of the PCASS-H4/-D4 reagent. The fairly small size and the water-soluble property of the reagent ensures reaction with only surface-exposed functional groups of the proteins. C. Representative MS spectra of peptides containing differentially-modified residues. Using the H4 and D4 forms of the reagent leads to a specific isotopic signature for the modified peptides in the mass spectrum: a doublet of signals separated by 4.03 Da (the mass difference between four hydrogen and four deuterium atoms). Isotopic coding provides a relative quantitation of the differential residues' reactivities and therefore provides a quantitative measurement of the residue's accessibilities to a small probe (modification reagent) via the ratios of the intensities of the light and heavy forms of the peptides. Reprinted from Serpa et al. (22).

To ensure the hydrophilicity of the modification reagent, I used the sulfated form of the NHS-ester, which is fully ionized over a wide pH range (Figure 24B). The reactivity of NHS esters is mainly directed towards the amino groups of the N-termini and K, but also can include hydroxyl groups of Y, S, and T residues. Surface accessibility of the latter residues is particularly of interest, as they can be buried as well as surface-exposed. To prevent hydrolysis of these PCASS-modified residues, I performed the pepsin digestion at low pH.

Differential modification of multiple residues in both the PrP^{C} and PrP^{β} forms of protein was detected (Table 6, Figure 24C). Approximately equal intensities of light and heavy signals for the N-terminal peptide, modified at the α-amino group of the N-terminus, were used as an internal control for both reactions. Several tyrosine residues were preferentially modified in the PrP^{β} form: Y128, Y149, Y150, Y157, Y163, and Y169. Modification of Y149 and Y150, found exclusively in the PrP^{β} form, was also found in the tyrosine nitration experiments (316). All of these residues are buried in the native PrP^{C} structure and are located on the interface between helix1–beta sheet 2 (H1–β2) and the helix 2 -helix 3 (H2–H3) core of the molecule. Interestingly, Y163 and Y169, which are preferentially modified in PrP^{β} form, are located on a "rigid loop" between β2 and H2 (residues aa163–172), which has been shown to be a primary epitope for oligomer-specific antibodies (240). This implies that these residues are located on the surface of the protein in the PrP^{β} form, but not in the PrP^{C} form.

m/z H form	m/z D form	Intensity H form	Intensity D form	Δ	RT	Res start	Res end	Sequence	Modified residue	Modified residue number	H/D Intensity ratio
1521.72	1525.74	81	85	−0.0014	8	68	80	(–)GSSHHHHHHSSGL(M)	G	68	0.95
2155.10	2159.13	258	173	0.0052	13	68	86	(–)GSSHHHHHHSSGLVPRGSH(M)	G	68	1.49
2286.18	2290.20	199	158	−0.0080	17	68	87	(–)GSSHHHHHHSSGLVPRGSHM(L)	G	68	1.26
2514.40	2518.42	148	92	−0.0024	36	88	109	(M)LEGQGGGTHNQWNKPSKPKTNM(K)	K	106	1.61
757.28	765.34	367	186	0.0055	19	81	86	(L)VPRGSH(M)	S	85	1.97
861.41	865.43	680	235	−0.0047	8	110	117	(M)KHMAGAAA(A)	K	110	2.89
932.47	936.49	1243	741	−0.0052	11	110	118	(M)KHMAGAAAA(G)	K	110	1.68
989.49	993.51	22,789	4985	−0.0031	9	110	119	(M)KHMAGAAAAG(A)	K	110	4.57
1060.53	1064.55	4084	523	−0.0024	12	110	120	(M)KHMAGAAAAGA(V)	K	110	7.81
746.22	750.25	72	124	0.0071	35	128	133	(G)YMLGSA(M)	Y	128	0.58
897.38	901.41	390	1014	−0.0009	19	120	128	(G)AVVGGLGGY(M)	Y	128	0.38
1015.46	1019.48	148	60	−0.0028	21	132	139	(G)SAMSRPMM(H)	S	132	2.47
1296.60	1300.64	1582	558	0.0129	36	135	144	(M)SRPMMHFGND(W)	S	135	2.84
1427.65	1431.67	292	96	−0.0059	36	134	144	(A)MSRPMMHFGND(W)	S	135	3.04
873.29	877.31	435	1764	−0.0088	13	145	149	(D)WEDRY(Y)	Y	149	0.25
817.22	821.24	83	234	−0.0076	35	150	154	(Y)YRENM(N)	Y	150	0.35
896.43	900.45	182	1465	0.0003	14	155	160	(M)NRYPNQ(V)	Y	157	0.12
1144.59	1148.61	125	1368	0.0085	28	161	168	(Q)VYYRPVDQ(Y)	Y	162	0.09
882.44	886.47	65	613	0.0008	16	163	168	(Y)YRPVDQ(Y)	Y	163	0.11
1045.41	1049.44	93	1180	−0.0044	27	162	168	(V)YYRPVDQ(Y)	Y	163	0.08
1045.35	1049.37	122	1603	0.0009	30	163	169	(Y)YRPVDQY(N)	Y	163	0.08
1208.37	1212.40	460	3040	0.0048	32	162	169	(V)YYRPVDQY(N)	Y	169	0.15
1307.42	1311.45	342	713	0.0088	36	161	169	(Q)VYYRPVDQY(N)	Y	169	0.48
931.52	935.54	2815	522	0.0005	8	184	190	(T)IKQHTVT(T)	K	185	5.39
958.45	962.46	563	249	−0.0122	7	218	224	(Q)YQKESQA(Y)	K	220	2.26
1108.53	1112.56	1577	368	0.0024	16	225	232	(A)YYDGRRSS(–)	Y	225,226	4.29
945.45	949.47	565	180	−0.0042	7	226	232	(Y)YDGRRSS(–)	Y	226	3.14
1108.52	1112.55	12,838	4974	−0.0006	11	225	232	(A)YYDGRRSS(–)	S	231,232	2.58

Table 6: Differential chemical surface modification of the PrP^C and PrP^β with PCASS-H4/-D4.

PrP^C and PrP^β were modified with light or heavy isotopic forms of the reagent, respectively. The reaction mixtures were quenched, combined, and digested with pepsin, and the digests (combined in a 1:1 ratio) were analyzed by MALDI LC-MS. PCASS-H4/-D4 modified peptides which had H4/D4 intensity ratios of >2 and or <0.5 were considered to correspond to differentially-modified residues in PrP^C and PrP^β, respectively. Δ=m/z D4–m/z H4−4.02508. Reprinted from Serpa et al. (22).

A number of residues were preferentially modified in the PrP^C form: K110 (located on N-terminal portion of the protein), S132, S135, (located on the β1–H1 loop, residues 128–142), and K220, Y225, Y226, and S231 on the C-terminal portion of H3 (residues 200–232). Preferential modification of the Y225 and Y226 in PrP^C was also in agreement with previously-reported tyrosine nitration experiments on oligomers and fibrils (25,316). Changes in reactivities for these residues, as a result of PrP^C to PrP^β conversion, may indicate involvement of these regions in new intra- and/or inter-protein interactions within β-oligomers.

3.3.3. Hydrogen/Deuterium Exchange

The hydrogen/deuterium (H/D) exchange method is based on the principle that backbone hydrogens can be exchanged with deuterium upon exposure of a protein to a D_2O-based buffer. The exchange rates at individual peptide-bond amides are dependent on the protein's structural context (318-320). Tightly hydrogen-bonded segments

undergo very slow exchange, while disordered regions exchange much more rapidly. Thus, this approach can provide information on an amino acid residue's hydrogen bonding, which in turn may reflect involvement in secondary structure motifs and/or exposure to the solvent.

Hydrogen/deuterium exchange experiments were performed using top-down ECD-FTICR mass spectrometry (325,326). This approach relies on the rapid scrambling-free fragmentation of the intact protein by ECD. The deuteration level of each amino acid residue then can be deduced from the c- and z-ion series produced. A protein solution is continuously mixed in a capillary — first with D_2O, then with an acidic quenching solution, and then the solution is directly infused into the mass spectrometer. In this analytical format, higher deuteration levels would reflect less protection of the amide protons and disruption of hydrogen bonding due to loss of secondary structure. Using 10-second exchange times, I have determined that approximately 38 amides are protected in PrP^C, while only 23 are protected in the oligomer (Figure 25). In other words, approximately 15 amides become unprotected as PrP changes from the monomer to oligomer, which indicates that a significant conformational change occurs during this process.

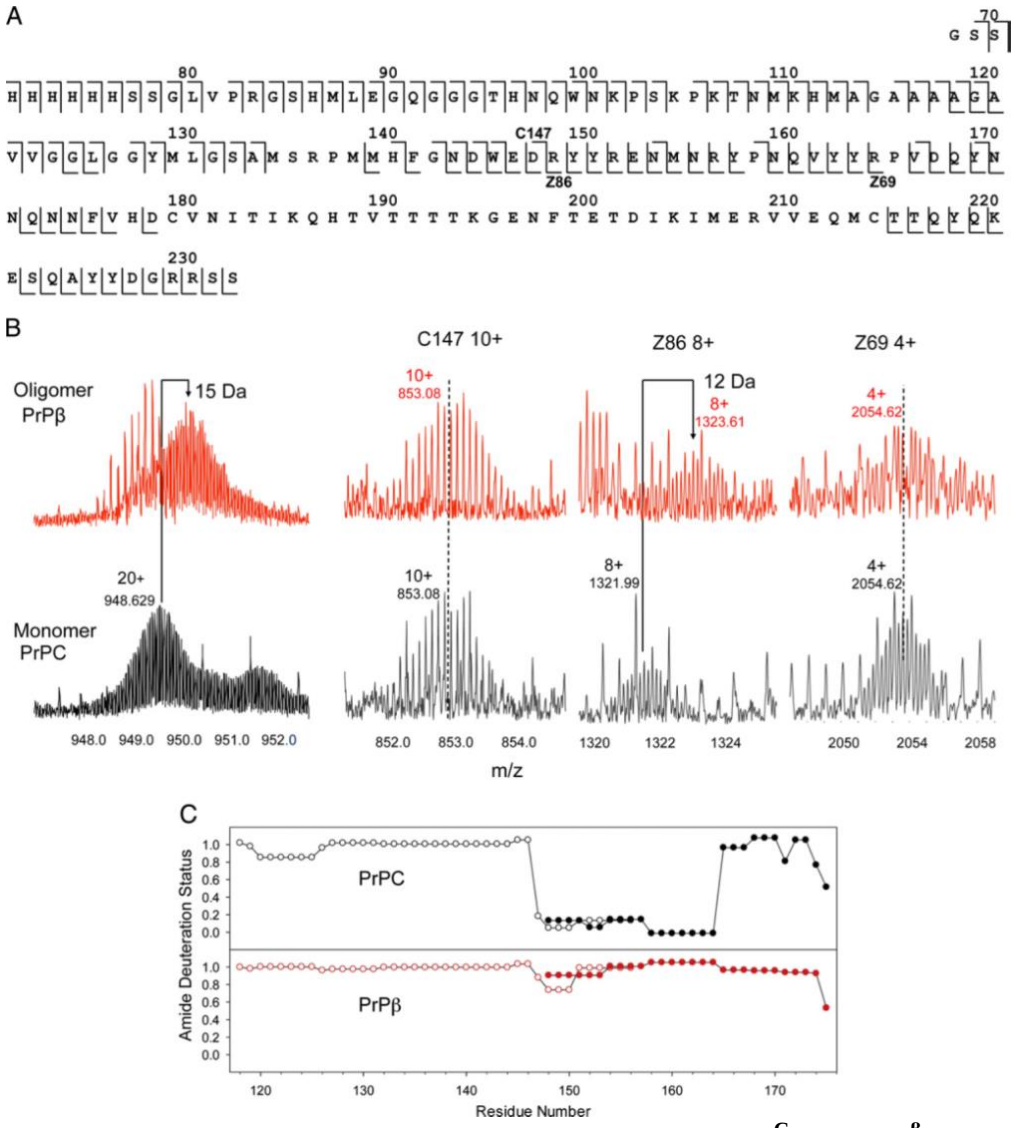

Figure 25: Hydrogen/deuterium exchange analysis of PrP^{C} and PrP^{β} by ECD-FTICR-MS.

A. Sequence coverage of the Syrian hamster $PrP_{90–232}$ by top-down ECD FTICR MS/MS. B. Different hydrogen/deuterium exchange patterns, observed for the PrP^{C} (black) and PrP^{β} (red) forms. Representative c- and z-ions series, observed for PrP^{C} and PrP^{β}, indicate that there is no significant difference in H-to-D exchange within the N- and C-terminal regions. However, there is a significant difference in exchange for fragments from the aa148–164 regions. C. Deuteration plot of the PrP^{C} and PrP^{β} residues. Reprinted from Serpa et al. (22).

Analysis of the deuteration status of the c- and z- fragment-ion series using a previously-developed strategy (325) allowed us to localize the region of major differences in the protection to residues aa148–164 (Figure 25C), which is the stretch of

the protein sequence encompassing H1–β2 residues aa148–164. Hydrogen/deuterium exchange deprotection of this region would indicate a loss of the secondary structure (i.e., the melting of helix 1, disassembly of the β-sheet involving the β2 strand) and/or disruption of the H1–β2/H2–H3 interface).

3.3.4. Crosslinking

Crosslinking analysis provides the distance between two crosslinked amino acid residues. The basis of this method is a chemical reaction of the crosslinking reagent with functional groups on a protein, leading to the formation of a covalent bond between two amino acid residues of the protein. The distance between the two crosslinked sites is determined by the length of the spacer in the crosslinking reagent. Thus, identification of the crosslinked sites on a protein or a protein complex provides spatial information and distance constraints for the two amino acid residues that are crosslinked.

I performed crosslinking experiments using our recently developed isotopically-coded CID-cleavable affinity-purifiable amine-reactive crosslinker CBDPS-H8/D8 (342), combined with proteinase K digestion (see Chapter 2. Use of Proteinase K non-specific digestion for selective and comprehensive identification of inter-peptide crosslinks: Application to prion proteins) (301). This approach allows robust identification of the inter-peptide crosslinks in the prion protein, which has only a few tryptic cleavage sites and where the aggregated forms are resistant to enzymatic digestion by high-specificity enzymes. Proteins were crosslinked with CBDPS-H8/D8, digested, and the crosslinks were affinity purified with immobilized avidin. These crosslinks were then identified by LC-MALDI MS and LC-MALDI MS/MS (342). We were able to detect and identify numerous crosslinks, some of which were preferentially found in either the PrP^{C} or PrP^{β} forms of the protein (Figure 26, Figure 27, Figure 28).

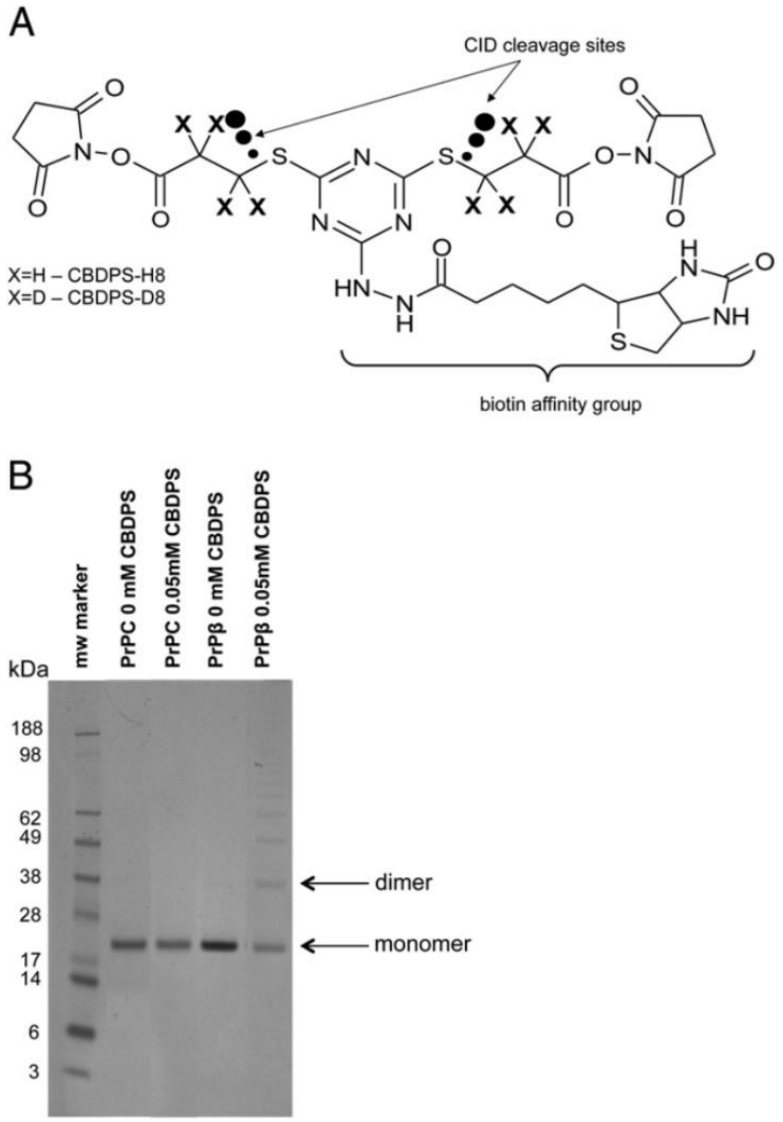

Figure 26: Differential crosslinking analysis of PrP^{C} and PrP^{β}.
A. CBDPS structure of PrP^{C} and PrP^{β} crosslinking reactions. PrP^{C} and PrP^{β} were crosslinked with 0.05 mM of CBDPS for 30 minutes. Reactions were quenched with ammonium bicarbonate and submitted to SDS-PAGE. Inter-protein crosslinked species were observed only for the PrP^{β} sample. Reprinted from Serpa et al. (22).

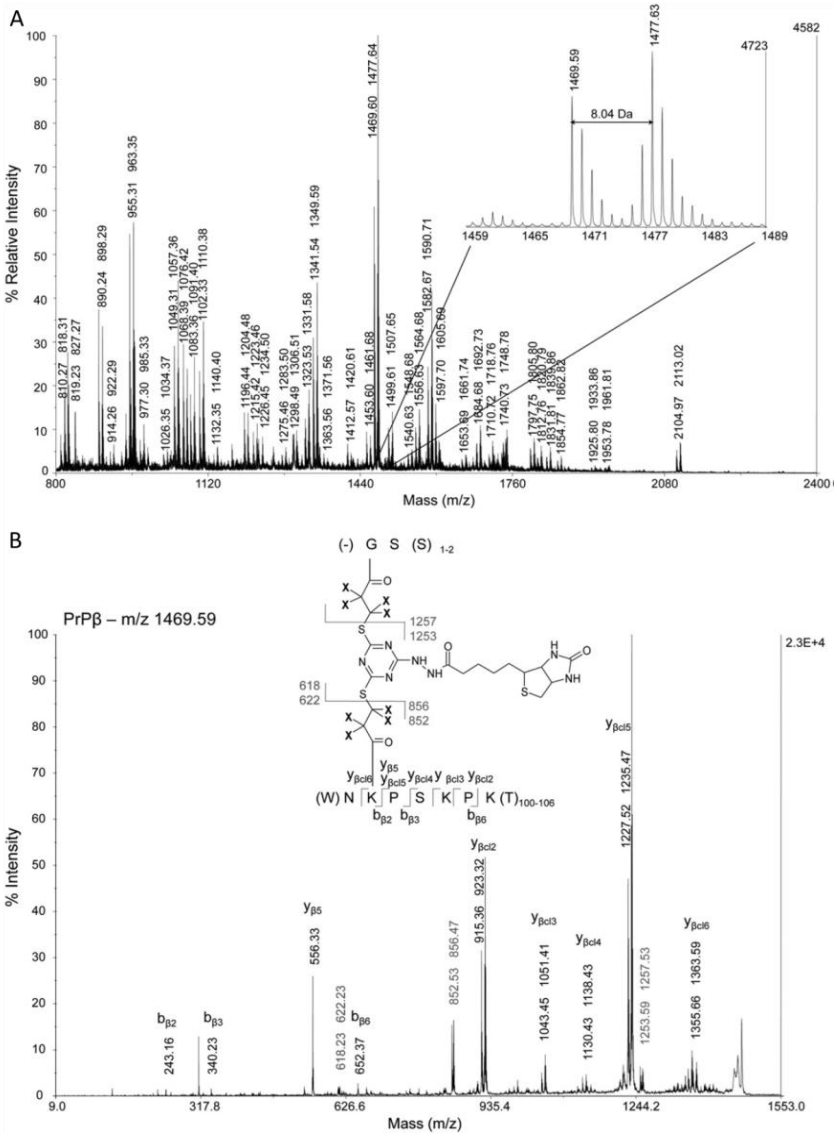

Figure 27: Differential crosslinking analysis of PrP^{C} and PrP^{β}.
A. MALDI-MS spectrum of peptides in a HPLC fraction from a proteinase K digest of the β-oligomeric sample crosslinked with equimolar ratio of CBDPS-H8/D8. The crosslinks were affinity purified with immobilized avidin, separated by HPLC, and analyzed by MALDI-MS and MS/MS. Inset: a differential crosslink, present only in the β-oligomer sample. B. MS/MS spectrum of the m/z 1469 crosslink identified as a G68-K101 inter-peptide crosslink. Reprinted from Serpa et al. (22).

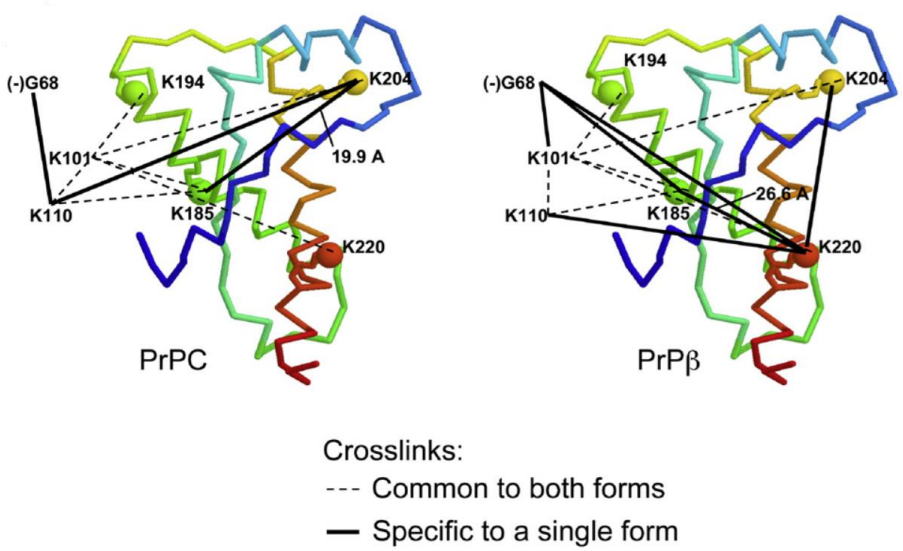

Figure 28: Differential crosslinking analysis of PrP^{C} and PrP^{β}. Structure of the native form of the $PrP_{90–231}$ showing differential inter-lysine residues crosslinks. Several crosslinks are not compatible with the structure of the native form, suggesting a conformational change in PrP^{β}. Reprinted from Serpa et al. (22).

Homo-oligomerization of the PrP^{β} adds another level of complexity to the interpretation of this crosslinking data, as we cannot determine whether some of the inter-peptide crosslinks in this approach are intra-protein or inter-protein in origin. To address this issue, the Borchers lab is in the process of analyzing the individual species of crosslinked prion proteins (the PrP^{C} monomer, the PrP^{β} monomer, and the PrP^{β} dimer) after separation by SDS-PAGE, using both in-gel digestion after gel fixing (376) and out-gel digestion, where the proteins are digested in solution after diffusion out of an unfixed gel (343). Crosslinks that are observed in the PrP^{β} dimer band, but not in the PrP^{β} monomer band, are considered to be inter-protein crosslinks. Further experiments have also been performed using metabolically ^{15}N-labeled prion protein to assist in distinguishing between inter- and intra-protein crosslinks (see Chapter 5. Structure of prion β-oligomers as determined by structural proteomics with crosslinking constraint-guided molecular dynamic simulations.

Analysis of the crosslinked sites has already revealed that some of the crosslinks which were observed in PrP^{β}, are not compatible with the NMR structure of PrP^{C} (377), implying that a conformational change or formation of new inter-protein contacts are taking place in PrP^{β}. Specifically, the K185–K220 crosslink is incompatible with the

crystal structure of PrP^C and would have to transverse the protein globule if it were in its native conformation. This crosslink was detected only in the PrP^β dimer band and, therefore, most likely represents an inter-protein contact, newly-formed in the PrPβ oligomer. Similarly, the K204–K220 crosslink, which was detected only in the monomer and the dimer PrP^β bands, is also incompatible with the native structure of PrP^C, as the crosslinker would have to travel through the β1–H1 loop in order to connect those residues. Rearrangement of this region, however, would open up the protein and would provide the space needed for the formation of this crosslink.

3.3.5. Interpretation of results from the multiple structural proteomic approaches

Limited proteolysis with trypsin showed increased protection of the K110 cleavage site in PrP^β compared to PrP^C. The accessibility of K110 to a small probe, as found in the chemical surface modification experiments, was also lower in PrP^β than in PrP^C. Limited proteolysis experiments using pepsin showed increased cleavage at sites in the aa149 to aa156 regions of PrP^β, but not PrP^C, indicating increased exposure of the hydrophobic residues in this region. The increased modification of residues on the H1–β2/H2–H3 interface (Y128, Y149, Y150, Y157, Y163, and Y169) in PrP^β as compared to PrP^C, also suggests a conformational change/rearrangement of this same region. These surface modification and limited proteolysis results are also in agreement with the results from the hydrogen/deuterium exchange experiments, where a major decrease in the protection of aa148 to aa164 (the sequence encompassing H1–β2) was found. These results are also in agreement with the enzymatic-digestion-based bottom-up hydrogen/deuterium exchange results reported previously (26). Crosslinking experiments also indicate rearrangement of this region, as the observed K185–K220 and K204–K220 crosslinks are incompatible with the structure of PrP^C.

To summarize, the combined analysis of the results from these different approaches gives remarkably consistent results (Figure 29). All the methods point to a rearrangement of the H1–β2/H2–H3 interface as the major structural difference between PrP^C and PrP^β. A conformational change in the H1–β2-rigid loop region and distortion of its contact with helices 2 and 3 would create new hydrophobic patches on the surface of the molecule, which, in turn, could be responsible for driving the aggregation process.

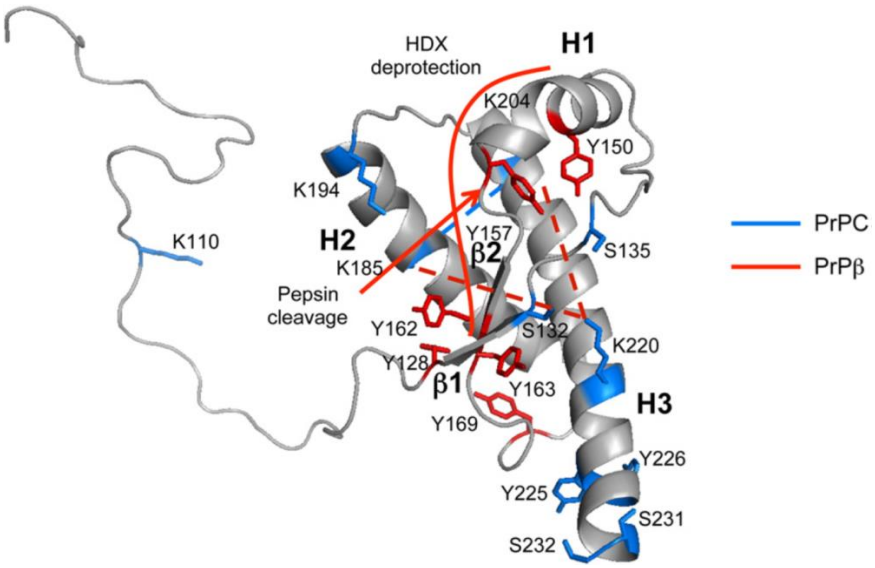

Figure 29: Summary of the structural differences between PrP^{C} and PrP^{β}, as revealed by structural proteomics methods.
The structure of the native form of ShPrP $_{90–232}$ (PDB 1B10) was used, with the addition of N-terminal residues aa68–124. The residues, which are preferentially modified or crosslinked in the native PrP^{C} and oligomeric PrP^{β} samples, are highlighted in blue and red, respectively. The preferential pepsin cleavage site for PrP^{β} is indicated by a red arrow. The region of the structure which loses protection from hydrogen/deuterium exchange in the PrP^{β} sample is indicated by the red arc. The K185–K204, K185–K220 and K204–K220 CBDPS crosslinks (red dashed lines) are present only in the oligomeric PrP^{β} sample. The K185–K220 and K204–K220 crosslinks are incompatible with the native PrP^{C} structure, which suggests a possible conformational change in the PrP^{β} aggregated form of the protein. The data from multiple approaches collectively suggests rearrangement of the β1–H1–β2–H2 region in the PrP^{β}. Reprinted from Serpa et al. (22).

3.4. Conclusion

Overall, this study illustrates and validates the usefulness of applying the entire available arsenal of structural proteomics methods for the characterization of conformational changes. We believe that accumulation of numerous structural constraints from these multiple approaches will allow to unequivocally solve the structure of prion aggregates.

I have applied a combination of the limited proteolysis, surface modification, hydrogen/deuterium exchange, and crosslinking to the differential characterization of the native PrP^{C} and the acid-induced oligomeric PrP^{β} forms of the prion protein. The results

obtained from these multiple structural proteomics approaches are in agreement with each other and indicate a rearrangement of the H1–β2-rigid loop region of the protein as the major structural difference between these two forms of the prion protein. Application of these multiple structural proteomics approaches, each of which provides unique structural information on the protein system studied, supports the findings of each method and validates the overall conclusions on the structural changes involved in the conversion of the native PrP^{C} to the acid-induced aggregated PrP^{β} form of the prion protein.

The combination of structural proteomic methods provided rich structural information on acid-induced PrP^{β}. Based on the successful implementation of this combined approach, I sought to increase the amino acid residue repertoire that could be used for surface modification experiments (see Chapter 4: Using isotopically-coded hydrogen peroxide as a surface modification reagent for the structural characterization of prion protein aggregates) and applied all methods to the structural study of urea-acid induced PrP^{β} oligomers (see Chapter 5. Structure of prion β-oligomers as determined by structural proteomics with crosslinking constraint-guided molecular dynamic simulations).

Chapter 4: Using isotopically-coded hydrogen peroxide as a surface modification reagent for the structural characterization of prion protein aggregates

Work in this chapter was a collaborative effort involving two laboratories. Native (PrP^C) and acid-induced oligomeric (PrP^β) prion protein was recombinantly expressed and purified in the laboratory of Dr. David Wishart in the Prion Protein and Plasmid Production Platform Facility (PrP5) (University of Alberta, Edmonton, AB, Canada), and supplied to the Borchers lab at University of Victoria as PrP^C and PrP^β stock solutions. Experimental design was performed by Jason Serpa, Evgeniy Petrotchenko, and Christoph Borchers. Comparative ratio formulas were derived by Evgeniy Petrotchenko. Software to extract isotopic cluster information was created by Karl Makepeace. LC-ESI-MSMS data analysis and experimentation for surface modification and crosslinking was done by Jason Serpa and Tristan Borchers. Christoph Borchers oversaw the project.

This chapter was adapted in part from the publication (302):

Serpa JJ, Makepeace KAT, Borchers TH, Wishart DS, Petrotchenko EV, Borchers CH. 2013. ***Using Isotopically-Coded Hydrogen Peroxide as a Surface Modification Reagent for the Structural Characterization of Prion Protein Aggregates*****. Journal of Proteomics.**

4.1. Introduction

Chemical surface modification of the protein surface allows the determination of the regions of the proteins that are exposed to the solvent. This makes this technique particularly suitable for the characterization of conformational changes in proteins. Identification of the actual modification sites reveals which amino acid residues are on the protein surface and therefore in contact with the solvent. Determining differences in reactivity of amino acid residues between different conformational states of the protein enables localization of regions of protein surfaces that undergo conformational changes during these transitions. Recently, mass spectrometry has become the method of choice for determining the extent of modification of specific amino acid residues in proteins, and the use of the isotopically-coded modification reagents allows the quantitation of the modification yield by mass spectrometry. Using MS, distinct stable isotopic forms of the reagents, which differ in mass, but are otherwise chemically identical, can be used for the comparison of the separate samples. As described in Chapter 3, combining the differentially modified samples allows detection of the reaction products within the same mass spectrum, thus eliminating run-to-run signal variability and providing reliable relative quantitation of the reaction products. Several examples of applying such isotopically-coded chemical surface modification reagents to the study of protein structure with mass spectrometry have recently been reported (22,378).

Oxidation of amino acid residues can be considered as a particular type of surface modification, and different types of oxidation reactions can be used for this purpose. These methods include the use of hydroxyl radicals (·OH) as a covalent labeling agent (379-381) and FPOP (fast photochemical oxidation of proteins) (382,383). H_2O_2 has been successfully used to analyse protein-ligand binding of multi-component protein mixtures (384). H_2O_2 can be used to specifically oxidize methionine residues (317,385) and tryptophan (386,387). In-vitro methionine oxidation studies of PrP^C using hydrogen peroxide have also been performed (317,388-392). I decided to take advantage of the availability of isotopically-coded hydrogen peroxide ($H_2{}^{18}O_2$) in order to perform relative quantitation of the oxidative reaction between two different conformational states of the prion protein, -- i.e., by combining oxidative labeling with isotopic coding of the H_2O_2 reagent. In these experiments, I used the same experimental conditions for oxidation that

were previously used by Requena et al. (317), where the results were verified by CD. Under these experimental conditions, the initial stages of these modification reactions are mainly expected to be captured.

In the case of prion protein, where there are at least two conformationally different states, a comparison of the oxidation levels of specific methionine and tryptophan residues between these states can provide details of their structural differences. However, obtaining an accurate quantitative comparison of amino acid residues oxidation reactivities for different prion forms would be difficult without using isotopically-labeled reagents. To quantify the oxidation levels between two different conformational states of PrP, we therefore used light and heavy isotopic forms of the H_2O_2 reagent ($H_2{}^{16}O_2$ and $H_2{}^{18}O_2$ respectively). Using this approach, I could directly compare the relative reactivities of specific amino acid residues in the PrP^C and the acid-induced $PrP^{ß}$ forms. This, in turn, allowed me to determine changes in the surface exposure of specific methionine and tryptophan residues, and, from these changes, I was able to determine the structural differences between these two prion forms.

4.2. Materials and methods

All chemicals were from Sigma-Aldrich, unless noted otherwise. Native and acid-induced β-oligomeric Syrian hamster 90-232 prion proteins (278) were obtained from PrioNet's PrP5 facility (University of Alberta, Canada).

The model peptide (-)EGFRCHMLPSPTDSNFYR was used to optimize the reaction conditions. PrP^C and $PrP^{β}$ samples were bubbled with nitrogen gas (Figure 30) prior to modification with 10 mM (final concentration) heavy or light H_2O_2. Reactions were performed in triplicate (three replicates with PrP^C +$H_2{}^{16}O_2$ and $PrP^{ß}$ +$H_2{}^{18}O_2$, and three replicates with $PrP^{ß}$ +$H_2{}^{16}O_2$ and PrP^C +$H_2{}^{18}O_2$), at 37 °C for 15 min (Figure 32). Modified PrP^C and $PrP^{β}$ samples were quenched with 150 mM methionine (Figure 31) and combined in a 1:1 molar ratio. Samples were mixed with equal volumes of 8 M urea, bubbled with nitrogen gas, and incubated at 20 °C for 2.5 h. DTT was added to give a final concentration of 10 mM, and the samples were incubated at 37 °C for 30 minutes. Samples were then diluted five-fold with PBS pH 7.4 and digested with trypsin at a 1:1 (w/w) ratio at 37 °C for 6 h. Completeness of digestion was confirmed by SDS-PAGE for all samples. Samples were further reduced by the addition of TCEP to give a final

concentration of 5 mM, and acidified with TFA to give a 0.1% final concentration, prior to LC-ESI-MS and MS/MS analysis.

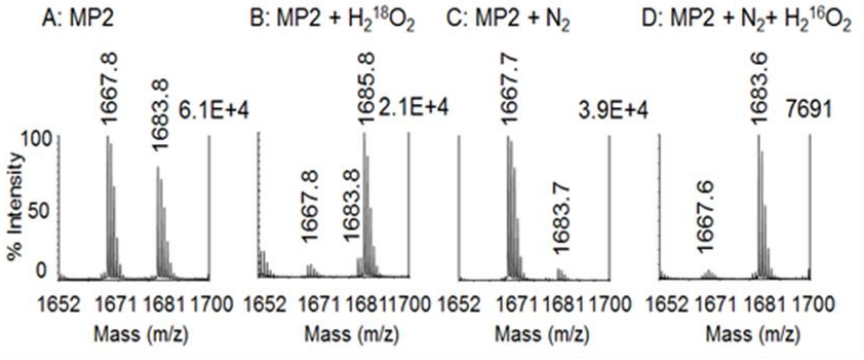

Figure 30: Use of N_2 gas to prevent endogenous oxidation.
A) Model peptide (-)EGFRCHMLPSPTDSNFYR (MP2) 37 ^{o}C 15 min. B) MP2 with 10 mM $H_2{}^{18}O_2$ at 37 ^{o}C 15 min. C) MP2 with N^2 gas at 37^{o}C 15 min. D) MP2 with N_2 gas then 10 mM $H_2{}^{16}O_2$ at 37 ^{o}C 15 min. Reprinted from Serpa et al. (302).

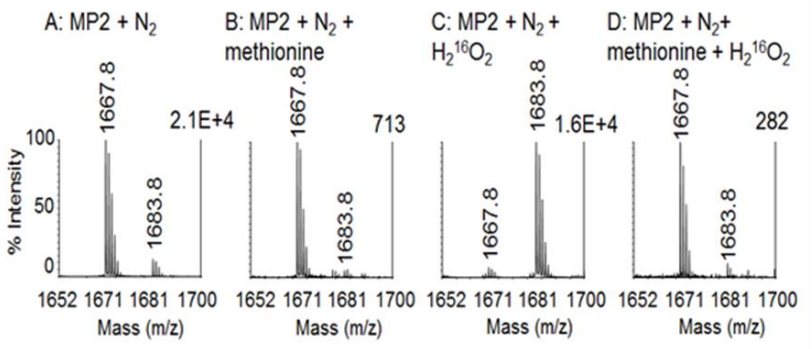

Figure 31: Use of methionine to quench H_2O_2 oxidation.
A) Model peptide (-)EGFRCHMLPSPTDSNFYR (MP2) with N_2 gas at 37 ^{o}C 15 min. B) MP2 with N_2 gas and 150 mM methionine at 37 ^{o}C 15 min. C) MP2 with N_2 gas and 10 mM $H_2{}^{16}O_2$ at 37 ^{o}C 15 min. D) MP2 with N_2 gas, methionine, and 10 mM $H_2{}^{16}O_2$ at 37 ^{o}C 15 min. Reprinted from Serpa et al. (302).

Mass spectrometric analysis was performed with a nano-HPLC system (Easy-nLC II, ThermoFisher Scientific, Bremen, Germany) coupled to the electrospray ionization source of an LTQ Orbitrap Velos mass spectrometer (ThermoFisher Scientific). Samples were injected onto a 100 µm ID, 360 µm OD trap column packed with Magic C18AQ (Bruker-Michrom, Auburn, CA), 100 Å, 5 µm pore size (prepared in-house), and desalted by washing for 15 minutes with 0.1% formic acid (FA). Separations were done on a 75 µm ID, 360 µm OD analytical column packed (in-house) with Magic C18AQ, 100 Å

particle size, 5 μm pore size, and with an IntegraFrit (New Objective Inc. Woburn, MA). The column was equilibrated with 95 % solvent A (2% acetonitrile and 98% water, both containing 0.1% FA) before the peptides were separated with a 60 min acetonitrile:water gradient. The gradient used was 0–60 min: 4–40% B, 60–62 min: 40–80% B, 62–70 min: 80%B, with solvent B containing 90% acetonitrile and 10% water, both containing 0.1% FA.

MS data were acquired in data-dependent MS/MS mode with the six most intense peaks in each full MS scan being selected for fragmentation. Dynamic exclusion was set to 60 s with 2 as the repeat count. MS scans (m/z 400–2000 range) and MS/MS scans were acquired at 60,000 and 30,000 resolution, respectively. MS/MS fragmentation was performed by collision-induced dissociation activation at a normalized collision energy of 35%, and measured in the FT.

Proteome Discoverer (Ver. 1.4.0.288) was used to generate .MGF files from .RAW files. Oxidized peptides were identified with MASCOT using a custom Syrian hamster prion sequence database, with open enzyme cleavage, oxidation of methionine, tryptophan, histidine, and tyrosine residues as variable modifications, a peptide mass tolerance of 8 ppm, MS/MS mass tolerance of 0.03 amu, and instrument set at ESI-TRAP. The list of oxidized peptides identified by MASCOT was compiled for all runs, grouping those peptides with similar retention times and highest MASCOT ion scores. Each modified peptide assignment was verified manually.

For each modified peptide containing one modification from each $PrP^{C} + H_2{}^{16}O_2/PrP^{ß} + H_2{}^{18}O_2$ and $PrP^{\beta} + H_2{}^{16}O_2/PrP^{C} + H_2{}^{18}O_2$ run we used Thermo Xcalibur 2.2 Qual Browser to obtain the MS isotopic cluster. Isotopic distributions of the oxidized peptides were obtained using the MS-Isotope program in Protein Prospector (393). From these isotopic distributions, a ratio of the 3rd isotopic peak versus the 1st isotopic peak was calculated (r_{nat}). The experimental ratios of the 3rd isotopic peak versus the 1st isotopic peak of the labeled and reverse-labeled oxidized peptides ($r_{\beta C}$ and $r_{C\beta}$) were also calculated. Differences in oxidation levels between PrP^{C} and $PrP^{ß}$ samples were determined by comparing ^{18}O oxidation contributions using Equation 2.

$$\frac{(r_{nat}-r_{\beta C}-1)(r_{C\beta}-r_{nat})}{(r_{nat}-r_{C\beta}-1)(r_{\beta C}-r_{nat})}$$

Equation 2: Formula for determination of differences in oxidation levels between PrP^C and $PrP^{ß}$ samples
From the theoretical isotopic distribution patterns of each singly oxidized peptide, a ratio of the 3rd isotopic peak versus the 1st isotopic peak (r_{nat}) is calculated. Ratios of the 3rd isotopic peak versus the 1st isotopic peak of the labeled and reverse-labeled oxidized peptides ($r_{\beta C}$ and $r_{C\beta}$) are also calculated. If samples are mixed in a 1:1 ratio, then peptides with residues having a higher oxidation level in the PrP^C form have values less than 1.0, while residues with higher oxidation levels in $PrP^{ß}$ have values greater than 1.0. Reprinted from Serpa et al. (302).

4.3. Results and discussion

Oxidation of amino acid residues, in particular oxidation of methionine, can occur during the general handling of a protein (394-396), during the electrospray ionization process (397,398) and/or during SDS-PAGE (399,400). With this approach, the background oxidation is superimposed on the oxidation levels created by the modification reactions. The effects of the background oxidation is balanced out by additional experiments where the isotopic forms of H_2O_2 for the modification were reversed, so that the contribution of background oxidation is accounted for.

The calculation of differential oxidation levels could be done in a number of different ways. In the study of protein–ligand binding using labeled hydrogen peroxide, DeArmond et al. (384) quantified the extent of oxidation using a weighted average molecular weight of each oxidized peptide. I tried this method of calculation on a number of PrP^C and $PrP^{ß}$ oxidized residues, and found that the results were comparable with those obtained using the comparative ratio formula presented above.

It has been reported that the methionines in PrP are particularly prone to oxidation (317,392,401), but it has been shown that conditions employed here can be used for PrP studies as the reactions are relatively rapid. It has also been shown that similar reaction conditions result in only minimal conformational change of the prion (317). Furthermore, the use of H_2O_2 without metal results in only one oxidation of methionine to methionine sulfoxide, and not the second oxidation to methionine sulfone (317).

Although it may be tempting to pursue oxidation of other amino acid residues in order to obtain more detailed structural information, the equisite use of harsher or alternative oxidation techniques, such as combination of hydrogen peroxide with metal ions (at least in the case of prion), can alter the conformation of the prion form being studied. PrP is a protein with high affinity, histidine-based copper binding sites (242,402). As such, it is very susceptible to metal-catalyzed oxidation. There are a number of additional amino acid residues (tyrosine, histidine) which would be expected to be oxidized under these conditions, but this reaction will also result in the misfolding and accumulation of PrP resulting from histidine oxidation (390) and has been shown to initiate aggregation of the protein (390) and PK resistance (403). Furthermore, the addition of H_2O_2 and Cu^{2+} leads to widespread fragmentation of PrP (404).

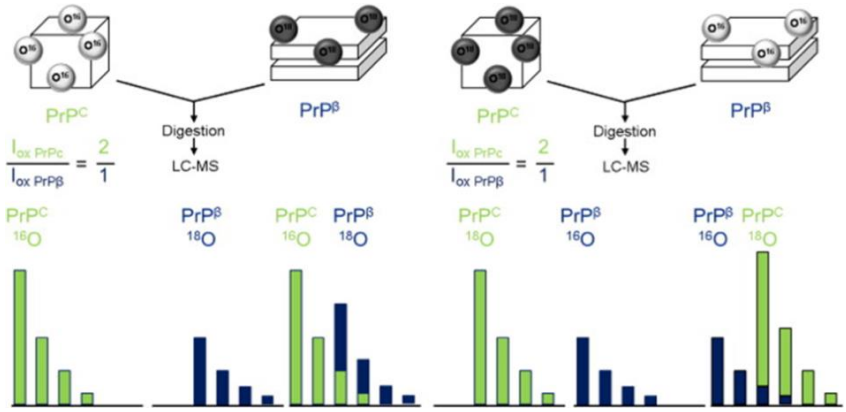

Figure 32: Experimental scheme for differential modification of native and β-oligomeric forms of prion protein using 1:1 ratio of $H_2{}^{16}O_2$ and $H_2{}^{18}O_2$.

The isotopic distributions shown are for oxidized peptides from PrP^C (green) and PrP^β (blue), with intensity ratios of 2:1. These distributions were derived from PrP^C + $H_2{}^{16}O_2$ and PrP^β + $H_2{}^{18}O_2$ (left), and from the alternative labeling scheme with PrP^C + $H_2{}^{18}O_2$ and PrP^β + $H_2{}^{16}O_2$ (right). Reprinted from Serpa et al. (302).

Using the isotopically-coded H_2O_2 modification approach (Figure 32), several residues were detected that were differentially modified between the PrP^C and PrP^β prion isoforms. Differential modification levels were calculated by superimposing the MS isotopic distributions of a $H_2{}^{18}O_2$ modified peptide and the known isotopic distribution of $H_2{}^{16}O_2$ modified peptide, leading to a ratio representing the difference in modification between two forms of the prion protein (Figure 33). PrP^C and PrP^β were also labeled in

reverse with $H_2{}^{16}O_2$ and $H_2{}^{18}O_2$ to account for any possible differences in reactivities between the $H_2{}^{16}O_2$ and $H_2{}^{18}O_2$ preparations, and any possible background oxidation of the protein samples prior to MS analysis. The analyses were performed in triplicate and detected nine of the ten methionines and one of the two tryptophan residues Table 7. Differential modification of multiple residues in both PrP^C and PrP^β forms of prion were observed (Figure 34), with many of the differentially-labeled methionine residues localized in what are already known to be critical regions for the conformational change of the prion protein (317). Differences in oxidation of these residues can give insights into structural changes that occur during PrP^C to PrP^β conversion.

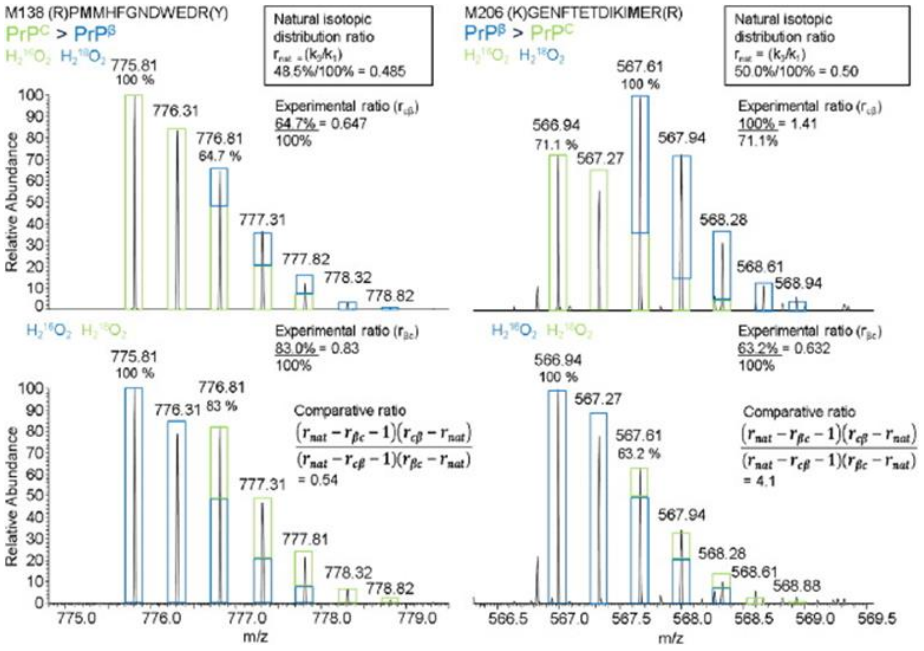

Figure 33: Mass spectra of oxidized peptides containing differentially modified residues Met138 and Met206.

Contributions of signals from the PrP^C and PrP^β forms are highlighted with green and blue boxes, respectively. Top: PrP^C has been modified with $H_2{}^{16}O_2$ and PrP^β has been modified with equimolar amount of $H_2{}^{18}O_2$. Bottom: PrP^C has been modified with $H_2{}^{18}O_2$ and PrP^β has been modified with $H_2{}^{16}O_2$. Differences in modification levels for two forms of the protein can be calculated by deconvoluting the superimposed isotopic distributions from the $H_2{}^{16}O_2$- and $H_2{}^{18}O_2$- modified peptides. Reprinted from Serpa et al. (302).

Residue	Sequence	$r_{c\beta}$		$r_{\beta c}$		Comparative ratio	PrP^C	PrP^β
		Average	SD	Average	SD			
M87	(R)GSH**M**LEGQGGGTHNQW(N)	0.70	0.09	0.69	0.10	1.01	X	X
W99	(R)GSHMLEGQGGGTHNQ**W**(N)	0.44	0.04	0.47	0.04	1.96		X
M112	(K)H**M**AGAAAAGAVVGGLGGY(M)	0.61	0.17	0.73	0.08	1.76		X
M129	(A)GAVVGGLGGY**M**LGSAMSR(P)	0.88	0.26	0.92	0.04	0.92	X	
M134	(A)GAVVGGLGGYMLGSA**M**SR(P)	0.78	0.11	0.68	0.21	1.59		X
M138	(R)P**M**MHFGNDWEDR(Y)	0.66	0.09	0.74	0.21	0.72	X	
M139	(R)PM**M**HFGNDWEDR(Y)	0.60	0.19	0.57	0.15	1.31		X
M206	(K)GENFTETDIKI**M**ER(V)	1.45	0.59	0.65 [a]	0.02	3.85		X
M213	(R)VVEQ**M**CTTQYQK(E)	0.41	0.05	0.60	0.07	−0.19	X	

[a] Note: this peptide was found in only two of the three runs.

Table 7: Differentially oxidized amino acids of PrP^C and PrP^β.
The ratios ($r_{c\beta}$ and $r_{\beta c}$) representing the differential modification of the specific residues are calculated as an average of three pairs of replicate runs, which are then input into Equation 2 from which the comparative ratio is calculated. Since samples are mixed in a 1:1 ratio, values greater than 1.0 indicate preferential modification of the residues in the PrP^β form, while ratios less than 1.0 indicate preferential modification of the residues in the PrP^C form. Reprinted from Serpa et al. (302).

A comparative ratio of 1.01 was found for M87 indicative of a residue with similar oxidation levels in both PrP^C and PrP^β. M87 is a part of an artificially introduced N-terminal tag and is located close to the beginning of the flexible N-terminal region. An equal modification rate of this residue most likely indicates its equal accessibility, due to the absence of a defined structure at the N-terminus in both forms. This can serve as an internal control of the labeling efficiency for both the light and heavy forms of the modification reagents, and confirms the ratio calculations.

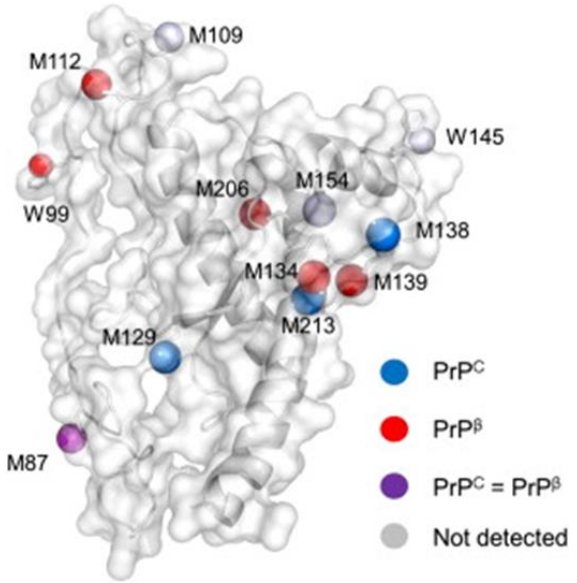

Figure 34: Oxidized residues highlighted on the PrP^C structure.

Residues that are preferentially oxidized in PrP^{C} and PrP^{β} are marked in blue and red, respectively; residues that are equally oxidized are marked in purple; residues for which singly oxidized peptides were not detected are marked in grey. Reprinted from Serpa et al. (302).

Several residues were preferentially modified in the PrP^{C} form: Met129, Met138, and Met213. Met129 is located in the beginning of the β-sheet 1 of PrP^{C}. This region is thought to be involved in the formation of the final stacked β-sheet structure in amyloid fibrils and has been previously shown to be strongly protected from the solvent in this form of PrP (405). Based on my data, there is only mild preferential protection of this residue, which may imply that an extensive β-sheet structure has not yet formed in the β-oligomeric form. This is in agreement with my previous findings on the exposure of the tyrosine residues in this region of the PrP^{β}, based on surface modification experiments with pyridine carboxylic acid N-hydroxysulfosuccinimide ester (PCASS) (see Chapter 3. Using multiple structural proteomic approaches for the characterization of prion proteins) (22). The Met138 residue is located within the strand between β1 and H1, and is readily exposed in PrP^{C}. Rearrangement of the β1-H1-β2 loop might therefore account for a change in the microenvironment of this residue in PrP^{β}. Met213 is the part of the same region – the β1-H1-β2/H3 interface – and is also situated on the protein surface in PrP^{C}. Moving the β1-H1-β2 loop away from the H2-H3 core would open up the hydrophobic internal region of β1-H1-β2/H2-H3, where M213 is located. My crosslinking data on PrP^{β} (see Chapter 5. Structure of prion β-oligomers as determined by structural proteomics with crosslinking constraint-guided molecular dynamic simulations) suggests that this region becomes occupied with different portion of the prion molecule in the β-oligomer aggregate. This would therefore be in agreement with the absence of oxidation of this residue in PrP^{β}, which was observed in this study.

A number of residues were preferentially modified in the PrP^{β} form: Trp99, Met112, Met134, Met139, and Met206. The Trp99 and Met112 residues are located in the N-terminal flexible portion of the 90-232 PrP molecule. I proposed earlier that this region may transiently interact with the PrP^{C} protein surface which is composed of the C-terminal portion of H2 and the H2-H3 loop (see Chapter 2. Use of Proteinase K non-specific digestion for selective and comprehensive identification of inter-peptide crosslinks: Application to prion proteins) (301). The oxidation data (Table 7, Figure 34)

may suggest relocation of this region in PrP^{β}. Met134 and Met139 are located in the β1-H1 region with side chains oriented towards the interior H2-H3 core in PrP^{C} structure. Rearrangement and movement of the β1-H1-β2 loop away from the PrP core would therefore expose this region to the solvent if it does not get involved in any additional contacts in PrP^{β}.

Overall, these current results on the H_2O_2 differential oxidation of PrP^{C} and PrP^{β} are in good agreement with our previous surface modification results, performed using reagent PCASS (see Chapter 3. Using multiple structural proteomic approaches for the characterization of prion proteins) (22) which preferably modifies lysines and the N-terminus but also reacts with tyrosines, serines, and threonines. With PCASS, Tyr150 and Tyr157 showed preferential modification in PrP^{β}, which shares the same internal face of the β1-H1-β2 loop with Met134 and Met139 (see Chapter 3. Using multiple structural proteomic approaches for the characterization of prion proteins) (22). The same movement of H1 away from the core would also allow H_2O_2 access to the Met206 residue, which is situated internally between the C-terminal portion of H2 and the N-terminal part of H3. Furthermore, these oxidation results are in good agreement with our hydrogen/deuterium exchange experiments on acid-induced PrP indicating rearrangement of the same region (see Chapter 3. Using multiple structural proteomic approaches for the characterization of prion proteins) (22). Specifically, previous HDX results indicated that residues aa148-164 (H1-β2) and aa132-167 (β1-H1-β2) are protected in the oligomeric form (see Chapter 3. Using multiple structural proteomic approaches for the characterization of prion proteins) (22) and Chapter 2. Use of Proteinase K non-specific digestion for selective and comprehensive identification of inter-peptide crosslinks: Application to prion proteins (301), respectively) and as evidenced by my PCASS surface-modification studies (see Chapter 3. Using multiple structural proteomic approaches for the characterization of prion proteins) (22), the rearrangement of the β1-H1-β2 in the oligomeric form can lead to an increased exposure of residues involved in the interface of the β1-H1-β2 loop with the H2-H3 core and, as shown by this study, leads to increased exposure of residues Met134, Met139, and Met206.

4.4. Conclusion

I have presented here the use of ^{16}O and ^{18}O isotopically-coded hydrogen peroxide oxidation as a surface modification reagent for comparing the extent of modification of methionine and tryptophan residues in two different conformational states of a protein. This approach allowed for the detection of several differentially oxidized residues between the native and the acid-induced β-oligomeric forms of the prion protein. The differences found can be explained by a flip of the β1-H1-β2 loop away from the core of the molecule during conversion, and indicates specific residues of prion protein which are involved in the conformational change and the formation of acid-induced PrP^{β} aggregates.

The addition of methionine and tryptophan residues to the amino acid repertoire that can be targeted using this surface modification approach is important for the study of prion oligomers, as many of these residues are located in critical regions of sequence that are implicated in the conversion. The introduction of this technology is important to obtain additional structural constraints for use in our study of urea-acid induced PrP^{β} structure (see Chapter 5. Structure of prion β-oligomers as determined by structural proteomics with crosslinking constraint-guided molecular dynamic simulations).

Chapter 5. Structure of prion β-oligomers as determined by structural proteomics with crosslinking constraint-guided molecular dynamic simulations

Work in this chapter was a collaborative effort involving two laboratories. Native (PrP^{C}) and urea-acid induced oligomeric (PrP^{β}) prion protein was recombinantly expressed and purified in-house. Experimental design was performed by Jason Serpa, Evgeniy Petrotchenko, and Christoph Borchers. All experimentation and data analysis was performed by Jason Serpa. Crosslinker-based structural constraints were submitted to the laboratory of Nikolay Dokholyan at Department of Biochemistry and Biophysics, University of North Carolina, Chapel Hill, NC, 27599, USA, where they were incorporated into crosslinking constraint guided molecular dynamic simulations (CL-DMD) by Konstantin I. Popov and Nikolay Dokholyan, which was used to generate a model. Karl Makepeace assisted in creating Pymol figures. Christoph Borchers oversaw the project.

The work presented in this chapter is a manuscript in preparation as (303):

Serpa, J. J.; Petrotchenko, E. V.; Dokholyan, N. V.; Borchers, C. H. (2017) *Manuscript in preparation.*

5.1. Introduction

The study of the molecular mechanisms involved in the conformational change of PrP^C leading to the assembly and final structure of β-oligomers is critical to understanding the aggregation process in prion disease. Conversion of PrP^C to $PrP^{ß}$ oligomers can be studied *in vitro* using non-glycosylated recombinantly expressed proteins. These oligomers carry structural features that are believed to resemble those existing *in vivo* during prion disease pathogenesis. Conversion to a β-rich intermediate form, PrP^{β}, can be induced by a number of different methods (see 1.7.2.1. Conversion methods, characteristics, and infectivity). Conversion of PrP^C to PrP^{β} can be confirmed using methods such as dynamic light scattering, proteinase-K resistance assay, 1-anilinonapthalene-8-sulfonate fluorescence, and circular dichroism. In this chapter, I used urea-acid (pH 4) converted prion protein, which is generally believed to resemble the existing *in vivo* converted species, as it occurs in an acidic pH environment comparable to that of endocytic vesicles (18,60). These β-rich forms are still inherently challenging to study using conventional structural biology methods, such as liquid-state NMR spectroscopy, and X-ray crystallography, due to their poor solubility and heterogeneity.

Despite these difficulties, significant understanding of prion aggregate structures has been obtained using alternative methods such as protease accessibility, X-ray diffraction, spin labeling, computer modeling, infrared spectroscopy, electron microscopy, and antibody mapping (see 1.7.2.1. Conversion methods, characteristics, and infectivity). Although important structural insights have been gained by these methods, there is still little agreement between the different proposed structures for the prion oligomer (24,207,220,223,312,313).

For a more complete characterization of prion aggregate structures, additional approaches can be used. Structural proteomics can be defined as a combination of protein chemistry methods -- such as limited proteolysis, surface chemical modification, hydrogen/deuterium exchange, and chemical crosslinking -- in combination with contemporary mass spectrometry (see 1.8. Studying prion conformational change and structure using protein chemistry methods combined with mass spectrometry). By using these methods, specific structural details of protein and protein complexes can be attained

and are especially useful in situations such as prion aggregates (see Chapter 3. Using multiple structural proteomic approaches for the characterization of prion proteins) (21,22). Numerous publications using structural proteomics methods for the study of prions have been reported (see 1.8. Studying prion conformational change and structure using protein chemistry methods combined with mass spectrometry).

I and others have shown, that during PrP^{C} to PrP^{β} conversion, the prion protein undergoes a significant conformational rearrangement and that for this to occur, there must be a disengagement of the H1 α-helix and a separation of contacts between the β1-H1-β2 domain and the H2-H3 core (22-26), consistent with the β-nucleation model (see 1.8. Studying prion conformational change and structure using protein chemistry methods combined with mass spectrometry). This rearrangement is thought to result in previously-buried surfaces becoming exposed to solvent, from which new inter-protein contacts can develop. This conversion is also thought to involve the formation of a β-sheet nucleation site, which initiates the maturation to fibrillar forms.

To further my investigations of prion oligomers, I performed a comprehensive study using multiple proteomic techniques for the determination of the urea-acid induced prion oligomer structure. A panel of proteolytic enzymes was used for limited proteolysis: ^{12}C and ^{13}C PCAS were used for differential modification of K, Y, S, and T residues, and isotopically-labeled hydrogen peroxide was used to induce differential oxidation of W and M residues, in order to determine changes in surface exposure as a result of the conversion. HDX was used to assess changes in secondary structure between PrP^{C} and PrP^{β}. A panel of crosslinking reagents, including zero-length and short- and long- range reagents was applied to an equimolar mixture of $^{14}N/^{15}N$-metabolically labeled β-oligomer, and used to identify intra- and inter- protein crosslinks. A combination of these structural proteomic methods was also used to compare the structure of PrP^{C} before and after conversion to urea-acid induced PrP^{β} oligomers.

This experimentally derived information allowed us to assemble a CL-DMD model of the β-oligomer, based on all of the crosslinking constraints obtained. This β-oligomer model is consistent with the rearrangement and disassembly of the β1-H1-β2 region from the H2-H3 core, and the consequent development of an apparent β-sheet nucleation site,

and the formation of new inter-protein hydrophobic contacts, resulting from the change in exposure of hydrophobic residues, as pivotal to the conversion of PrP^C to PrP^β.

5.2. Materials and methods

5.2.1. Materials

All chemicals were from Sigma-Aldrich, unless noted otherwise. Crosslinking reagents azido-benzoic-acid-succinimide (ABAS) (339), CyanurBiotinDimercaptoPropionylSuccinimide (CBDPS) (342), DiSuccinimidylAdipate (DSA), DiSuccinimidylGlutarate (DSG), DiSuccinimidylSuberate (DSS), succinimidyl 4,4'-azipentanoate (SDA) (406), and 2,4,6-triazido-1,3,5-triazine (TATA) (340) were obtained from Creative Molecules Inc..

5.2.2. Prion protein expression and urea-acid induced conversion to PrP^β

A synthetic gene, corresponding to Syrian hamster prion protein residues 90-232 ($ShPrP_{90-232}$) which included a 22-residue N-terminal fusion tag with a thrombin cleavage site and 6x-His, was obtained from the laboratory of Dr. David Wishart (University of Alberta). $ShPrP_{90-232}$ was expressed with or without minimal (^{15}N-labeled) media in *E. coli*, as previously described (278,407). Cells were sonicated, and -- in order to purify the expressed PrP protein from inclusion bodies -- cell lysates were resuspended in guanidine-solubilizing buffer and the protein was loaded onto immobilized nickel-nitrilotriacetic acid (Ni-NTA) beads *via* their fused histidine tail (253). To ensure the correct folding to native PrP^C, the bound protein was re-folded on-column with a decreasing urea concentration gradient over a 12 hour time period (278). PrP immobilized on-column favours the formation of an intramolecular disulfide bond and prevents protein aggregation (253). It has been determined that protein refolded using this method is predominantly in the native PrP^C form, with little or no β-isoform present (279). Refolded soluble protein was eluted with imidazole in sodium phosphate buffer without urea. Then the buffer was exchanged and concentrated using 10 KDa cut-off centrifugal filters (Amicon) and 20mM NaOAc, pH 5.2. SDS-PAGE was used to determine PrP^C purity and the protein was further characterized by NMR, CD, and fluorescence spectroscopy (253). PrP^C was dialysed against a low-salt buffer such as

20mM sodium acetate (NaOAc) and has been found to remain stable for at least 5 weeks at 4 ^{o}C (279).

The β-oligomeric form was created as previously described (279). Briefly, protein is reconstituted to 5M urea, 200mM NaCl, 20mM NaOAc, 60mM AcOH at 1mg/ml for 20 hours at 25^{o}C. After conversion, oligomers were dialysed into 20mM NaOAc (pH 5.2) (10mM ammonium acetate for HDX experiments) using dialysis buttons (Hampton Research) and dialysed at 4 ^{o}C for 180 minutes 3 times into 50mL of 20mM NaOAc, pH 5.2. The protein concentration was determined by measuring the absorbance at 280nm. Oligomer formation was confirmed by performing a comparative crosslinking assay between PrP^{C} and PrP^{β} using SDA, by PK-resistance assay, and by circular dichroism.

5.2.3. Circular dichroism

Circular dichroism spectra were recorded on a Jasco J-720 spectropolarimeter using a temperature-regulated cell with a 1mm optical path length quartz cell. Spectra were recorded in the UV region (190-250nm) in 20mM NaOAc (pH 5.2) at a protein concentration of 0.5mg/mL. Estimation of secondary structure content was performed using secondary-structure prediction and fold-recognition software for circular dichroism spectroscopy, specialized for β-structure selection (BeStSel) (408).

5.2.4. Limited proteolysis

Limited proteolysis was performed using Arg-C (in 20mM Na_2HPO_4), Asp-N (in 100mM ammonium bicarbonate (ABC)), chymotrypsin (in PBS and 10mM CaCl2), Glu-C (in either 50mM ABC or PBS, pH 7.4), pepsin (in 20mM HEPES 6.9), proteinase K (in PBS) and trypsin (in PBS, pH 7.4). For each experiment, a 15-µg aliquot of PrP^{C} and PrP^{β} was incubated at 37^{o}C with an enzyme: substrate ratio of 1:25 for pepsin, 1:500 for proteinase-K, and 1:50 for all other enzymes. Three-µg aliquots were removed at time 0, 1, 5, 10, and 30 minutes, and each was immediately mixed with NuPage lithium dodecyl sulfate (LDS) Sample Buffer 4x (Invitrogen) and heated at 100 ^{o}C for 10 minutes. All samples were then separated by SDS-PAGE. Individual bands -- corresponding to different proteolytic fragments of the prion protein -- were individually excised and prepared by in-gel tryptic digestion (376). The digestion sites were determined by

LC/ESI-MS/MS on a LTQ Orbitrap Velos mass spectrometer, using PEAKS Client 7.0 software.

5.2.5. Surface modification

PrP^{C} and PrP^{β} were modified with either the heavy or light form of the modification reagent, pyridine carboxylic acid N-hydroxysulfosuccinimide ester (PCAS-^{12}C6 and ^{13}C6) (Creative Molecules Inc.), which modifies the N-terminus, K, Y, S, or T residues (Figure 35) (22) and heavy or light hydrogen peroxide ($H_2{}^{16}O_2$ or $H_2{}^{18}O_2$) for modification of W or M residues (Figure 32) (see Chapter 4: Using isotopically-coded hydrogen peroxide as a surface modification reagent for the structural characterization of prion protein aggregates) (302).

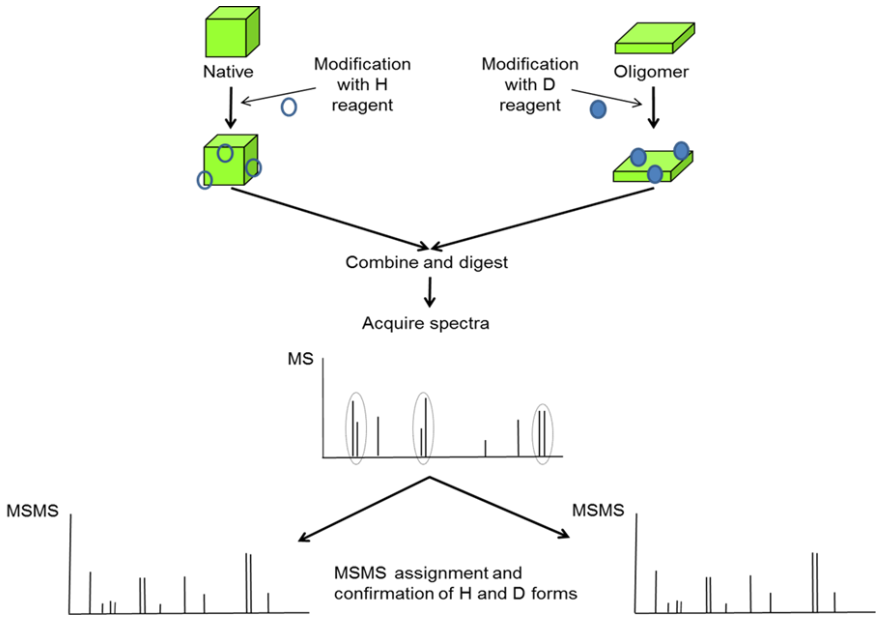

Figure 35: PCAS surface modification workflow.
Differential surface modification. PrP^{C} and PrP^{β} were modified with either the heavy or light forms of pyridine carboxylic acid N-hydroxysulfosuccinimide ester (PCAS-^{12}C6,-^{13}C6) in a 1:1 ratio. Samples were quenched, then combined and digested prior to MS and MS/MS acquisition and analysis (302). Reprinted from Serpa et al. (303).

For differential surface modification with PCAS, 6.5µg aliquots of PrP^{C} or PrP^{β} were prepared at 4.0 µM. Reaction mixtures included 10 mM PCAS light (PCAS-^{12}C6) or heavy (PCAS-^{13}C6), added to either PrP^{C} or PrP^{β}. Reactions were allowed to proceed for 30 minutes at 25 ^{o}C, then were quenched with 25 mM ABC, and then the reaction mixture acidified with 10% acetic acid (AcOH) to pH 2 Prior to the addition of pepsin,

samples were combined (PrP^C + PCAS-^{12}C6 and PrP^β + PCAS-^{13}C6 or PrP^C + PCAS-^{13}C6 and PrP^β + PCAS-^{12}C6) then digested with pepsin at a 1:10 enzyme: substrate ratio and incubated for 12 hours at 37^{o}C. Digests were analyzed by LC/ESI-MS/MS on a LTQ Orbitrap Velos mass spectrometer, and peptides containing a modification were identified using Peaks Client 7.0, and their peak areas were determined.

For H_2O_2 differential oxidation, 6.5µg aliquots of PrP^C or PrP^β at 4.0 µM were bubbled with nitrogen gas prior to the addition of H_2O_2. 10m M H_2O_2 light ($H_2{}^{16}O_2$) or heavy ($H_2{}^{18}O_2$) was added to either PrP^C or PrP^β, and the solution was incubated for 30 minutes at 25 ^{o}C and samples were quenched with 10% acetic acid to pH 2. Prior to the addition of pepsin, samples were combined (PrP^C + $H_2{}^{16}O_2$ and PrP^β + $H_2{}^{18}O_2$ or PrP^C + $H_2{}^{18}O_2$ and PrP^β + $H_2{}^{16}O_2$ light), bubbled with nitrogen gas, and digested with pepsin at a 1:10 enzyme: substrate ratio for 12 hours at 37^{o}C. Digests were analyzed by LC/ESI-MS/MS on a LTQ Orbitrap Velos mass spectrometer, and peptides containing a modification were identified using Peaks Client 7.0 and their peak areas were determined.

For experiments involving PCAS modification, the mean of the log peak area ratios (PrP^C with PCAS-^{12}C6/ PrP^β with PCAS-^{13}C6 or PrP^C with PCAS-^{13}C6/ PrP^β with PCAS-^{12}C6) for each modified residue were calculated. The antilog of the mean of the ratio provided a value representative of the relative exposure of a residue in PrP^C versus PrP^β.

For modification experiments with H_2O_2, the log of the peak area ratios (PrP^C with $H_2{}^{16}O_2$/ PrP^β with $H_2{}^{18}O_2$ or PrP^C with $H_2{}^{18}O_2$/ PrP^β with $H_2{}^{16}O_2$) for each modified residue was calculated. Differences in the oxidation levels of a residue between PrP^C and PrP^β were calculated using a comparative ratio formula (Figure 33) (302) which accounts for endogenous oxidation of the residues. The resulting ratio provides a value indicative of the relative exposure of a residue in PrP^C versus PrP^β.

5.2.6. Hydrogen/deuterium exchange

HDX using FTMS-ECD top-down analysis was performed on a Bruker 12T-FTICR mass spectrometer. Experiments were carried out under “exchange-in” conditions, using a two-stage continuous-flow mixer as described previously (22,325). The protein solution and D_2O (from separate syringes) were mixed continuously in a 1:4 ratio (80% D_2O) through a three-way tee connected to a 100 µm × 21 cm capillary, resulting in a 10-

second labeling time. The outflow from this capillary was mixed with a quenching solution (0.4% formic acid in 80% D_2O) from third syringe *via* a second three-way tee. The outflow from this last capillary was injected into a Bruker 12T Apex-Qe hybrid Fourier Transform mass spectrometer, equipped with an Apollo II electrospray source. In-cell ECD fragmentation experiments were performed with an m/z 900–1200 precursor selection range, using a grid potential of 12 V and cathode filament current of 1.2 Amps. Approximately 1200 scans were accumulated over the 250–2600 m/z range, resulting in an approximate acquisition time of 30 minutes for each ECD spectrum. FT-MS calibration was performed using the ECD fragments of PrP^{β}. The HDX Match software of the ICC-CLASS software suite was used to determine the deuteration levels of the amino acid residue's amide groups, based on the centroid masses of the c- and z- ion series (409).

5.2.7. Crosslinking

Crosslinking was performed on an $^{14}N^{15}N$-equimolar mixture of PrP^{β} (Figure 36) (333), using a panel of crosslinking reagents: ABAS (339), CBDPS, 4-(4, 6-dimethoxy-1,3,5-triazin-2-yl)-4-methylmorpholinium chloride (DMTMM) (410,411), DSA, DSG, DSS, and 1-ethyl-3-(3-dimethylaminopropyl) carbodiimide hydrochloride (EDC) (412). Photo-induced crosslinking of the unmodified proteins was performed with (PICUP) (361), SDA (406), and TATA (340), which differ in reactivity and spacer length (see Table 8 for crosslinking conditions for each reagent). After the crosslinking reaction, a 1% (final concentration) solution of deoxycholate was added to each sample and incubated at 25 ^{o}C for 30 minutes. Samples were then digested with proteinase K (see Chapter 2. Use of Proteinase K non-specific digestion for selective and comprehensive identification of inter-peptide crosslinks: Application to prion proteins) (301) at a 1:25 enzyme: substrate ratio for 2.25 hours at 37 ^{o}C at 400rpm, and then acidified to 0.9% (final concentration) triflouroacetic acid for 5 minutes. Samples were then spun down at 21130 x g on a desktop centrifuge for 10 minutes, and the supernatant was removed to separate Eppendorf tube prior to C_{18} stage-tip (Thermo Scientific) clean-up, and then analyzed by LC/ESI-MS/MS on an LTQ Orbitrap Velos or an Orbitrap Fusion mass spectrometer, followed by crosslinking site assignment using our $^{14}N^{15}N$ DXMSMS Match software (334).

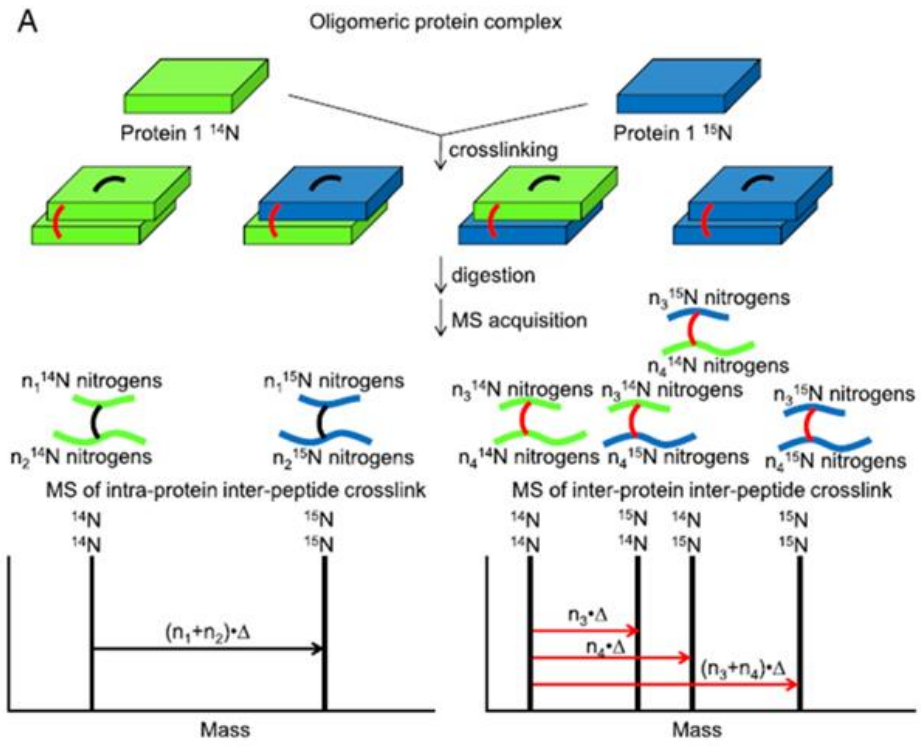

Figure 36: Workflow for crosslinking of 1:1 molar ratio mixture of ^{14}N (green) and ^{15}N (blue) metabolically labeled PrP^{β}.
Intra-protein inter-peptide crosslinks are shown in black and inter-protein inter-peptide crosslinks are shown in red. Each type of either intra-protein inter-peptide or inter-protein inter-peptide crosslinks is represented by doublets of signals in the MS spectra, separated by a mass difference corresponding to the ^{15}N isotope content of the peptides (334). Reprinted from Serpa et al. (303).

Crosslinking reagent	Buffer	pH	PrP concentration	Reagent 1	Reagent 2	Notes
ABAS	PBS 7.4	7.4	4 µM	0.9mM ABAS		UV short wavelength 10 minutes
CBDPS	PBS 7.4	7.4	4 µM	0.025mM CBDPS		
DMTMM	0.2M HEPES 6.9	6.9	4 µM	12 mg/ml DMTMM		
DSA	PBS 7.4	7.4	4 µM	0.025mM DSA		
DSG	PBS 7.4	7.4	4 µM	0.025mM DSG		
DSS	PBS 7.4	7.4	4 µM	0.025mM DSS		
PICUP	PBS 7.4	7.4	4 µM	1mM Ammonium persulfate	0.05 Ruthenium-tris(2,2'-bipyridyl) dichloride	5 flashes 1cm distance from eppendorf using (Sony DSC-S90 camera flash)
SDA	PBS 7.4	7.4	4 µM	400uM SDA		UV long wavelength 10 minutes
TATA	PBS 7.4	7.4	4 µM	1.25mM TATA		UV short wavelength 5 minutes

Table 8: Table of crosslinking reaction conditions.
Crosslinking conditions, reagents, buffer, protein concentration, and relevant reagents and notes are given for each crosslinking reaction. Reprinted from Serpa et al. (303).

5.3. Results and discussion

5.3.1. Formation of oligomers

In order to characterize the conformational change from PrP^{C} to PrP^{β}, and to determine the arrangement of the subunits in the aggregate, I compared both forms of the N-terminal histidine-tagged Syrian hamster prion protein (90-232), recombinantly expressed in *E. coli* by multiple structural proteomic techniques. This construct contains aa90 - aa128 of the aa29 – aa128 flexible and unstructured N-terminal region (373). Even with the truncation, the construct represents PrP 27-30, the hallmark proteinase K-resistant core region of pathogenic PrP^{Sc} which was identified *in vivo* (44,106) and which carries all of the necessary features for conversion and the propagation of aggregates (48,250-252).

The expressed protein was purified from the *E. coli* inclusion bodies. Cells were sonicated, the lysate was resuspended in guanidine solubilizing buffer, and the protein was loaded onto Ni-NTA column. The bound protein was re-folded on-column with a decreasing urea concentration gradient over a 12-hour time period to ensure correct folding to native PrP^{C} form (278). The refolded soluble protein was eluted with imidazole in sodium phosphate buffer without urea, and was analyzed by SDS-PAGE to determine its purity.

Of the multiple conversion methods reported, we chose urea-acid conversion, as it uses conditions that are thought to be comparable to those occurring *in vivo* (18,60) and may, therefore, accurately represent the aggregation mechanism involved in pathogenesis. To convert the purified soluble PrP^{C}, the protein was incubated in the conversion buffer (5M urea, 20 mM NaOAc, 200 mM NaCl, 60 mM AcOH) for 20 hours at 25 ^{o}C, and then dialyzed into 20 mM NaOAc pH 5.2. β-oligomers obtained using this method exhibit an increased resistance to proteinase-K digestion (Figure 37: Confirmation of urea-acid induced conformational change.) and an increase in β-sheet structure, as determined by CD (11.8% β-sheet content in PrP^{C} and 20.1% in PrP^{β}) (Figure 38: Confirmation of urea-acid induced conformational change.). A crosslinking titration assay of PrP^{C} and PrP^{β} showed a significant differential formation of the inter-protein crosslinked species on SDS-PAGE gel for PrP^{β}, but not for PrP^{C} (Figure 39: Confirmation of urea-acid induced

conformational change.) Structural characterization of PrP^{β} was done using HDX, crosslinking, limited proteolysis, and surface modification.

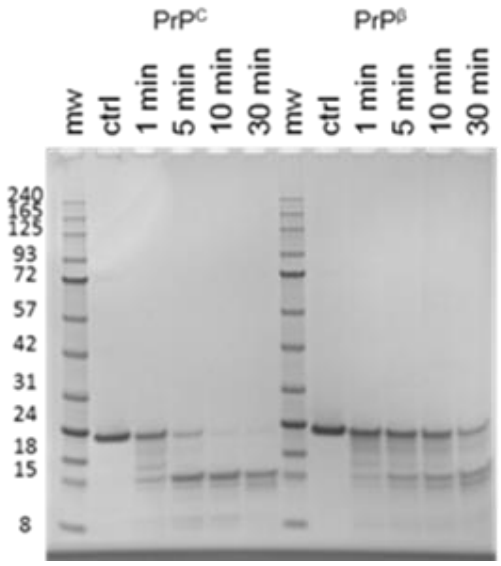

Figure 37: Confirmation of urea-acid induced conformational change. Differences in the relative resistance to Proteinase K (1:250 enzyme:substrate ratio) between PrP^{C} and PrP^{β} over a 30 minute time-course at 37 ^{o}C. Reprinted from Serpa et al. (303).

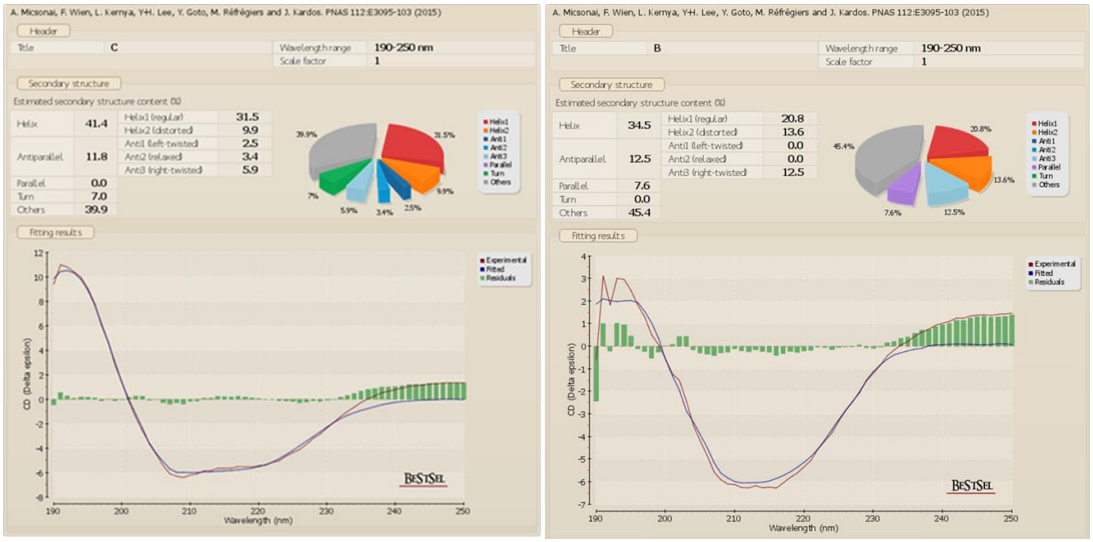

Figure 38: Confirmation of urea-acid induced conformational change. CD results for PrP^{C} (left pane) showing 41.4% alpha-helix and β-strand 11.8%. CD results PrP^{β} (right pane) showing 34.5% alpha helix and 20.1% β-sheet. Calculations were performed and the graph was created using BeStSel (408). Reprinted from Serpa et al. (303).

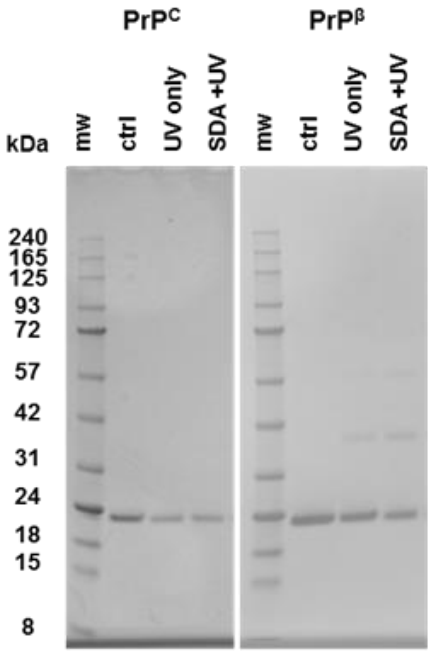

Figure 39: Confirmation of urea-acid induced conformational change. Crosslinking titration using SDA illustrating the differences in crosslinking efficiencies between PrP^{C} and PrP^{β}. Reprinted from Serpa et al. (303).

5.3.2. Hydrogen/deuterium exchange

The principle of the hydrogen/deuterium exchange method is that backbone amide hydrogens exchange with deuterium at different rates based on their hydrogen-bonding status. Consequently, the deuteration status of the backbone amides reflects their involvement in secondary structure (318-320). Here, I used top-down ECD-FTICR mass spectrometry to determine the boundaries of the secondary-structure motifs. based on the deuteration values of the amino acid residue (325,326).

PrP^{β} showed an increase in protection compared to PrP^{C} of approximately 11 protons, as evidenced by the total deuteration values of the intact proteins (Figure 40, Figure 41, Figure 42, Figure 43, Figure 44). This increase in protection of PrP^{β}, in combination with the CD data, suggests an increase in β-structure, a hallmark of the subsequent maturation of the oligomers to fibrils.

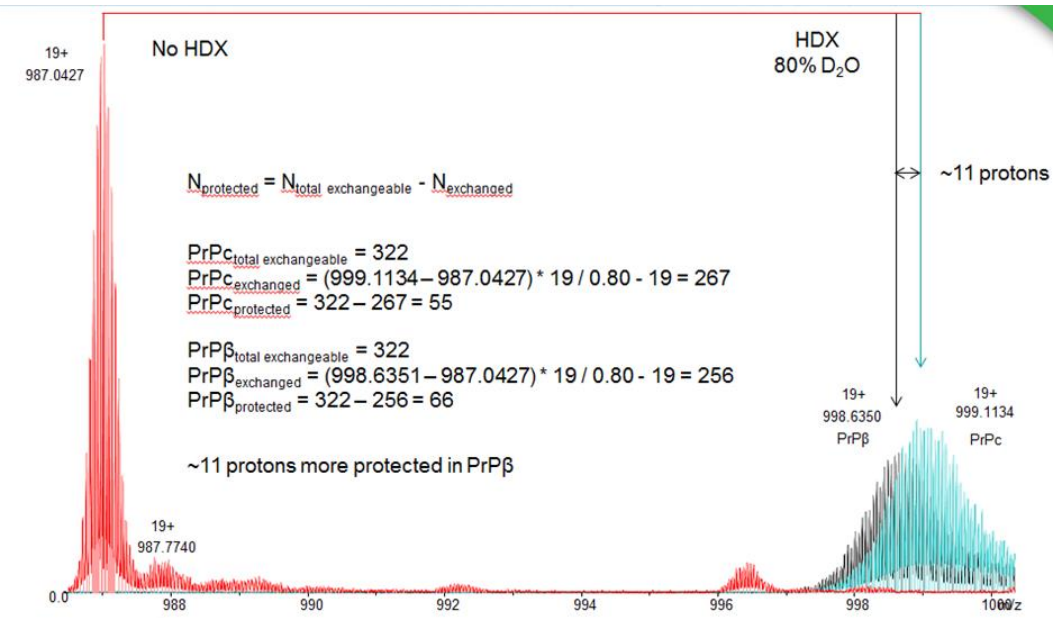

Figure 40: Top-down HDX total exchange of PrP^{C} and PrP^{β}.
The total exchange for PrP^{C} (cyan) and PrP^{β} (black) shows increased protection of PrP^{β} by 11 protons. PrP^{C} without exchange is shown in red. Reprinted from Serpa et al. (303).

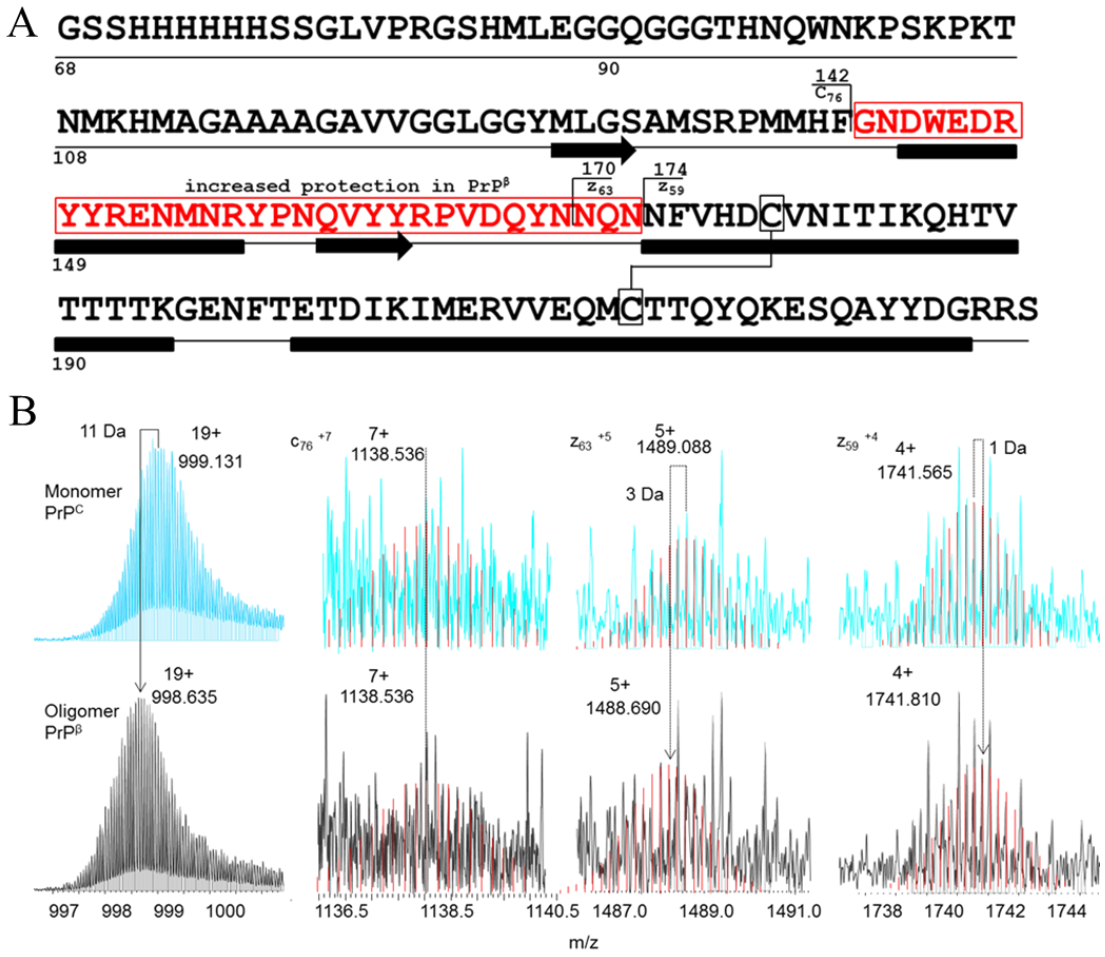

Figure 41: Top-down HDX analysis of PrP^{C} versus PrP^{β}.
A) ShPrP $_{90\text{-}232}$ sequence with the His-tag. PrP^{C}'s secondary-structure motifs are indicated below the amino acid sequence. Black arrows indicate β-sheets and black rectangles represent α-helices. The disulfide bond between cys179 and cys214 is indicated. The region of the PrP^{β} sequence showing increased protection in HDX is highlighted in red. B) The overall increase in protection in PrP^{β} is 11Da, and specific fragments, indicating the region responsible for the increased overall protection in PrP^{β} compared to PrP^{C} (aa143-aa173). The theoretical isotopic distribution for given fragment, based on the number of exchanged hydrogens, is overlaid in red over the experimental distribution patter (black). The region of increased protection indicates areas undergoing structural rearrangement and may represent the β-nucleation core of PrP^{β}. Reprinted from Serpa et al. (303).

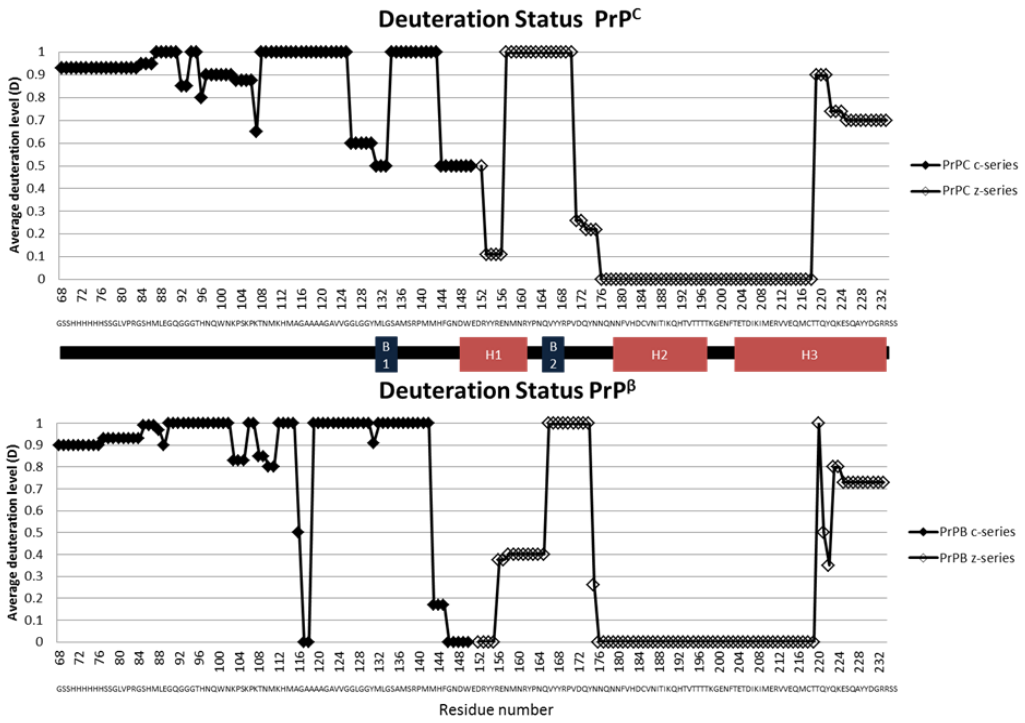

Figure 42: Deuteration status of backbone amide sites obtained from PrP^{C} and PrP^{β}.
c-ions are shown as filled diamonds and z-ions are shown as non-filled diamonds. Reprinted from Serpa et al. (303).

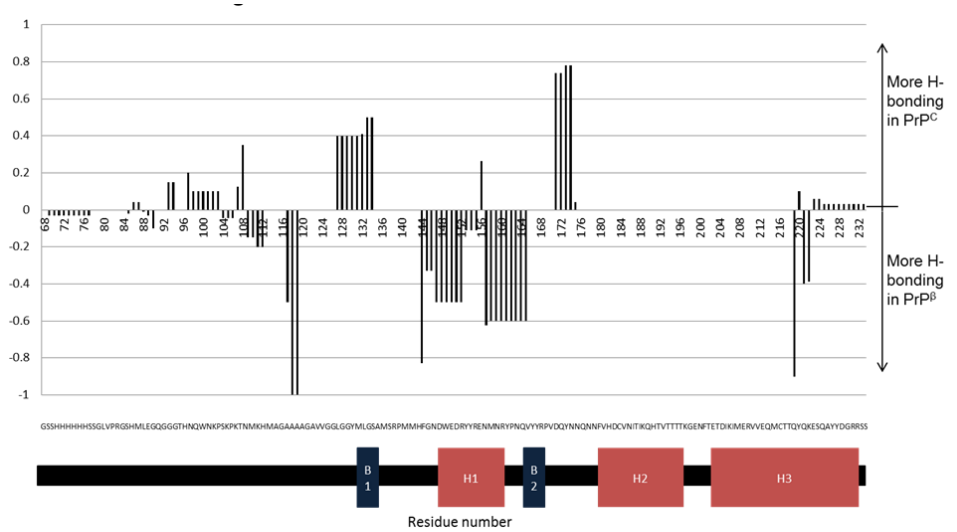

Figure 43: Differences in deuteration status between PrP^{C} and PrP^{β}.
Change in deuteration status of PrP^{C} and PrP^{β}, indicating the region of PrP^{β} that showed the greatest increase in hydrogen bonding (aa143-aa164). Reprinted from Serpa et al. (303).

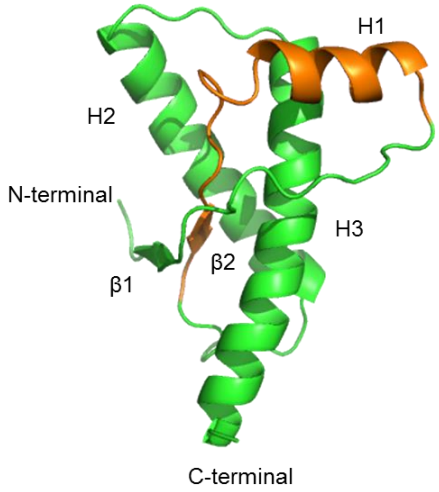

Figure 44: Region of PrP^{β} showing greatest increase in hydrogen bonding superimposed on PrP^{C} structure.
Region aa143-aa164 (orange) representing region of greatest increase in hydrogen bonding in PrP^{β} superimposed over $ShPrP^{C}{}_{90\text{-}232}$ (PDB:1B1O) structure with secondary structural elements labeled. Reprinted from Serpa et al. (303).

Analysis of the c- and z- ion fragment series (409) revealed that the aa144-aa165 region of PrP^{β} (the region encompassing the H1, the H1-β2 loop and β2) (Figure 44) was responsible for the increased protection and, therefore showed increased hydrogen bonding of this segment in the aggregated form. These HDX results were encouraging, as they indicated a rearrangement or restructuring to β-sheets in the aa144-aa165 region and may highlight a putative β-sheet initiation site, crucial to the progression of the aggregation process. Indeed, total numbers of the protected backbone amide protons in PrP^{C} and PrP^{β} measured by HDX of intact proteins were 55 and 66, respectively. H2 and H3 contain 52 residues and account for 39 (PrP^{C}) and 38 (PrP^{β}) protected protons (Figure 42). Aa68-aa142 (the N-terminal portion of the protein) accounts for 7 protected protons in both forms. H1, β1, and β2 contain 21 residues and account for 13 (PrP^{C}) and 24 (PrP^{β}) protected protons (Figure 38). Moreover, an increase of β-structure content in PrP^{β} -- up to 20.1% from 11.8% in PrP^{C}, as determined by CD (Figure 38) -- point out the disassembly of H1 helix and the formation of new β-structure in the aa143-aa164 region (Figure 43). This rearrangement was further characterized by crosslinking analysis of the PrP^{β} oligomer.

5.3.3. Crosslinking

Crosslinking combined with mass spectrometry provides distance information between pairwise crosslinked amino acid residues. Crosslinking reagents can vary in their specificities and can include NHS-ester base (e.g. CBDPS, which reacts primarily with amino groups of the N-terminus and K, but can also react with the hydroxyl groups of Y, S, T residues), amine to carboxyl specific (e.g. EDC or DMTMM which links lysine to aspartic or glutamic acid), specific photo-reactive (PICUP which links tyrosine to tyrosine), and non-specific photo-reactive (e.g. TATA). The spacer arm length between covalently bound functional groups in crosslinks dictates the distance constraints obtained, which can vary from 14 Å in the case of CBDPS to shorter range constraints (e.g. 8 Å DSG and 5 Å TATA) or zero-length crosslinks (<1 Å) (e.g. EDC and PICUP). After reaction, the crosslinked proteins are enzymatically digested and analyzed by LC-MS/MS.

By crosslinking an equimolar mixture of ^{14}N- and ^{15}N-PrP$^{\beta}$, one can determine if the crosslinks occur within the same protein (intra-protein crosslinks) or between two protein molecules (inter-protein crosslinks) (333) (Figure 36). Determining whether a crosslink is of intra- or inter- protein origin (334) is critical in guiding the modeling of the PrP$^{\beta}$ subunit structure (intra-protein crosslinks) and the PrP$^{\beta}$ assembly (inter-protein crosslinks).

Using a panel of crosslinking reagents (DMTMM, PICUP, TATA, ABAS, SDA, DSA, DSG, DSS, CBDPS) (Figure 45) we detected 14 intra-protein and 48 inter-protein inter-peptide crosslinks (Appendix A: Table of all urea-acid induced PrP$^{\beta}$ intra-protein crosslinked sites identified and Appendix B: Table of all urea-acid induced PrP$^{\beta}$ inter-protein crosslinked sites identified). The oligomer model was then built by satisfying all of the intra-protein and inter-protein constraints (Figure 46). Zero-length crosslinks obtained are especially important in the modeling process as they provide the strictest constraints. Intra-protein DMTMM crosslink D167-K204 requires rearrangement of the native β2-H2 loop (containing D167) to satisfy the crosslinking distance constraint to K204 within the H3 helix, while the PICUP inter-protein crosslinks Y225 to Y157, Y162, and Y163 anchor the region of increased HDX protection to the C-terminal end of helix H3 from another subunit (Figure 47A). Furthermore, the PICUP inter-protein crosslinks

Y128 to Y128 and Y128 to Y162 or Y163 form a triangle with Y157, Y162, or Y163 to Y225 and provide evidence for the rearrangement of the β1-H1-β2 and formation of the compact hydrophobic region of the inter-protein contacts (Figure 47A).

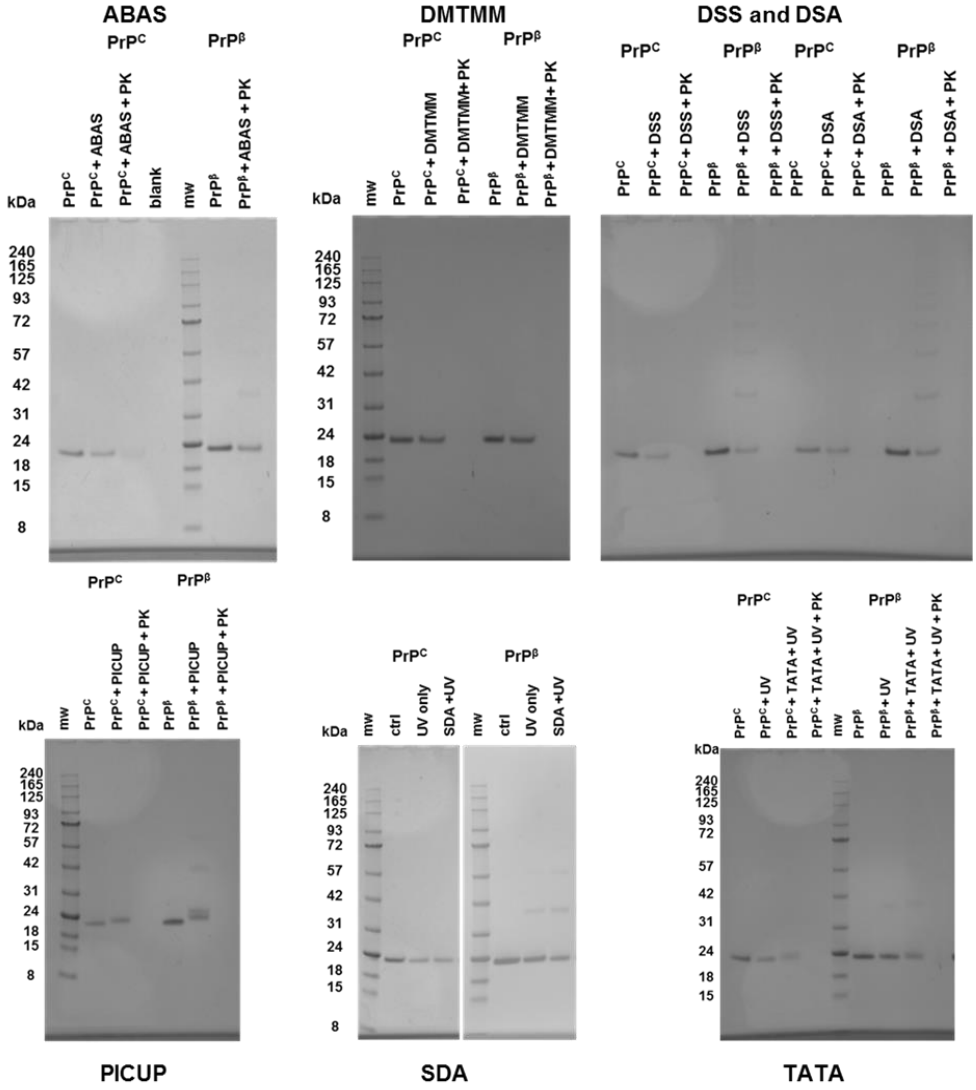

Figure 45: SDS-PAGE gel images of crosslinking reaction mixtures. Crosslinking conditions (Table 8). Crosslinking reagent used and lane descriptions as indicated. Reprinted from Serpa et al. (303).

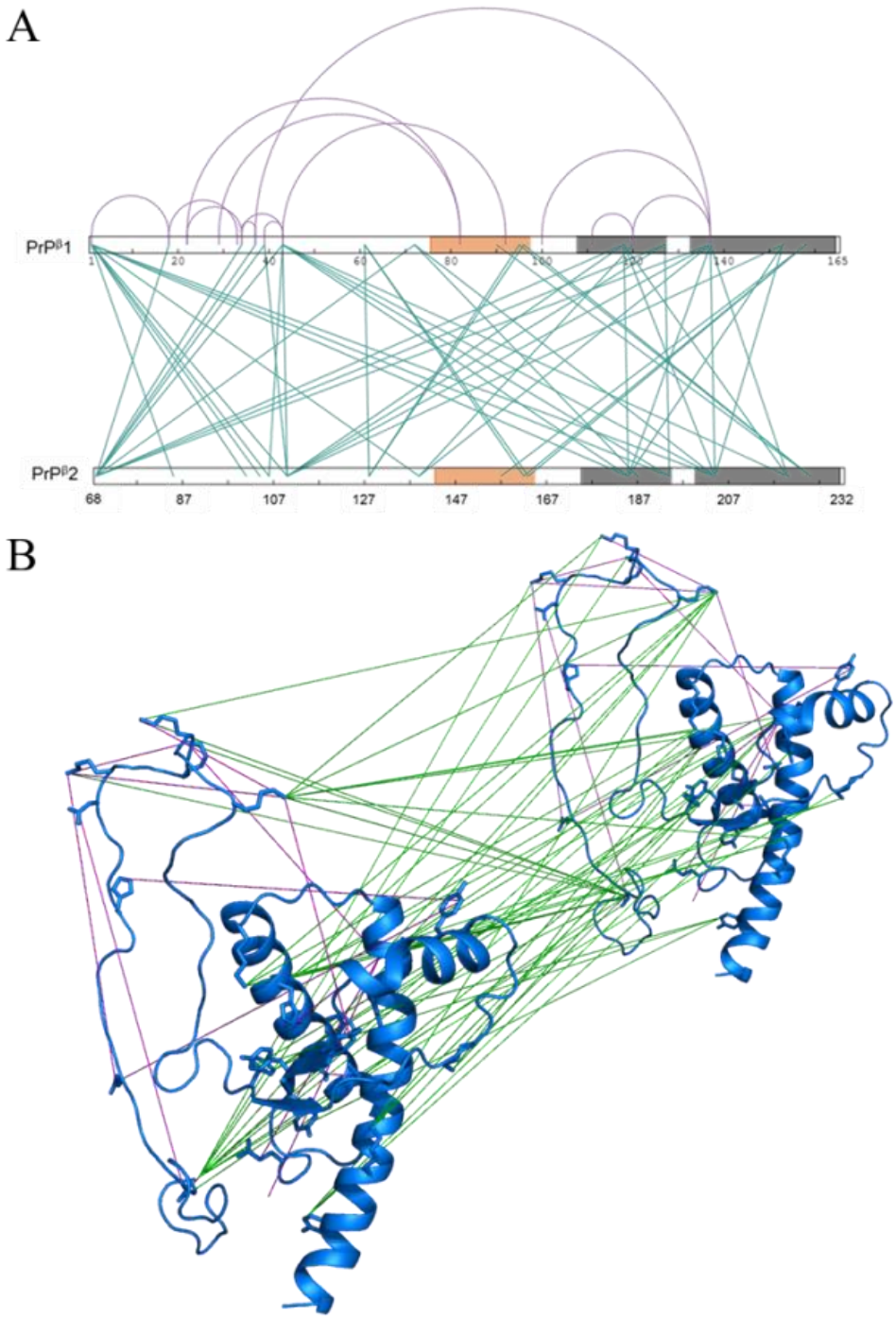

Figure 46: Crosslinking analysis of PrP^{β}.
A) Representation of all intra- and inter-protein constraints obtained by crosslinking a 1:1 equimolar mixture of ^{14}N- and ^{15}N-PrP^{β} (Appendix A: Table of all urea-acid induced PrPβ intra-protein crosslinked sites identified and Appendix B: Table of all urea-acid induced PrPβ inter-protein crosslinked sites identified). Sequences of two PrP^{β} monomers are

represented. The orange shading in the sequence represents a newly formed β-nucleation site and the grey shading represents the H2-H3 core α-helices. Intra-protein inter-peptide crosslinks are shown as purple arcs and inter-protein inter-peptide crosslinks are shown as green lines. This figure was created using xiNet (413). (B) Short-distance crosslinking constraints guide the PrP^{β} model. All intra- and inter- protein crosslinks are shown on a model of two PrP^{β} monomers. Crosslinks are shown as intra-protein crosslinks (purple) and inter-protein crosslinks (green). Intra-protein crosslinks indicate that a conformational change is taking place during conversion, and inter-protein crosslinks allow arrangement of monomers. Reprinted from Serpa et al. (303).

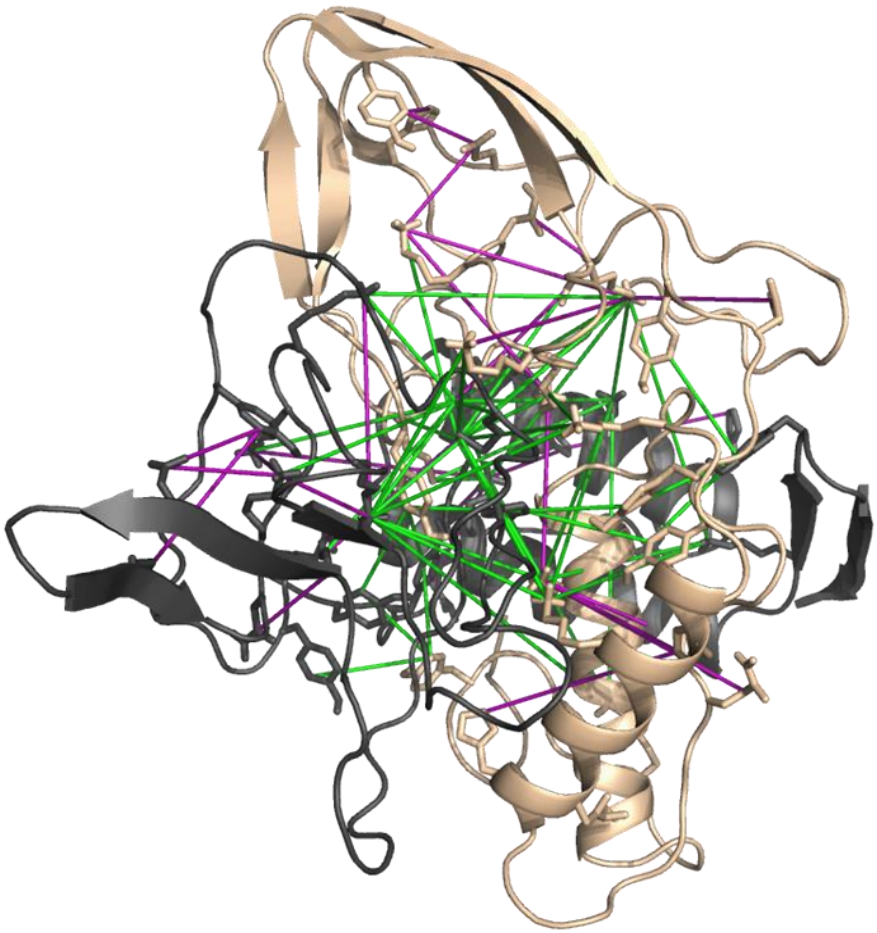

Figure 47: PrP^{β} dimer obtained by discrete molecular dynamics. Representation of all intra- and inter-protein constraints obtained by crosslinking a 1:1 equimolar mixture of ^{14}N- and ^{15}N-PrP^{β} displayed with PrP^{β} dimer obtained by discrete molecular dynamics. Intra-protein crosslinks are shown in purple (Appendix A: Table of all urea-acid induced PrPβ intra-protein crosslinked sites identified) and inter-protein crosslinks are shown in

green (Appendix B: Table of all urea-acid induced PrPβ inter-protein crosslinked sites identified). Reprinted from Serpa et al. (303).

A set of inter-protein crosslinks (particularly those from amine-reactive reagents, such as DSG, DSA, DSS, and CBDPS) guides the further assembly and placement of the H2-H3 cores of each subunit. CBDPS K194 – K194, K185 – K185, and DSG K204 – K204, K185 – K204, and K204 – K220) reveals that the subunits are packed together in a twisting stack-like arrangement (Figure 47).

The N-terminal part of the protein can be positioned in slightly different regions of the oligomer depending on whether intra-protein or inter-protein crosslinks are used (Figure 46A, Figure 47). The intra-protein DSG crosslink K104-K204 anchors the N-terminal region to the start of H3, and the SDA crosslinks K110-N159, E89-Y149, and H96-Y149 anchor the N-terminal region to the rearranged β1-H1-β2 region (Figure 47). Based on the inter-protein crosslinks, the N-terminal region of one subunit interacts with the newly rearranged β1-H1-β2 of an adjacent subunit and the C-terminal end of H2 (Figure 47), as indicated by ABAS crosslinks K110-K194 (N-terminal region to C-terminal end of H2) and M139-K194 (re-arranged β1-H1 loop to C-terminal end of H2) (Figure 47). This may be evidence that the N-terminal portion of the protein can occupy similar sites on both the subunit from which it originates and on the adjacent neighbouring subunit.

Crosslinking data has allowed us to assemble a β-oligomer structure that satisfies all of the constraints obtained. In the model, region aa144-aa165, which showed an increased protection in HDX, and the hydrophobic residues from this region (e.g. Y157, Y161, Y162, and Y169) may be involved in the newly formed β-strands of the putative β-nucleation site. The hydrophobic residue Y128 is outside of the aa151-173 region, but may also be interacting with this β-sheet structure, since it is in close proximity (based on PICUP crosslinking) to Y128, Y162, and/or Y163 of the adjacent subunit (Figure 47). The model obtained was further validated by additional results from both limited proteolysis and surface modification experiments.

5.3.4. Limited proteolysis

Limited proteolysis provides surface accessibility information to a large (enzyme) probe. The first cleavage sites, obtained after short incubation times, should be restricted to the outermost regions (i.e., the surfaces) of the protein subunit, which are accessible to

the active site of the proteolytic enzyme. Under limited proteolysis with pepsin, a different pattern of digestion for PrP^{C} versus PrP^{β} was observed (Figure 47, Figure 48). The native form exhibited a rapid accumulation of a C-terminal ~15 kDa product. In contrast, virtually no proteolysis was evident for the oligomeric form. This indicates a lack of enzyme access to the Trp99 cleavage site in this region of the oligomer (Figure 47). Limited proteolysis with chymotrypsin also highlighted Trp99 as being more protected from cleavage in PrP^{β} than in PrP^{C}. Chymotrypsin also showed greater protection of residues Y149, Y150, Y162, Y163, F175, and M206 in PrP^{β} relative to PrP^{C} (Figure 47). Arg-C cleavage of the N-terminal region (R83) was reduced in PrP^{β} compared to PrP^{C} (Figure 47), which is indicative of the delocalization of the N-terminal region in the oligomeric form to either the start of N-terminal region of H3 or C-terminal region of H2, based on the crosslinking results (see above) (Figure 47). Trypsin also indicated somewhat higher protection of the R83 and K110 cleavage sites in PrP^{β}, which is consistent with the Arg-C results (Figure 47). AspN digestion occurred at D227 in the PrP^{C}-terminal region and was equally susceptible to digestion in both prion forms. These results are in contrast with those from GluC digestion, which also indicated digestion in the PrP^{C}-terminal region at E221, except that proteolysis occurred more rapidly in PrP^{β} versus PrP^{C} (Figure 47). This might be the result of the β2-H2 loop moving away from H3 in PrP^{β}. In summary, limited proteolysis data were consistent with the HDX and crosslinking findings for the PrP^{β} and, therefore, can serve as a positive confirmation of the proposed structure (Figure 47).

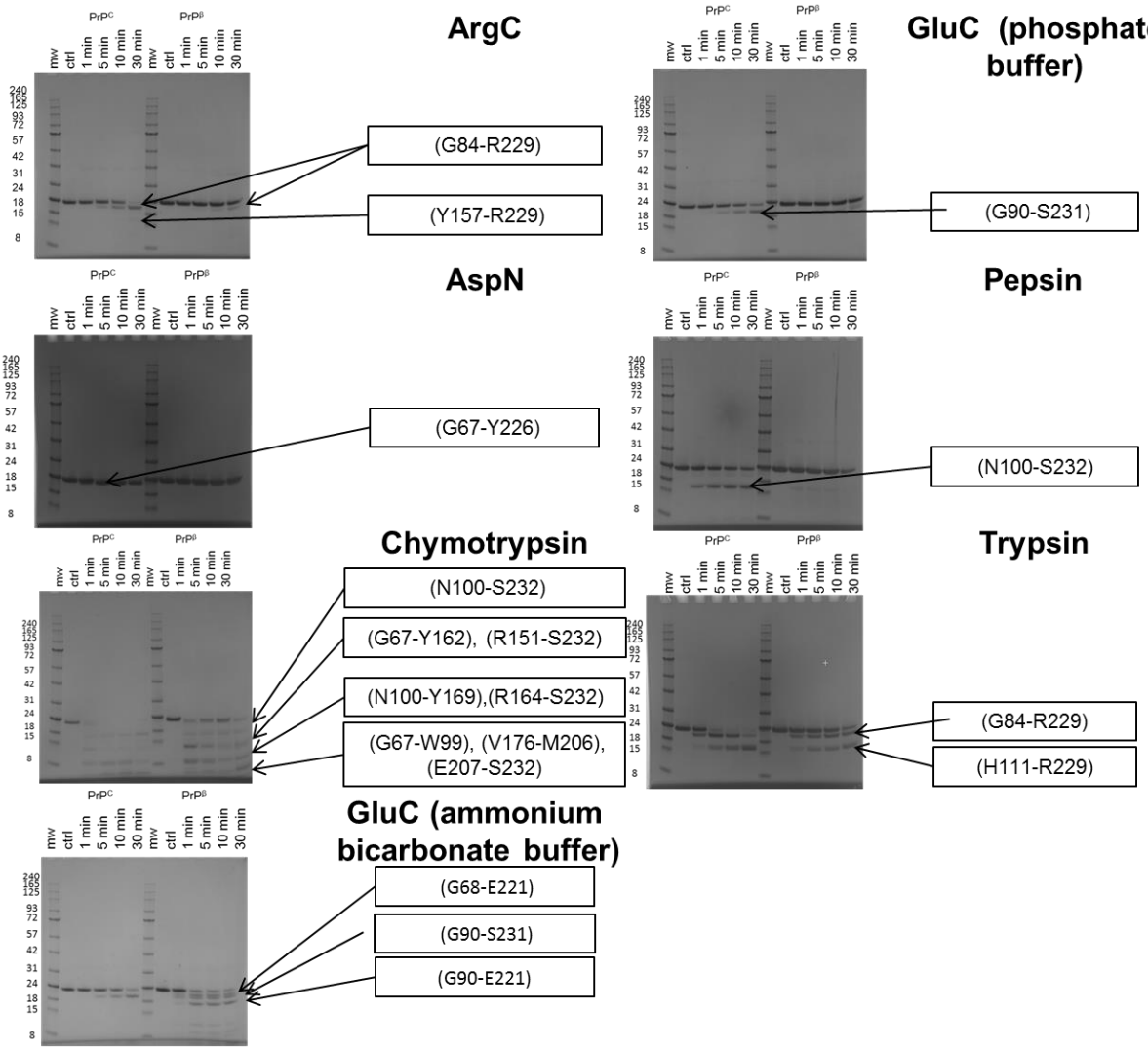

Figure 48: Limited proteolysis analysis of PrP^C and PrP^β.
PrP^C and PrP^β were digested with indicated enzymes, at 37 ^oC. Aliquots were taken at the indicated time points, and were separated by SDS-PAGE. The gel was stained with Coomassie blue, and the marked bands were excised for trypsin in-gel digestion and peptide identification by LC/ESI-MS/MS. Amino acid residues present in each excised band are indicated. Reprinted from Serpa et al. (303).

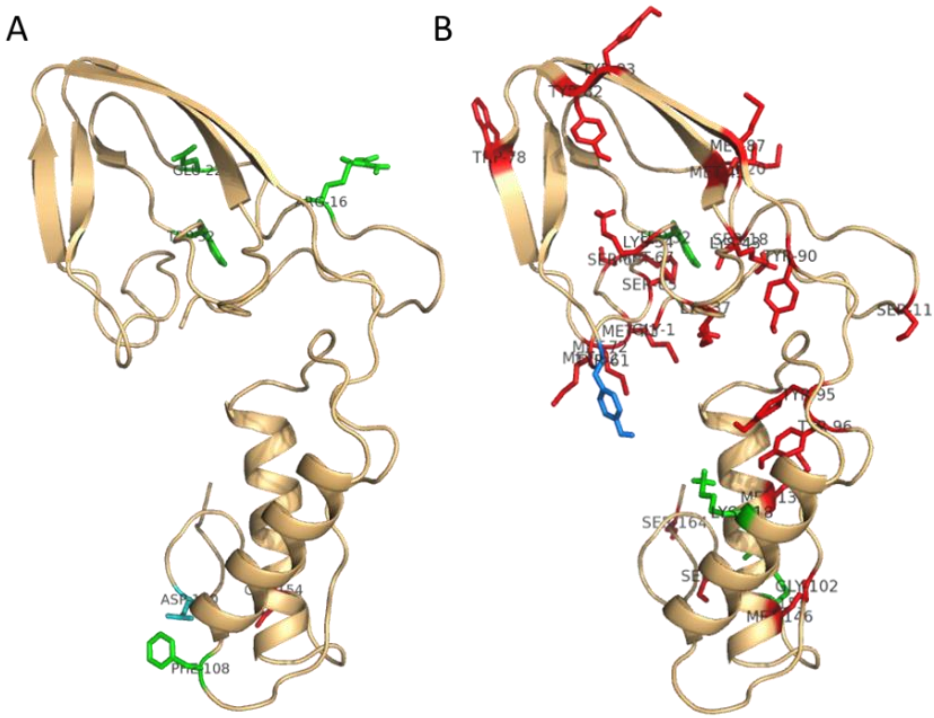

Figure 49: Limited proteolysis analysis results shown on a model of the PrP^{β} monomer.
A) Limited proteolysis results. Residues more exposed in PrP^{β} than in PrP^{C} are shown in red; residues equally exposed in PrP^{β} and PrP^{C} are shown in blue; residues more exposed in PrP^{C} than in PrP^{β} are shown in green. B) Surface modification results for PCAS (Table 9) and H_2O_2 (Table 10), shown on a model of the PrP^{β} oligomer. Residues more exposed in PrP^{β} than in PrP^{C} are shown in red; residues equally exposed in PrP^{β} and PrP^{C} are shown in blue; residues more exposed in PrP^{C} than in PrP^{β} are shown in green. Reprinted from Serpa et al. (303).

5.3.5. Surface modification

Surface modification provides information on the accessibility of residues to small (modification reagent) probes. I used isotopically-coded amine-reactive PCAS (Figure 35) (22) and isotopically-coded hydrogen-peroxide for differential surface modification experiments on PrP^{C} versus PrP^{β} (Figure 32) (302). In these experiments, PrP^{C} and PrP^{β} were modified with either the light or heavy isotopic forms of the reagents. The reactions were quenched, samples from both protein forms were combined in a 1:1 ratio, digested, and analyzed by LC-MS/MS. In this experimental design, residues that are equally exposed in both protein forms result in doublets of peaks of equal intensity. Residues

which will differ in surface accessibility between the two protein states will show a higher degree of modification in one of the states, resulting in doublets of peaks with unequal intensity ratios.

In the PCAS surface modification experiments, we detected several differentially-modified residues between the PrP^{C} and PrP^{β} forms (Table 9, Figure 47). Differentially modified tyrosine residues Y149, Y150, Y157, Y162, and Y169 are located within the β1-H1-β2 region and showed increased exposure in PrP^{β}. Tyrosines Y149, Y150, and Y157 contact the internal regions of H2 and H3 and are buried in the native PrP^{C} structure (Figure 47). Interestingly, Y149, Y150, Y162, and Y163 were preferentially modified with PCAS, but were protected from chymotryptic proteolysis (Figure 47), possibly indicating a tight packing of this re-formed region in the PrP^{β} form. Y128, which was shown by crosslinking to be in close proximity to this region, exhibited an equal degree of modification in PrP^{C} and PrP^{β} and therefore was equally exposed in the two prion forms (Figure 47). These tyrosine residues (Y128, Y149, Y150, Y157, Y162, Y163, Y169) may represent adjacent interacting residues with the apparent β-nucleation site. Both K185 and K220 were less accessible in PrP^{β} than in PrP^{C}, possibly indicating involvement of these residues in the stacking of the subunits and interaction with the relocated N-terminal part in the oligomer (Table 9, Figure 49).

Residue	Residue #	Peptide	Mean of log cβ	Mean of log βc	antilog of mean of log cβ	antilog of mean of log βc	PrP c	PrP β
G	67	**G**SSHHHHHHSSGLVPRGSHM.L	-2.7 +/- 2.12	-2.42 +/- 2.32	0.002	0.004		X
S	78	S.**S**GLVPRGSHM(+15.99).L	-0.24 +/- 0.02	-0.08 +/- 0.04	0.570	0.825		X
S	85	L.VPRG**S**HM(+15.99).L	-0.27 +/- 0.05	-0.21 +/- 0.05	0.532	0.610		X
K	101	LEGQGGGTHNQWN**K**PSKPKTNM	-3.47 +/- 0.06	-2.23 +/- 1.94	0.000	0.006		X
K	104	M.LEGQGGGTHNQWNKP(+15.99)SKP**K**TNM.K	-4.53 +/- 2.06	-2.51 +/- 2.3	0.000	0.003		X
K	110	M.**K**HM(+15.99)AGAAAAG.A	-0.63 +/- 0.03	-0.57 +/- 0.10	0.234	0.266		X
Y	128	G.AAAAGAVVGGLGG**Y**MLG.S	0.02 +/- 0.1	-0.37 +/- 0.05	1.040	0.428	X	X
S	132	G.**S**AM(+15.99)SRPMM(+15.99).H	-0.08 +/- 0.09	-0.47 +/- 0.10	0.841	0.340		X
S	135	A.M**S**RPM(+15.99)M(+15.99)HFGND.W	-0.01 +/- 0.01	-0.23 +/- 0.19	0.985	0.588		X
Y	149	M.HFGNDWEDR**Y**.Y	-0.86 +/- 0.12	-1.03 +/- 0.10	0.139	0.094		X
Y	150	Y.**Y**RENM(+15.99).N	-1.04 +/- 0.14	-1.05 +/- 0.11	0.092	0.089		X
Y	157	M.NR**Y**PNQV.Y	-1.12 +/- 0.14	-1.12 +/- 0.07	0.075	0.076		X
Y	162	M.NRYPNQV**Y**.Y	-1.03 +/- 0.04	-1.03 +/- 0.03	0.093	0.094		X
Y	163	Q.V**YY**RPVDQY.N	-0.65 +/- 0.06	-0.85 +/- 0.06	0.224	0.141		X
Y	169	V.YYRPVDQ**Y**NNQNN.F	-0.51 +/- 0.09	-0.54 +/- 0.08	0.310	0.288		X
K	185	T.I**K**QHTVT.T	-0.74 +/- 0.78	1.56 +/- 0.56	5.433	36.176	X	
K	220	E.RVVEQMCTTQYQ**K**ESQA.Y	-1.4 +/- 0.36	0.96 +/- 0.08	24.882	9.044	X	
S	222	E.**S**QAYYDGRRSS	-2.94 +/- 1.89	-4.22 +/- 1.96	0.001	0.000		X
Y	226	Q.AY**Y**DGRRSS	-0.93 +/- 0.23	-1.09 +/- 0.17	0.118	0.082		X
S	231	Q.AYYDGRS**S**	-2.37 +/- 1.83	-2.33 +/- 1.59	0.004	0.005		X

Table 9: Differential surface modification (PCAS modification) of PrP^{C} and PrP^{β}.

Table indicating residues that were differentially modified with PCAS. The mean of the log of the ratio of peak areas for PrP^{C} versus PrP^{β} (cβ) and for

PrP^{β} versus PrP^{C} are listed as are the antilog of the mean log of cβ and βc. Colours and represent PCAS's preferential modification of PrP^{C} (green), PrP^{β} (red), or the equal modification of both forms(blue). Reprinted from Serpa et al. (303).

Using surface modification with isotopically coded hydrogen peroxide, we also detected several residues that were differentially modified in the PrP^{C} versus the PrP^{β} forms (Table 10, Figure 47). Residues that are preferentially modified in PrP^{β} (M129, M134, M138, M139, W145 and M154) indicate increased exposure and are located within the rearranged β1-H1-β2 region (Figure 47). W99 was shown to be less exposed in PrP^{β} than in PrP^{C}. This is in agreement with both the chymotrypsin and the pepsin limited-proteolysis results, indicating this residue is buried in PrP^{β} (Figure 47).

Residue	Residue #	Peptide	log rcβ	log rβc	antilog of comparitive ratio	PrPc	PrPβ
M	87	R.GSH**M**LEGQGGGTHNQWNK.P	-0.08 +/- 0.08	-0.15 +/- 0.04	2.11		X
W	99	R.GSHMLEGQGGGTHNQ**W**NKPSKPK.T	0.02 +/- 0.02	0.03 +/- 0.02	0.6	X	
M	112	H.**M**AGAAAAGAVVGGLGGYMLGSAMSR.P	0.05 +/- 0.03	0.02 +/- 0.04	1.61		X
M	129	G.LGGY**M**LGSAMSR.P	-0.25 +/- 0.1	-0.32 +/- 0.07	1.52		X
M	134	G.AVVGGLGGYMLGSA**M**SR.P	0 +/- 0.17	-0.05 +/- 0.16	1.22		X
M	138	R.P**M**MHFGNDWEDRYYR.E	-0.06 +/- 0.06	-0.07 +/- 0.04	1.33		X
M	139	M.**M**HFGNDWEDR.Y	-0.42 +/- 0.02	-0.47 +/- 0	431.35		X
W	145	R.PMMHFGND**W**EDR.Y	-0.02 +/- 0.04	-0.29 +/- 0.01	12.39		X
M	154	R.EN**M**NRYPNQVYYR.P	0.07 +/- 0.08	-0.14 +/- 0.03	1.59		X
M	206	K.GENFTETDIK**M**ER.V	-0.05 +/- 0.08	-0.28 +/- 0.01	15.09		X
M	213	R.VVEQ**M**CTTQYQK.E	-0.06 +/- 0.1	-0.33 +/- 0.06	8.68		X

Table 10: Differential surface modification (hydrogen peroxide oxidation) of PrP^{C} and PrP^{β}.

Table indicating residues that are differentially H_2O_2 modified. The log and standard deviation of the ratio of peak areas for PrP^{C} versus PrP^{β} (rcβ) and PrP^{β} versus PrP^{C} (rβc) are indicated. The antilog of the comparative ratio, and the preferential modification by H_2O_2 of PrP^{C} (green) or PrP^{β} (red) are displayed. Reprinted from Serpa et al. (303).

5.3.6. PrP^{β} model

Our PrP^{β} model is consistent with experimental data obtained using numerous other methods. Wille et al. (58) used negative stain electron microscopy to determine recombinant $ShPrP_{90-231}$ fibrils as having an average diameter of 79 +/- 38 Å which compares to the diameter of our trimer model, which is approximately 48 Å (Figure 50). Peretz et al. (414) used a panel of recombinant antibodies to $ShPrP^{C}$, with linear epitopes, to determine that residues within the N-terminal region (aa90 –aa120) were largely unaccessible in hamster brain derived PrP 27-30 and remained accessible in PrP^{C} (Figure

51A). Numerous monoclonal antibody studies have also described the N-terminal domain as important in the conversion of PrP^{C} to PrP^{Sc} and implicate this domain as critical to the binding of PrP^{C} to PrP^{Sc} (Figure 51A)(415-419). These studies indicate that the major change in conformation to PrP^{Sc} occurs within this region, which is in agreement with our PrP^{β} model (Figure 49, Figure 50, Figure 51).

The PrP^{C}-selective antibody D18 (416) binds the β1-H1 loop and the H1 helix (aa132 – aa156) and has no reactivity with PrP^{Sc}, which is also consistent with our model which shows that this region has undergone significant structural rearrangement (Figure 51B). Epitopes for PrP^{Sc} specific YYR antibody (420) (aa148- aa150 and 161 - aa163) are both exposed in our model (Figure 51C). The PrP^{Sc}-specific monoclonal antibody 6H10 has a discontinuous epitope located at the C-terminal region of helix H3 (aa215 – aa216, aa221- aa223, aa228) (421) where our model also shows structural rearrangement of the helix (Figure 51D).

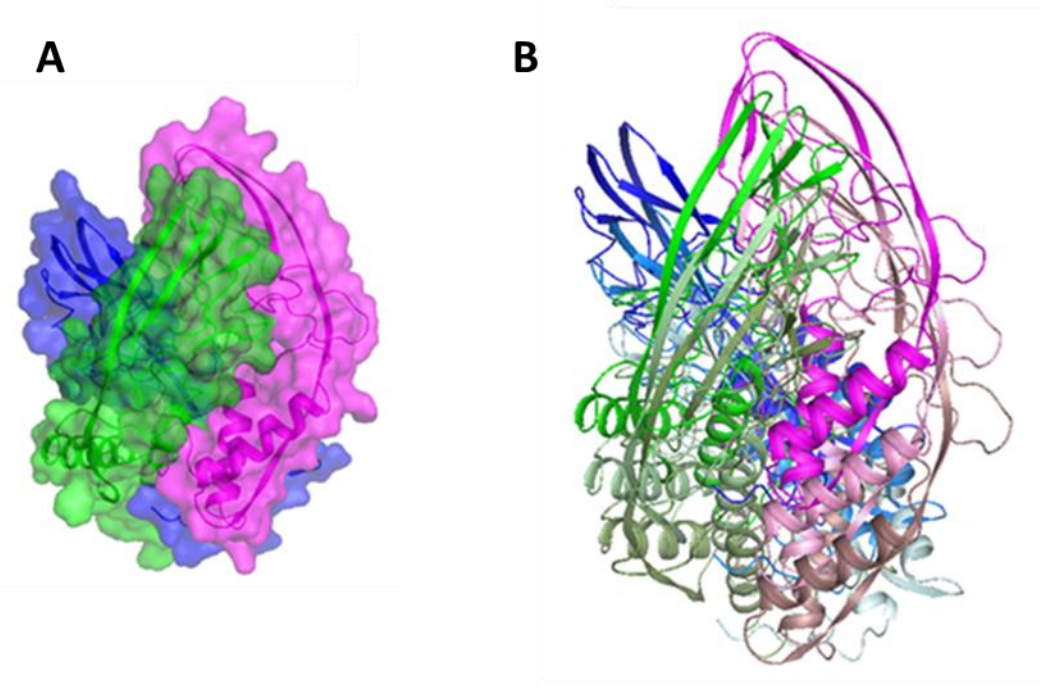

Figure 50: Arrangement of subunits of PrP^{β} oligomer.
A) Three PrP^{β} oligomers (magenta, green, and blue) are shown in a possible trimer arrangement. B) Alignment of subunits in the oligomer. PrP^{β} monomers are arranged to represent the putative assembly. β-strands on the periphery along the length of the axis may explain the creation of β-nucleation site. Reprinted from Serpa et al. (303).

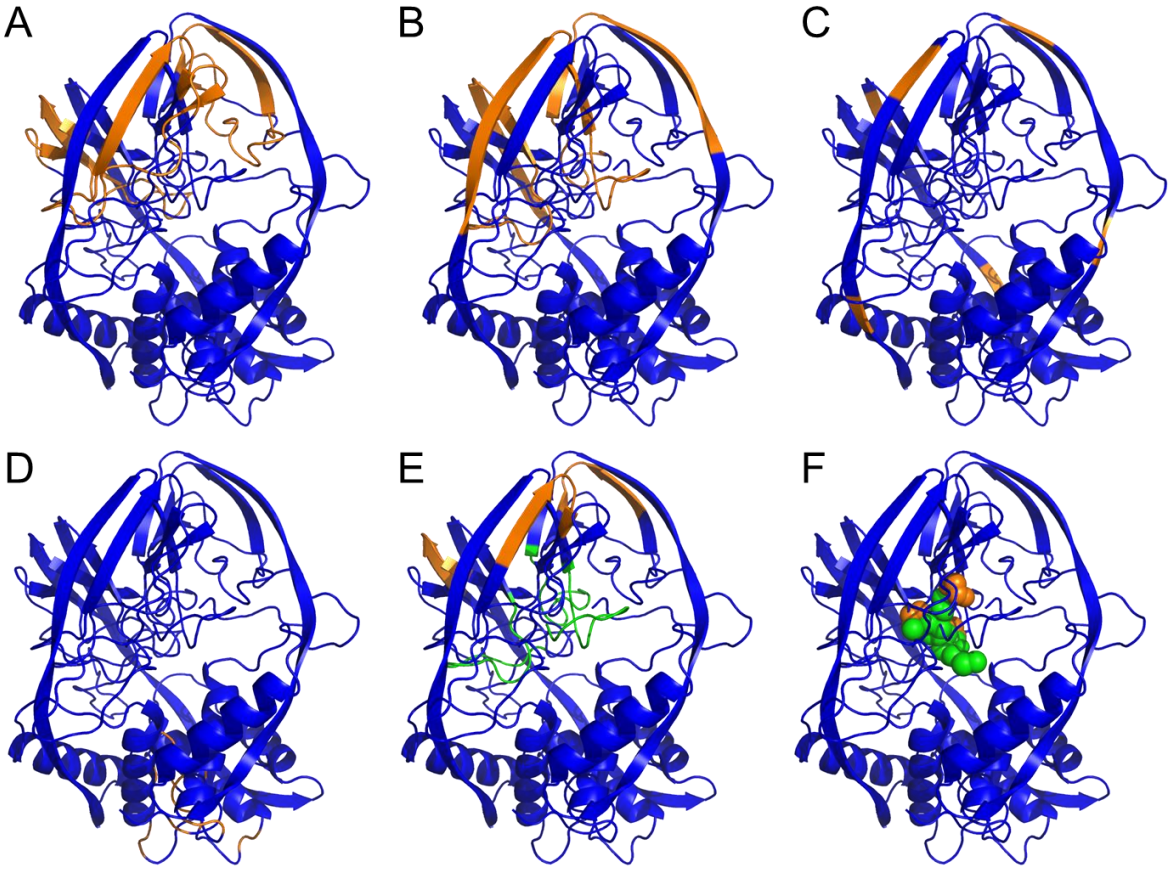

Figure 51: Model of PrP^{β} oligomer assembled as a trimer.
Three monomers of PrP^{β} are illustrated (blue). A) Residues within the N-terminal region (aa90 – aa120) are accessible to antibodies used against PrP^{C} but not PrP27-30 (green). B) The PrP^{C}-specific antibody D18 binds to PrP^{C} at the β1-H1 loop and helix H1 (aa 132 – aa156). This region shows a marked structural rearrangement in the model of the oligomer (orange). C) Epitopes of the PrP^{Sc}-specific YYR antibody (aa148 – aa150 and aa161 – 163) are exposed in the model of the trimer (shown in orange). D) The PrP^{Sc}-specific monoclonal antibody has a discontinuous epitope (aa215 – aa216, aa221 – aa223, aa228). Residues that formed the discontinuous epitope (orange) have undergone structural rearrangement from C-terminal end of the H3 helix in PrP^{C}. E) Synthetic peptides of residues aa113 – aa120 (orange) and aa129 – aa141 (green) can inhibit the formation of protease-resistant prion. F) Polymorphic variants of *PRNP* involved in protection against prion infection. Residues 129 (orange) and 127 (green) are illustrated. Reprinted from Serpa et al. (303)

Chabry et al. (422) demonstrated that synthetic peptides corresponding to aa113 - aa120 and aa129 – aa141 can inhibit the formation of protease-resistant prion protein *in vitro*. These peptides represent regions in our model which may be implicated in conversion (Figure 51E). Recombinant antibody antigen-binding fragments (Fabs) of D18 antibody (416) (described above) has also been shown to inhibit the conversion of PrP^{C} to PrP^{Sc} and to inhibit the development of prion disease *in vivo* (96,423).

A common polymorphism of human prion protein has either methionine or valine at residue 129. M129V heterozygotes have relative protection from sporadic, acquired, and some inherited forms of prion disease (424-426). This protection is thought to occur by inhibiting homotropic protein-protein interactions (425,427). Residue 129 may also directly effect the propagation of some prion strains by conformational selection (94,428). Polymorphism at codon 127 (G127V) has been shown to be protective against Kuru and, interestingly, has only been identified among natives of Papua New Guinea (429). PICUP inter-protein crosslinks between Y128 of different subunits (Appendix B: Table of all urea-acid induced PrPβ inter-protein crosslinked sites identified) demonstrate the close inter-protein proximity of these critical polymorphic variants at residues 127 and 129. In our PrP^{β} trimer model, these residues are localized in the central region of the trimer where inter-protein contacts are known to occur, which may explain why G127V may have importance for protective effects against conversion (Figure 51F). Our model confirms that the conformational change occurring during urea-acid conversion results from the rearrangement of the PrP^{C} β1-H1-β2 region and disruption of its original contacts with the H2-H3 core. It shows that the H2-H3 core area becomes involved in contacts with the rearranged aa126-aa170 region of an adjacent monomer (Figure 47). The aa144-aa165 region shows increased protection in HDX and is involved in numerous crosslinks (3 intra-protein, 5 inter-protein). This region also appears to participate in the formation of new hydrophobic patches and is thought to be involved in the formation of a β-sheet nucleation site and new inter-protein contacts.

5.4. Conclusion

Data from multiple structural proteomics approaches have enabled us to determine the structure of urea-acid converted prion oligomers. The structure obtained explains the mechanism of the conformational change involved in the conversion, the early formation

of the β-structure nucleation site, and describes the mode of assembly of the subunits within the oligomer.

Chapter 6: Discussion and Future Directions

6.1. Summary of research objectives

My research hypothesis was that a rearrangement of the H1-β2-H2 interface in normal PrP^C monomers leads to the formation of new inter-subunit interaction interfaces in the prion aggregates, thereby leading to aggregation.

My objective was to use constraints obtained by structural proteomics methods to determine the 3D structure of urea-acid induced recombinant prion oligomers (PrP^β). This structure would explain the mechanism of the conformational change involved in the conversion, the early formation of the β-structure nucleation site, and would describe the mode of assembly of the subunits within the oligomer.

In Chapter 2, I was able to demonstrate the use of proteinase-K digestion for crosslinking combined with mass spectrometry. By using proteinase-K, the broad specificity and high activity of this enzyme leads to extensive digestion of the crosslinked proteins, providing comprehensive coverage of the crosslinked sites. Furthermore, the digestion produces a series of related inter-peptide crosslink species differing by one amino acid residue, which provides additional conformation of the crosslink assignments. This was especially useful for prion oligomers which are poorly digested by trypsin, the most common enzyme used in crosslinking workflows. Indeed, proteinase K digestion was essential for obtaining acid-induced PrP^β oligomer crosslinking constraints described in Chapters 2, 3, and 5 of this thesis (Chapter 2. Use of Proteinase K non-specific digestion for selective and comprehensive identification of inter-peptide crosslinks: Application to prion proteins, Chapter 3. Using multiple structural proteomic approaches for the characterization of prion proteins, Chapter 5. Structure of prion β-oligomers as determined by structural proteomics with crosslinking constraint-guided molecular dynamic simulations). Proteinase K was also crucial for obtaining sufficient crosslinking constraints for the modeling of urea-acid converted PrP^β, using a variety of crosslinking reagents.

In Chapter 3, I showed that a combination of structural proteomic approaches allowed us to compare the findings from each method, cross-validate the results, and solidify the overall conclusions. In this chapter, I also introduced the differential surface modification experimental approach to compare PrP^C and acid-induced PrP^β, as well as

the PCAS modification reagent that reacts with the N-terminus, and K, Y, S, and T residues. I showed that data on the structural differences between the native and aggregated forms of the prion protein, obtained from multiple structural proteomics approaches (limited proteolysis, surface modification, HDX, and crosslinking), consistently implicates the same regions of the molecule in the acid-induced PrP^{β} oligomer conversion process. This confirms that application of these multiple complementary structural proteomics approaches leads to a reliable structural characterization of a protein or protein complexes.

In chapter 4, I demonstrated that, in the case of prion protein where there are at least two conformationally different states, a comparison of the oxidation levels of specific methionine and tryptophan residues between these states can provide details of the structural differences between the two states. However, obtaining an accurate quantitative comparison of amino acid residues oxidation reactivities for different prion forms would be difficult without the use of isotopically-labeled reagents. To quantify the oxidation levels between two different conformational states of PrP, I therefore used light and heavy isotopic forms of the H_2O_2 reagent ($H_2{}^{16}O_2$ and $H_2{}^{18}O_2$, respectively). Using this approach, I was able to directly compare the relative reactivities of specific amino acid residues in PrP^{C} and the acid-induced $PrP^{ß}$ form. This, in turn, allowed me to determine changes in the surface exposure of specific methionine and tryptophan residues, and, from these changes, I was able to determine differences in the structures of these two prion forms.

In Chapter 5, to further my investigation of the PrP^{β} structure, I performed a comprehensive study using multiple proteomic techniques for the determination of urea-acid induced prion oligomer structure. A panel of proteolytic enzymes was used for limited proteolysis: ^{12}C and ^{13}C PCAS were used for differential modification of the N-terminus, K, Y, S, and T residues, and isotopically-labeled hydrogen peroxide was used to induce differential oxidation of W and M residues. The results of these experiments were used to determine changes in surface exposure resulting from the conversion. HDX was used to assess changes in secondary structure between PrP^{C} and PrP^{β}. A panel of crosslinking reagents, including zero-length and short- and long- range crosslinking reagents was applied to an equimolar mixture of $^{14}N/^{15}N$-metabolically labeled β-

oligomer, and used to identify intra- and inter- protein crosslinks. A combination of these structural proteomic methods was also used to compare the structures of PrP^{C} before and after conversion to the urea-acid induced PrP^{β} oligomeric form.

This experimentally derived information allowed us to assemble a CL-DMD model of the β-oligomer, based on all of the crosslinking constraints obtained. This model is in agreement with my research hypothesis that a rearrangement of the H1-β2-H2 interface in normal PrP^{C} monomers leads to the formation of new inter-subunit interaction interfaces in the prion aggregates, thereby leading to aggregation. Our model confirms that the conformational change occurring during urea-acid conversion results from the rearrangement of the PrP^{C} β1-H1-β2 region and disruption of its original contacts with the H2-H3 core. It shows that the H2-H3 core area becomes involved in contacts with the rearranged aa126-aa170 region of an adjacent monomer. The aa144-aa165 region shows increased protection in HDX and is involved in numerous crosslinks (3 intra-protein, 5 inter-protein). This region appears to participate in the formation of new hydrophobic patches and is thought to be involved in the formation of a β-sheet nucleation site and new inter-protein contacts.

We have contributed to the field of prion research by explaining how the oligomer forms. We did this by determining the structure of the β-oligomer, from which we were able to propose the mechanism of assembly of oligomers. This structure allowed us to understand the process of oligomerization, as well as how the assembled structure can grow, and -- quite probably -- how these structures can mature into fibrils. We show that most of the important residues and regions involved in the conformational change are located in the central axis of our assembled oligomer, which is consistent with the experimental data from the literature. Our findings can represent the structural basis of understanding how prion disease progresses.

6.2. Future Directions

The use of proteomic techniques to study protein structure is an evolving field. New techniques and specialized reagents continue to be developed. For example, the Borchers laboratory recently published work (335) on α-synuclein protein using the same isotopically-coded PCAS surface modification reagent, but for surface modification of

folded and urea-unfolded versions of the protein. In this scheme, the protein is modified with the modification reagent in the light or heavy form, and with or without 8 molar urea, which leads to unfolding of the protein. Since all modifiable residues should be modified when in the denatured form, it is possible to determine the relative accessibility of a given residue when modified in its native structural state. Although, in our case, we obtained important information by comparing PrP^{C} to PrP^{β} using isotopically-coded PCAS, this new approach could provide valuable constraints that could help confirm the surface accessibility of residues in their misfolded form.

Crosslinking is an expanding technology for determining protein structure. Future work in this area could involve the use of more recently developed crosslinking reagents, in particular short-range non-specific crosslinking reagents which continue to be developed by the Borchers laboratory. To deconstruct the assembly process of urea-acid induced oligomers, an in-gel digestion approach could be used. In this method, PrP^{β} would be crosslinked with a panel of crosslinking reagents and separated on an SDS-PAGE gel. Bands corresponding to the monomer, dimer, and trimer, would be excised and proteinase-K in-gel digested. The goal of this experiment would be to find crosslinks that are unique to one of the bands. For example, a crosslink identified in the trimer band but not in the monomer or dimer band could be a crosslink which could confirm the assembly of the trimer. This could remove some of the ambiguity from inter-protein crosslinks such as those obtained using $^{14}N/^{15}N$ crosslinking.

Crosslinking could also be used to directly study the kinetics of conversion of PrP^{C} to PrP^{β}. In this experiment aliquots, would be removed during the conversion process and crosslinked with the heavy form of the crosslinker. If the prion monomer, prior to conversion, is crosslinked with the light form of the crosslinker, it would be possible to quantitatively compare the emergence of certain crosslinks and the disappearance of others. This type of detailed kinetic analysis might provide information on the first regions to undergo conformational change and could allow one to distinguish between multiple conversion mechanisms provided the conversion reaction is not too rapid.

In order to understand prion diseases, it is critical to understand the details of prion biosynthesis and the posttranslational processes that are involved in the PrP^{C} to PrP^{Sc} conversion. Furthermore, the connections between the structure and function of the

native form of the prion protein, and the structure and function of the misfolded isoforms -- including their relation to infectivity, conversion, and pathogenesis -- need to be further elucidated. All of these questions are still unanswered. All of the technologies developed and used in this dissertation could be applied to other misfolded forms of prion protein including those obtained from in vivo samples. Such studies could also be performed with prion isoforms having various single point mutations which are known to make them more or less susceptible to conversion. Structures obtained from these methods would help understand which regions of the protein make it susceptible to conversion and infectivity. All of the structures obtained can be used for rational structure-based drug design and specific interrogation of regions shown to be involved in early misfolding events could be targeted in order to prevent misfolding.

Advances in prion research may be directly applicable to other neurodegenerative diseases in which aggregates are believed to transmit disease in a 'prion-like' mechanism. Proteins involved in these diseases include: amyloid beta (Aβ), tau, and α-synuclein (Alzheimer's disease), superoxide dismutase 1 (SOD1) (amyotrophic lateral sclerosis), and possibly huntingtin (Huntington's chorea) (104). Advances in the treatments of all of these diseases require a clearer understanding of the conversion mechanism that occurs *in vivo*. The similarity between the etiologies of these diseases and that of prion-related disease means that technologies developed for prions can be used to study the proteins involved these other diseases; this may eventually lead to therapies or ways to mitigate the effects of these diseases.

References

1. Lawson, V. A., Collins, S. J., Masters, C. L., and Hill, A. F. (2005) *Journal of neurochemistry* **93**, 793-801
2. Soto, C., and Castilla, J. (2004) *Nature medicine* **10 Suppl**, S63-67
3. Prusiner, S. B. (1998) *Proceedings of the National Academy of Sciences of the United States of America* **95**, 13363-13383
4. Collinge, J. (2001) *Annual review of neuroscience* **24**, 519-550
5. Soto, C., and Satani, N. (2011) *Trends in molecular medicine* **17**, 14-24
6. Prusiner, S. B. (1982) *Science* **216**, 136-144
7. Alper, T., Cramp, W. A., Haig, D. A., and Clarke, M. C. (1967) *Nature* **214**, 764-766
8. Bellinger-Kawahara, C., Diener, T. O., McKinley, M. P., Groth, D. F., Smith, D. R., and Prusiner, S. B. (1987) *Virology* **160**, 271-274
9. Duguid, J. R., Rohwer, R. G., and Seed, B. (1988) *Proceedings of the National Academy of Sciences of the United States of America* **85**, 5738-5742
10. Meyer, N., Rosenbaum, V., Schmidt, B., Gilles, K., Mirenda, C., Groth, D., Prusiner, S. B., and Riesner, D. (1991) *The Journal of general virology* **72 (Pt 1)**, 37-49
11. Kupfer, L., Hinrichs, W., and Groschup, M. H. (2009) *Current molecular medicine* **9**, 826-835
12. Prusiner, S. B., Scott, M., Foster, D., Pan, K. M., Groth, D., Mirenda, C., Torchia, M., Yang, S. L., Serban, D., Carlson, G. A., and et al. (1990) *Cell* **63**, 673-686
13. Pan, K. M., Baldwin, M., Nguyen, J., Gasset, M., Serban, A., Groth, D., Mehlhorn, I., Huang, Z., Fletterick, R. J., Cohen, F. E., and et al. (1993) *Proceedings of the National Academy of Sciences of the United States of America* **90**, 10962-10966
14. Cohen, F. E., and Prusiner, S. B. (1998) *Annual review of biochemistry* **67**, 793-819
15. Horiuchi, M., and Caughey, B. (1999) *The EMBO journal* **18**, 3193-3203
16. Oesch, B., Westaway, D., Walchli, M., McKinley, M. P., Kent, S. B., Aebersold, R., Barry, R. A., Tempst, P., Teplow, D. B., Hood, L. E., and et al. (1985) *Cell* **40**, 735-746
17. Sokolowski, F., Modler, A. J., Masuch, R., Zirwer, D., Baier, M., Lutsch, G., Moss, D. A., Gast, K., and Naumann, D. (2003) *The Journal of biological chemistry* **278**, 40481-40492
18. Lu, B. Y., and Chang, J. Y. (2002) *The Biochemical journal* **364**, 81-87
19. Caughey, B., Baron, G. S., Chesebro, B., and Jeffrey, M. (2009) *Annual review of biochemistry* **78**, 177-204
20. Serpa, J. J., Parker, C. E., Petrotchenko, E. V., Han, J., Pan, J. X., and Borchers, C. H. (2012) *Eur J Mass Spectrom* **18**, 251-267
21. Silva, C. J. (2014) *Prion* **8**, 42-50
22. Serpa, J. J., Patterson, A. P., Pan, J., Han, J., Wishart, D. S., Petrotchenko, E. V., and Borchers, C. H. (2012) *Journal of proteomics*

23. Wille, H., Michelitsch, M. D., Guenebaut, V., Supattapone, S., Serban, A., Cohen, F. E., Agard, D. A., and Prusiner, S. B. (2002) *Proceedings of the National Academy of Sciences of the United States of America* **99**, 3563-3568
24. Govaerts, C., Wille, H., Prusiner, S. B., and Cohen, F. E. (2004) *Proceedings of the National Academy of Sciences of the United States of America* **101**, 8342-8347
25. Gong, B., Ramos, A., Vazquez-Fernandez, E., Silva, C. J., Alonso, J., Liu, Z., and Requena, J. R. (2011) *Biochemistry* **50**, 4963-4972
26. Eghiaian, F., Daubenfeld, T., Quenet, Y., van Audenhaege, M., Bouin, A. P., van der Rest, G., Grosclaude, J., and Rezaei, H. (2007) *Proceedings of the National Academy of Sciences of the United States of America* **104**, 7414-7419
27. Morrissey, M. P., and Shakhnovich, E. I. (1999) *Proceedings of the National Academy of Sciences of the United States of America* **96**, 11293-11298
28. Brown, P. (2013) Transmissible Spongiform Encephalopathy: From its Beginnings to Daniel Carlton Gajdusek. in *Prions and Diseases* (Zou, W. Q., Gambetti, P. ed.), Springer Science + Business Media, New York. pp 1-19
29. Horwich, A. L., and Weissman, J. S. (1997) *Cell* **89**, 499-510
30. Cuille, J., Chelle, P.L. (1939) *C. R. Acad. Aci.* **208**, 1058-1160
31. Chandler, R. L. (1961) *Lancet* **1**, 1378-1379
32. Gajdusek, D. C. (1977) *Science* **197**, 943-960
33. Hadlow, W. J. (1959) *The Lanet* **274**, 289-290
34. Gajdusek, D. C., Gibbs, C. J., and Alpers, M. (1966) *Nature* **209**, 794-796
35. Klatzo, I., Gajdusek, D. C., and Zigas, V. (1959) *Laboratory Investigation* **8**, 799-&
36. Gibbs, C. J., Jr., Gajdusek, D. C., Asher, D. M., Alpers, M. P., Beck, E., Daniel, P. M., and Matthews, W. B. (1968) *Science* **161**, 388-389
37. Masters, C. L., Gajdusek, D. C., and Gibbs, C. J., Jr. (1981) *Brain : a journal of neurology* **104**, 559-588
38. Cho, H. J. (1976) *Nature* **262**, 411-412
39. Latarjet, R., Muel, B., Haig, D. A., Clarke, M. C., and Alper, T. (1970) *Nature* **227**, 1341-1343
40. Alper, T., Haig, D. A., and Clarke, M. C. (1966) *Biochemical and biophysical research communications* **22**, 278-284
41. Prusiner, S. B., Bolton, D. C., Groth, D. F., Bowman, K. A., Cochran, S. P., and Mckinley, M. P. (1982) *Biochemistry* **21**, 6942-6950
42. Prusiner, S. B., McKinley, M. P., Groth, D. F., Bowman, K. A., Mock, N. I., Cochran, S. P., and Masiarz, F. R. (1981) *Proceedings of the National Academy of Sciences of the United States of America* **78**, 6675-6679
43. Bolton, D. C., McKinley, M. P., and Prusiner, S. B. (1982) *Science* **218**, 1309-1311
44. Prusiner, S. B., Groth, D. F., Bolton, D. C., Kent, S. B., and Hood, L. E. (1984) *Cell* **38**, 127-134
45. McKinley, M. P., Bolton, D. C., and Prusiner, S. B. (1983) *Cell* **35**, 57-62
46. Bolton, D. C., McKinley, M. P., and Prusiner, S. B. (1984) *Biochemistry* **23**, 5898-5906
47. Griffith, J. S. (1967) *Nature* **215**, 1043-1044

48. Legname, G., Baskakov, I. V., Nguyen, H. O., Riesner, D., Cohen, F. E., DeArmond, S. J., and Prusiner, S. B. (2004) *Science* **305**, 673-676
49. Castilla, J., Saa, P., Hetz, C., and Soto, C. (2005) *Cell* **121**, 195-206
50. Deleault, N. R., Harris, B. T., Rees, J. R., and Supattapone, S. (2007) *Proceedings of the National Academy of Sciences of the United States of America* **104**, 9741-9746
51. Deleault, N. R., Walsh, D. J., Piro, J. R., Wang, F., Wang, X., Ma, J., Rees, J. R., and Supattapone, S. (2012) *Proceedings of the National Academy of Sciences of the United States of America* **109**, E1938-1946
52. Colby, D. W., Wain, R., Baskakov, I. V., Legname, G., Palmer, C. G., Nguyen, H. O., Lemus, A., Cohen, F. E., DeArmond, S. J., and Prusiner, S. B. (2010) *PLoS pathogens* **6**, e1000736
53. Kim, J. I., Cali, I., Surewicz, K., Kong, Q., Raymond, G. J., Atarashi, R., Race, B., Qing, L., Gambetti, P., Caughey, B., and Surewicz, W. K. (2010) *The Journal of biological chemistry* **285**, 14083-14087
54. Makarava, N., Kovacs, G. G., Bocharova, O., Savtchenko, R., Alexeeva, I., Budka, H., Rohwer, R. G., and Baskakov, I. V. (2010) *Acta neuropathologica* **119**, 177-187
55. Timmes, A. G., Moore, R. A., Fischer, E. R., and Priola, S. A. (2013) *PloS one* **8**, e71081
56. Wang, F., Wang, X., Yuan, C. G., and Ma, J. (2010) *Science* **327**, 1132-1135
57. Aguzzi, A., and Calella, A. M. (2009) *Physiological reviews* **89**, 1105-1152
58. Wille, H., Bian, W., McDonald, M., Kendall, A., Colby, D. W., Bloch, L., Ollesch, J., Borovinskiy, A. L., Cohen, F. E., Prusiner, S. B., and Stubbs, G. (2009) *Proceedings of the National Academy of Sciences of the United States of America* **106**, 16990-16995
59. Stohr, J., Weinmann, N., Wille, H., Kaimann, T., Nagel-Steger, L., Birkmann, E., Panza, G., Prusiner, S. B., Eigen, M., and Riesner, D. (2008) *Proceedings of the National Academy of Sciences of the United States of America* **105**, 2409-2414
60. Baskakov, I. V., Legname, G., Baldwin, M. A., Prusiner, S. B., and Cohen, F. E. (2002) *J Biol Chem* **277**, 21140-21148
61. Aguzzi, A., and Weissmann, C. (1997) *Nature* **389**, 795-798
62. Collinge, J., Palmer, M. S., Sidle, K. C. L., Gowland, I., Medori, R., Ironside, J., and Lantos, P. (1995) *Lancet* **346**, 569-570
63. Campana, V., Sarnataro, D., and Zurzolo, C. (2005) *Trends in cell biology* **15**, 102-111
64. Mabbott, N. A., and MacPherson, G. G. (2006) *Nature Reviews Microbiology* **4**, 201-211
65. Collins, S. J., Lawson, V. A., and Masters, C. L. (2004) *Lancet* **363**, 51-61
66. Collinge, J., Whitfield, J., McKintosh, E., Beck, J., Mead, S., Thomas, D. J., and Alpers, M. P. (2006) *Lancet* **367**, 2068-2074
67. Bongianni, M., Orru, C., Groveman, B. R., Sacchetto, L., Fiorini, M., Tonoli, G., Triva, G., Capaldi, S., Testi, S., Ferrari, S., Cagnin, A., Ladogana, A., Poleggi, A., Colaizzo, E., Tiple, D., Vaianella, L., Castriciano, S., Marchioni, D., Hughson, A. G., Imperiale, D., Cattaruzza, T., Fabrizi, G. M., Pocchiari, M., Monaco, S., Caughey, B., and Zanusso, G. (2016) *JAMA neurology*

68. Wadsworth, J. D., Hill, A. F., Beck, J. A., and Collinge, J. (2003) *British medical bulletin* **66**, 241-254
69. Will, R. G. (2003) *British medical bulletin* **66**, 255-265
70. Collinge, J. (1997) *Human molecular genetics* **6**, 1699-1705
71. Brown, P., Cathala, F., Raubertas, R. F., Gajdusek, D. C., and Castaigne, P. (1987) *Neurology* **37**, 895-904
72. Godsave, S. F., Peters, P. J., and Wille, H. (2015) *Virus research*
73. Prusiner, S. B. (1997) *Science* **278**, 245-251
74. Huang, Z. W., Gabriel, J. M., Baldwin, M. A., Fletterick, R. J., Prusiner, S. B., and Cohen, F. E. (1994) *Proceedings of the National Academy of Sciences of the United States of America* **91**, 7139-7143
75. Cohen, F. E., Pan, K. M., Huang, Z., Baldwin, M., Fletterick, R. J., and Prusiner, S. B. (1994) *Science* **264**, 530-531
76. Riek, R., Wider, G., Billeter, M., Hornemann, S., Glockshuber, R., and Wuthrich, K. (1998) *Proceedings of the National Academy of Sciences of the United States of America* **95**, 11667-11672
77. Swietnicki, W., Petersen, R. B., Gambetti, P., and Surewicz, W. K. (1998) *J Biol Chem* **273**, 31048-31052
78. Collinge, J., Owen, F., Poulter, M., Leach, M., Crow, T. J., Rossor, M. N., Hardy, J., Mullan, M. J., Janota, I., and Lantos, P. L. (1990) *Lancet* **336**, 7-9
79. Collinge, J., Brown, J., Hardy, J., Mullan, M., Rossor, M. N., Baker, H., Crow, T. J., Lofthouse, R., Poulter, M., Ridley, R., Owen, F., Bennett, C., Dunn, G., Harding, A. E., Quinn, N., Doshi, B., Roberts, G. W., Honavar, M., Janota, I., and Lantos, P. L. (1992) *Brain : a journal of neurology* **115**, 687-710
80. Collinge, J., Harding, A. E., Owen, F., Poulter, M., Lofthouse, R., Boughey, A. M., Shah, T., and Crow, T. J. (1989) *Lancet* **2**, 15-17
81. Safar, J. G., Geschwind, M. D., Deering, C., Didorenko, S., Sattavat, M., Sanchez, H., Serban, A., Vey, M., Baron, H., Giles, K., Miller, B. L., DeArmond, S. J., and Prusiner, S. B. (2005) *Proceedings of the National Academy of Sciences of the United States of America* **102**, 3501-3506
82. Gabizon, R., McKinley, M. P., and Prusiner, S. B. (1987) *Proceedings of the National Academy of Sciences of the United States of America* **84**, 4017-4021
83. Bueler, H., Fischer, M., Lang, Y., Bluethmann, H., Lipp, H. P., DeArmond, S. J., Prusiner, S. B., Aguet, M., and Weissmann, C. (1992) *Nature* **356**, 577-582
84. Prusiner, S. B. (1991) *Science* **252**, 1515-1522
85. Collins, S., Boyd, A., Lee, J. S., Lewis, V., Fletcher, A., McLean, C. A., Law, M., Kaldor, J., Smith, M. J., and Masters, C. L. (2002) *Neurology* **59**, 1365-1371
86. Cousens, S. N., Zeidler, M., Esmonde, T. F., De Silva, R., Wilesmith, J. W., Smith, P. G., and Will, R. G. (1997) *BMJ* **315**, 389-395
87. Parchi, P., Giese, A., Capellari, S., Brown, P., Schulz-Schaeffer, W., Windl, O., Zerr, I., Budka, H., Kopp, N., Piccardo, P., Poser, S., Rojiani, A., Streichemberger, N., Julien, J., Vital, C., Ghetti, B., Gambetti, P., and Kretzschmar, H. (1999) *Annals of neurology* **46**, 224-233
88. Krasnianski, A., Schulz-Schaeffer, W. J., Kallenberg, K., Meissner, B., Collie, D. A., Roeber, S., Bartl, M., Heinemann, U., Varges, D., Kretzschmar, H. A., and Zerr, I. (2006) *Brain : a journal of neurology* **129**, 2288-2296

89. Puoti, G., Bizzi, A., Forloni, G., Safar, J. G., Tagliavini, F., and Gambetti, P. (2012) *Lancet neurology* **11**, 618-628
90. Parchi, P., de Boni, L., Saverioni, D., Cohen, M. L., Ferrer, I., Gambetti, P., Gelpi, E., Giaccone, G., Hauw, J. J., Hoftberger, R., Ironside, J. W., Jansen, C., Kovacs, G. G., Rozemuller, A., Seilhean, D., Tagliavini, F., Giese, A., and Kretzschmar, H. A. (2012) *Acta neuropathologica* **124**, 517-529
91. Zerr, I., Pocchiari, M., Collins, S., Brandel, J. P., de Pedro Cuesta, J., Knight, R. S., Bernheimer, H., Cardone, F., Delasnerie-Laupretre, N., Cuadrado Corrales, N., Ladogana, A., Bodemer, M., Fletcher, A., Awan, T., Ruiz Bremon, A., Budka, H., Laplanche, J. L., Will, R. G., and Poser, S. (2000) *Neurology* **55**, 811-815
92. Budka, H., Aguzzi, A., Brown, P., Brucher, J. M., Bugiani, O., Gullotta, F., Haltia, M., Hauw, J. J., Ironside, J. W., Jellinger, K., Kretzschmar, H. A., Lantos, P. L., Masullo, C., Schlote, W., Tateishi, J., and Weller, R. O. (1995) *Brain Pathology* **5**, 459-466
93. Bell, J. E., Gentleman, S. M., Ironside, J. W., McCardle, L., Lantos, P. L., Doey, L., Lowe, J., Fergusson, J., Luthert, P., McQuaid, S., and Allen, I. V. (1997) *Neuropathology and applied neurobiology* **23**, 26-35
94. Collinge, J., and Clarke, A. R. (2007) *Science* **318**, 930-936
95. Brundin, P., Melki, R., and Kopito, R. (2010) *Nature reviews. Molecular cell biology* **11**, 301-307
96. White, A. R., Enever, P., Tayebi, M., Mushens, R., Linehan, J., Brandner, S., Anstee, D., Collinge, J., and Hawke, S. (2003) *Nature* **422**, 80-83
97. Perrier, V., Solassol, J., Crozet, C., Frobert, Y., Mourton-Gilles, C., Grassi, J., and Lehmann, S. (2004) *Journal of neurochemistry* **89**, 454-463
98. Korth, C., May, B. C., Cohen, F. E., and Prusiner, S. B. (2001) *Proceedings of the National Academy of Sciences of the United States of America* **98**, 9836-9841
99. Atkinson, C. J., Zhang, K., Munn, A. L., Wiegmans, A., and Wei, M. Q. (2016) *Prion* **10**, 63-82
100. Perrier, V., Wallace, A. C., Kaneko, K., Safar, J., Prusiner, S. B., and Cohen, F. E. (2000) *Proceedings of the National Academy of Sciences of the United States of America* **97**, 6073-6078
101. Canada, P. H. A. o. (2016) Creutzfeldt-Jakob Disease: CJD-Surveillance System: Statistics.
102. instiute, A. p. r. (2016) Prion Basics: Why prion research?
103. Mitura, V., Di Pietro, L. (2004) Canada‟s beef cattle sector and the impact of BSE on farm family income 2000-2003. in *Agriculture and Rural Working Paper Series 2004*, Statistics Canada, Agriculture Division
104. Prusiner, S. B. (2013) *Annual review of genetics* **47**, 601-623
105. Chesebro, B., Race, R., Wehrly, K., Nishio, J., Bloom, M., Lechner, D., Bergstrom, S., Robbins, K., Mayer, L., Keith, J. M., and et al. (1985) *Nature* **315**, 331-333
106. Basler, K., Oesch, B., Scott, M., Westaway, D., Walchli, M., Groth, D. F., McKinley, M. P., Prusiner, S. B., and Weissmann, C. (1986) *Cell* **46**, 417-428
107. Sparkes, R. S., Simon, M., Cohn, V. H., Fournier, R. E., Lem, J., Klisak, I., Heinzmann, C., Blatt, C., Lucero, M., Mohandas, T., and et al. (1986)

Proceedings of the National Academy of Sciences of the United States of America **83**, 7358-7362
108. Liao, Y. C., Lebo, R. V., Clawson, G. A., and Smuckler, E. A. (1986) *Science* **233**, 364-367
109. Robakis, N. K., Devinegage, E. A., Jenkins, E. C., Kascsak, R. J., Brown, W. T., Krawczun, M. S., and Silverman, W. P. (1986) *Biochemical and biophysical research communications* **140**, 758-765
110. Hsiao, K., Baker, H. F., Crow, T. J., Poulter, M., Owen, F., Terwilliger, J. D., Westaway, D., Ott, J., and Prusiner, S. B. (1989) *Nature* **338**, 342-345
111. Gabriel, J. M., Oesch, B., Kretzschmar, H., Scott, M., and Prusiner, S. B. (1992) *Proceedings of the National Academy of Sciences of the United States of America* **89**, 9097-9101
112. Westaway, D., Goodman, P. A., Mirenda, C. A., McKinley, M. P., Carlson, G. A., and Prusiner, S. B. (1987) *Cell* **51**, 651-662
113. McKinley, M. P., Hay, B., Lingappa, V. R., Lieberburg, I., and Prusiner, S. B. (1987) *Developmental biology* **121**, 105-110
114. Kretzschmar, H. A., Prusiner, S. B., Stowring, L. E., and DeArmond, S. J. (1986) *The American journal of pathology* **122**, 1-5
115. Manson, J., West, J. D., Thomson, V., McBride, P., Kaufman, M. H., and Hope, J. (1992) *Development* **115**, 117-122
116. Turk, E., Teplow, D. B., Hood, L. E., and Prusiner, S. B. (1988) *European journal of biochemistry / FEBS* **176**, 21-30
117. Haraguchi, T., Fisher, S., Olofsson, S., Endo, T., Groth, D., Tarentino, A., Borchelt, D. R., Teplow, D., Hood, L., Burlingame, A., Lycke, E., Kobata, A., and Prusiner, S. B. (1989) *Archives of biochemistry and biophysics* **274**, 1-13
118. Haraguchi, T., Fisher, S., Olofsson, S., Endo, T., Groth, D., Tarentino, A., Borchelt, D. R., Teplow, D., Hood, L., Burlingame, A., and et al. (1989) *Archives of biochemistry and biophysics* **274**, 1-13
119. Katorcha, E., Makarava, N., Savtchenko, R., D'Azzo, A., and Baskakov, I. V. (2014) *PLoS pathogens* **10**, e1004366
120. Stahl, N., Borchelt, D. R., Hsiao, K., and Prusiner, S. B. (1987) *Cell* **51**, 229-240
121. Stahl, N., Baldwin, M. A., Hecker, R., Pan, K. M., Burlingame, A. L., and Prusiner, S. B. (1992) *Biochemistry* **31**, 5043-5053
122. Simons, K., and Ikonen, E. (1997) *Nature* **387**, 569-572
123. Barmada, S., Piccardo, P., Yamaguchi, K., Ghetti, B., and Harris, D. A. (2004) *Neurobiology of disease* **16**, 527-537
124. Hay, B., Barry, R. A., Lieberburg, I., Prusiner, S. B., and Lingappa, V. R. (1987) *Molecular and cellular biology* **7**, 914-920
125. Hay, B., Prusiner, S. B., and Lingappa, V. R. (1987) *Biochemistry* **26**, 8110-8115
126. Hegde, R. S., Mastrianni, J. A., Scott, M. R., DeFea, K. A., Tremblay, P., Torchia, M., DeArmond, S. J., Prusiner, S. B., and Lingappa, V. R. (1998) *Science* **279**, 827-834
127. Kim, S. J., Rahbar, R., and Hegde, R. S. (2001) *The Journal of biological chemistry* **276**, 26132-26140
128. Hegde, R. S., Tremblay, P., Groth, D., DeArmond, S. J., Prusiner, S. B., and Lingappa, V. R. (1999) *Nature* **402**, 822-826

129. Stewart, R. S., and Harris, D. A. (2001) *J Biol Chem* **276**, 2212-2220
130. Holscher, C., Bach, U. C., and Dobberstein, B. (2001) *The Journal of biological chemistry* **276**, 13388-13394
131. Chakrabarti, O., Ashok, A., and Hegde, R. S. (2009) *Trends in biochemical sciences* **34**, 287-295
132. Varki, A. (1999) Sialic Acids. in *Essentials of Glycobiology* (Ajit Varki, R. C., Jeffrey Asko, Hudson Freezwe, Gerals Hart, Jamey Math ed., Cold Springs Harbor Laboratory Press, Cold Spring Harbor (NY)
133. Varki, A. (2008) *Trends in molecular medicine* **14**, 351-360
134. Brown, G. C., and Neher, J. J. (2014) *Nature reviews. Neuroscience* **15**, 209-216
135. Collins, B. E., Blixt, O., DeSieno, A. R., Bovin, N., Marth, J. D., and Paulson, J. C. (2004) *Proceedings of the National Academy of Sciences of the United States of America* **101**, 6104-6109
136. DeArmond, S. J., Qiu, Y., Sanchez, H., Spilman, P. R., Ninchak-Casey, A., Alonso, D., and Daggett, V. (1999) *Journal of neuropathology and experimental neurology* **58**, 1000-1009
137. Bolton, D. C., Meyer, R. K., and Prusiner, S. B. (1985) *Journal of virology* **53**, 596-606
138. Rudd, P. M., Endo, T., Colominas, C., Groth, D., Wheeler, S. F., Harvey, D. J., Wormald, M. R., Serban, H., Prusiner, S. B., Kobata, A., and Dwek, R. A. (1999) *Proceedings of the National Academy of Sciences of the United States of America* **96**, 13044-13049
139. Borchelt, D. R., Scott, M., Taraboulos, A., Stahl, N., and Prusiner, S. B. (1990) *The Journal of cell biology* **110**, 743-752
140. Prado, M. A., Alves-Silva, J., Magalhaes, A. C., Prado, V. F., Linden, R., Martins, V. R., and Brentani, R. R. (2004) *Journal of neurochemistry* **88**, 769-781
141. Borchelt, D. R., Taraboulos, A., and Prusiner, S. B. (1992) *The Journal of biological chemistry* **267**, 16188-16199
142. Godsave, S. F., Wille, H., Pierson, J., Prusiner, S. B., and Peters, P. J. (2013) *Neurobiology of aging* **34**, 1621-1631
143. Goold, R., Rabbanian, S., Sutton, L., Andre, R., Arora, P., Moonga, J., Clarke, A. R., Schiavo, G., Jat, P., Collinge, J., and Tabrizi, S. J. (2011) *Nature communications* **2**, 281
144. Marijanovic, Z., Caputo, A., Campana, V., and Zurzolo, C. (2009) *PLoS pathogens* **5**, e1000426
145. Rouvinski, A., Karniely, S., Kounin, M., Moussa, S., Goldberg, M. D., Warburg, G., Lyakhovetsky, R., Papy-Garcia, D., Kutzsche, J., Korth, C., Carlson, G. A., Godsave, S. F., Peters, P. J., Luhr, K., Kristensson, K., and Taraboulos, A. (2014) *The Journal of cell biology* **204**, 423-441
146. Caughey, B., and Raymond, G. J. (1991) *The Journal of biological chemistry* **266**, 18217-18223
147. Gilch, S., Winklhofer, K. F., Groschup, M. H., Nunziante, M., Lucassen, R., Spielhaupter, C., Muranyi, W., Riesner, D., Tatzelt, J., and Schatzl, H. M. (2001) *The EMBO journal* **20**, 3957-3966
148. Abid, K., Morales, R., and Soto, C. (2010) *FEBS letters* **584**, 2409-2414

149. Kim, J. I., Surewicz, K., Gambetti, P., and Surewicz, W. K. (2009) *FEBS letters* **583**, 3671-3675
150. Beranger, F., Mange, A., Goud, B., and Lehmann, S. (2002) *The Journal of biological chemistry* **277**, 38972-38977
151. Fevrier, B., Vilette, D., Archer, F., Loew, D., Faigle, W., Vidal, M., Laude, H., and Raposo, G. (2004) *Proceedings of the National Academy of Sciences of the United States of America* **101**, 9683-9688
152. Westaway, D., Carlson, G. A., and Prusiner, S. B. (1989) *Trends in neurosciences* **12**, 221-227
153. Harris, D. A., Falls, D. L., Johnson, F. A., and Fischbach, G. D. (1991) *Proceedings of the National Academy of Sciences of the United States of America* **88**, 7664-7668
154. Pauly, P. C., and Harris, D. A. (1998) *The Journal of biological chemistry* **273**, 33107-33110
155. Brown, D. R., and Besinger, A. (1998) *The Biochemical journal* **334 (Pt 2)**, 423-429
156. Walz, R., Amaral, O. B., Rockenbach, I. C., Roesler, R., Izquierdo, I., Cavalheiro, E. A., Martins, V. R., and Brentani, R. R. (1999) *Epilepsia* **40**, 1679-1682
157. Roesler, R., Walz, R., Quevedo, J., de-Paris, F., Zanata, S. M., Graner, E., Izquierdo, I., Martins, V. R., and Brentani, R. R. (1999) *Brain research. Molecular brain research* **71**, 349-353
158. Sakaguchi, S., Katamine, S., Nishida, N., Moriuchi, R., Shigematsu, K., Sugimoto, T., Nakatani, A., Kataoka, Y., Houtani, T., Shirabe, S., Okada, H., Hasegawa, S., Miyamoto, T., and Noda, T. (1996) *Nature* **380**, 528-531
159. Tobler, I., Gaus, S. E., Deboer, T., Achermann, P., Fischer, M., Rulicke, T., Moser, M., Oesch, B., McBride, P. A., and Manson, J. C. (1996) *Nature* **380**, 639-642
160. Prince, R. C., and Gunson, D. E. (1998) *Trends in biochemical sciences* **23**, 197-198
161. Brown, D. R. (1999) *Journal of neuroscience research* **58**, 717-725
162. White, A. R., Collins, S. J., Maher, F., Jobling, M. F., Stewart, L. R., Thyer, J. M., Beyreuther, K., Masters, C. L., and Cappai, R. (1999) *The American journal of pathology* **155**, 1723-1730
163. Wong, B. S., Pan, T., Liu, T., Li, R., Gambetti, P., and Sy, M. S. (2000) *Biochemical and biophysical research communications* **273**, 136-139
164. Frederikse, P. H., Zigler, S. J., Jr., Farnsworth, P. N., and Carper, D. A. (2000) *Current eye research* **20**, 137-143
165. Brown, D. R., Clive, C., and Haswell, S. J. (2001) *Journal of neurochemistry* **76**, 69-76
166. Brown, D. R., Nicholas, R. S., and Canevari, L. (2002) *Journal of neuroscience research* **67**, 211-224
167. Dupuis, L., Mbebi, C., Gonzalez de Aguilar, J. L., Rene, F., Muller, A., de Tapia, M., and Loeffler, J. P. (2002) *Molecular and cellular neurosciences* **19**, 216-224
168. Huber, R., Deboer, T., and Tobler, I. (2002) *Neuroreport* **13**, 1-4
169. Miele, G., Jeffrey, M., Turnbull, D., Manson, J., and Clinton, M. (2002) *Biochemical and biophysical research communications* **291**, 372-377

170. Curtis, J., Errington, M., Bliss, T., Voss, K., and MacLeod, N. (2003) *Neurobiology of disease* **13**, 55-62
171. Zeng, F., Watt, N. T., Walmsley, A. R., and Hooper, N. M. (2003) *Journal of neurochemistry* **84**, 480-490
172. Rachidi, W., Vilette, D., Guiraud, P., Arlotto, M., Riondel, J., Laude, H., Lehmann, S., and Favier, A. (2003) *The Journal of biological chemistry* **278**, 9064-9072
173. Brown, D. R. (2004) *Neurobiology of disease* **15**, 534-543
174. Brown, L. R., and Harris, D. A. (2003) *Journal of neurochemistry* **87**, 353-363
175. Lee, K. S., Linden, R., Prado, M. A., Brentani, R. R., and Martins, V. R. (2003) *Reviews in medical virology* **13**, 399-408
176. Linden, R., Martins, V. R., Prado, M. A., Cammarota, M., Izquierdo, I., and Brentani, R. R. (2008) *Physiological reviews* **88**, 673-728
177. Martins, V. R., Beraldo, F. H., Hajj, G. N., Lopes, M. H., Lee, K. S., Prado, M. A., and Linden, R. (2010) *Current issues in molecular biology* **12**, 63-86
178. Beraldo, F. H., Arantes, C. P., Santos, T. G., Queiroz, N. G., Young, K., Rylett, R. J., Markus, R. P., Prado, M. A., and Martins, V. R. (2010) *The Journal of biological chemistry* **285**, 36542-36550
179. Roffe, M., Beraldo, F. H., Bester, R., Nunziante, M., Bach, C., Mancini, G., Gilch, S., Vorberg, I., Castilho, B. A., Martins, V. R., and Hajj, G. N. (2010) *Proceedings of the National Academy of Sciences of the United States of America* **107**, 13147-13152
180. Santos, T. G., Beraldo, F. H., Hajj, G. N., Lopes, M. H., Roffe, M., Lupinacci, F. C., Ostapchenko, V. G., Prado, V. F., Prado, M. A., and Martins, V. R. (2013) *Journal of neurochemistry* **124**, 210-223
181. Lopes, M. H., Hajj, G. N., Muras, A. G., Mancini, G. L., Castro, R. M., Ribeiro, K. C., Brentani, R. R., Linden, R., and Martins, V. R. (2005) *The Journal of neuroscience : the official journal of the Society for Neuroscience* **25**, 11330-11339
182. Santuccione, A., Sytnyk, V., Leshchyns'ka, I., and Schachner, M. (2005) *The Journal of cell biology* **169**, 341-354
183. Beraldo, F. H., Arantes, C. P., Santos, T. G., Machado, C. F., Roffe, M., Hajj, G. N., Lee, K. S., Magalhaes, A. C., Caetano, F. A., Mancini, G. L., Lopes, M. H., Americo, T. A., Magdesian, M. H., Ferguson, S. S., Linden, R., Prado, M. A., and Martins, V. R. (2011) *FASEB journal : official publication of the Federation of American Societies for Experimental Biology* **25**, 265-279
184. Mouillet-Richard, S., Ermonval, M., Chebassier, C., Laplanche, J. L., Lehmann, S., Launay, J. M., and Kellermann, O. (2000) *Science* **289**, 1925-1928
185. Mouillet-Richard, S., Pietri, M., Schneider, B., Vidal, C., Mutel, V., Launay, J. M., and Kellermann, O. (2005) *The Journal of biological chemistry* **280**, 4592-4601
186. Mouillet-Richard, S., Schneider, B., Pradines, E., Pietri, M., Ermonval, M., Grassi, J., Richards, J. G., Mutel, V., Launay, J. M., and Kellermann, O. (2007) *Annals of the New York Academy of Sciences* **1096**, 106-119

187. Loubet, D., Dakowski, C., Pietri, M., Pradines, E., Bernard, S., Callebert, J., Ardila-Osorio, H., Mouillet-Richard, S., Launay, J. M., Kellermann, O., and Schneider, B. (2012) *Faseb Journal* **26**, 678-690
188. Pietri, M., Caprini, A., Mouillet-Richard, S., Pradines, E., Ermonval, M., Grassi, J., Kellermann, O., and Schneider, B. (2006) *J Biol Chem* **281**, 28470-28479
189. Hirsch, T. Z., Hernandez-Rapp, J., Martin-Lanneree, S., Launay, J. M., and Mouillet-Richard, S. (2014) *Biochimie*
190. Moreno, J. A., Radford, H., Peretti, D., Steinert, J. R., Verity, N., Martin, M. G., Halliday, M., Morgan, J., Dinsdale, D., Ortori, C. A., Barrett, D. A., Tsaytler, P., Bertolotti, A., Willis, A. E., Bushell, M., and Mallucci, G. R. (2012) *Nature* **485**, 507-511
191. Beraldo, F. H., Ostapchenko, V. G., Caetano, F. A., Guimaraes, A. L., Ferretti, G. D., Daude, N., Bertram, L., Nogueira, K. O., Silva, J. L., Westaway, D., Cashman, N. R., Martins, V. R., Prado, V. F., and Prado, M. A. (2016) *The Journal of biological chemistry* **291**, 21945-21955
192. Kuffer, A., Lakkaraju, A. K., Mogha, A., Petersen, S. C., Airich, K., Doucerain, C., Marpakwar, R., Bakirci, P., Senatore, A., Monnard, A., Schiavi, C., Nuvolone, M., Grosshans, B., Hornemann, S., Bassilana, F., Monk, K. R., and Aguzzi, A. (2016) *Nature* **536**, 464-468
193. Carneiro, M. V., Americo, T. A., Guimaraes, M. Z., and Linden, R. (2016) *Biochemical and biophysical research communications* **472**, 293-298
194. Watt, N. T., Taylor, D. R., Kerrigan, T. L., Griffiths, H. H., Rushworth, J. V., Whitehouse, I. J., and Hooper, N. M. (2012) *Nature communications* **3**, 1134
195. You, H., Tsutsui, S., Hameed, S., Kannanayakal, T. J., Chen, L., Xia, P., Engbers, J. D., Lipton, S. A., Stys, P. K., and Zamponi, G. W. (2012) *Proceedings of the National Academy of Sciences of the United States of America* **109**, 1737-1742
196. Um, J. W., Kaufman, A. C., Kostylev, M., Heiss, J. K., Stagi, M., Takahashi, H., Kerrisk, M. E., Vortmeyer, A., Wisniewski, T., Koleske, A. J., Gunther, E. C., Nygaard, H. B., and Strittmatter, S. M. (2013) *Neuron* **79**, 887-902
197. Haas, L. T., Salazar, S. V., Kostylev, M. A., Um, J. W., Kaufman, A. C., and Strittmatter, S. M. (2016) *Brain : a journal of neurology* **139**, 526-546
198. Amin, L., Nguyen, X. T., Rolle, I. G., D'Este, E., Giachin, G., Tran, T. H., Serbec, V. C., Cojoc, D., and Legname, G. (2016) *J Cell Sci*
199. Riek, R., Hornemann, S., Wider, G., Billeter, M., Glockshuber, R., and Wuthrich, K. (1996) *Nature* **382**, 180-182
200. Riek, R., Hornemann, S., Wider, G., Glockshuber, R., and Wuthrich, K. (1997) *FEBS letters* **413**, 282-288
201. Schrodinger, L. (2014) The PyMOL Molecular Graphics System, Version 1.3.
202. Zahn, R., Liu, A., Luhrs, T., Riek, R., von Schroetter, C., Lopez Garcia, F., Billeter, M., Calzolai, L., Wider, G., and Wuthrich, K. (2000) *Proceedings of the National Academy of Sciences of the United States of America* **97**, 145-150
203. DeMarco, M. L., and Daggett, V. (2005) *Comptes rendus biologies* **328**, 847-862
204. Merz, P. A., Somerville, R. A., Wisniewski, H. M., and Iqbal, K. (1981) *Acta neuropathologica* **54**, 63-74
205. Prusiner, S. B., McKinley, M. P., Bowman, K. A., Bolton, D. C., Bendheim, P. E., Groth, D. F., and Glenner, G. G. (1983) *Cell* **35**, 349-358

206. Vazquez-Fernandez, E., Vos, M. R., Afanasyev, P., Cebey, L., Sevillano, A. M., Vidal, E., Rosa, I., Renault, L., Ramos, A., Peters, P. J., Fernandez, J. J., van Heel, M., Young, H. S., Requena, J. R., and Wille, H. (2016) *PLoS pathogens* **12**, e1005835
207. Kunes, K. C., Clark, S. C., Cox, D. L., and Singh, R. R. (2008) *Prion* **2**, 81-90
208. Sim, V. L., and Caughey, B. (2009) *Neurobiology of aging* **30**, 2031-2042
209. Kocisko, D. A., Lansbury, P. T., Jr., and Caughey, B. (1996) *Biochemistry* **35**, 13434-13442
210. Zou, W. Q., Capellari, S., Parchi, P., Sy, M. S., Gambetti, P., and Chen, S. G. (2003) *The Journal of biological chemistry* **278**, 40429-40436
211. Zanusso, G., Farinazzo, A., Prelli, F., Fiorini, M., Gelati, M., Ferrari, S., Righetti, P. G., Rizzuto, N., Frangione, B., and Monaco, S. (2004) *The Journal of biological chemistry* **279**, 38936-38942
212. Sajnani, G., Pastrana, M. A., Dynin, I., Onisko, B., and Requena, J. R. (2008) *Journal of molecular biology* **382**, 88-98
213. Vazquez-Fernandez, E., Alonso, J., Pastrana, M. A., Ramos, A., Stitz, L., Vidal, E., Dynin, I., Petsch, B., Silva, C. J., and Requena, J. R. (2012) *PloS one* **7**, e50111
214. Safar, J., Roller, P. P., Gajdusek, D. C., and Gibbs, C. J., Jr. (1993) *The Journal of biological chemistry* **268**, 20276-20284
215. Caughey, B. W., Dong, A., Bhat, K. S., Ernst, D., Hayes, S. F., and Caughey, W. S. (1991) *Biochemistry* **30**, 7672-7680
216. Baron, G. S., Hughson, A. G., Raymond, G. J., Offerdahl, D. K., Barton, K. A., Raymond, L. D., Dorward, D. W., and Caughey, B. (2011) *Biochemistry* **50**, 4479-4490
217. Nguyen, J. T., Inouye, H., Baldwin, M. A., Fletterick, R. J., Cohen, F. E., Prusiner, S. B., and Kirschner, D. A. (1995) *Journal of molecular biology* **252**, 412-422
218. Safar, J., Wille, H., Itri, V., Groth, D., Serban, H., Torchia, M., Cohen, F. E., and Prusiner, S. B. (1998) *Nature medicine* **4**, 1157-1165
219. Downing, D. T., and Lazo, N. D. (1999) *Biochem J* **343**, 453-460
220. DeMarco, M. L., and Daggett, V. (2004) *Proceedings of the National Academy of Sciences of the United States of America* **101**, 2293-2298
221. Stork, M., Giese, A., Kretzschmar, H. A., and Tavan, P. (2005) *Biophys J* **88**, 2442-2451
222. Yang, S., Levine, H., Onuchic, J. N., and Cox, D. L. (2005) *FASEB journal : official publication of the Federation of American Societies for Experimental Biology* **19**, 1778-1782
223. Langedijk, J. P., Fuentes, G., Boshuizen, R., and Bonvin, A. M. (2006) *Journal of molecular biology* **360**, 907-920
224. Groveman, B. R., Dolan, M. A., Taubner, L. M., Kraus, A., Wickner, R. B., and Caughey, B. (2014) *The Journal of biological chemistry*
225. Mornon, J. P., Prat, K., Dupuis, F., Boisset, N., and Callebaut, I. (2002) *Cellular and Molecular Life Sciences* **59**, 2144-2154

226. Onisko, B., Fernandez, E. G., Freire, M. L., Schwarz, A., Baier, M., Camina, F., Garcia, J. R., Rodriguez-Segade Villamarin, S., and Requena, J. R. (2005) *Biochemistry* **44**, 10100-10109
227. Wille, H., Govaerts, C., Borovinskiy, A., Latawiec, D., Downing, K. H., Cohen, F. E., and Prusiner, S. B. (2007) *Archives of biochemistry and biophysics* **467**, 239-248
228. Cobb, N. J., Sonnichsen, F. D., McHaourab, H., and Surewicz, W. K. (2007) *Proceedings of the National Academy of Sciences of the United States of America* **104**, 18946-18951
229. Lu, X., Wintrode, P. L., and Surewicz, W. K. (2007) *Proceedings of the National Academy of Sciences of the United States of America* **104**, 1510-1515
230. Smirnovas, V., Baron, G. S., Offerdahl, D. K., Raymond, G. J., Caughey, B., and Surewicz, W. K. (2011) *Nature structural & molecular biology* **18**, 504-506
231. Silva, C. J. (2012) *Prion* **6**, 163-173
232. Amenitsch, H., Benetti, F., Ramos, A., Legname, G., and Requena, J. R. (2013) *Prion* **7**, 496-500
233. Terry, C., Wenborn, A., Gros, N., Sells, J., Joiner, S., Hosszu, L. L., Tattum, M. H., Panico, S., Clare, D. K., Collinge, J., Saibil, H. R., and Wadsworth, J. D. (2016) *Open biology* **6**
234. Ghetti, B., Piccardo, P., Frangione, B., Bugiani, O., Giaccone, G., Young, K., Prelli, F., Farlow, M. R., Dlouhy, S. R., and Tagliavini, F. (1996) *Brain Pathology* **6**, 127-145
235. Requena, J. R., and Wille, H. (2014) *Prion* **8**, 60-66
236. Bolton, D. C., Bendheim, P. E., Marmorstein, A. D., and Potempska, A. (1987) *Archives of biochemistry and biophysics* **258**, 579-590
237. Huang, Z. W., Prusiner, S. B., and Cohen, F. E. (1996) *Folding & design* **1**, 13-19
238. Gasset, M., Baldwin, M. A., Lloyd, D. H., Gabriel, J. M., Holtzman, D. M., Cohen, F., Fletterick, R., and Prusiner, S. B. (1992) *Proceedings of the National Academy of Sciences of the United States of America* **89**, 10940-10944
239. Bowie, J. U., Luthy, R., and Eisenberg, D. (1991) *Science* **253**, 164-170
240. Korth, C., Stierli, B., Streit, P., Moser, M., Schaller, O., Fischer, R., Schulz-Schaeffer, W., Kretzschmar, H., Raeber, A., Braun, U., Ehrensperger, F., Hornemann, S., Glockshuber, R., Riek, R., Billeter, M., Wuthrich, K., and Oesch, B. (1997) *Nature* **390**, 74-77
241. Richardson, J. S., and Richardson, D. C. (2002) *Proceedings of the National Academy of Sciences of the United States of America* **99**, 2754-2759
242. Stockel, J., Safar, J., Wallace, A. C., Cohen, F. E., and Prusiner, S. B. (1998) *Biochemistry* **37**, 7185-7193
243. James, T. L., Liu, H., Ulyanov, N. B., Farr-Jones, S., Zhang, H., Donne, D. G., Kaneko, K., Groth, D., Mehlhorn, I., Prusiner, S. B., and Cohen, F. E. (1997) *Proceedings of the National Academy of Sciences of the United States of America* **94**, 10086-10091
244. Swietnicki, W., Morillas, M., Chen, S. G., Gambetti, P., and Surewicz, W. K. (2000) *Biochemistry* **39**, 424-431
245. Silveira, J. R., Raymond, G. J., Hughson, A. G., Race, R. E., Sim, V. L., Hayes, S. F., and Caughey, B. (2005) *Nature* **437**, 257-261

246. Mehlhorn, I., Groth, D., Stockel, J., Moffat, B., Reilly, D., Yansura, D., Willett, W. S., Baldwin, M., Fletterick, R., Cohen, F. E., Vandlen, R., Henner, D., and Prusiner, S. B. (1996) *Biochemistry* **35**, 5528-5537
247. Wopfner, F., Weidenhofer, G., Schneider, R., von Brunn, A., Gilch, S., Schwarz, T. F., Werner, T., and Schatzl, H. M. (1999) *Journal of molecular biology* **289**, 1163-1178
248. Schatzl, H. M., Dacosta, M., Taylor, L., Cohen, F. E., and Prusiner, S. B. (1995) *Journal of molecular biology* **245**, 362-374
249. Telling, G. C., Scott, M., Mastrianni, J., Gabizon, R., Torchia, M., Cohen, F. E., Dearmond, S. J., and Prusiner, S. B. (1995) *Cell* **83**, 79-90
250. Colby, D. W., Giles, K., Legname, G., Wille, H., Baskakov, I. V., DeArmond, S. J., and Prusiner, S. B. (2009) *Proceedings of the National Academy of Sciences of the United States of America* **106**, 20417-20422
251. Ghaemmaghami, S., Colby, D. W., Nguyen, H. O., Hayashi, S., Oehler, A., DeArmond, S. J., and Prusiner, S. B. (2013) *The American journal of pathology* **182**, 866-874
252. Le, N. T., Narkiewicz, J., Aulic, S., Salzano, G., Tran, H. T., Scaini, D., Moda, F., Giachin, G., and Legname, G. (2015) *Virus research* **207**, 25-37
253. Zahn, R., von Schroetter, C., and Wuthrich, K. (1997) *FEBS letters* **417**, 400-404
254. Hornemann, S., Korth, C., Oesch, B., Riek, R., Wider, G., Wuthrich, K., and Glockshuber, R. (1997) *FEBS letters* **413**, 277-281
255. Negro, A., De Filippis, V., Skaper, S. D., James, P., and Sorgato, M. C. (1997) *FEBS letters* **412**, 359-364
256. Aguzzi, A., Heikenwalder, M., and Polymenidou, M. (2007) *Nat Rev Mol Cell Bio* **8**, 552-561
257. Hill, A. F., Joiner, S., Linehan, J., Desbruslais, M., Lantos, P. L., and Collinge, J. (2000) *Proceedings of the National Academy of Sciences of the United States of America* **97**, 10248-10253
258. Schaller, O., Fatzer, R., Stack, M., Clark, J., Cooley, W., Biffiger, K., Egli, S., Doherr, M., Vandevelde, M., Heim, D., Oesch, B., and Moser, M. (1999) *Acta neuropathologica* **98**, 437-443
259. Lasmezas, C. I., Deslys, J. P., Robain, O., Jaegly, A., Beringue, V., Peyrin, J. M., Fournier, J. G., Hauw, J. J., Rossier, J., and Dormont, D. (1997) *Science* **275**, 402-405
260. Schulz-Schaeffer, W. J., Tschoke, S., Kranefuss, N., Drose, W., Hause-Reitner, D., Giese, A., Groschup, M. H., and Kretzschmar, H. A. (2000) *The American journal of pathology* **156**, 51-56
261. Hilton, D. A., Ghani, A. C., Conyers, L., Edwards, P., McCardle, L., Penney, M., Ritchie, D., and Ironside, J. W. (2002) *BMJ* **325**, 633-634
262. Weissmann, C. (1991) *Nature* **352**, 679-683
263. Bartz, J. C., DeJoia, C., Tucker, T., Kincaid, A. E., and Bessen, R. A. (2005) *Journal of virology* **79**, 11858-11863
264. Telling, G. C., Scott, M., Hsiao, K. K., Foster, D., Yang, S. L., Torchia, M., Sidle, K. C., Collinge, J., DeArmond, S. J., and Prusiner, S. B. (1994) *Proceedings of the National Academy of Sciences of the United States of America* **91**, 9936-9940
265. Hill, A. F., and Collinge, J. (2003) *Trends in microbiology* **11**, 578-584

266. Benestad, S. L., Sarradin, P., Thu, B., Schonheit, J., Tranulis, M. A., and Bratberg, B. (2003) *Veterinary Record* **153**, 202-+
267. Orge, L., Galo, A., Machado, C., Lima, C., Ochoa, C., Silva, J., Ramos, M., and Simas, J. P. (2004) *Journal of General Virology* **85**, 3487-3491
268. Klingeborn, M., Wik, L., Simonsson, M., Renstrom, L. H. M., Ottinger, T., and Linne, T. (2006) *Journal of General Virology* **87**, 1751-1760
269. Safar, J. G., Scott, M., Monaghan, J., Deering, C., Didorenko, S., Vergara, J., Ball, H., Legname, G., Leclerc, E., Solforosi, L., Serban, H., Groth, D., Burton, D. R., Prusiner, S. B., and Williamson, R. A. (2002) *Nature biotechnology* **20**, 1147-1150
270. Pastrana, M. A., Sajnani, G., Onisko, B., Castilla, J., Morales, R., Soto, C., and Requena, J. R. (2006) *Biochemistry* **45**, 15710-15717
271. Tzaban, S., Friedlander, G., Schonberger, O., Horonchik, L., Yedidia, Y., Shaked, G., Gabizon, R., and Taraboulos, A. (2002) *Biochemistry* **41**, 12868-12875
272. Kelly, J. W. (1998) *Current opinion in structural biology* **8**, 101-106
273. Surewicz, W. K., Jones, E. M., and Apetri, A. C. (2006) *Accounts of chemical research* **39**, 654-662
274. Bucciantini, M., Giannoni, E., Chiti, F., Baroni, F., Formigli, L., Zurdo, J., Taddei, N., Ramponi, G., Dobson, C. M., and Stefani, M. (2002) *Nature* **416**, 507-511
275. Lansbury, P. T., Jr., and Caughey, B. (1995) *Chemistry & biology* **2**, 1-5
276. Caughey, B., Kocisko, D. A., Raymond, G. J., and Lansbury, P. T., Jr. (1995) *Chemistry & biology* **2**, 807-817
277. De Simone, A., Zagari, A., and Derreumaux, P. (2007) *Biophys J* **93**, 1284-1292
278. Bjorndahl, T. C., Zhou, G. P., Liu, X., Perez-Pineiro, R., Semenchenko, V., Saleem, F., Acharya, S., Bujold, A., Sobsey, C. A., and Wishart, D. S. (2011) *Biochemistry* **50**, 1162-1173
279. Baskakov, I. V., Legname, G., Prusiner, S. B., and Cohen, F. E. (2001) *The Journal of biological chemistry* **276**, 19687-19690
280. Leffers, K. W., Wille, H., Stohr, J., Junger, E., Prusiner, S. B., and Riesner, D. (2005) *Biological chemistry* **386**, 569-580
281. Luhrs, T., Zahn, R., and Wuthrich, K. (2006) *Journal of molecular biology* **357**, 833-841
282. Sanghera, N., and Pinheiro, T. J. (2002) *Journal of molecular biology* **315**, 1241-1256
283. Wang, F., Yang, F., Hu, Y., Wang, X., Jin, C., and Ma, J. (2007) *Biochemistry* **46**, 7045-7053
284. Deleault, N. R., Piro, J. R., Walsh, D. J., Wang, F., Ma, J., Geoghegan, J. C., and Supattapone, S. (2012) *Proceedings of the National Academy of Sciences of the United States of America* **109**, 8546-8551
285. Deleault, N. R., Lucassen, R. W., and Supattapone, S. (2003) *Nature* **425**, 717-720
286. Miller, M. B., Wang, D. W., Wang, F., Noble, G. P., Ma, J., Woods, V. L., Jr., Li, S., and Supattapone, S. (2013) *Structure* **21**, 2061-2068

287. Jackson, G. S., Hosszu, L. L. P., Power, A., Hill, A. F., Kenney, J., Saibil, H., Craven, C. J., Waltho, J. P., Clarke, A. R., and Collinge, J. (1999) *Science* **283**, 1935-1937
288. Morillas, M., Vanik, D. L., and Surewicz, W. K. (2001) *Biochemistry* **40**, 6982-6987
289. Apetri, A. C., and Surewicz, W. K. (2003) *The Journal of biological chemistry* **278**, 22187-22192
290. Saleem, F., Bjorndahl, T. C., Ladner, C. L., Perez-Pineiro, R., Ametaj, B. N., and Wishart, D. S. (2014) *Prion* **8**
291. Ladner-Keay, C. L., Griffith, B. J., and Wishart, D. S. (2014) *PloS one* **9**
292. da Luz, M. H. M., Peres, I. T., Santos, T. G., Martins, V. R., Icimoto, M. Y., and Lee, K. S. (2015) *Frontiers in cellular neuroscience* **9**
293. Wong, E., Thackray, A. M., and Bujdoso, R. (2004) *The Biochemical journal* **380**, 273-282
294. Brown, D. R., Hafiz, F., Glasssmith, L. L., Wong, B. S., Jones, I. M., Clive, C., and Haswell, S. J. (2000) *The EMBO journal* **19**, 1180-1186
295. Jansen, K., Schafer, O., Birkmann, E., Post, K., Serban, H., Prusiner, S. B., and Riesner, D. (2001) *Biological chemistry* **382**, 683-691
296. Xiong, L. W., Raymond, L. D., Hayes, S. F., Raymond, G. J., and Caughey, B. (2001) *Journal of neurochemistry* **79**, 669-678
297. Leffers, K. W., Schell, J., Jansen, K., Lucassen, R., Kaimann, T., Nagel-Steger, L., Tatzelt, J., and Riesner, D. (2004) *Journal of molecular biology* **344**, 839-853
298. Post, K., Pitschke, M., Schafer, O., Wille, H., Appel, T. R., Kirsch, D., Mehlhorn, I., Serban, H., Prusiner, S. B., and Riesner, D. (1998) *Biological chemistry* **379**, 1307-1317
299. Supattapone, S. (2010) *Science* **327**, 1091-1092
300. Noble, G. P., Wang, D. W., Walsh, D. J., Barone, J. R., Miller, M. B., Nishina, K. A., Li, S., and Supattapone, S. (2015) *PLoS pathogens* **11**, e1005017
301. Petrotchenko, E. V., Serpa, J. J., Hardie, D. B., Berjanskii, M., Suriyamongkol, B. P., Wishart, D. S., and Borchers, C. H. (2012) *Molecular & cellular proteomics : MCP*
302. Serpa, J. J., Makepeace, K. A., Borchers, T. H., Wishart, D. S., Petrotchenko, E. V., and Borchers, C. H. (2013) *Journal of proteomics*
303. Serpa, J. J. P., K. I.; Petrotchenko, E. V.; Dokholyan, N. V.; Borchers, C. H. (2017) *Manuscript in preparation*
304. Gerber, R., Tahiri-Alaoui, A., Hore, P. J., and James, W. (2007) *The Journal of biological chemistry* **282**, 6300-6307
305. Rezaei, H., Eghiaian, F., Perez, J., Doublet, B., Choiset, Y., Haertle, T., and Grosclaude, J. (2005) *Journal of molecular biology* **347**, 665-679
306. Kosmac, M., Koren, S., Giachin, G., Stoilova, T., Gennaro, R., Legname, G., and Serbec, V. C. (2011) *Molecular immunology* **48**, 746-750
307. Kang, H. E., Weng, C. C., Saijo, E., Saylor, V., Bian, J., Kim, S., Ramos, L., Angers, R., Langenfeld, K., Khaychuk, V., Calvi, C., Bartz, J., Hunter, N., and Telling, G. C. (2012) *The Journal of biological chemistry* **287**, 37219-37232
308. van der Kamp, M. W., and Daggett, V. (2011) *Topics in current chemistry* **305**, 169-197

309. Gasset, M., Baldwin, M. A., Fletterick, R. J., and Prusiner, S. B. (1993) *Proceedings of the National Academy of Sciences of the United States of America* **90**, 1-5
310. Sajnani, G., Silva, C. J., Ramos, A., Pastrana, M. A., Onisko, B. C., Erickson, M. L., Antaki, E. M., Dynin, I., Vazquez-Fernandez, E., Sigurdson, C. J., Carter, J. M., and Requena, J. R. (2012) *PLoS pathogens* **8**, e1002547
311. Yang, C., Lo, W. L., Kuo, Y. H., Sang, J. C., Lee, C. Y., Chiang, Y. W., and Chen, R. P. (2014) *ACS chemical biology*
312. Schlepckow, K., and Schwalbe, H. (2013) *Angew Chem Int Ed Engl* **52**, 10002-10005
313. Singh, J., and Udgaonkar, J. B. (2015) *Biochemistry* **54**, 4431-4442
314. Rezaei, H., Marc, D., Choiset, Y., Takahashi, M., Hoa, G. H. B., Haertle, T., Grosclaude, J., and Debey, P. (2000) *Eur J Biochem* **267**, 2833-2839
315. Silva, C. J., Erickson-Beltran, M. L., and Dynin, I. C. (2016) *Biochemistry* **55**, 894-902
316. Lennon, C. W., Cox, H. D., Hennelly, S. P., Chelmo, S. J., and McGuirl, M. A. (2007) *Biochemistry* **46**, 4850-4860
317. Requena, J. R., Dimitrova, M. N., Legname, G., Teijeira, S., Prusiner, S. B., and Levine, R. L. (2004) *Archives of biochemistry and biophysics* **432**, 188-195
318. Tsutsui, Y., and Wintrode, P. L. (2007) *Current medicinal chemistry* **14**, 2344-2358
319. Kaltashov, I. A., and Eyles, S. J. (2002) *Mass spectrometry reviews* **21**, 37-71
320. Konermann, L., Pan, J., and Liu, Y. H. (2011) *Chemical Society reviews* **40**, 1224-1234
321. Nazabal, A., Hornemann, S., Aguzzi, A., and Zenobi, R. (2009) *Journal of mass spectrometry : JMS* **44**, 965-977
322. Singh, J., Sabareesan, A. T., Mathew, M. K., and Udgaonkar, J. B. (2012) *Journal of molecular biology* **423**, 217-231
323. Sabareesan, A. T., Singh, J., Roy, S., Udgaonkar, J. B., and Mathew, M. K. (2016) *Biophys J* **110**, 1766-1776
324. Cobb, N. J., Apostol, M. I., Chen, S., Smirnovas, V., and Surewicz, W. K. (2014) *The Journal of biological chemistry* **289**, 2643-2650
325. Pan, J., Han, J., Borchers, C. H., and Konermann, L. (2009) *Journal of the American Chemical Society* **131**, 12801-12808
326. Pan, J., Han, J., Borchers, C. H., and Konermann, L. (2010) *Analytical chemistry* **82**, 8591-8597
327. Back, J. W., de Jong, L., Muijsers, A. O., and de Koster, C. G. (2003) *Journal of molecular biology* **331**, 303-313
328. Sinz, A. (2007) Chemical cross-linking and mass spectrometry for investigation of protein-protein interactions in *Mass spectrometry of protein interactions* (Downward, K. ed.), John Wiley and sons. pp
329. Novak, P., and Giannakopulos, A. E. (2007) *Eur J Mass Spectrom (Chichester)* **13**, 105-113
330. Sinz, A. (2006) *Mass spectrometry reviews* **25**, 663-682
331. Petrotchenko, E. V., and Borchers, C. H. (2010) *Mass spectrometry reviews* **29**, 862-876

332. Kaimann, T., Metzger, S., Kuhlmann, K., Brandt, B., Birkmann, E., Holtje, H. D., and Riesner, D. (2008) *Journal of molecular biology* **376**, 582-596
333. Taverner, T., Hall, N. E., O'Hair, R. A., and Simpson, R. J. (2002) *The Journal of biological chemistry* **277**, 46487-46492
334. Petrotchenko, E. V., Serpa, J. J., Makepeace, K. A., Brodie, N. I., and Borchers, C. H. (2014) *Journal of proteomics* **109**, 104-110
335. Brodie, I. B. P., K.I.; Petrotchenko, E.V.; Dokholyan, N.V.; Borchers, C.H. (2017) *Manuscript in preparation*
336. Jin Lee, Y. (2008) *Molecular bioSystems* **4**, 816-823
337. Petrotchenko, E. V., Makepeace, K. A., Serpa, J. J., and Borchers, C. H. (2014) *Methods Mol Biol* **1156**, 447-463
338. Rappsilber, J. (2011) *Journal of structural biology* **173**, 530-540
339. Brodie, N. I., Makepeace, K. A., Petrotchenko, E. V., and Borchers, C. H. (2015) *Journal of proteomics* **118**, 12-20
340. Brodie, N. I., Petrotchenko, E. V., and Borchers, C. H. (2016) *Journal of proteomics*
341. Petrotchenko, E. V., Serpa, J. J., and Borchers, C. H. (2010) *Analytical chemistry* **82**, 817-823
342. Petrotchenko, E. V., Serpa, J. J., and Borchers, C. H. (2011) *Molecular & cellular proteomics : MCP* **10**, M110 001420
343. Petrotchenko, E. V., Serpa, J. J., Cabecinha, A. N., Lesperance, M., and Borchers, C. H. (2014) *Journal of proteome research*
344. Petrotchenko, E. V., and Borchers, C. H. (2010) *BMC bioinformatics* **11**, 64
345. Petrotchenko, E. V., and Borchers, C. H. (2014) *Proteomics*
346. Petrotchenko, E. V., Makepeace, K. A., and Borchers, C. H. (2014) *Current protocols in bioinformatics / editoral board, Andreas D. Baxevanis ... [et al.]* **48**, 8 18 11-18 18 19
347. Petrotchenko, E. V., Xiao, K., Cable, J., Chen, Y., Dokholyan, N. V., and Borchers, C. H. (2009) *Molecular & cellular proteomics : MCP* **8**, 273-286
348. Petrotchenko, E. V., Borchers, C.H. (2008) Cross-linking as a tool to examine protein complexes: examples of cross-linking strategies and computational modeling. in *Mass Spectrometry Analysis for Protein-Protein Interactions and Dynamics* (Chance, M. ed.), Wiley and Sons, Hoboken, NJ. pp
349. Petrotchenko, E. V., Olkhovik, V. K., and Borchers, C. H. (2005) *Molecular & Cellular Proteomics* **4**, 1167-1179
350. Leitner, A., Walzthoeni, T., Kahraman, A., Herzog, F., Rinner, O., Beck, M., and Aebersold, R. (2010) *Molecular & cellular proteomics : MCP* **9**, 1634-1649
351. Muller, D. R., Schindler, P., Towbin, H., Wirth, U., Voshol, H., Hoving, S., and Steinmetz, M. O. (2001) *Analytical chemistry* **73**, 1927-1934
352. Soderblom, E. J., and Goshe, M. B. (2006) *Analytical chemistry* **78**, 8059-8068
353. Hurst, G. B., Lankford, T. K., and Kennel, S. J. (2004) *Journal of the American Society for Mass Spectrometry* **15**, 832-839
354. (2011) PrioNet_Canada PrP5: The PrioNet Prion Protein & Plasmid Production Platform Facility (PrP5).
355. (2011) PrioNet_Canada

356. Schwieters, C. D., Kuszewski, J. J., Tjandra, N., and Clore, G. M. (2003) *J Magn Reson* **160**, 65-73
357. Powell, M. J. D. (1973) *Math Program Stud* **4**, 193-201
358. Koradi, R., Billeter, M., and Wuthrich, K. (1996) *Journal of molecular graphics* **14**, 51-55, 29-32
359. Wu, C. C., MacCoss, M. J., Howell, K. E., and Yates, J. R., 3rd. (2003) *Nature biotechnology* **21**, 532-538
360. Roche_Diagnostics_GmbH. (2006) Proteinase K, recombinant, PCR grade.
361. Fancy, D. A., and Kodadek, T. (1999) *Proceedings of the National Academy of Sciences of the United States of America* **96**, 6020-6024
362. Biljan, I., Ilc, G., Giachin, G., Raspadori, A., Zhukov, I., Plavec, J., and Legname, G. (2011) *Journal of molecular biology* **412**, 660-673
363. Tench, R. J., Balooch, M., Bernardez, L., Allen, M. J., Siekhaus, W. J., Olander, D. R., and Wang, W. (1991) *J Vac Sci Technol B* **9**, 820-824
364. Chen, X., Westphall, M. S., and Smith, L. M. (2003) *Analytical chemistry* **75**, 5944-5952
365. Trauger, S. A., Webb, W., and Siuzdak, G. (2002) *Spectrosc-Int J* **16**, 15-28
366. Tran, B. Q., Hernandez, C., Waridel, P., Potts, A., Barblan, J., Lisacek, F., and Quadroni, M. (2011) *Journal of proteome research* **10**, 800-811
367. Laskin, J., and Futrell, J. H. (2003) *Rapid Commun Mass Sp* **17**, 2694-2694
368. Prusiner, S. B., Groth, D. F., Cochran, S. P., Masiarz, F. R., McKinley, M. P., and Martinez, H. M. (1980) *Biochemistry* **19**, 4883-4891
369. Diener, T. O., McKinley, M. P., and Prusiner, S. B. (1982) *Proceedings of the National Academy of Sciences of the United States of America* **79**, 5220-5224
370. Pruisiner, S. B., Safar, J. (2000) Method for detecting prions. (office, U. s. p. a. t. ed., A01N 1/02 (20060101); C12N 11/00 (20060101); G01N 33/531 (20060101); G01N 33/566 (20060101); G01N 033/531 () Ed., The Regents of the University of California (Oakland, CA) United States
371. Calzolai, L., and Zahn, R. (2003) *The Journal of biological chemistry* **278**, 35592-35596
372. Bae, S. H., Legname, G., Serban, A., Prusiner, S. B., Wright, P. E., and Dyson, H. J. (2009) *Biochemistry* **48**, 8120-8128
373. Donne, D. G., Viles, J. H., Groth, D., Mehlhorn, I., James, T. L., Cohen, F. E., Prusiner, S. B., Wright, P. E., and Dyson, H. J. (1997) *Proceedings of the National Academy of Sciences of the United States of America* **94**, 13452-13457
374. Hall, M. C., Shcherbakova, P. V., Fortune, J. M., Borchers, C. H., Dial, J. M., Tomer, K. B., and Kunkel, T. A. (2003) *Nucleic acids research* **31**, 2025-2034
375. Glocker, M. O., Borchers, C., Fiedler, W., Suckau, D., and Przybylski, M. (1994) *Bioconjugate chemistry* **5**, 583-590
376. Shevchenko, A., Tomas, H., Havlis, J., Olsen, J. V., and Mann, M. (2006) *Nature protocols* **1**, 2856-2860
377. Liu, H., Farr-Jones, S., Ulyanov, N. B., Llinas, M., Marqusee, S., Groth, D., Cohen, F. E., Prusiner, S. B., and James, T. L. (1999) *Biochemistry* **38**, 5362-5377
378. Hochleitner, E. O., Borchers, C., Parker, C., Bienstock, R. J., and Tomer, K. B. (2000) *Protein science : a publication of the Protein Society* **9**, 487-496
379. Xu, G., and Chance, M. R. (2007) *Chemical reviews* **107**, 3514-3543

380. Stocks, B. B., and Konermann, L. (2009) *Analytical chemistry* **81**, 20-27
381. Stocks, B. B., and Konermann, L. (2010) *Journal of molecular biology* **398**, 362-373
382. Hambly, D. M., and Gross, M. L. (2005) *Journal of the American Society for Mass Spectrometry* **16**, 2057-2063
383. Gau, B. C., Sharp, J. S., Rempel, D. L., and Gross, M. L. (2009) *Analytical chemistry* **81**, 6563-6571
384. DeArmond, P. D., Xu, Y., Strickland, E. C., Daniels, K. G., and Fitzgerald, M. C. (2011) *Journal of proteome research* **10**, 4948-4958
385. Heegaard, P. M. H., Pedersen, H. G., Flink, J., and Boas, U. (2004) *FEBS letters* **577**, 127-133
386. Kell, G., and Steinhart, H. (1990) *Journal of food science* **55**, 1120-&
387. Maleknia, S. D., Brenowitz, M., and Chance, M. R. (1999) *Analytical chemistry* **71**, 3965-3973
388. Nadal, R. C., Abdelraheim, S. R., Brazier, M. W., Rigby, S. E., Brown, D. R., and Viles, J. H. (2007) *Free radical biology & medicine* **42**, 79-89
389. Wolschner, C., Giese, A., Kretzschmar, H. A., Huber, R., Moroder, L., and Budisa, N. (2009) *Proceedings of the National Academy of Sciences of the United States of America* **106**, 7756-7761
390. Requena, J. R., Groth, D., Legname, G., Stadtman, E. R., Prusiner, S. B., and Levine, R. L. (2001) *Proceedings of the National Academy of Sciences of the United States of America* **98**, 7170-7175
391. Younan, N. D., Nadal, R. C., Davies, P., Brown, D. R., and Viles, J. H. (2012) *The Journal of biological chemistry* **287**, 28263-28275
392. Wong, B. S., Wang, H., Brown, D. R., and Jones, I. M. (1999) *Biochemical and biophysical research communications* **259**, 352-355
393. ProteinProspector. ProteinProspector. v 5.10.11 Ed.
394. Kotiaho, T., Eberlin, M. N., Vainiotalo, P., and Kostiainen, R. (2000) *Journal of the American Society for Mass Spectrometry* **11**, 526-535
395. Guan, Z., Yates, N. A., and Bakhtiar, R. (2003) *Journal of the American Society for Mass Spectrometry* **14**, 605-613
396. Chowdhury, S. K., Eshraghi, J., Wolfe, H., Forde, D., Hlavac, A. G., and Johnston, D. (1995) *Analytical chemistry* **67**, 390-398
397. Morand, K., Talbo, G., and Mann, M. (1993) *Rapid Commun Mass Sp* **7**, 738-743
398. Chen, M., and Cook, K. D. (2007) *Analytical chemistry* **79**, 2031-2036
399. Swiderek, K. M., Davis, M. T., and Lee, T. D. (1998) *Electrophoresis* **19**, 989-997
400. Sun, G., and Anderson, V. E. (2004) *Electrophoresis* **25**, 959-965
401. Breydo, L., Bocharova, O. V., Makarava, N., Salnikov, V. V., Anderson, M., and Baskakov, I. V. (2005) *Biochemistry* **44**, 15534-15543
402. Jackson, G. S., Murray, I., Hosszu, L. L., Gibbs, N., Waltho, J. P., Clarke, A. R., and Collinge, J. (2001) *Proceedings of the National Academy of Sciences of the United States of America* **98**, 8531-8535
403. Canello, T., Frid, K., Gabizon, R., Lisa, S., Friedler, A., Moskovitz, J., and Gasset, M. (2010) *PLoS pathogens* **6**, e1000977

404. McMahon, H. E., Mange, A., Nishida, N., Creminon, C., Casanova, D., and Lehmann, S. (2001) *The Journal of biological chemistry* **276**, 2286-2291
405. Skora, L., Fonseca-Ornelas, L., Hofele, R. V., Riedel, D., Giller, K., Watzlawik, J., Schulz-Schaeffer, W. J., Urlaub, H., Becker, S., and Zweckstetter, M. (2013) *The Journal of biological chemistry* **288**, 2994-3002
406. Gomes, A. F., and Gozzo, F. C. (2010) *Journal of mass spectrometry : JMS* **45**, 892-899
407. Ladner, C. L., and Wishart, D. S. (2012) *Analytical biochemistry* **426**, 54-62
408. Micsonai, A., Wien, F., Kernya, L., Lee, Y. H., Goto, Y., Refregiers, M., and Kardos, J. (2015) *Proceedings of the National Academy of Sciences of the United States of America* **112**, E3095-3103
409. Petrotchenko, E. V., and Borchers, C. H. (2015) *Journal of the American Society for Mass Spectrometry* **26**, 1895-1898
410. Leitner, A., Joachimiak, L. A., Unverdorben, P., Walzthoeni, T., Frydman, J., Forster, F., and Aebersold, R. (2014) *Proceedings of the National Academy of Sciences of the United States of America* **111**, 9455-9460
411. Kunishima, M., Kawachi, C., Morita, J., Terao, K., Iwasaki, F., and Tani, S. (1999) *Tetrahedron* **55**, 13159-13170
412. Novak, P., and Kruppa, G. H. (2008) *Eur J Mass Spectrom (Chichester, Eng)* **14**, 355-365
413. Combe, C. W., Fischer, L., and Rappsilber, J. (2015) *Molecular & cellular proteomics : MCP* **14**, 1137-1147
414. Peretz, D., Williamson, R. A., Matsunaga, Y., Serban, H., Pinilla, C., Bastidas, R. B., Rozenshteyn, R., James, T. L., Houghten, R. A., Cohen, F. E., Prusiner, S. B., and Burton, D. R. (1997) *Journal of molecular biology* **273**, 614-622
415. Yuan, F. F., Biffin, S., Brazier, M. W., Suarez, M., Cappai, R., Hill, A. F., Collins, S. J., Sullivan, J. S., Middleton, D., Multhaup, G., Geczy, A. F., and Masters, C. L. (2005) *Immunology and cell biology* **83**, 632-637
416. Williamson, R. A., Peretz, D., Pinilla, C., Ball, H., Bastidas, R. B., Rozenshteyn, R., Houghten, R. A., Prusiner, S. B., and Burton, D. R. (1998) *Journal of virology* **72**, 9413-9418
417. Kim, C. L., Umetani, A., Matsui, T., Ishiguro, N., Shinagawa, M., and Horiuchi, M. (2004) *Virology* **320**, 40-51
418. Eghiaian, F., Grosclaude, J., Lesceu, S., Debey, P., Doublet, B., Treguer, E., Rezaei, H., and Knossow, M. (2004) *Proceedings of the National Academy of Sciences of the United States of America* **101**, 10254-10259
419. Trevitt, C. R., Hosszu, L. L., Batchelor, M., Panico, S., Terry, C., Nicoll, A. J., Risse, E., Taylor, W. A., Sandberg, M. K., Al-Doujaily, H., Linehan, J. M., Saibil, H. R., Scott, D. J., Collinge, J., Waltho, J. P., and Clarke, A. R. (2014) *The Journal of biological chemistry*
420. Paramithiotis, E., Pinard, M., Lawton, T., LaBoissiere, S., Leathers, V. L., Zou, W. Q., Estey, L. A., Lamontagne, J., Lehto, M. T., Kondejewski, L. H., Francoeur, G. P., Papadopoulos, M., Haghighat, A., Spatz, S. J., Head, M., Will, R., Ironside, J., O'Rourke, K., Tonelli, Q., Ledebur, H. C., Chakrabartty, A., and Cashman, N. R. (2003) *Nature medicine* **9**, 893-899

421. Saijo, E., Hughson, A. G., Raymond, G. J., Suzuki, A., Horiuchi, M., and Caughey, B. (2016) *Journal of virology* **90**, 4905-4913
422. Chabry, J., Caughey, B., and Chesebro, B. (1998) *J Biol Chem* **273**, 13203-13207
423. Peretz, D., Williamson, R. A., Kaneko, K., Vergara, J., Leclerc, E., Schmitt-Ulms, G., Mehlhorn, I. R., Legname, G., Wormald, M. R., Rudd, P. M., Dwek, R. A., Burton, D. R., and Prusiner, S. B. (2001) *Nature* **412**, 739-743
424. Wu, X., Chavez, J. D., Schweppe, D. K., Zheng, C., Weisbrod, C. R., Eng, J. K., Murali, A., Lee, S. A., Ramage, E., Gallagher, L. A., Kulasekara, H. D., Edrozo, M. E., Kamischke, C. N., Brittnacher, M. J., Miller, S. I., Singh, P. K., Manoil, C., and Bruce, J. E. (2016) *Nature communications* **7**, 13414
425. Wu, X., Chavez, J. D., Schweppe, D. K., Zheng, C. X., Weisbrod, C. R., Eng, J. K., Murali, A., Lee, S. A., Ramage, E., Gallagher, L. A., Kulasekara, H. D., Edrozo, M. E., Kamischke, C. N., Brittnacher, M. J., Miller, S. I., Singh, P. K., Manoil, C., and Bruce, J. E. (2016) *Nature communications* **7**
426. Collinge, J. (2005) *Journal of neurology, neurosurgery, and psychiatry* **76**, 906-919
427. Lanni, C., Racchi, M., Mazzini, G., Ranzenigo, A., Polotti, R., Sinforiani, E., Olivari, L., Barcikowska, M., Styczynska, M., Kuznicki, J., Szybinska, A., Govoni, S., Memo, M., and Uberti, D. (2008) *Molecular psychiatry* **13**, 641-647
428. Collinge, J. (1999) *Lancet* **354**, 317-323
429. Mead, S., Whitfield, J., Poulter, M., Shah, P., Uphill, J., Campbell, T., Al-Dujaily, H., Hummerich, H., Beck, J., Mein, C. A., Verzilli, C., Whittaker, J., Alpers, M. P., and Collinge, J. (2009) *The New England journal of medicine* **361**, 2056-2065

Appendix A: Table of all urea-acid induced PrP^{β} intra-protein crosslinked sites identified

Crosslinking reagent	Arm length (Ao)	AA# Start (1)	AA# End (1)	AA Modified (1)	AA# Modified (1)	AA-1 (1)	Peptide Sequence (1)	AA+1 (1)	AA# Start (2)	AA# End (2)	AA Modified (2)	AA# Modified (2)	AA-1 (2)	Peptide Sequence (2)	AA+1 (2)
DMTMM	0	89	94	**E**	**89**	L	EGQGGG	T	99	101	**K**	**101**	Q	WNK	P
DMTMM	0	166	171	**D**	**167**	P	VDQYNN	Q	203	206	**K**	**204**	D	IKIM	E
TATA	5	84	87	**G**	**85**	R	GSHM	L	100	108	**N**	**100**	W	NKPSKPKTN	M
TATA	5	177	183	**H**	**177**	V	HDCVNIT	I	187	189	**H**	**187**	Q	HTV	T
SDA	5	87	93	**E**	**89**	H	MLEGQGG	G	142	149	**Y**	**149**	F	GNDWEDRY	Y
SDA	5	93	97	**H**	**96**	G	GGTHN	Q	139	149	**Y**	**149**	M	MHFGNDWEDRY	Y
SDA	5	108	114	**K**	**110**	T	NZKHZAG	A	159	169	**N**	**159**	P	NQVYYRPVDQY	N
ABAS	7	98	101	**K**	**101**	N	QWNK	P	102	108	**K**	**104**	K	PSKPKTN	M
ABAS	7	186	192	**H**	**187**	K	QHTVTTT	T	199	204	**K**	**204**	F	TETDIK	I
DSG	8	100	108	**K**	**101**	W	NKPSKPKTN	M	109	111	**K**	**110**	N	MKH	M
DSG	8	103	104	**K**	**104**	P	SK	P	200	204	**K**	**204**	T	ETDIK	I
DSA	9	99	108	**K**	**101**	Q	WNKPSKPKTN	M			**K**	**104**		i	
DSA	9	98	108	**K**	**106**	N	QWNKPSKPKTN	M	109	112	**K**	**110**	N	MKHM	A
DSS	11	68	69	**G**	**68**	-	GS	S	79	85	**S**	**85**	S	GLVPRGS	H

Table 11: Intra-protein crosslinked sites identified for urea-acid induced PrP^{β} oligomers.

Crosslinking reagent and corresponding arm length identified. Peptide information for each component of crosslink indicated. 'z' indicates oxidized methionine and 'i' indicates intra-peptide crosslink.

Appendix B: Table of all urea-acid induced PrP^{β} inter-protein crosslinked sites identified

Crosslinking reagent	Arm length (Ao)	AA# Start (1)	AA# End (1)	AA Modified (1)	AA# Modified (1)	AA-1 (1)	Peptide Sequence (1)	AA+1 (1)	AA# Start (2)	AA# End (2)	AA Modified (2)	AA# Modified (2)	AA-1 (2)	Peptide Sequence (2)	AA+1 (2)
PICUP	0	124	128	Y	128	G	GLGGY	M	126	130	Y	128	L	GGYML	G
PICUP	0	126	130	Y	128	L	GGYML	G	161	169	Y	162	Q	VYYRPVDQY	N
PICUP	0	124	128	Y	128	G	GLGGY	M	163	169	Y	163	Y	YRPVDQY	N
PICUP	0	154	162	Y	157	N	MNRYPNQVY	Y	222	225	Y	225	E	SQAY	Y
PICUP	0	161	169	Y	162	Q	VYYRPVDQY	N	222	225	Y	225	E	SQAY	Y
PICUP	0	163	169	Y	163	Y	YRPVDQY	N	222	225	Y	225	E	SQAY	Y
ABAS	7	139	142	M	139	M	MHFG	N	184	187	K	187	T	IKQH	T
ABAS	7	68	71	G	68	-	GSSH	H	193	198	K	194	T	TKGENF	T
ABAS	7	139	142	M	139	M	MHFG	N	199	204	K	204	F	TETDIK	I
ABAS	7	68	71	G	68	-	GSSH	H	139	145	M	139	M	MHFGNDW	E
ABAS	7	109	113	K	110	N	MKHMA	G	193	198	K	194	T	TKGENF	T
DSG	8	68	71	G	68	-	GSSH	H	97	108	K	101	H	NQWNKPSKPKTN	M
DSG	8	68	71	G	68	-	GSSH	H	98	108	K	104	N	QWNKPSKPKTN	M
DSG	8	68	71	G	68	-	GSSH	H	98	108	K	106	N	QWNKPSKPKTN	M
DSG	8	68	71	G	68	-	GSSH	H	109	112	K	110	N	MKHM	A
DSG	8	68	71	G	68	-	GSSH	H	193	198	K	194	T	TKGENF	T
DSG	8	68	71	G	68	-	GSSH	H	202	206	K	204	T	DIKIM	E
DSG	8	109	111	K	110	N	MKH	M	193	198	K	194	T	TKGENF	T
DSG	8	110	111	K	110	M	KH	M	199	206	K	204	F	TETDIKIM	E
DSG	8	184	186	K	185	T	IKQ	H	199	204	K	204	F	TETDIK	I
DSG	8	193	196	K	194	T	TKGE	N	193	198	K	194	T	TKGENF	T
DSG	8	199	206	K	204	F	TETDIKIM	E	204	205	K	204	I	KI	M
DSG	8	202	206	K	204	T	DIKIM	E	220	221	K	220	Q	KE	S
DSA	9	68	71	G	68	-	GSSH	H	79	85	S	85	S	GLVPRGS	H
DSA	9	68	71	G	68	-	GSSH	H	98	108	K	101	N	QWNKPSKPKTN	M
DSA	9	68	71	G	68	-	GSSH	H	98	108	K	104	N	QWNKPSKPKTN	Z
DSA	9	68	71	G	68	-	GSSH	H	98	108	K	106	N	QWNKPSKPKTN	M
DSA	9	68	71	G	68	-	GSSH	H	193	198	K	194	T	TKGENF	T
DSA	9	98	108	K	106	N	QWNKPSKPKTN	M	109	112	K	110	N	MKHM	A
DSA	9	184	185	K	185	T	IK	Q	199	206	K	204	F	TETDIKIM	E
DSA	9	199	206	K	204	F	TETDIKIM	E	203	204	K	204	D	IK	I
DSS	11	68	69	G	68	-	GS	S	79	85	S	85	S	GLVPRGS	H
DSS	11	68	69	G	68	-	GS	S	99	108	K	101	Q	WNKPSKPKTN	M
DSS	11	68	69	G	68	-	GS	S	99	108	K	104	Q	WNKPSKPKTN	M
DSS	11	68	69	G	68	-	GS	S	99	108	K	106	Q	WNKPSKPKTN	M
DSS	11	68	71	G	68	-	GSSH	H	193	198	K	194	T	TKGENF	T
DSS	11	68	71	G	68	-	GSSH	H	199	206	K	204	F	TETDIKIM	E
DSS	11	184	186	K	185	T	IKQ	H	199	206	K	204	F	TETDIKIM	E
DSS	11	194	198	K	194	T	KGENF	T	192	198	K	194	T	TTKGENF	T
DSS	11	202	206	K	204	T	DIKIM	E	204	205	K	204	I	KI	M
CBDPS	14	68	69	G	68	-	GS	S	109	112	K	110	N	MKHM	A
CBDPS	14	68	69	G	68	-	GS	S	184	187	K	185	T	IKQH	T
CBDPS	14	109	111	K	110	N	MKH	M	109	111	K	110	N	MKH	M
CBDPS	14	109	111	K	110	N	MKH	M	184	186	K	185	T	IKQ	H
CBDPS	14	109	111	K	110	N	MKH	M	220	223	K	220	Q	KESQ	A
CBDPS	14	184	186	K	185	T	IKQ	H	184	187	K	185	T	IKQH	T
CBDPS	14	184	187	K	185	T	IKQH	T	220	223	K	220	Q	KESQ	A
CBDPS	14	192	194	K	194	T	TTK	G	193	198	K	194	T	TKGENF	T

Table 12: Table of all inter-protein crosslinked sites identified for urea-acid induced PrP^{β} oligomers.

Crosslinking reagent and corresponding arm length identified. Peptide information for each component of crosslink indicated.